Fire behaviour of selected polymeric materials

Numerical modelling and validation using microscale and bench scale test methods

Bhargava, Abhishek

2020

Document Version:
Publisher's PDF, also known as Version of record

Fire behaviour of selected polymeric materials

Numerical modelling and validation using microscale and bench scale test methods

ABHISHEK BHARGAVA | DIVISION OF FIRE SAFETY ENGINEERING | LUND UNIVERSITY

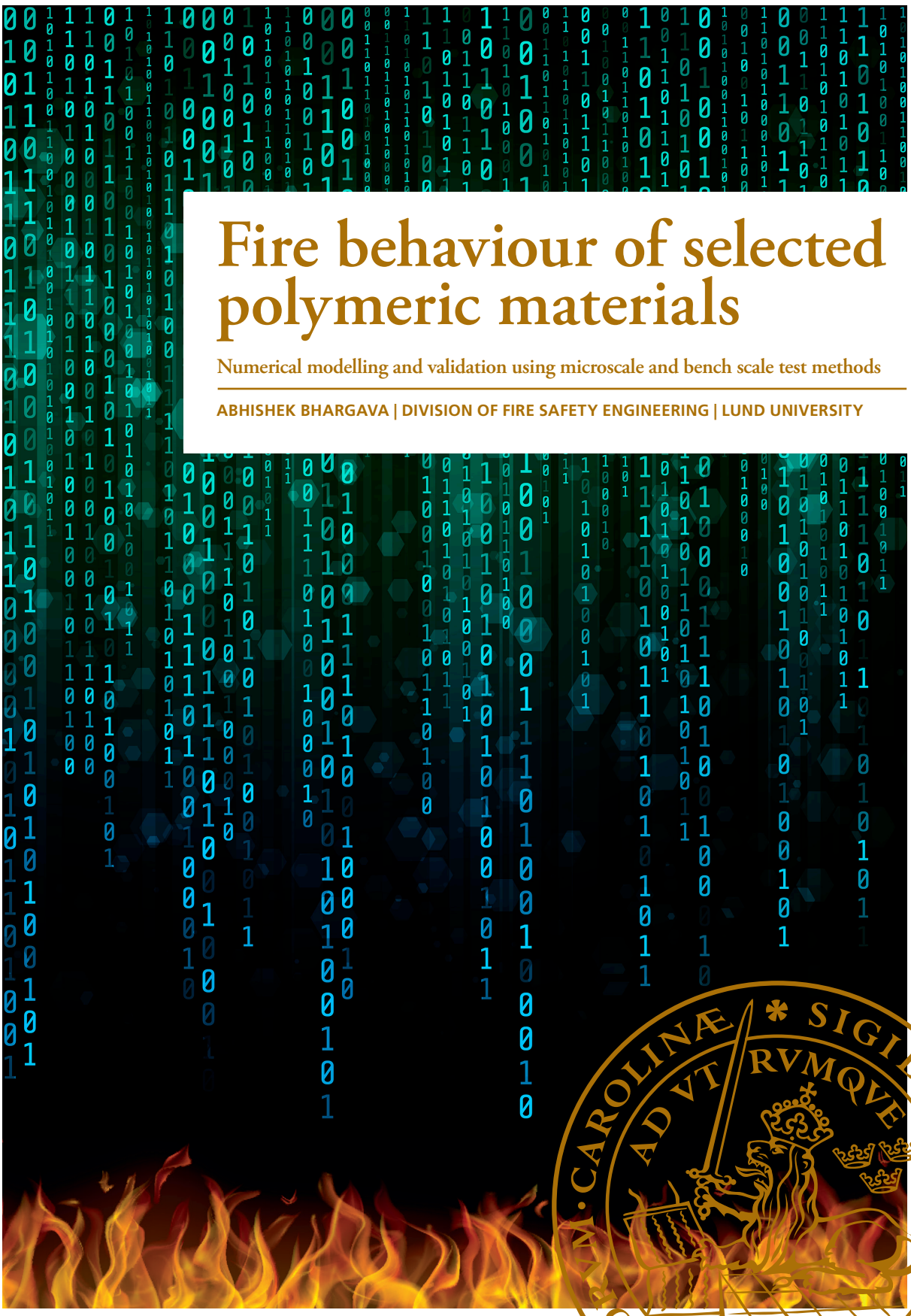

Fire behaviour of selected polymeric materials

Numerical modelling and validation using microscale and bench scale test methods

Abhishek Bhargava

LUND
UNIVERSITY

DOCTORAL THESIS

by due permission of the Faculty of Engineering, Lund University, Sweden
To be defended in lecture hall V:B on

Friday the 20th of March, 2020 at 09:15 am

Opponent

Prof. Serge Bourbigot, Unité Matériaux et Transformations (UMET)
UMR CNRS 8207, École Nationale Supérieure de Chimie de Lille (ENSCL),
France

Organization: Division of Fire Safety Engineering Faculty of Engineering Lund University P.O BOX 118 22100 Lund	Document Name: DOCTORAL THESIS
Author: Abhishek Bhargava	Date of Issue: 20th of March 2020
	Sponsoring Organizations: European Commission 7th Framework Program (Grant# 316991) and DBI

Title: Fire behaviour of selected polymeric materials - Numerical modelling and validation using microscale and bench scale test methods

Abstract

The ability to predict fire behaviour of materials is of key interest to building materials industry. The main reason for it is expensive fire testing and certification costs borne by the manufacturers to bring a finished product to market. Failure in a fire test leads to increased expenses in the product development cycle leading to delayed realization of profits and low cost competitiveness in the market. Numerical modelling and fire simulations is a less expensive method to predict the outcomes of a real fire test. However, the state of the art models existing in literature suffer from several shortcomings. A few of them are related to inadequacies related to material property data used in them as input values. Others include modelling deficiencies pertaining to accurate description of physicochemical processes involved in materials during the fire. Often hurdles in implementation of appropriate numerical methods are also a cause of poor predictability of mathematical models. In this industrial PhD work, a novel one-dimensional computational pyrolysis model was developed using a combination of deterministic and stochastic approach. The tool is capable of prediction of key fire technical properties of interest obtained in a standard cone calorimeter device such as mass loss rate (MLR), heat release rate (HRR), total heat released (THR). The developed model could be incorporated into a bigger CFD code and can be used for estimation of fire growth rate on successively bigger material scale. The performance of novel pyrolysis model considers several physicochemical transformation complexities occurring in the material and renders a satisfactory performance of the investigated materials on microscale and bench scale level simulations.

Keywords: DAEM; Pyrolysis Modelling; Polymer Flammability; Mass Loss Rate; Heat Release

Classification System if any

Supplementary bibliographical information Report 1063 ISRN LUTVDG/TVBB--1063—SE	Language: English
ISSN and key title 1402- 3504	ISBN 978-91-7895-408-7 (Print) 978-91-7895-409-4 (Pdf)
Recipient Notes	Number of pages 198 | Price
	Security classification Open

Signature 

Date: 10th of February 2020

Fire behaviour of selected polymeric materials

Numerical modelling and validation using microscale and bench scale test methods

Abhishek Bhargava

LUND
UNIVERSITY

Supervisor
Prof. Patrick van Hees, Division of Fire Safety Engineering, Faculty of Engineering, Lund University, Sweden

Co-Supervisor
Dr. Bjarne Paulsen Husted, Division of Fire Safety Engineering, Faculty of Engineering, Lund University, Sweden

Mr. Dan Lauridsen, Danish Institute of Fire and Security Technology, Hvidovre, Denmark

Opponent
Prof. Serge Bourbigot, Unité Matériaux et Transformations (UMET) UMR/CNRS 8207, École Nationale Supérieure de Chimie de Lille (ENSCL), France

Assessment Committee
Prof. Guillermo Rein, Department of Mechanical Engineering, Imperial College London, U.K.

Prof. Baljinder Kaur Kandola, Institute for Materials Research and Innovation, University of Bolton, U.K.

Dr. Andrea Klippel, Institute for Apparatus and Environmental Technology, Otto-von-Guericke University Magdeburg, Germany

Division of Fire Safety Engineering
Lund University, P.O Box 118, SE-2201 00 Lund, Sweden

Report 1063
ISSN 1402-3504
ISRN LUTVDG/TVBB--1063—SE
ISBN 978-91-7895-408-7 (Print)
ISBN 978-91-7895-409-4 (Pdf)

Printed in Sweden by Media-Tryck, Lund University
Lund 2020

Acknowledgements

I would like to take this opportunity to express my sincere gratitude to my supervisor Prof. Patrick van Hees and co-supervisor Dr. Bjarne Husted and Dr. Berit Andersson (retired) for their immense support, patience and deep knowledge in guiding me through the research process and writing my PhD thesis. I have benefited enormously from their broad knowledge and experience during the last six years. Without their continuous support and motivation, this work would not have been possible.

Second, I owe my sincere thanks Mr. Jesper Ditlev, (CEO) Danish Institute of Fire and Security Technology for providing me with this excellent opportunity and letting me be the part of the Fire Tools project at DBI. The financial support for this project was jointly provided by DBI and European Commission's seventh framework program under Marie Skłodowska-Curie actions (EU Grant# 316991), which is gratefully acknowledged. Also, many thanks to our project partners including Fire Testing Technology (FTT), Kingspan Insulation, Saint Gobain Isover, Rockwool International A/S, Interscience Communications Ltd., Ghent University for facilitating industrial visits, providing excellent internship opportunities and have fruitful discussions during the course of the project.

Special thanks to Dan Lauridsen, and the fire testing team at DBI for insightful technical discussions and sharing practical knowhow into industrial fire testing at every point during the project. In particular, I am also thankful to Carsten Damgaard, and Poul Bjerre Toftild and Fanny Guay for providing their continuous support in project management issues and keeping the team closely knitted together. I thank my fellow colleagues Karlis Livkiss, Blanca Andres Valiente, Frida Vermina Plathner, Konrad Wilkens Flecknoe Brown and Thomas Hullin for stimulating technical discussions and all the good moments we had in the last four years during conference trips and team building activities together.

I would also like to express my sincere gratitude to the staff at Lund University in particular, Dr. Daniel Nilsson, Dr. Nils Johansson, Dr. Jonathan Wahlqvist and Prof. Lars Wadsö for sharing their deep knowledge in core fire engineering subjects, laboratory work and imparting relevant programming skills which proved to be very helpful during the course of my research work. Also, special

thanks to Dr. Marc Janssens, Dr. Bertrand Girardin, Dr. Anna Matala, Dr. Hossein Sina, Prof. Srinivasan Iyengar and Dr. Lucas Bustamante for sharing the resources for model development work and providing technical insights during the project as and when required.

Finally, I would like to thank my parents Mrs. Ela and Mr. Chaitan Bhargava who have been a source of constant motivation and encouragement during my life so far. Their support and motivation has been the sole force to keep me motivated during my research journey. I would also like to thank my sister, Mansi who has been supportive throughout my life and took care of my parents during my absence.

Popular Science Summary

Computational fluid dynamics (CFD) based fire models are used for the prediction of heat and smoke spread in building spaces. Such models use some form of Navier-Stokes equations representative of different transport processes (physical and chemical) occurring in the considered spatial domain during the course of fire. Typically, these equations consist of mass, energy and momentum conservation along with applicable boundary conditions, which are solved using appropriate numerical methods for different field variables (typically, pressure, density, temperature and velocity). With increasing computational power, such calculations can be applied to numerous fire scenarios and completed in time bound manner to provide improved fire safe building design solutions to architects, fire engineers and regulatory bodies. However, CFD based simulations face several challenges related to prediction accuracy and computational costs.

To improve upon the speed and prediction ability of CFD based fire models, it is necessary to upgrade not only the computational infrastructure, but also invest enough resources to explore new and accurate sub models and acquire better experimental devices to provide material input parameters for simulating a given fire scenario. Unless the material fire behavior cannot be predicted accurately in microscale and bench scale studies, it is likely there will be large deviations in the prediction accuracy of field models also.

A large number of polymers are used in building and construction sector, whose fire performance is of particular interest from safety point of view. In this industrial PhD work, the main research objective was to improve prediction of fire performance of common polymer materials using numerical modelling and simulation tools. To achieve that aim a novel one-dimensional computational pyrolysis model was developed and validated for the solid phase. The method followed a combination of deterministic and stochastic means following a multiscale approach. The material property input parameters were acquired using experiments performed in microscale analytical devices while validation was performed on bench scale device. Another focus of the work was to explore stand alone chemical reaction sub-models that can describe multiple reactions in polymeric materials of common and industrial relevance. A sensitivity analysis framework for standalone chemical kinetic models was also presented.

The overall results show the model is capable of predicting key fire technical properties of interest obtained in a standard cone calorimeter device such as mass loss rate (MLR), heat release rate (HRR), total heat released (THR). The developed model could be incorporated it into a bigger CFD code and can be used for estimation of fire propagation rate on successively incremental scale. The performance of novel pyrolysis model considers several physicochemical transformation complexities occurring in the material and renders a satisfactory performance of the investigated materials on microscale and bench scale level simulations.

A discussion section is also presented on how to incorporate higher degree of complexity for gas diffusion and in depth radiation absorption for improving the prediction ability of the current form of the model. In conclusion, the material presented in this thesis contributes to better understanding of burning behavior of selected polymers. These findings can be used as a foundation for expanding the current level of understanding for flame spread calculations. It is envisaged that the work shall be useful for practicing engineers and researchers involved in the field of fire development and CFD based fire risk assessment.

List of Publications and Author's Contribution

This thesis is based on the following research papers that have been accepted in international peer reviewed scientific journals:

Paper I — A. Bhargava, P. van Hees, and B. Andersson, "Pyrolysis modeling of PVC and PMMA using a distributed reactivity model," *Polymer Degradation and Stability* (2016), Vol 129 pp. 199-211;DOI: https://doi.org/10.1016/j.polymdegradstab.2016.04.016

Paper II — A. Bhargava, B. Andersson, P. van Hees, H. Sina, and S. Iyengar, " Distributed Reactivity Model to Predict Multistage Pyrolysis of Polymeric Materials and Sensitivity Analysis," *Interflam'16, 14th International Conference and Exhibition on Fire Science and Engineering, London, UK*, 4- 6th July 2016

Paper III — A. Bhargava, P. van Hees, B. Husted, A. R. Junior, and C. Neumeister, "Performance analysis of a coupled heat transfer and sub-grid chemical reaction distributed activation energy model for fire simulations," *Journal of Fire Sciences*, (2019), Vol 37 (1) pp 18-46; DOI: https://doi.org/10.1177/0734904118808009

Paper IV — A. Bhargava and P. van Hees, "Pyrolysis Modelling of PVC using Distributed Activation Energy Model (DAEM) – micro scale testing," Proceedings of the *International Conference of Applications of structural fire engineering Dubrovnik, Croatia*, 15-16th October 2015. ISBN-978-8001-05204-4, pp 448-453; DOI: https://doi.org/10.14311/asfe.2015.071

The author's contribution to the papers are presented in the following table.

Table 1 Author's Contribution

Paper	Author's Contribution
I	The author wrote the full paper, did background research, developed the model algorithm into software code for parameter estimation and did all the data analysis. The co-authors and the main supervisor provided comments.
II	The author wrote the full paper, did background research, performed experiments, data analysis and developed the model algorithm into software code for sensitivity analysis. S. Iyengar and author's main supervisor provided comments. Part of the experimental work was also done by Hossien Sina (co-author) and partly sourced from external research lab for model development.
III	The author wrote the full paper, did background research, implemented the sub-grid model into the software, and did all the data analysis. Experimental work was supported by co-authors. Author's main and co-supervisor provided comments.
IV	The author wrote the full paper, did background research and performed all the data analysis. Author's supervisor provided comments. Experimental work was supported from external laboratory.

Other Contributions

- K. Livkiss, B. Andres, A. Bhargava, and P. van Hees, "Characterization of stone wool properties for fire safety engineering calculations," *Journal of Fire Sciences*. Vol. 36, Issue 3, Pages 202-223; DOI: https://doi.org/10.1177/0734904118761818

- B. Andres, K. Livkiss, J. Hindalgo, P. van Hees, L. Bisby, N. Johansson and A.Bhargava, "Response of Stone Wool Insulated Building Barriers under Severe Heating Exposures," *Journal of Fire Sciences*. Vol. 36, Issue 4, Pages 315-341; DOI: https://doi.org/10.1177/0734904118783942

Conferences

- Cone calorimeter studies on cable sheathing polymers to evaluate flame retardancy effect of aluminium trihydroxide (ATH), Nordic Fire Safety Day, Trondheim, Norway. 8th June 2018

- Using Distributed Activation Energy Model (DAEM) to predict mass loss rates in PMMA, European Meeting on Fire Retardancy and Protection of Materials Berlin, Germany, 21-25th June 2015

List of Abbreviations

NFPA	National Fire Protection Association
ASTM	American Society for Testing and Materials
FDS	Fire Dynamics Simulator
PVC	Polyvinyl chloride
CFD	Computational Fluid Dynamics
PMMA	Poly-methyl methacrylate
EVA	Ethylene vinyl acetate
ATH	Aluminium tri-hydroxide
TGA	Thermo-gravimetric analysis
DTG	Differential thermogravimetry
HRR	Heat release rate
THR	Total heat release
DAEM	Distributed Activation Energy Model
MLR	Mass loss rate
FDM	Finite difference method
FVM	Finite volume method
EHC	Effective heat of combustion
DIDP	Diisodecyl phthalate
AMEO	Aminopropyltriethoxysilane

TTI	Time to ignition
DSC	Differential scanning calorimetry
TPS	Transient plane source
OF	Objective function
PHR	Parts per hundred of rubber
DTA	Differential thermal analysis
H-TRIS	Heat-Transfer Rate Inducing System

Nomenclature

Symbols

m	Mass	[mg]
A	Pre-exponential factor	[s^{-1}]
E	Activation Energy	[kJ mol^{-1}]
t	Time	[s]
T	Temperature	[K]
E_0	Mean activation energy	[kJ mol^{-1}]
c_p	Specific heat	[kJ kg^{-1} K^{-1}]
H	Heat of pyrolysis	[kJ kg^{-1}]
x	Spatial co-ordinate	[m]
D	Diffusivity	[m^2 s^{-1}]
G	Incident heat flux from cone heater	[kW m^{-2}]
L	Length	[m]
k	Thermal conductivity	[W m^{-1} K^{-1}]
$\ddot{q}$	Heat flux	[kW m^{-2}]

Subscript

o	Initial
f	Final
T	Total
exp	Experimental
max	Maximum
cal	Calculated

i	Index for experiment
j	Index for data point
s	Solid phase
$char$	Char
g	Gas
amb	Ambient
fl	Flame
$virgin$	Virgin
p	Peak
$flame\ out$	Flame out
rad	Radiation

Greek letters

α	Conversion	[-]
β	Heating Rate	[K min^{-1}]
φ	Temperature integral	[-]
σ	Standard deviation	[kJ mol^{-1}]
ρ	Density	[kg m^{-3}]
ω	Reaction rate	[s^{-1}]
η	Char fraction	[-]
ε	Emissivity	[-]
κ	Absorption coefficient	[-]

Constants

R	Real gas constant	[8.314 J K^{-1} mol^{-1}]
σ_c	Stefan Boltzman constant	[5.67x10^{-8} W m^{-2} K^{-4}]

List of Figures

List of Tables

Table of Contents

The boy stood on the burning deck,
Whence all but he had fled;
The flame that lit the battle's wreck,
Shone round him o'er the dead.

Yet beautiful and bright he stood,
As born to rule the storm;
A creature of heroic blood,
A proud, though childlike form.

The flames rolled on – he would not go,
Without his father's word;
That father, faint in death below,
His voice no longer heard.

He called aloud – 'Say, father, say
If yet my task is done?'
He knew not that the chieftain lay
Unconscious of his son.

'Speak, father!' once again he cried,
'If I may yet be gone!'
– And but the booming shots replied,
And fast the flames rolled on….

by F.D Hemans

1 Introduction

1.1 The Fear of Fire

The above lines have been taken from the poem Casabianca composed by the English poet Felicia Hemans in 1826. As a school-going boy, I learnt different stanzas of the above poem for participating in poetry recitation competitions in my high school. The different lines of this poem have been echoing in my head, ever since I took up research work in the area of fire safety engineering. The very thought of being caught in a fire like situations can run down shivers to most of us. The above lines are no exception; F. D Hemans portrays the apathy, tension and plight of a young boy who waited for his father's signal to vacate his post on the ship that was caught on fire. Unfortunately, he was not aware of the fact that his father, also the captain of the ship, was already dead and the boy kept battling flames instead of trying to escape.

In general, these lines symbolize true actions and feelings of committed individuals who value relationships and duties surrounding them, irrespective of impending danger they may fall prey to. In case of acute trauma and emergency like situation such as fire, their behaviour can become irrational and emotions may take precedence over pragmatic actions. The field of fire safety engineering supports rationality in the face of fire as a counterbalance of the risk for irrational or emotional response to developing incidents.

1.2 Goals of Fire Safety Engineering

The field of Fire Safety engineering is committed to protect human lives and structures by channelizing their scientific and engineering capabilities via rational way of thinking so that emergency rescue situations may be dealt with high degree of maturity. This includes taking active and pro-active measures to ward off dangers associated with fire with the aim of protecting lives, and property or both. However, despite several efforts the history has witnessed many fire accidents. There is no dearth of the list of number of people who have succumbed to deaths by burns and smoke inhalation. Recent fire statistics from National Fire Protection Association (NFPA) in the United States reveal the year 2017, alone saw 3400 civilian fire fatalities, 14,670 civilian fire injuries and an estimated $23 billion in direct property losses [1]. Out of this, home fires caused maximum number of civilian fire deaths (2630 lives or 77 % of the total number of deaths).

These staggering statistics reveal the gravity of the situation and high degree of vulnerability of the people with respect to an omnipresent fire risk hazard they live in their own built environment. The issue of potential dangers associated with fire affects people in other situational circumstances also. This risk is not only limited to building spaces but also present when people travel via road/rail/air, or during their presence in industrial workspaces and often getting affected of the acts of arson due to malicious intent of the perpetrators.

The fire engineering community has formed a structured preventive approach by clearly defining fire safety objectives and acceptable levels of safety [2,3]. In case of building fires, the primary safety objective is to ensure the life safety of occupants. This is achieved by promoting building designs that allow sufficient egress times before untenable conditions in the compartment are reached [4]. Other fire safety objectives are to prevent the spread of fire to other compartments/buildings and avoid serious injuries to fire fighters.

1.3 Regulatory Framework and Testing Methodology

In the present scenario, in order to meet the above discussed fire safety objectives, the methodology of fire testing has been instituted via harmonized codes and test standards published by International Standardization Organization (ISO) [5] or other notified and standardization bodies. The main purpose of fire testing is to assess the fire performance of individual building material, components and products in standard test conditions for classification purpose. This process involves following standard methods for preparing, conditioning and mounting of the test specimens in accordance with relevant test methods and product standards prior to any testing. The 'Reaction to fire' product classification is performed based on the European standard EN 13501-1 [6], which lays down general requirements, provides a model for reporting and gives background information of the testing and classification system. This document applies to three categories, namely construction products, floorings and linear pipes thermal insulation. Based on the performance in a test, a Euroclass (A1, A2, B, C, D, E and F) is awarded to a lining product. In Euroclasses, A1 and A2 represent different degrees of limited combustibility. For linings, Euroclasses B-E represents products that may go to flashover in a room at certain times. Products which do not live up to the classification demands and cannot be classified in one of the classes A1, A2, B, C, D, E are awarded class F. For linear pipe insulations and flooring materials, subscripts L and fl are added. Thus there are seven classes for linings and seven classes for floor coverings [4]. All the materials classified as A2, B, C, D obtain an additional classification regarding emission of smoke (s=1 (weak) to s= 3 (high)) and production of flaming droplets (d=0 (absent) to d=2 (high dripping)). The `Reaction to Fire´ testing methodology mainly focuses on consideration of the fire risks in the initial developmental

stages (pre-flashover) of fire. This is done via assessment of ignition, flame spread and heat release and smoke generation.

Some examples of standard reaction to fire tests are[1]:

a) EN ISO 1716 [7] - Bomb calorimeter test to determine gross calorific potential of a material. This test is relevant for classes A1, A2, $A1_{fl}$, $A2_{fl}$
b) EN ISO 1182 [8] – Non-combustibility test to identify products that will not or will not significantly contribute to fire regardless of their end use. This test is relevant for classes A1, A2, $A1_{fl}$, $A2_{fl}$, $A1_{L}$, $A2_{L}$
c) EN 13823 [9] – Single Burning Item (SBI) test to evaluate the potential contribution of a product to the development of a fire, under a fire situation simulating a single burning item in a room corner near to that product. The test is relevant for classes A1, A2, B, C, D. Subscripts L and fl are added for linear pipe insulation and flooring materials.
d) ISO 9705 [10] – Room corner test is a large scale test method to measure burning behaviour of construction products in a room scenario. The principal output is the occurrence and time to flashover.
e) EN ISO 11925-2 [11] – Small flame test to evaluate the ignitability of a product under exposure to a small flame. The test is relevant for classes B, C, D, E, B_{fl}, C_{fl}, D_{fl}, E_{fl}. B_{L}, C_{L}, D_{L}, E_{L}.
f) EN ISO 9239-1 [12] is a floor covering test to evaluate critical radiant flux below which flames no longer spread over a horizontal flooring surface. The test is relevant for classes $A2_{fl}$, B_{fl}, C_{fl}, D_{fl}.
g) EN ISO 5660-1 [13] is a bench scale test to evaluate heat release and smoke production characteristics of a product specimen by impinging external heat flux from a cone heater above the sample.

On the other hand, when the objective is to ensure the stability of the structure and prevention of fire spread, testing methodology focuses on load bearing (R), insulation (I) and integrity (E) of the structures via 'Resistance to fire' tests conducted in large scale industrial sized furnaces of horizontal or vertical type (EN 1363-1 [14] and EN 13501-2 [15]). The method provides the ability to quantify the capacity of an element, or a construction, to withstand high temperatures when exposed to different type of fire curves (e.g. ISO 834 fire curve; hydrocarbon curve). The main outcome is a report carrying the information about the fire performance of the product in a given test conditions, which may be used to seek a type approval from the relevant certification authorities to get a fire rating/CE marking of the product specimen.

[1] Subscript (fl) here refers to classification for flooring materials

1.4 Numerical Simulations for Product Development

In this gamut of adhering to prescribed fire testing procedures for the scrutiny of building material and products, the repercussions of a failure or underperformance leads the onus of product redevelopment cost on the manufacturer. Such detrimental issues hamper innovation; lead to poor cost efficiency and delay in reaching the benefits of the product to the end customer. In light of this problem, it is interesting to study and explore the fire behaviour of materials via numerical simulations. This can aid the manufacturer in fine-tuning their design in the early product development stages to meet the fire safety requirements. These tasks may be accomplished under the activities of numerical modelling and simulation, where in the fire performance of products may be estimated based on close representation of physicochemical phenomenon occurring in the material during a fire test via application of the principles of heat and mass transfer. In a more simplified language, modelling and simulation tasks aim to convert physicochemical nature of the fire problem into actual mathematical governing equations, that have the capability to resolve various fire technical properties of interest, predicting their performance in a standard fire test. Some examples of the variables are time evolution of temperature distributions, mass loss rate, heat release rates and smoke development. The proliferation of mathematical models and their eventual solution using numerical methods using advanced computational resources has rendered a way to solve the very theoretical nature of the problem into quantifiable entities in form of different fire technical properties. To cite a few examples out of large number of computer software packages used in this domain are based on CFD based programs such as (Fire Dynamics Simulator (FDS) [16], FireFoam [17]), FEM based programs such as (TASEF [18]; Comsol) and other pyrolysis models based on finite difference numerical schemes such as Thermakin [19], Pyropolis [20]. In addition, stand-alone mathematical software packages are also available for performing mathematical computations such as individual Matlab and Python based scripts.

1.5 Research Objectives

The overarching research objective of this work aims to improve prediction of fire performance of materials using numerical modelling and simulation tools. To achieve this goal the work has been sub-divided into the following specific objectives:

Research Objective 1:

To investigate major experimental techniques used for evaluating the fire behaviour of polymeric building materials.

This part of the research aims to investigate major experimental techniques used for evaluation of fire behaviour of polymers on different length scales starting from microscale to bench scale level. These set of techniques evaluate the thermal decomposition, heat release and smoke emission characteristics exhibited by the sample specimen upon exposure to heat. The evaluation is not exhaustive. It excludes those techniques that characterize other phenomena experienced by the materials during combustion process such as flame spread, burning droplets and gas composition analysis. Chapter 3 covers the main points outlined for this part of the research work.

Research Objective 2:

To investigate which numerical models and simulation techniques are suitable for predicting the fire behaviour of building materials.

This part of the research investigates which mathematical models and numerical methods may be used for prediction of fire behaviour of polymeric materials on two separate length scales namely microscale and bench scale. This evaluation does not cover all the models existing in literature but encompass some of the main works done in the recent past that may be considered as reference points in developing new ideas in the field of fire simulations. It is believed the results obtained during this task will pave the way for modifications and development of new models with distinct features. Chapter 4 covers the main aspects for this portion of research work.

Research Objective 3:

To identify the gaps in the mathematical models found in literature on microscale and bench scale models and find new sub-grid models for rendering improvements in their overall prediction ability.

This part of the research aims to identify gaps in the identified mathematical models and aims to seek modifications that could be made in microscale and

bench scale models in order to improve the overall prediction ability and address various physicochemical transformations occurring in the material via suitable governing equations. Further, this work aims to explore new sub-grid models prevalent in other research areas such as combustion of solid fuels in industrial power plants. Those sub-grid models could find new applications in fire simulation work. The scope of investigation is limited to chemical kinetic models and excludes several other sub-grid models (e.g. radiative char model, porosity models, volume expansion/shrinking models etc.) which may be evaluated that are existent in literature. Hence, performance evaluation of stand-alone sub-grid chemical kinetic models and sensitivity analysis in combustion literature forms one of the main area explored in this section. The main aspects of this research objective are presented in chapter 4 and 5.

Research Objective 4:

To identify how material behaviour can be linked from test data acquired from microscale characterization experiments to predict bench scale fire behaviour, through numerical modelling.

This part of the research work aims to highlight, how material property data acquired using microscale material characterization tests be used for providing input data to newly developed bench scale model for prediction of fire properties. The work encompasses model development tasks displaying the interlinking of microscale sub-grid model to the bench scale model.

Later sections of Chapter 4 (Section 4.5) and Chapter 5 provide answers to the main goals of this research objective.

1.6 Limitations

The discussion on main limitations of the study is divided into experimental and numerical aspects of the work. For the experimental part, it can be stated, only few selected materials were used in this thesis as a point of evaluation for the model development process. In addition, the list of materials used as specimens is only representative of common building materials. The list is not exhaustive but rather representative of what can be found as combustibles in common residential buildings. Secondly, some input data required for simulation work was not acquired by means of experiments, but sourced from literature values. In addition, direct acquisition of experimental data was subject to access to analytical devices.

Moreover, the study focused to simulate most significant bench scale fire properties of interest that may be obtained via cone calorimeter such as time to ignition and heat release rate, peak heat release rate and total heat release rates.

The study does not address and simulate many other bench scale fire properties of interest such as evolution of various gas species via quantification of concentrations, flame spread rate, mechanical behaviour (bending, cracking, swelling, shrinkage), phase change phenomenon such as melting, formation of bubbles, melt and plastic behaviour and burning droplet formation.

Also, only few microscale and bench devices depending upon the availability of the analytical equipment were used to acquire input data relevant for simulations. Henceforth, the study does not address/reflect the material fire performance in many other standard bench scale devices for fire tests such as non-combustibility apparatus (EN ISO 1182 [8]), lateral ignition and flame spread (ASTM E 1321) apparatus (LIFT), smoke density chamber (ISO 5659), small flame test (EN ISO 11925 [11]) to evaluate ignitability.

With reference to simulation work, the study is mainly focused on solid phase material decomposition only; the model in current form is not capable of resolving gas phase parameters. Although, the model discusses several complexities in the solid phase during thermal decomposition such as gas diffusion and in-depth radiation absorption but these physical phenomena have not been implemented in its current form of the model. For instituting the sub-model on bench scale level, an analytical approximation has been used as mathematical difficulties were unresolved in its current form. The main reason for it was attributed to presence of Gaussian integral and error function in the solution of coupled partial differential equations.

2 Theory

2.1 Multi-scale Approach for Fire Simulations

In view of the multitude of products entering the building materials market, the need for meeting the fire safety requirements is ubiquitous. Recent trends in fire simulation studies show the adoption of multi-scale approach. The term 'multi-scale' refers to acquiring material property data using small-scale tests for using as inputs for performing fire simulations on progressively increasing scales. This involves obtaining knowledge about the individual building materials by deconstructing them into different components of which they are composed of and obtaining their individual physical and chemical properties relevant for providing inputs to fire simulation. Another dimension of this approach also refers to model validation tasks on each studied scale and analyse variation in fire behaviour of materials as the scale of fire testing changes. The term validation refers to the process of determining the appropriateness of the governing equations as a mathematical model of the physical phenomena of interest [21]. The work involves the evaluation of the quality of predictions made by the mathematical models by comparing the simulated results with the data obtained via experimental measurements. The main standard covering this area is published by American Society of Testing and Materials under the document ASTM E 1355 [22].

The items used in buildings are mainly classified into three main broad categories: Building content, Building Products and Building Barriers. Each of them may comprise of one or more constituting materials. The three main categories may be defined as:

- **Building content**: They are defined as interior objects that can be moved /and or are mobile, not attached or fastened/part of room construction – e.g. electronic goods (TV, Microwave oven), furniture (sofa, bed, drawer chests) etc.
- **Building products**: These are items used for the construction of building, consisting of one or more solid materials – e.g. gypsum plaster board, sandwich panels, electrical cables

- **Building barriers**: These are the boundaries of the fire compartment in which the fire is present and are used to separate one compartment from another in case of fire. E.g.- wall window, door, roof and floor

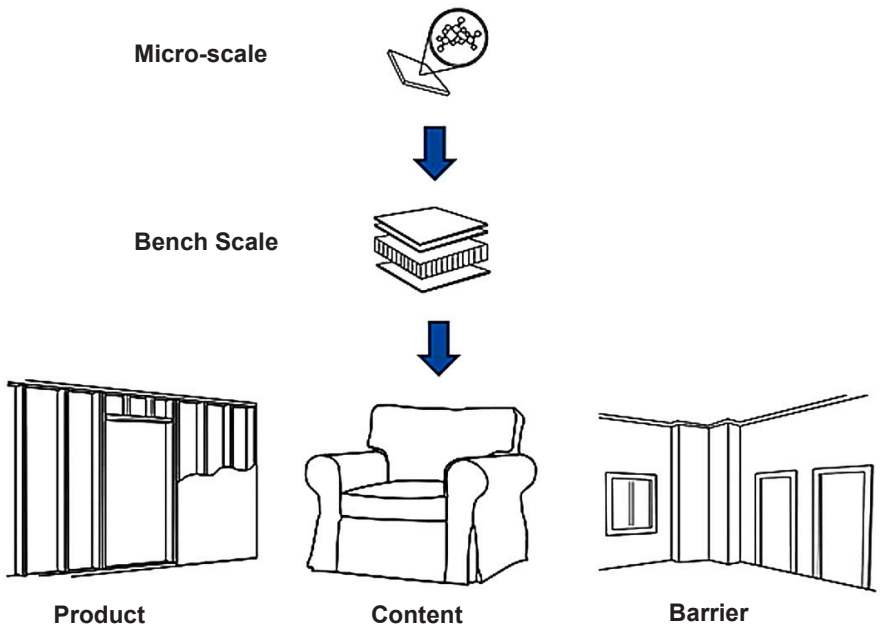

Fig. 1 Multi-Scale approach for fire modelling of building products, content and barriers

Microscale: The first step towards fire simulation is to acquire material property input data. In this stage, material analysis is performed on milligram sized test samples. As the sample sizes are small heat transfer effects may be neglected allowing investigation of chemical kinetic properties, combustion properties without added complexity of thermal gradients. Common devices used for such studies are simultaneous thermal analyser (STA), micro-combustion calorimeter (MCC) and bomb calorimeter. Such tests give initial estimates of mass loss profiles, heat released, exothermicity or endothermicity, heat of combustion of the reactions that occur in the materials and various points of material transformations in a dynamic heating experiment.

Bench Scale: This is the next stage of material analysis followed by microscale testing. For applications to building content and building products this size, falls in the range in which heat transfer effects are taken into account but flame spread effects are not part of the analysis. Specimen sizes are in the range of few centimeters. One example of such a specimen is the one used in cone calorimeter (square specimens of 10 cm by 10 cm) which is a standard size

used for the assessment of reaction to fire properties. In addition to that, some material properties such as the heat transfer properties are considered to be acquired on this level as the size of the sample required for measurements are bigger than that of microscale level by a few orders in magnitude. Common devices of acquiring heat transfer properties are slug calorimeter [23], guarded hot plate (GHP), transient plane source (TPS) and heat flow meter (HFM).

Intermediate Scale: This scale refers to fire testing of products and building barriers on a progressively larger samples in which the size of the samples are of order of few meters. On this scale, flame spread effects and heat transfer effects taken into consideration depending upon the choice of the apparatus. Common devices used for such studies are top/front loading gas fired furnace of size (1.46 x 1.46 x 1.5 m^3), single burning item test (SBI), lateral ignition and flame spread (LIFT) apparatus.

Large Scale: The large-scale fire behaviour comprises of combined fire behaviour of building product, content and barriers. The size of the specimens are typically several times bigger than the intermediate scale level. Common testing methodologies involve, placement of the test setup under an industrial hood, usage of large-scale furnace of size 3 m x 3 m in vertical or horizontal format or as free burning item. It may represent substantial part of the construction in its entity or in partial forms. For example, a portion of foam slab and gypsum plasterboard and stone-wool sandwich in placed in a corner arrangement tested for heat release rate, temperature development and flame spread. It can also represent testing of full-scale test specimens in large furnace or as in a free burning test. The sizes of the test specimen may represent the actual size of the real doors, windows, glass partitions and facades.

Overall model for fire simulation: The final phase of the multiscale approach is to integrate knowledge gained from experiments and simulations from each scale into a single model for fire simulation using a complex simulation code. This may be done using a complex fire simulation software, which involves many phenomenon e.g. fluid dynamics, heat transfer and pyrolysis, which may then be used for engineering product design calculations.

An example of this approach could be an electrical cable (designated as building product) which would comprise of a current carrying conductor (typically made up of copper), polymeric sheathing (such as PVC) and plastic insulation (polyethylene). The fire performance of a cable may be assessed by obtaining material properties of each constituting elements via small scale testing followed by simulating their fire performance in bench scale test configuration (such as a cone calorimeter) using suitable program such as Fire Dynamics Simulator.

Depending upon the response, this may further be extended to simulate heat release, smoke emission and flame propagation characteristics of a bunch of cables mounted on a vertical ladder (system level) in different mounting and backing conditions analogous to in a real fire test. An example of such a fire test can be exemplified via standards EN 50399 [24] in which a bunch of cables are mounted on a vertical ladder and combusted with a gas burner in corner configuration.

The test outputs from such simulations will encompass key parameters such as flame spread (m), peak heat release rate (p-HRR) (kW), total heat release (THR) (MJ), total smoke production (TSP) (m^2) values. This would enable significant help to the manufacturers in assessing the fire behaviour of cables during product development stages and make modifications without actually testing the semi-finished products.

2.2 Pyrolysis Modelling

The pyrolysis phenomenon can be described as the release of volatile gaseous components from the material upon exposure to heat. In the last decades, rapid advances in the field of 1D comprehensive pyrolysis modelling have been witnessed.

Several computer programs based on computational fluid dynamics (CFD) framework have been developed such as Fire Dynamics Simulator (FDS) [16,25], Thermakin [26], Pyropolis [20], Comsol [27] and Matlab [28] based applications. Some of the notable works in the field of comprehensive pyrolysis modelling include those of McGrattan [16], Stoliarov et al. [19,29], Snegirev et al. [30], Marquis et al. [31,32], Ghorbani et al. [33], DiBlasi [34] and Bustamante [28]. Their models incorporate different physicochemical processes to describe material response to heat in form of mass and energy conservation equations. Despite elaborate efforts, the results of such simulations deviate considerably from experiments in large number of cases for a variety of materials under different heat exposure conditions and specimen dimensions [26,33]. The main factors accountable for incongruence between experimental and simulated results are lack of material property data, deficiencies in mathematical model describing the underlying physics and numerical problems in computation of governing equations. To account for such deficiencies, acquisition of direct material property data and modifications performed on sub-model is one way forward for resolve such issues in an effort to improve the predictive capability of model equations. In this work both, the approaches have been adopted depending upon the availability of experimental resources and instituting modifications on sub-model level to seek improvements in bench scale fire simulations. For direct acquisition of material property data, microscale material characterization

experiments have been performed while on modelling level, new sub-model based on probability and statistics have been instituted to account for variations in key input values. The main concept of probability distribution function (PDF) based on Gaussian distribution of activation energies has been used in chemical reaction sub-model, which accounts for the variations observed in chemical kinetic parameters a key input in fire simulations.

3 Materials and Methods

3.1 Research Methodology for Model Development

The strategy followed for the model development process is broadly summarized using a seven-point process. It has been largely derived from the project work performed under the individual tasks and work packages of the bigger project Fire Tools [35].

The various steps are as follows:

1. Identification of multi-scale studies prevailing in scientific literature.
2. Reviewing existing mathematical models for fire simulations on microscale and bench scale studies.
3. Reviewing experimental methods used for retrieving material property data for providing inputs to identified models.
4. Determining gaps in existing modelling studies and exploring scope of improvements for target fire technical properties of interest.
5. Material selection and acquisition of experimental data for comparison with test data during model development process to assess the model performance.
6. Shortlisting of models, proposing modifications and their conversion to relevant computer programs for model fitting and comparison with experimental results.
7. Documenting model performance via publications in scientific journals related to fire behaviour of materials.

3.2 Choice of Materials

The main intent of the work was to demonstrate the model performance for a set of materials that are representative for those found in common buildings. Material selection decisions were also based on the joint collaborative work performed under the framework of Fire Tools project with other participant researchers [23,36,37]. It is to be noted that not all experimental techniques on investigated scale were used in this research work, however, some of them have been described in brief which were found to be helpful in sourcing data from literature. In this section, justification for the choice of materials is presented.

The choice involves two widely used thermoplastics in electrical cables. Since cables are prone to short circuits due to insulation malfunction resulting in eventual fires. Hence, polyvinyl chloride (PVC) and ethylene vinyl acetate (EVA) were chosen in a few of the studies. Both the materials were obtained in neat as well as industrial formulation form and are reported in Paper I and III respectively. Poly-methyl methacrylate (PMMA) was another material chosen because it has been widely studied as a reference material in fire safety engineering domain. In addition, the material is widely used as lightweight replacement of glass in doors and windows. The third set of materials are also polymeric in nature and used in building and construction sector in the form of covering for gypsum plasterboard wall partitions. Therefore, cellulosic paper sample retrieved from a commercial gypsum plasterboard was also part of the study. Finally, a fabric composed of a blend of cotton and polyester was included to represent furniture fire issue as it is used as an upholstery material for foam-based materials such as cushions, sofas and mattresses.

3.3 Studies encompassing chosen materials

It is to be clarified that not all the materials were part of all the publications. For the first publication, PVC and PMMA specimens were used on which a detailed analysis on kinetic modelling has been performed. In the subsequent paper on sensitivity analysis, the list of test specimens was expanded to paper (retrieved from a gypsum plasterboard), ethyl vinyl acetate (EVA), fabric used in furniture which is a blend of cotton and polyester. Later other formulations of EVA having ATH impregnated in the polymer matrix. In the third paper another commercial formulation of cable sheathing polymer of PVC was used which was supplied by Braskem, while EVA-ATH formulation was supplied by Nabaltec AG.

In other studies stone wool, steel, and gypsum plasterboard based constructions were used as test specimens (but are not discussed in this framework of thesis). Table 2 outlines the list of materials and equipment used in various studies and their corresponding sources of data acquisition.

Table 2 List of materials and experimental equipment used for data acquisition

Paper #	Materials	Techniques	Data Sources
I	PVC PMMA	STA	VTT (Finland) SwRI (USA)
II	PVC PMMA EVA Paper (Plaster board covering) Fabric (25% Polyester rest cotton)	STA	VTT (Finland) Lund University (Sweden) SwRI (USA) University of Lille (France)
III	PVC (Industrial Formulation) EVA-ATH (Industrial Formulation)	STA Cone Calorimeter Twin screw extruder Hot pressing Machine	Nabaltec AG (Germany), Braskem SA (Brazil)
IV	PVC	STA	VTT (Finland)
Other publications*	Stonewool	STA MCC Bomb Calorimeter Slug Calorimeter	DBI (Denmark) Lund University (Sweden) University of Edinburgh (U.K) Rockwool International A/S (Denmark)
Other publications*	Gypsum plasterboard Stonewool Steel	STA H-TRIS Intermediate Scale Furnace Large Scale Furnace	DBI (Denmark) University of Edinburgh (U.K)

*Results obtained in other publications are not discussed under the current document but have been part of fire tools activities. For details, reference to individual publications should be made.

3.4 Microscale Equipment

3.4.1 Simultaneous Thermal Analyser (STA–TGA, DTA/DSC)

Simultaneous thermal analysers (STA) have dual capabilities of performing thermogravimetric analysis (TGA) and differential scanning calorimetry (DSC) tests [38,39]. In this work, test data was largely acquired using Netzsch 449 F3 STA and hence this section is based on design specification and working principle of that instrument. Variations in instrument design is common among manufacturers. In the standalone TGA mode weight changes, temperature stability, oxidation and reduction behaviour, decomposition can be evaluated. While in DSC mode melting, crystallization, oxidative stability, evaluation of specific heat may be studied. When the device is connected to a Fourier Transform Infrared Spectrometer (FTIR) and/or a Gas Chromatograph-Mass Spectrometer (GC-MS) various chemical functions of complex gas blends may be evaluated from the evolved fragments during operation, enabling detailed gas analysis.

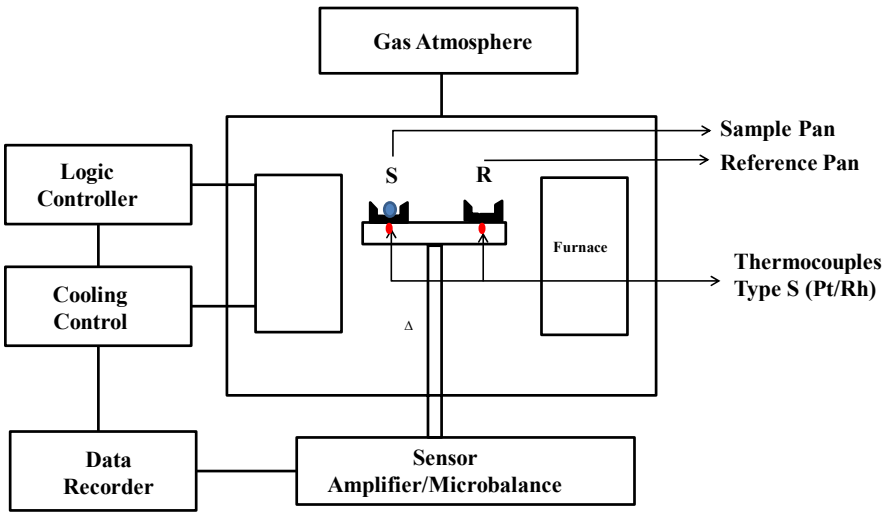

Fig. 2 Schematic of a TGA-DSC/TGA-DTA (Δ represents the differential signal ΔT for DTA and ΔP for DSC) (Reproduced from [40])

The working principle of TGA is based on monitoring of weight changes while the sample is exposed to a specified heating program. For DSC, the working principle is based on monitoring of heat flow rate to the sample against time, while the samples are exposed to a temperature program. The DSC used in Netzsch 449 F3 is a heat flux type DSC, in which the temperature difference between sample and reference is recorded, after a suitable calorimetric

calibration as a direct measure of the difference in heat flow rate or the difference in power. The schematic diagram of the device is shown (Fig. 2), showing the placement of the rod type sensor connected to a sensor signal amplifier, data recorder and cooling control and logic controller. Also shown are pans for sample and reference material in contact with thermocouple of the rod sensor. The sample carrier is placed concentrically within the radiation shield surrounding it. The radiation shield is used for even distribution of gas around the sample.

The temperature range of the instrument depends upon the type and properties of the furnace used. Some examples of different form of furnaces used are Steel (up to 1000 °C), Platinum (up to 1500 °C), Silicon Carbide (up to 1600 °C), Graphite (up to 2000 °C) and Tungsten (up to 2400 °C). The device is equipped with a top loading balance. This type of design allows ease of operation as samples can be introduced in the machine from the top in the sample holding crucibles. Some other manufacturers use hanging samples in basket type of crucibles. The simultaneous analysis is possible via replacement of plug and play sensors for desired mode of operation each for TGA-DTA, TGA- DSC and TGA-DSC-Cp sensor. The sample carrier rods have thermocouples embedded on the bottom part of the platform on which sample pans are kept. The thermocouples having a wide range of measurement capability (such as type S allowing temperatures measurement up to 1650 °C). The device can be programmed for temperature scanning rates from 0.001 to 50 degrees °C/min (for higher heating rate up to 1000 °C /min are possible but it depends on the furnace used). Often, the device is provided with two purge gas options (inert, oxidative, corrosive) and one as a protective gas for the balance. The microbalance connected to the rod sensor is used to log weight changes.

3.4.2 Microscale Combustion Calorimeter (MCC)

The microscale combustion calorimeter (MCC) was developed by Federal Aviation Administration (in the United States) in the late nineties so as to study the flammability of the polymeric materials used in commercial aircrafts [41]. Fig. 3 shows the schematic diagram of MCC. The device consists of two chambers namely a pyrolyzer and combustor. Each chamber is supplied with a gas line of nitrogen and oxygen respectively. The working principle is based on stimulating the actual conditions in a flaming solid, in which two zones exist in the case of specimen is on fire. The first zone at the sample gas interface is the pyrolysis zone (oxygen deficient zone) where fuel conversion to volatiles take place, followed by combustion zone where volatile gas generated interacts with a reactive gas atmosphere such as bulk oxygen from air to release heat and smoke. In the MCC, the pyrolyzer chamber is equipped with a nitrogen gas line and a furnace, which heats up the sample in oxygen deficient environment. The products of pyrolysis are swept away to the combustion zone

via nitrogen and combusted in presence of excess of oxygen and high temperature.

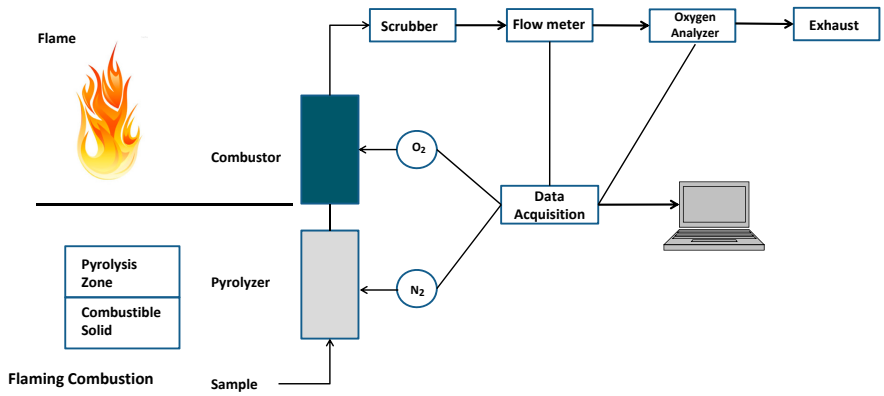

Fig. 3 A schematic diagram of Microscale Combustion Calorimeter (MCC) (Reproduced from Ref. [41])

The Heat release rate (HRR) at different sample heating rates and heat release capacity (HRC) are calculated based on the oxygen consumption, heating rate, flow rate and the sample weight. The other related flammability parameters provided by a single MCC experiment include temperature at peak heat release rate (TPHRR), total heat release (THR) and percent char yield. In this research work, the experimental work on MCC has been restricted mainly for obtaining heat of combustion of stone wool [23] and to corroborate with the data reported in literature on combustibility values for PVC [42]. Nevertheless, the device is gaining wide acceptance in fire safety engineering community hence this has been briefly discussed.

3.5 Sample Preparation (Bench Scale Specimens)

3.5.1 Screw Extruder and Hot Pressing

Polymer compounding and extrusion is an important step in the sample preparation process before any bench scale fire testing may be performed on them. The compounding and extrusion were done mainly for PVC and EVA-ATH polymers in two different industrial labs (Nabaltec AG and Braskem) hence; a generalized schematic is shown in Fig. 4. No detailed description of the individual equipment is shown in this section. The schematic illustrates the feed charging of the polymer mixture and extruding the pellets out of it. The reader may refer to Paper III for further details in preparation of each formulation used in the study. For initiating the compounding process, additives for desired polymer formulation were gathered in respective proportion for mixing along with the pellets of neat polymers. This was

followed by transferring the mixture to single screw extruder hopper to extrude small pellets of the formulation. In some cases, the heated mixing chamber, also called as kneader and that one was used for pre-mixing the various polymer additives before charging to screw extruder. The last step is the hot pressing of the pelletized material under pressurized conditions, by applying hydraulic force equivalent to approximately twenty tons. The result is a plastic sheet of defined thickness.

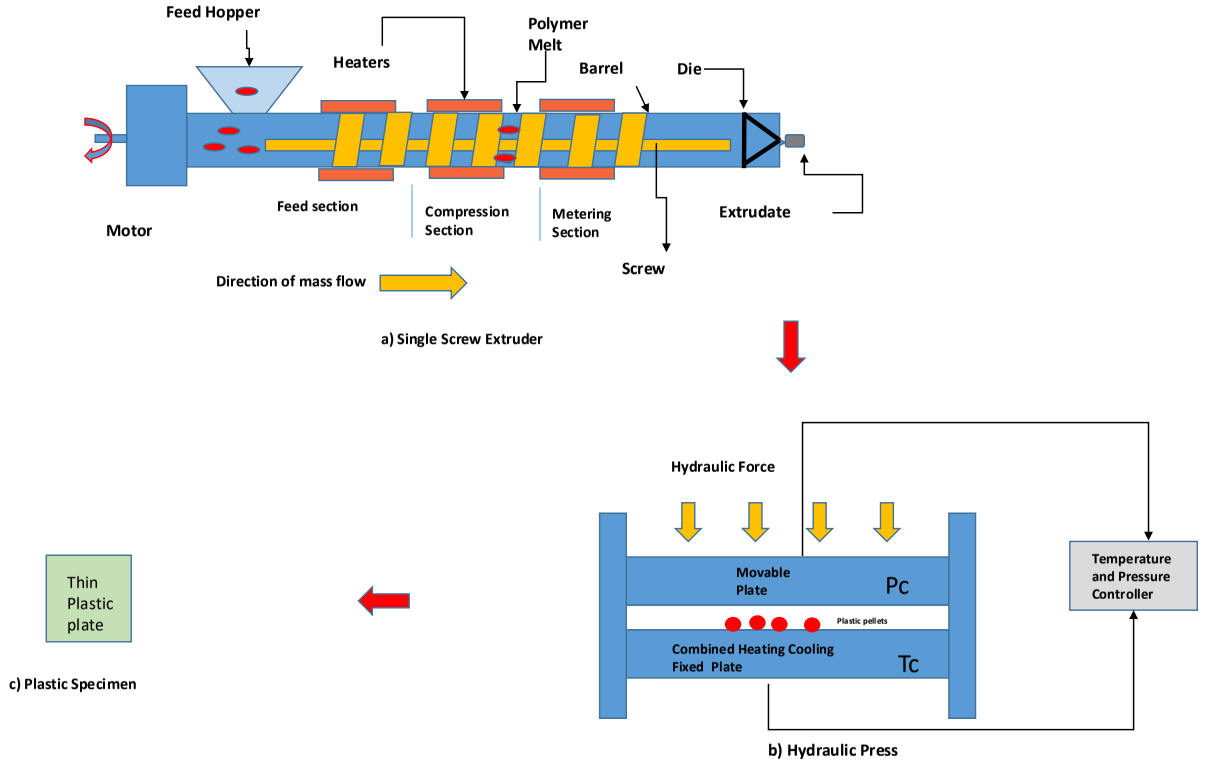

Fig. 4 Schematic illustrating the screw extrusion and hot-pressing process for preparation of plastic specimens for testing in cone calorimeter a) Single screw extruder, b) Hydraulic press, c) Plastic specimen

3.6 Bench Scale Fire Testing Equipment

3.6.1 Cone Calorimeter

The Cone calorimeter is widely used as a bench scale test equipment for measuring reaction to fire characteristics. The working principle of the device is based on oxygen consumption calorimetry. The device has been adopted by the International Organization for Standardization (ISO 5660-1) [13] for measuring heat release and smoke emission characteristics of a specimen. The main components of the device include a conical radiant heater, specimen holder, load cell, exhaust hood, oxygen concentration analyser. The specimen is usually cut into square shapes of size 10 cm x 10 cm for testing. It is placed on the edge frame backed by the aluminium foil and ceramic wool to avoid heat losses from the backside. The whole assembly is put on the load cell and irradiated with the cone heater at a predefined heat flux level. A schematic of cone calorimeter set up and sample preparation method is shown in Fig. 5 and Fig. 6 respectively. When the sample is irradiated the material shows emission of volatile gases and later appearance of a flame when the spark igniter ignites the volatiles. The gas mixture generated upon irradiating the sample are extracted by the hood for the measurement of oxygen concentration, smoke obscuration (via laser extinction) and quantification of heat release (HRR, THR) and smoke emission (TSP, RSR) characteristics. The device provides various possibilities of testing specimens of different thicknesses, configurations (vertical and horizontal) under varying incident heat flux conditions.

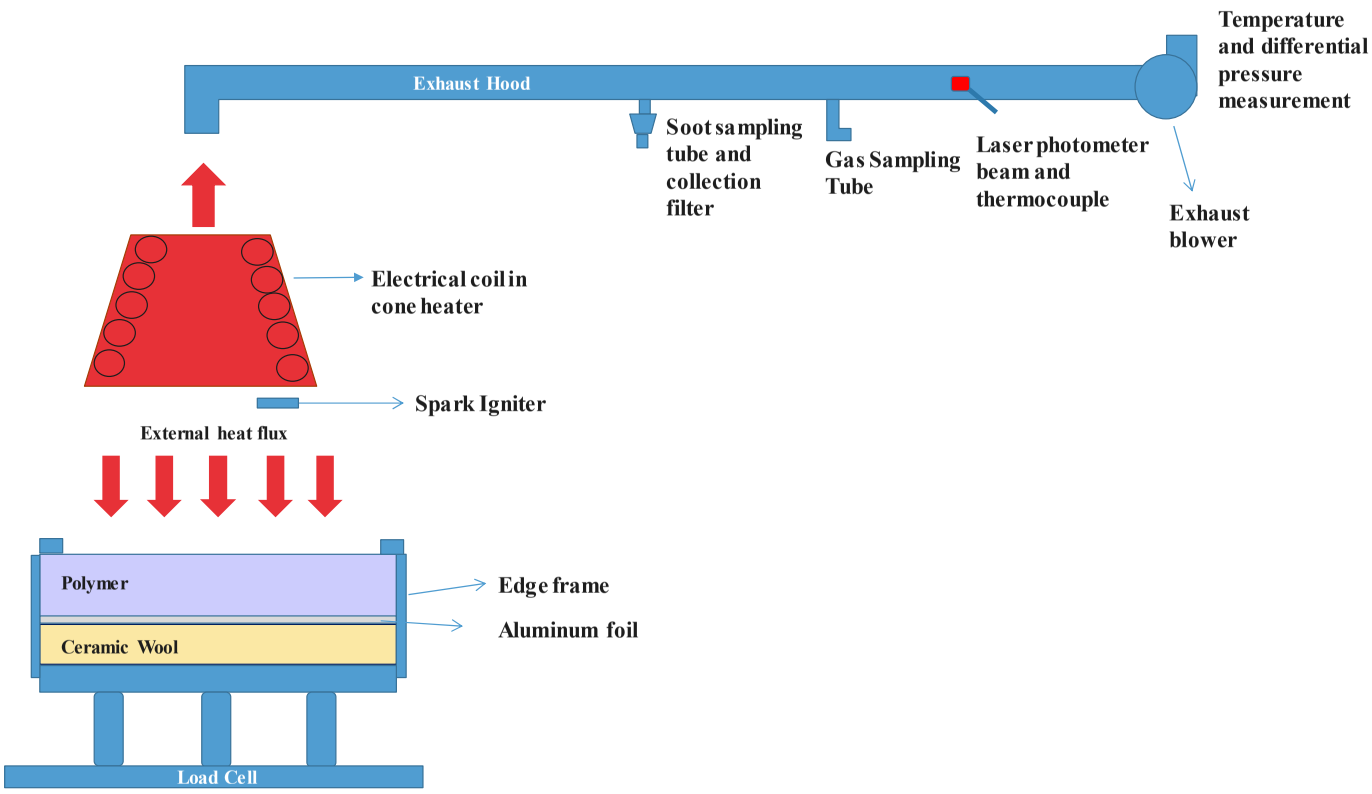

Fig. 5 Schematic of a cone calorimeter set up

Fig. 6 Polymer specimens prepared to be tested in cone calorimeter experiment

4 Numerical Modelling

4.1 Overview

In this chapter, a modified computational pyrolysis model developed for solid phase is presented. This chapter aims to provide the reader an overview of all the mathematical models used in this PhD work in a systematic and concise manner. The overall modelling and simulation work is aimed at developing the capability of simulating the pyrolysis and combustion phenomenon in charring and non-charring polymers. The approach followed here is a combination of deterministic and stochastic in nature. The deterministic aspects of modelling work comprise of forward solution of governing equations when input values are fed to the model. While the stochastic part of the model come into play when some of the key input parameters required to resolve the solution of governing equations are estimated by means of probabilistic approaches and parameter search algorithms (in this case chemical kinetic parameters).

The nature of a fire model is thermo-chemical in its character because it combines transient heat transfer equation and other sub-models (including chemical reaction, gas diffusion and in-depth radiation absorption) to describe the material transformation during fire. The key features of the developed model is illustrated by its capability of incorporating multiple chemical reactions and using temperature dependent physical and chemical properties as input values. One-dimensional version of the model is implemented via heat transfer problem analogous to the testing condition in a cone calorimeter.

The overall foundation of this chapter is largely sourced from the individual theoretical concepts presented in each paper; I [43], II [44], III [42] and IV [45] listed in the beginning of the document. For a detailed account of individual models shown in each publication, respective papers may also be referred.

Models covered under individual publications:

- **Paper I** presents detailed kinetic analysis on two different polymers (neat PVC and PMMA) using model free and model fitting methods.
- **Paper II** presents kinetic and sensitivity analysis of kinetic parameters estimated for multi-reaction chemical kinetic model. The concept is

extended to several materials (including Paper (used in common gypsum plasterboard), EVA-ATH, PVC, and Fabric).

- **Paper III** presents the implementation of a microscale chemical kinetic model in bench scale model for prediction of fire behaviour of materials corresponding to tests performed in cone calorimeters.
- **Paper IV** presents the DAEM model in its model free form and shows the effects of varying gas atmospheres and heating rates on the rate of thermal decomposition profiles of PVC samples.

The vital link from microscale studies to bench scale material flammability experiments performed typically in standard cone calorimeters is shown via the third paper. This is also in agreement with the aim to demonstrate the implementation of multi scalability of the problem up-to the bench scale level.

In view of that background, the next three paragraphs discuss the organization of this chapter. The first part of this chapter, (**Section 4.2.1**) focuses on Micro scale model. This part shows the derivation of equations used to retrieve chemical kinetic constants after processing of TGA data. In addition, background information about different reaction models existing in literature is shown in brief.

Section 4.2.2 is related to model fitting approaches (distributed reactivity models) to deal with the complexities involved in multiple reactions. The discussion shows procedures to extract chemical kinetic properties when the polymers display complex thermal decomposition profiles recorded in microscale devices. In this section, special emphasis is laid out on DAEM model, its solution methodology and corresponding sensitivity analysis.

Section 4.3 deals with bench scale modelling of pyrolysis phenomenon using one-dimensional heat transfer processes for computation of fire properties. In particular, implementation of a sub-grid chemical reaction DAEM model is shown for calculating key fire properties of interest.

Section 4.4 discusses about the temperature dependency of input data used in simulations such as thermal conductivity (k_s), specific heat (c_p).

Section 4.5 shows solution and computational workflow for bench scale model in form of a flowchart.

4.2 Microscale Model

4.2.1 Kinetic Analysis (Model Free - Iso-conversional methods)

Typically, the iso-conversional model free approach is a method to determine the kinetic parameters of the rate equation describing the thermal decomposition reaction. Experimentally, the rate is determined via a set of laboratory tests performed in a simultaneous thermal analyser (STA). For modelling purpose, the equation governing the rate of thermal decomposition reaction is solved numerically. Mathematically, the rate equation is expressed as shown in Eq 1. This equation is termed as Arrhenius equation, which was initially proposed by Swedish scientist, Svante Arrhenius in the year 1889.

$$\frac{d\alpha}{dt} = Aexp\left(\frac{-E}{RT}\right) f(\alpha) \quad [1]$$

where,

α = Normalized conversion (by weight change) [-]

t = Time [s]

A = Pre-exponential factor [1/s]

E = Activation energy [J/mol]

$f(\alpha)$ = Reaction model (conversion dependent)

T = Temperature [K]

R = Real gas constant 8.314 J/[K.mol]

In the above equation, α[-] is designated as a dependent variable, while, time t is an independent variable.

For a test performed in a STA, the normalized conversion is expressed as:

$$\alpha(T) = \frac{m_0 - m_T}{m_0 - m_f} \quad [2]$$

In STA, the instantaneous conversion at temperature *T* is given by equation 2. In this equation, the conversion, $\alpha(T)$ is normalized with respect to weight change. The ratio represents change in sample mass at any instant during the experiment to the final mass change when the test ends. Masses are denoted by m, the subscripts denote their values depending upon the when it was

measured. m_0 is the initial mass, m_f is the final mass and m_T is the mass at temperature T in a dynamic experiment with a linear heating rate. In the STA, as the temperature increases the sample decomposes and converts itself from virgin material to residue. Correspondingly, the conversion value varies between ($\alpha = 0$) to ($\alpha = 1$).

In equation 1, the entities parameterizing the Arrhenius equation are called as kinetic triplets ($E, A\ and\ f(\alpha)$). The activation energy E, is the minimum energy required that must be met for overcoming the potential energy barrier to propel the reaction forward and convert the reactants into products. While the pre-exponential factor A, refers to the frequency, at which the molecules collide effectively for allowing the conversion of reactants to products to happen. The reaction model $f(\alpha)$ is an analytical function of conversion. The most commonly used reaction model is first order $f(\alpha) = (1 - \alpha)$. A large number of reaction models sourced from the literature are shown in Table 3. Many literature sources also consider the order of the reaction (n) as the third kinetic triplet instead of using a generalized reaction model $[f(\alpha)]$. In this work a generalized treatment to the third kinetic triplet is undertaken via the use of reaction models $[f(\alpha)]$ rather than the order of the reaction.

Table 3 Kinetic Models used in solid state kinetics (reproduced from [46] and [47,48])

	Reaction model	Code	Model Type	f(α)	g(α)*
1	Power law	P4	Accelerating	$4\alpha^{3/4}$	$\alpha^{1/4}$
2	Power law	P3	Accelerating	$3\alpha^{2/3}$	$\alpha^{1/3}$
3	Power law	P2	Accelerating	$2\alpha^{1/2}$	$\alpha^{1/2}$
4	Power law	P2/3	Accelerating	$2/3\alpha^{-1/2}$	$\alpha^{3/2}$
5	One-dimensional diffusion	D1	Accelerating	$1/2\alpha^{-1}$	α^{2}
6	Mampel (first order)	F1	Deaccelerating	$1-\alpha$	$-\ln(1-\alpha)$
7	Avrami–Erofeev	A4	Sigmoidal	$4(1-\alpha)[-\ln(1-\alpha)]^{3/4}$	$[-\ln(1-\alpha)]^{1/4}$
8	Avrami–Erofeev	A3	Sigmoidal	$3(1-\alpha)[-\ln(1-\alpha)]^{2/3}$	$[-\ln(1-\alpha)]^{1/3}$
9	Avrami–Erofeev	A2	Sigmoidal	$2(1-\alpha)[-\ln(1-\alpha)]^{1/2}$	$[-\ln(1-\alpha)]^{1/2}$
10	Three-dimensional diffusion	D3	Diffusion	$3/2(1-\alpha)^{2/3}\left[1-(1-\alpha)^{1/3}\right]^{-1}$	$\left[1-(1-\alpha)^{1/3}\right]^{2}$
11	Contracting sphere	R3	Contracting volume	$3(1-\alpha)^{2/3}$	$1-(1-\alpha)^{1/3}$
12	Contracting cylinder	R2	Contracting area	$2(1-\alpha)^{1/2}$	$1-(1-\alpha)^{1/2}$
13	Two-dimensional diffusion	D2	Diffusion	$[-\ln(1-\alpha)]^{-1}$	$(1-\alpha)\ln(1-\alpha)+\alpha$

***g(α)* represents the integrated form of f(α);** $g(\alpha)=\int_0^{\alpha}\frac{d\alpha}{f(\alpha)}=A\int_0^{t}\exp\left(\frac{-E}{RT}\right)dt=\frac{A}{\beta}\int_{T_0}^{T}\exp\left(\frac{-E}{RT}\right)dT$ **; For details refer to Eq. 1.15 Ref.**[46] **and text following Eq. 4**

From a large number of reaction models available in literature (Table 3), which may be used to describe the rate equation, most of them may be divided into three categories: accelerating types, deaccelerating type and sigmoidal types. These types indicate towards the profile of mass loss curve in a STA device experienced by the sample. The accelerating type show quick rise of the conversion level in exponential manner, while the deaccelerating types show sluggish rise, and the sigmoidal types show initially quick rise but then slow down and exhibit a S type curve. For details detailed discussion by Vyazovkin [46] may be referred.

The rate is obtained via solution of ordinary differential equation (ODE) Eq 1. The solution is dependent on the thermal stimulation (i.e. temperature change) with time and the values parameterising the ODE. This is achieved in a two-step process. In the first step iso-conversional data analysis is performed to determine kinetic parameters. While in the second step the rate equation is simulated, using the parameters obtained in the first step using a suitable numerical method (e.g. 4^{th} order runge kutta method)

To put things in perspective of above shown model in relation with the STA which is used to obtain weight loss data while the sample is being heated. Consider a test sample material of measured weight undergoing thermal decomposition reaction at a given heating rate. The rate of change of sample weight as the temperature increases may be correlated to what happens inside the crucible of STA where the sample is placed. The applied heating rate to the test sample may be represented by equation 3.

Where T is a linear function of time and is expressed as:

$$T(t) = T_0 + \beta\, t \qquad [3]$$

Here,

T_0 – Initial temperature [K]

β - Heating rate [K/s]

t – Time [s]

The derivative of Eq. 3 may be expressed as Eq. 4

$$\beta = \frac{dT}{dt} \qquad [4]$$

For a constant heating rate, β (K/s) the rate equation 1 transforms itself itself into:

$$\beta \frac{d\alpha}{dT} = Aexp\left(\frac{-E}{RT}\right) f(\alpha) \quad [5]$$

After re-arrangement the following relation is obtained, which may be integrated on both sides to resolve conversion dependency on temperature (α vs T plot).

$$\int_0^{\alpha} \frac{d\alpha}{f(\alpha)} = \frac{A}{\beta} \int_{T_0}^{T} \exp\left(\frac{-E}{RT}\right) dT$$

Overall, the rate expression provides heat source term as input value for the energy conservation model and aids in computation of mass loss rate (MLR) experienced by the specimen upon exposure to heat. Further details of relevant governing equations linking the rate equations to the material level simulations are covered under subsequent section 4.3 (under bench scale model).

The way forward for determining kinetic parameters using iso-conversional approaches is based on conducting at least three TGA tests at different heating rates allowing determination of temperatures at fixed levels of conversions at each heating rate. The main steps and the key equations used for extraction of kinetic parameters are shown in Fig. 7.

The main assumption of the iso-conversional principle states that the reaction rate at constant extent of conversion is only a function of temperature. This is demonstrated by taking the logarithmic derivative of the reaction rate equation. 1, which yields the following relation:

$$\left[\frac{\partial \ln(\frac{d\alpha}{dt})}{\partial T^{-1}}\right]_{\alpha} = \left[\frac{\partial \ln(A(T))}{\partial T^{-1}}\right]_{\alpha} + \left[\frac{\partial \ln(f(\alpha)}{\partial T^{-1}}\right]_{\alpha}$$

Here the subscript α indicates iso-conversional values i.e. values related to same extent of conversion. The second term on the right hand side (RHS) disappears (being zero) since α is constant, hence $f(\alpha)$ is also constant and its derivative with respect to temperature has a null value. Thus the above expression transforms itself into the following expression:

$$\left[\frac{\partial \ln(\frac{d\alpha}{dt})}{\partial T^{-1}}\right]_{\alpha} = -\frac{E_{\alpha}}{R}$$

Hence it can be said that the temperature dependency of iso-conversional rate can be used to evaluate iso-conversional values of the activation energy, E_{α} without

assuming any form of the reaction model. Hence for this reason isoconversional methods are frequently called as 'model free methods'. Vyazovkin and co-workers [46] have suggested that as a part of any kinetic modelling study it is advisable to perform basic fitting using iso-conversional methods. In this analysis the three most commonly practiced iso-conversional methods, Friedman and Kissinger-Akhaira-Sunose (KAS), along with Kissinger method, are applied to calculate the activation energies for the pyrolysis of polymers. The corresponding equations for these methods are summarized in Table 4. The detailed discussion of these methods can be found in the cited references and in the first publication of the enclosed articles [43,45].

Table 4 Model equations for iso-conversional methods and the Kissinger method

S. No	Method	Equation	References
1	Friedman	$\ln\left[\beta_i \left(\frac{d\alpha}{dT}\right)_{\alpha,i}\right] = \ln(Af(\alpha)) - \left(\frac{E_\alpha}{RT_{\alpha,i}}\right)$	[49]
2	Kissinger-Akhaira-Sunose (KAS)	$\ln\left(\frac{\beta_i}{T_{\alpha,i}^2}\right) = \ln\left(\frac{AR}{g(\alpha)E_\alpha}\right) - \left(\frac{E_\alpha}{RT_\alpha}\right)$	[50]
3	Kissinger	$\ln\left(\frac{\beta_i}{T_{max,i}^2}\right) = \ln\left(-\frac{AR}{E_\alpha} f'(\alpha_{max})\right) - \left(\frac{E}{RT_{max,i}}\right)$	[51]

In all these methods activation energies are calculated by the analysis of multiple conversion curves measured at different heating rates at same level of conversions (α) assuming first order reaction model where $f(\alpha) = (1-\alpha)$ and $g(\alpha) = -\ln(1-\alpha)$. The reason for such an assumption stems from the fact that for most fire simulations, the reaction model is assumed to follow a single first order reaction. The main steps to retrieve activation energy and pre-exponential factor is illustrated by means of Fig. 7.

a) **Step 1 – Plotting of conversion curves (from STA test data) and extraction of temperatures at same conversion levels**

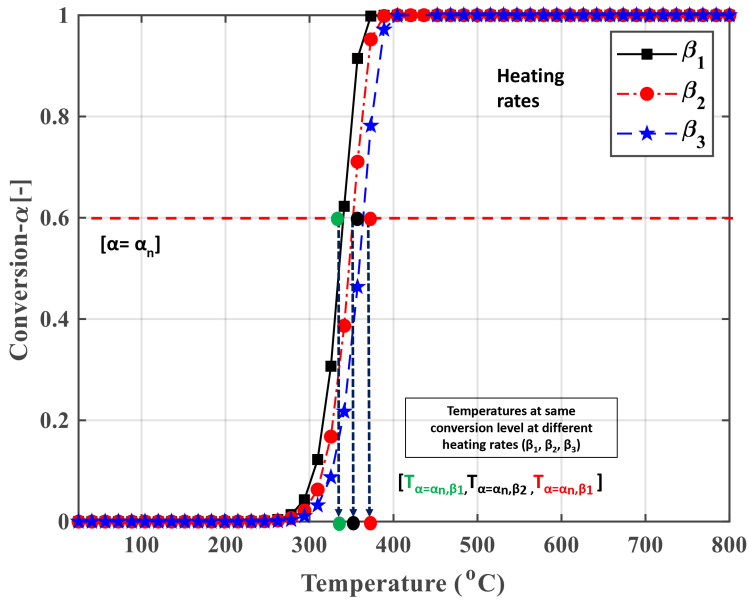

b) **Step 2- Extraction of Activation energy for each conversion level (α)**

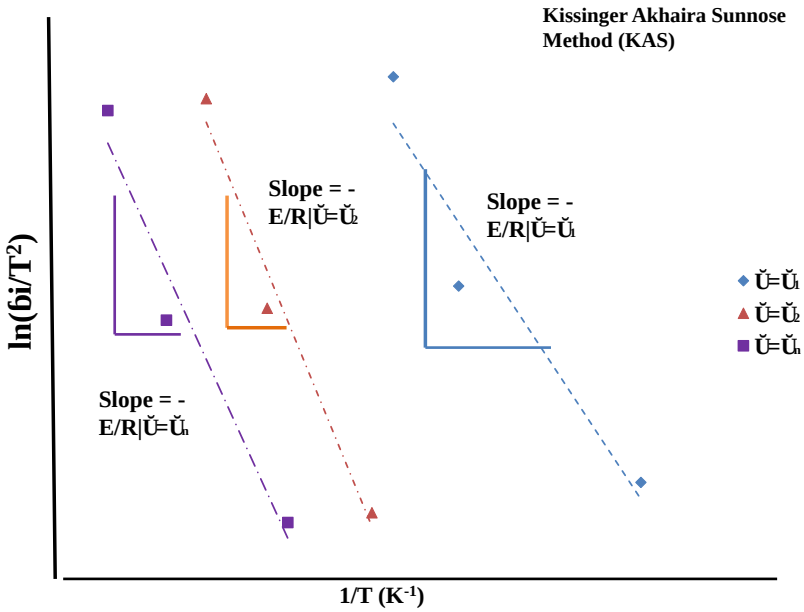

c) Step 3 – Plotting conversion dependent activation energy

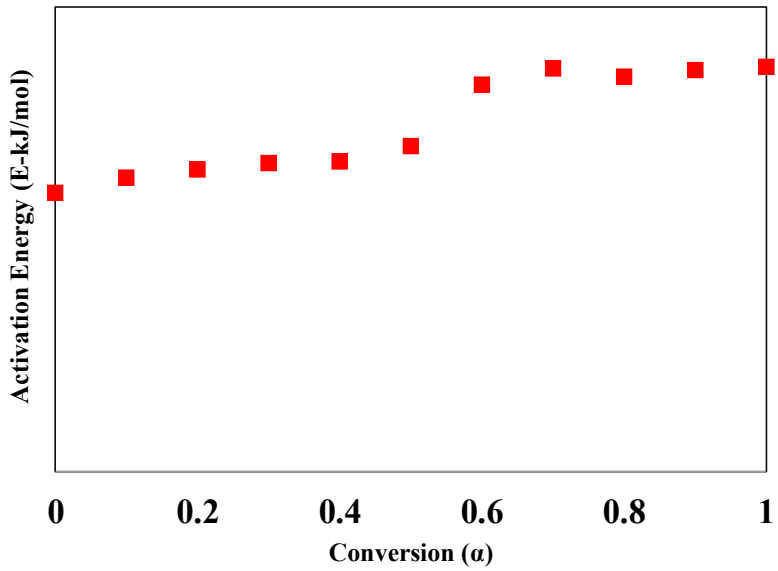

Fig. 7 Schematic diagram showing step by step extraction of kinetic parameters (E *and* A) using Iso-conversional-Kissinger Akhaira Sunnose Method (KAS).

The first part of the figure, Fig. 7 (a) shows plotting conversion curves at three different heating rates and extracting temperatures corresponding to same conversion levels. This is followed by plots of left hand side (LHS) of model equations shown in Table 4 against *1/T* for each conversion level. This allows obtaining linear fits (via regression analysis) as shown in Fig. 7 b. From the slope of each straight line, activation energy is determined and its conversion dependency may also be plotted as shown in Fig. 7(c). In case of KAS plots activation energy may be determined from the relation:

$$Slope_{\alpha} = -\frac{E_{\alpha}}{R}$$

This procedure may be repeated to calculate pre-exponential factor values from the intercept of each straight line and comparing with the first term on the RHS of the chosen model shown in Table 4. As an example, in KAS model at a certain conversion level, intercept is equated to first term on the RHS in which the only un-known is A.

$$Intercept_{\alpha} = \ln(\frac{AR}{g(\alpha)E_{\alpha}})$$

Once the values of activation energy and pre-exponential factor are obtained, equation 4 may be solved using 4th order Runge Kutta method to calculate the

conversion dependency on temperature and $\frac{d\alpha}{dt}$ curve may be simulated for desired heating rate.

The dependency of activation energy is important in detecting and treating multi-step kinetics. A significant variation in the plot of E_α vs α denotes that the process is kinetically complex and one cannot apply single step rate equation to describe throughout the whole range of experimental conversion and temperature [46]. This situation leads to involving multi-step reaction kinetics and model fitting methods to model reaction rate data. The next section is devoted such to multi-step model fitting methods using distributed activation energy model.

4.2.2 Kinetic Analysis (Model Fitting-Distributed Activation Energy Model -DAEM)

Unlike, the iso-conversional methods, the Distributed Activation Energy Model (DAEM) falls under the model fitting methods and is capable of description of complex kinetics in material undergoing thermal decomposition in multiple overlapping steps. In this model, each reaction step is assumed to consist of infinite number of simultaneously occurring parallel reactions having different activation energies (E) and pre-exponential factors (A). These different activation energies are assumed to follow a probability distribution function (PDF) denoted by the f(E) curve as shown in the following text. In this study, the distribution function of the activation energy has been modelled by a Gaussian function due to its symmetrical nature of its curve. However other distribution functions (such as logistic, gamma, log-normal etc.) can also be applied (see Bhargava et al. [42]).

The symmetrical nature of the bell shaped PDF whose mean is centred at its peak value ensures adequate complexity is taken into account in the model without adding further computational barriers due to the presence of double integrals in the governing equations.

DAEM uses the thermal decomposition data obtained in a dynamic TG experiment to retrieve the chemical kinetic parameters using an optimization technique. For non-isothermal TGA runs, where temperature is a linear function of time, and conversion is obtained by (Eq. 1). The temperature function is modelled as equation [3].

Equation 6 shows the change in amount of volatiles represented in the terms of the DAEM model.

$$\alpha(T) = \int_0^\infty \{1 - \varphi(E,T)\}\, f(E)\, dE \qquad \textbf{[6]}$$

In equation 7, $\varphi(E,T)$ is the term representing the temperature integral.

$$\varphi(E,T) = exp\left(\frac{-A}{\beta}\int_0^T e^{-E/RT}\, dT\right) \quad \textbf{[7]}$$

In equation 8, $f(E)$ is the probability distribution function of the activation energies having the conversion at temperature $T(K)$.

$$f(E) = \frac{1}{\sigma\sqrt{2\pi}} exp\left[-\frac{(E-E_0)^2}{2\sigma^2}\right] \quad \textbf{[8]}$$

The derivative form of equation 6 can be written as shown in equation (9)

$$\frac{d\alpha(T)}{dT} = \frac{1}{\sigma\sqrt{2\pi}}\int_0^\infty \frac{A}{\beta} exp\left[-\frac{E}{RT} - \frac{A}{\beta}\int_0^T exp(-\frac{E}{RT})\, dT - \frac{(E-E_0)^2}{2\sigma^2}\right] dE \quad \textbf{[9]}$$

Since there is no analytical solution for the inner temperature integral dT in equation 9, a large number of approximations that intend to approximate the values of temperature integral have been discussed in the literature [52–55]. Nevertheless, numerical integration for its evaluation is preferred. Hence, in our computations we have used adaptive quadrature method to evaluate the temperature integral. The algorithm of evaluation of DAEM is shown in the flowchart below (Fig. 8). The algorithm shows step by step working of parameter estimation process with the aim of minimizing the objective function equation 10.

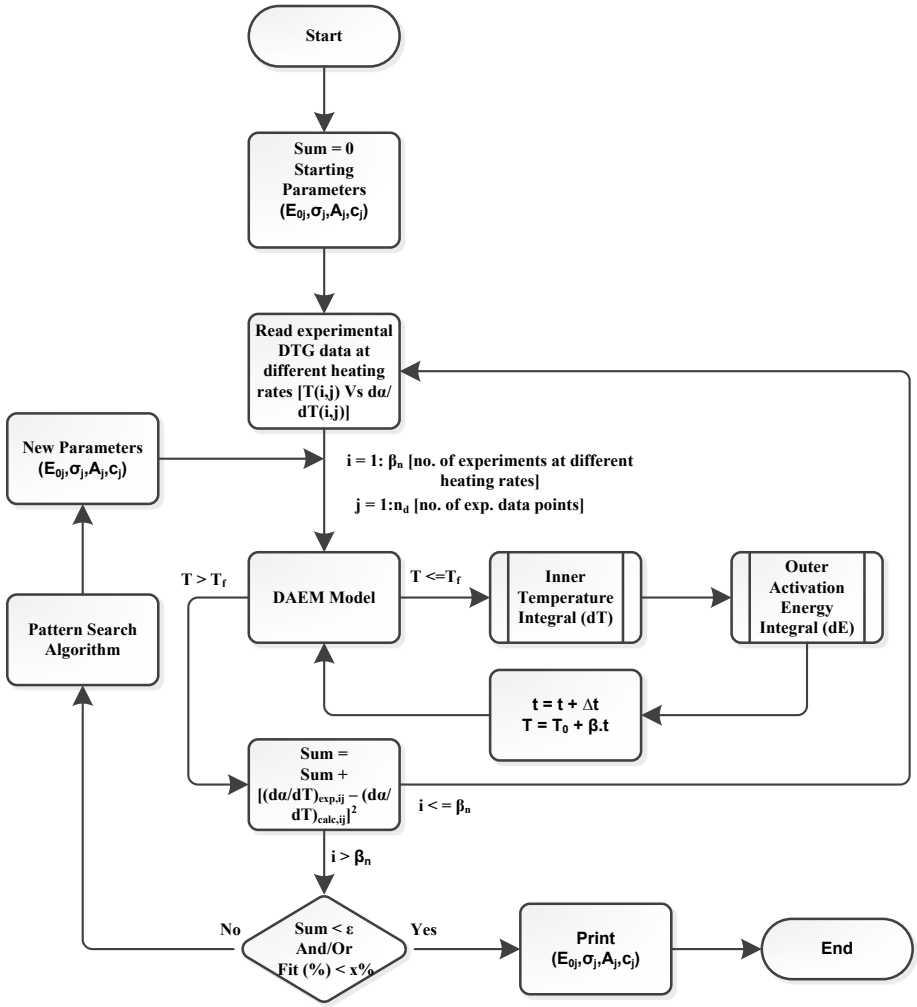

Fig. 8 Algorithm for the DAEM evaluation using a non-linear least square minimization using a set of three experiments at different heating rates showing rigorous minimization procedure

In this case, the minimization of the objective function (O.F.) (equation 10) is achieved by taking into consideration all the experimental tests performed at different heating rates. The corresponding fitness function is given by equation 11.

$$O.F. = \sum_{i=1}^{3}\sum_{j=1}^{n_d}\left[\left(\frac{d\alpha}{dT}_{exp,ij}\right) - \left(\frac{d\alpha}{dT}_{cal,ij}\right)\right]^2 \quad [10]$$

$$Fit(\%) = 100 * \frac{\left(\sqrt{\frac{O.F}{n_d}}\right)}{\sum_{j=1}^{3}\frac{d\alpha(T)}{dT}_{exp,max}} \quad [11]$$

The purpose of the O.F. is to minimize the difference between experimental and calculated values of the DTG curve using a non-linear least square method for certain chosen values of kinetic parameters. In equation (10 and 11), j is the serial number of the data point used; n_d is the total number of data points logged during the experiment. In equation (10), i =1 to 3 correspond to experiments at different heating rates (i = 1 represents 5K/min, i =2 represents 10K/min, and i =3 represents 20K/min). The term $\frac{d\alpha(T)}{dT}_{exp,ij}$ is the experimental DTG value, while $\frac{d\alpha(T)}{dT}_{cal,ij}$ is the calculated value using equation 9 for a given set of parameters of A, E_0, σ . The fitting quality as shown in equation 11 is based on a previous study by Zhang et. al. and Cai et. al. [56,57]. A lower value signifies better quality of fitting.

For complex materials decomposing in more than one reaction steps, the single Gaussian model has shown poor fitness quality. There is a significant interest in using multi-Gaussian approach to describe multiple reaction steps and to improve the comprehensiveness of the reaction model. In multi-Gaussian model, the overall $\frac{d\alpha(T)}{dT}$ curve is taken as a weighted sum of more than one individual $\frac{d\alpha(T)}{dT}$ curve. Similarly, the global f(E) curve is a weighted sum of linear combination of individual curves. Hence, equation 5 and 6 are replaced by equations 12 and 13 respectively for the multi-Gaussian fitting. The parameters representing individual weight are denoted by c_j and are also estimated for each reaction in the optimization calculation.

$$f(E) = \sum_1^n c_j f(E)_j \quad [12]$$

$$\frac{d\alpha(T)}{dT} = \sum_1^n c_j \frac{d\alpha_j}{dT} \quad [13]$$

In both equations 12 and 13 c_j physically represents the fraction of volatiles produced by the j^{th} peak and n is the number of peaks. c_j values were estimated between 0-1. For overall optimization calculations using this approach four parameters (E_0, σ, A, c_j) are optimized corresponding to each reaction step. As the number of assumed reactions, increase the number of parameters increase by four folds.

Solution Methodology and Parameter estimation using Pattern search

The solution is evaluated using a computer code based on flowchart shown in Fig. 8. The codes work in conjunction with the optimization toolbox of

MATLAB®. It invokes the pattern search algorithm with initial guess parameters (E_0, σ, A, c_j) to run the optimization process until a minimum tolerance value in the order 10^{-4} of the objective function is reached and the simulated DTG curve fits the experimental one.

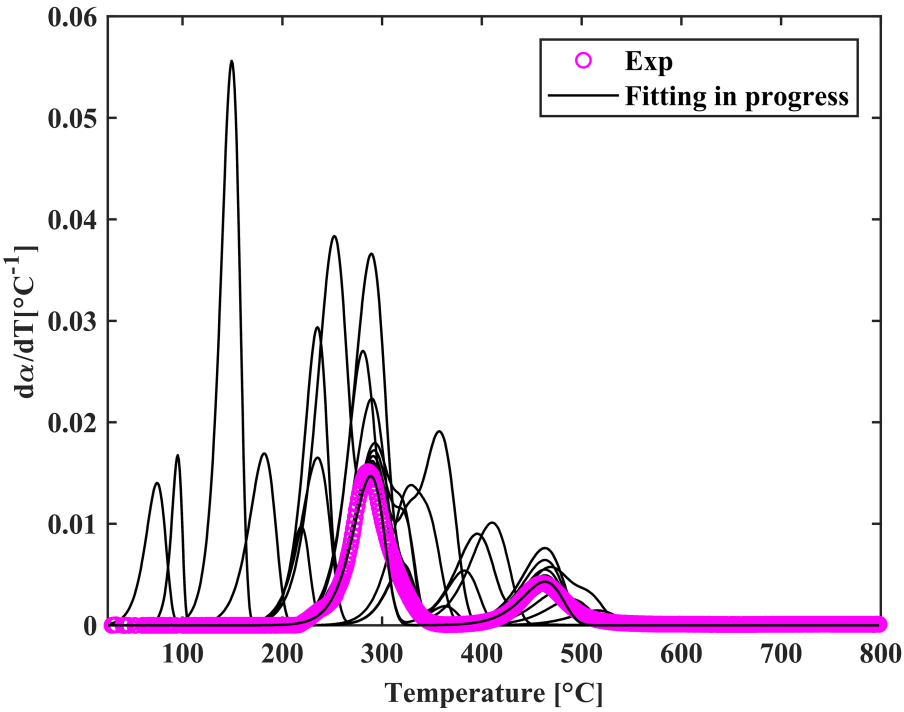

Fig. 9 Plot showing combined working of the pattern search and DAEM model fitting in progress.

In the above figure, the experimental DTG curve (in pink open circles) is the target curve, while each black curve shows a solution of DAEM model equation using unique set of kinetic parameters chosen by the pattern search algorithm as input to DAEM model. Pattern search is a derivative free direct search subroutine for minimizing the objective function (O.F.). It is considered to be better in terms of number of function evaluations as compared to other search methods such as Powell method and Simplex method [58]. However, in the last decades more studies in this domain have surfaced and researchers have evaluated several other methods for objective function minimization. Some of them are Genetic Algorithm, Levenberg Marquardt and Simulated annealing algorithm. The work done by Lautenberger et al. [25], Chaos et al. [59] are particularly significant point of reference in this domain, however these studies were more focused towards complete optimization of comprehensive pyrolysis model rather than stand alone kinetic model.

In the developed code, the arguments of the O.F. are varied until its minimum is obtained. A detailed account is available in reference [60]. In our case, the pattern search routine determines the sequence of values for variables (E_0, σ, A, c_j); while the DAEM code computes the functional values of O.F. During the parameter estimation process, successive values of variables are chosen as distinct points in the multi-dimensional space. For double Gaussian DAEM this value is 8 dimensional while for multi-Gaussian DAEM with four partial reactions, this value is 16 dimensional. The procedure for going from a given point to the next is called a move. This move is termed as a success if the value of objective function decreases; else it is a failure. The first move is exploratory in nature to gain knowledge about variations in the variables leading to a successful move. In each exploratory move only a single variable is changed in a particular direction. The exploratory moves form a vector base to pursue the search for the arguments in subsequent iterations. The second move is the pattern move, in which the knowledge gained in the exploratory moves is utilized to accomplish the actual minimization of the objective function by moving in the direction of the established pattern. The point from which the pattern move is made is called the base point, and the direct search procedure can be understood as moving from base point to base point. This procedure is repeated until the O.F. value meets the tolerance limit.

Sensitivity Analysis of DAEM Model

A sensitivity analysis allows the study of how changes in input parameters affect the model predictions. It provides a systematic way of analysing the model's performance, when one of the input parameters deviates from its optimum value. This technique has been used previously by (Cai and Rao) [61–63] to study parametric changes on their pyrolysis model outputs. In this study, the local sensitivity analysis of estimated DAEM model parameters has been done by varying each kinetic parameter, one at a time, in the range of ±20% of its optimum value at a step size of 5 percent (other parameters being held constant). A plot of the relative objective function against the relative parameter is the final outcome of sensitivity analysis. In this case the relative objective function (Eq. 14) can be defined as the ratio of the objective function value at the deviated parameter to its value calculated at the optimized parameter.

$$Relative\ O.F. = \frac{O.F._{Deviated\ Parameter}}{O.F._{Optimized\ Parameter}} \quad [14]$$

The relative parameter (Eq. 15) represents the ratio of the deviated parameter to its value at the optimized one.

$$Relative\ Parameter = \frac{Deviated\ Parameter}{Optimized\ Parameter} \quad [15]$$

Eq. 16 and Eq. 17 show the relative parameters with respect to mean activation energy and standard deviation of the j^{th} reaction peak respectively.

$$E_{0,j,relative} = \frac{E_{oj,deviated}}{E_{oj,optimized}} \quad [16]$$

$$\sigma_{j,relative} = \frac{\sigma_{j,deviated}}{\sigma_{j,optimized}} \quad [17]$$

4.3 Bench Scale Model

In this section, the main governing equations of the combined heat and chemical reaction model are illustrated for bench scale prediction of fire properties. The model is developed based on the work of Ghorbani et al.[33], Cai et al. [64] and solid phase model described in SFPE handbook [65]. It is mainly divided between equations of mass and energy conservation followed by description of initial and boundary conditions and finally computation of MLR. More conventionally, the Arrhenius model is used for describing source terms has been replaced with the above-discussed DAEM model.

4.3.1 Mass Conservation

If it is assumed that there are n number of reactions occurring in the polymer matrix during thermal decomposition, then the total rate of thermal decomposition reaction is the cumulative sum of the rate of individual sub-reactions multiplied by their assigned weights as shown in equations 18-21.

$$\frac{\partial \rho}{\partial t} = -\omega_s \quad [18]$$

$$\omega_s = A(\rho - \eta_{char}\rho_0) \int_0^\infty \exp\left(-\frac{E}{RT}\right) f(E) dE \quad [19]$$

$$f(E) = \frac{1}{\sigma\sqrt{2\pi}} exp\left[-\frac{(E-E_0)^2}{2\sigma^2}\right] \quad [20]$$

where, $\rho, \omega_s, \eta_{char}, A, E, E_0$ and σ are the density, reaction rate, char fraction, pre-exponential factor, activation energy, mean activation energy and standard deviation respectively. The total reaction rate is expressed as a weighted cumulative sum as shown in equation 21.

$$\frac{\partial \rho}{\partial t}_{Total} = \sum_{i=1}^{n} c_i \frac{\partial \rho}{\partial t}_i = \sum_{i=1}^{n} -c_i \omega_{s,i} \quad [21]$$

Here, c_i and $\omega_{s,i}$ denotes the weight and reaction rate of i^{th} individual reaction respectively. The parameters A_i, σ_i, E_{0i} and c_i are determined by optimization routine by minimization of the objective function using least sum of square (LSS) approach as shown in the previous section.

4.3.2 Energy Conservation

The second part of the model is the heat transfer model, in which the coupling is done via temperature. The main equation of the model formulation is given by equation 22, where $\rho, c_{p,}\, k_s$ and T describe the mass density, heat capacity, thermal conductivity and temperature of the solid material, x is the spatial coordinate normal to the exposed surface, $\omega_{s,Total}$ is the total mass reaction rate as described above (i.e. amount of virgin material converted to pyrolysis gas per unit time per unit volume) and $\Delta H_{r,i}$ is the heat of pyrolysis of the i^{th}reaction (i.e. heat required to generate unit mass of volatiles at temperature T). Equation 22 describes the heat conduction inside the solid and accounts for endothermic pyrolysis processes.

$$\rho c_p \frac{\partial T}{\partial t} = \frac{\partial}{\partial x}\left(k_s \frac{\partial T}{\partial x}\right) - \sum_{i=1}^{n} c_i \omega_{s,i}\, \Delta H_{r,i} \qquad [22]$$

Additional assumptions which are valid for this model are:

- In-depth generated volatiles are instantaneously transported to the surface;
- Surface regression is not captured by the model, the fuel thickness remains intact regardless of the amount of solid fuel consumption
- Volume expansion is not addressed under the current scope of the model;
- Specimens are assumed to be opaque and hence in-depth absorption of radiation is not considered under the current scope of the model;

4.3.3 Initial Conditions

The initial conditions for the model are described by the equation 23 below, which states that, before any exposure to thermal radiation, the sample temperature is that of ambient atmosphere and its density is same as that of virgin sample.

At, $t = 0$, for $0 \leq$ x $\leq$ L ; $T = T_0$; $\rho = \rho_0$ [23]

4.3.4 Boundary Conditions

The boundary conditions define the exposure and insulation on the surface and back side of the sample respectively. Equation 24 shows the insulated backside condition. While, equation 25 shows the exposed side conditions on the top surface of the polymer describing the exposure as a sum of incident heat flux from the cone, radiative heat losses and convective losses from the surface. The addition of flame heat flux is approximated until the attainment of threshold temperature value for the onset of degradation of polymer sample is reached. More conventionally, the ignition criteria is determined when the mass loss rate of the pyrolyzing gases attain the lower flammability limit until the critical mass flux value of 1g/(m^2.s) is reached also discussed by Lyon et al. [66]. Also, the above cases correspond to thermally thick solids whose Biot number (Bi= hl/k) was found to be higher than 0.1 indicating towards the existence of a temperature gradient in studied specimens.

Insulated backside:

For, t > 0, at $x = L$, $\frac{\partial T}{\partial x} = 0$ [24]

Exposed side:

For, t > 0, at x = 0,

$$\ddot{q_{w(t)}} = \varepsilon G - \varepsilon\sigma_c\left(T_s^4 - T_{amb}^4\right) - h(T_s - T_{amb}) + \ddot{q}_{fl} \quad [25]$$

In above equations, ε is the material emissivity, G the incident heat flux from the cone heater, σ_c is the Stefan-Boltzmann constant (5.67x10^{-8} W/m^2/K^4) and T_s is the surface temperature of the polymer surface, L the thickness of the material, h the convective heat transfer coefficient (W/m^2/K) and $\ddot{q_{fl}}$ is the flame heat flux (W/m^2/K).

4.3.5 Mass Loss Rate

The mass loss rate of the polymer is given by equation 26, which shows the total mass loss rate summed over the thickness of the sample at any instant. It is computed by the line integral of the total reaction rate with respect to the thickness of the sample.

Here, $m_f(t)$ is the mass loss rate per unit area of the sample.

$$m_f(t) = \int_0^L \omega_s(x,t)dx \quad [26]$$

4.4 Treatment of Thermal Properties

The model assumes the solid phase thermal conductivity (k_s[W/m/K]) and specific heat (c_p [kJ/kg/K]) to be a temperature dependent quantity. Additionally, they are assumed to be a composite function of the amount of virgin material converted into char. As the material is irradiated with the heat from the cone, the combustion reaction is triggered which leads to conversion of solid phase into intermediate and eventually char. The values of thermal conductivity, specific heat and reaction conversion (α) are co-related by equations 27-29 respectively, where k_s is the solid phase thermal conductivity given by Eq 27.

$$k_s = k_{virgin}(T)\alpha + k_{char}(1-\alpha) \quad [27]$$

c_p is the specific heat of the sample given by Eq. 28

$$c_p = c_{p,virgin}(T)\alpha + c_{p,char}(1-\alpha) \quad [28]$$

and α is the instantaneous conversion given by Eq. 29

$$\alpha = \frac{\rho_{virgin} - \rho(t)}{\rho_{virgin} - \rho_{char}} \quad [29]$$

4.5 Solution and Computational Workflow

The solution methodology is divided into two parts. In the first part, an analytical approximation to DAEM model is shown (see Paper III), while in the second part, the overall computational workflow is presented. The flowchart below shows the workflow of the model computation process. The procedure involves collection of different input parameters (chemical reaction, thermo-physical and geometrical parameters) for the material in consideration. Previously, such models have been solved with time split approach method as discussed in the introductory part of the Paper III. In this case, Comsol has been used to solve the differential equations using finite volume method (FVM), however, in this section only the sequential steps will be described in the form of a flowchart. It can be seen from Fig. 10 that in the first step reaction parameters, thermo-physical parameters and geometrical parameters are read. Thereafter the control passes to the DAEM sub-grid model followed by feeding of the calculated conversion values and the source terms to the thermo-physical property estimation module. This is followed by specification of the boundary conditions. With every increasing time step, the boundary conditions provide necessary increment in the temperature (due to irradiation from the cone and the flame heat flux) on the top side or insulation on the bottom surface of the domain. As the temperature increases in the calculation domain, the chemical reaction model is activated to provide inputs to heat transfer model and modification of thermo-physical

properties. As the conversion increases, the char and virgin material properties change depending upon the converted fraction. The chemical reaction model also provides necessary input in the form of heat generated/consumed from the source to the heat transfer model. Finally, at the end of the simulation time, the MLR is computed by integration of mass loss rates over the space domain i.e. over the thickness of the sample. The time to ignition, peak mass loss rate and time to extinction may be obtained from the MLR curve, while heat release rate curve may be obtained as a product of MLR curve and effective heat of combustion (EHC). Similarly, temperature profiles on the front and back side of the polymer sample may be computed once the heat transfer physics is resolved.

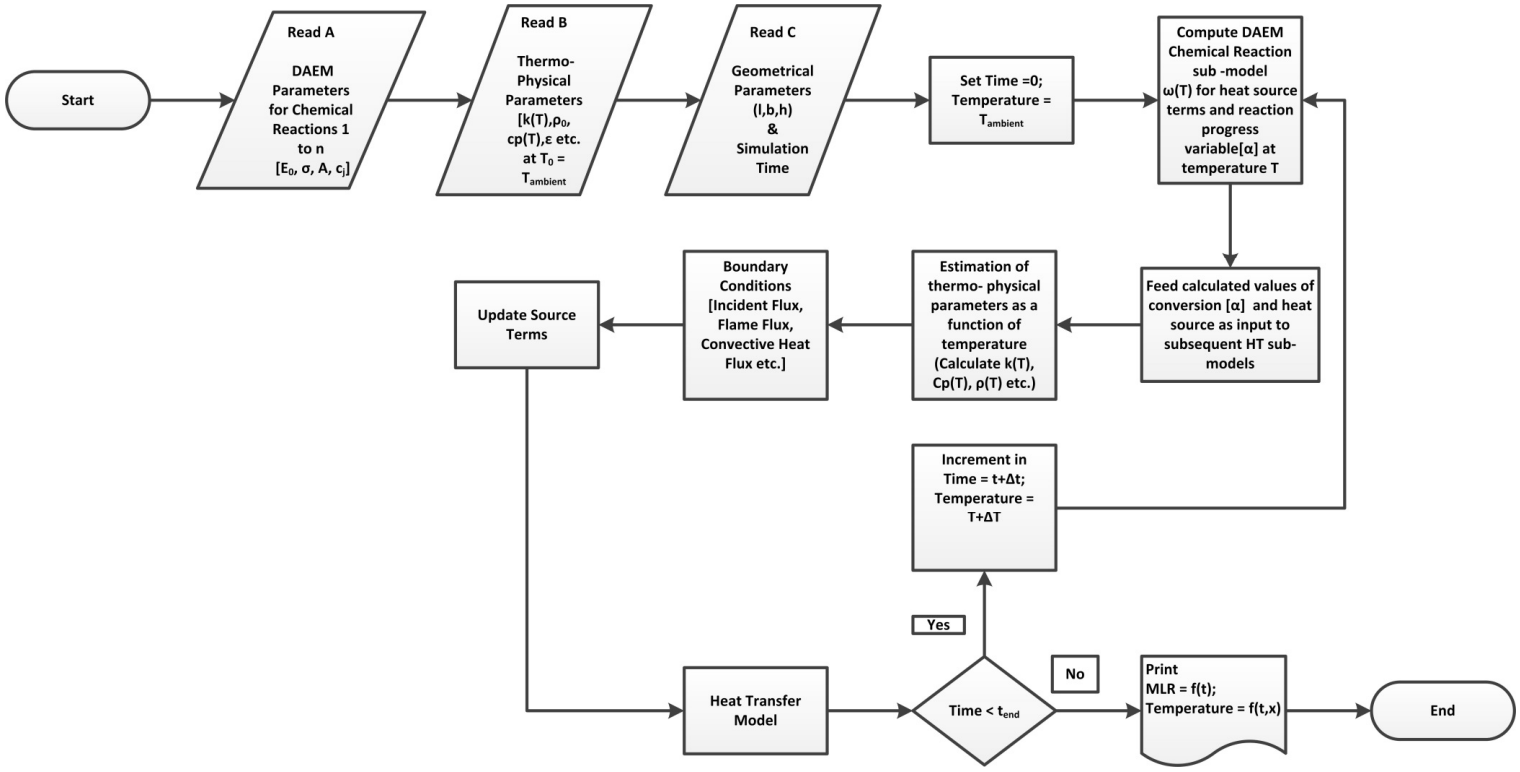

Fig. 10 Flowchart depicting combined working of heat transfer and DAEM reaction model for estimation of fire properties of charring polymers

5 Results and Analysis

An overview of the results and analysis is presented in the articles is given in this chapter. Discussions about the results is dealt separately in subsequent chapter.

Section 5.1 mainly covers the experimental results reported on pure form of PVC and PMMA samples. The sample sizes used in these set of experiments are on milligram level. The influence of varying gas atmosphere is discussed in the later section of 5.1 whose detailed reference account may be found in **Paper IV** [45]

Section 5.2 shows a detailed kinetic analysis on above set of materials. A comprehensive study on these set of neat polymers is presented in **Paper I** [37].

Section 5.3 is dedicated to modelling of complex multi-step reaction kinetics. For this task model fitting method involving DAEM is used. To demonstrate the model applicability to wide number of materials, the sample selection is expanded. The materials used in this study are pure form of PVC, PMMA (the same ones used in section 5.1), ethyl vinyl acetate (EVA), paper (used in common gypsum plasterboard) and a fabric blend of cotton and polyester.

Section 5.3.1 shows sensitivity analysis of kinetic parameters obtained. All results presented in this section are discussed in detail in **Paper II.**

Section 5.4 deals with materials, which are of industrial relevance and are significantly different than laboratory grade chemicals due to addition of several additives. The composition of such materials are used to make real materials such as cable sheathing polymers. Hence, experiments and model fittings performed on them are based on specimens received from two industrial partners in the project. All results presented in this section are discussed in detail in **Paper III** [42]**.**

5.1 Microscale Experiments (Thermogravimetric Analysis)

5.1.1 Polyvinyl chloride (PVC)

The experimental results obtained from the TG-DTG tests of PVC are shown in Fig. 11. Experiments were performed at three different heating rates in nitrogen atmosphere.

a)

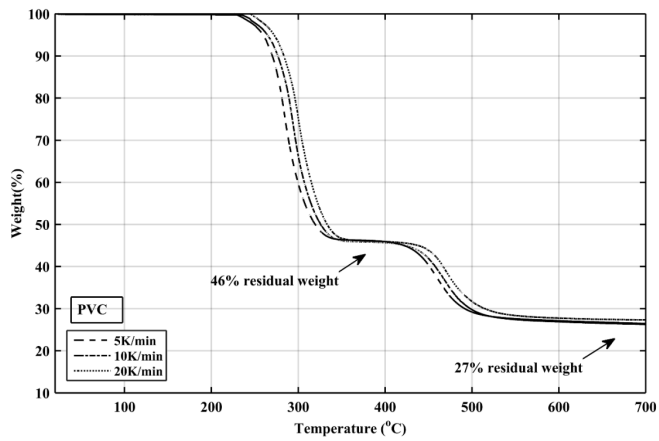

b)

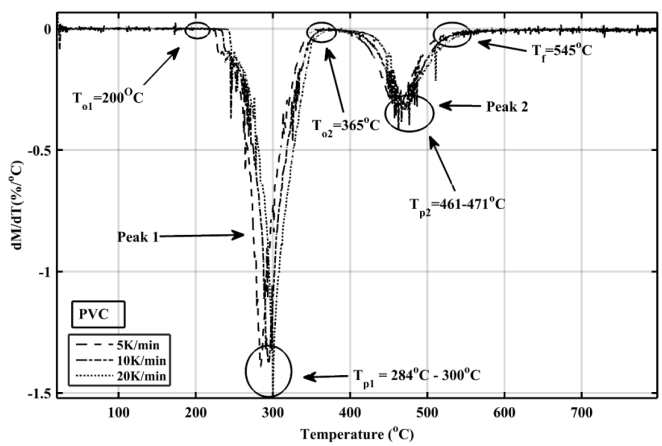

Fig. 11 Experimental TG (above) and DTG (below) curves for PVC in nitrogen at different heating rates

The TG curve Fig. 11 (a) shows that weight loss occurs in at least two stages. In the first stage the sample shows a weight loss of 54% (residual weight = 46%), while in the second stage, a further weight loss of 19% is recorded, leading to the final sample residual weight of 27%. The TG curve also shows the appearance of a small plateau between 340 to 420°C indicating a slight drop in the rate of weight loss during that temperature interval. The DTG curve Fig. 11 (b), shows that the first stage of decomposition occurs between 200 to 365 °C while the second stage of decomposition occurs in between 365 °C to 545 °C. The curves show slight sensitivity to the applied heating rate. The DTG curve peaks shift to the right as the heating rate increases. The peaks appear to fall in a very narrow temperature range of 10-15°C. It can be seen from Fig. 11 (b) that main peak temperatures *(T_{P1})* increases from 284°C to 300°C with increasing heating rate, while the minor peak (T_{P2}) is observed between 461-471°C. These results are consistent with the earlier studies performed by Miranda et al. [67]. For PVC, it is well known that during the first stage of pyrolysis, the mass loss is mainly attributed to the release of hydrogen chloride (HCl) and this phenomenon is termed as de-hydro-chlorination. Several authors mentioned that the first stage is a combination of two independent (parallel) reactions associated with head-to-head and head-to-tail linkages [67–69]. During this stage small amounts of other aromatic hydrocarbons (e.g. benzene, toluene, xylene and ethyl benzene) and condensed ring aromatics such as naphthalene, anthracene and indene are also evolved. McNiell et al. [68] have explained that most double bonds in such aromatic compounds get accumulated in the polymer to create cross linked network of cyclic compounds in the aliphatic matrix. In the second reaction step these cyclic compounds aromatize via chain scission reactions leading to further weight loss and formation of aliphatic and olefinic, aromatic hydrocarbons and char.

Table 5 Summary of DTG curves for PVC

Heating Rate	Main Peak Temperature	DTG(main peak)	Minor Peak Temperature	DTG(minor)	Residual Weight
β(K/min)	T_{P1}/ °C	$(dM/dT)_{P1}$	T_{P2}/°C	$(dM/dT)_{P2}$	Wt.%
5	284	-1.4	461	-0.3	26
10	295	-1.4	463	-0.4	26
20	300	-1.5	471	-0.3	27

In the past a number of experimental kinetic studies on the thermal decomposition of PVC have been reported by Hugget, McNiel et al. [67–72]. Many of the previous research works have shown that PVC degradation occurs

in two distinct reaction steps, however it is apparent only from the works of Miranda [67], Wu [69] and Maqueda and Criado [73,74], that DTG curves recorded for PVC have also been shown to exhibit three and four distinct peaks. As a consequence, the modelling work for those studies was performed using multiple step reactions through series and parallel kinetic models. The accuracy of these models is very good, however, a key issue in these models is to propose a reaction mechanism of the thermal degradation process.

For fire engineering work, this is a cumbersome and challenging task. In addition, the profile of the DTG curve is influenced by other factors such as the choice of gas atmosphere in which the TG experiments were performed e.g. N_2, CO_2, O_2, heating rates used and the chemical composition of the polymer. The material shows significantly different reaction profiles under ambient atmosphere due to oxidation reactions as shown by Bhargava et al. [45] (Paper IV). When the reactant gas atmosphere or chemical composition of the material is altered, a new reaction mechanism has to be proposed. This task poses a major challenge in the general implementation of this sub-model to simulate the overall pyrolysis model for HRR predictions for a cone calorimeter test. It is to be noted that for all practical applications the properties of PVC are modified by adding several additives, plasticizers and flame-retardants. The reaction mechanism originally proposed for a specific polymeric composition may not be generalized for a modified material. This problem may be mitigated by using the DAEM approach for the purpose of fire modelling due to its inherent modelling assumptions. In the DAEM model, it is assumed that each reaction step represents an infinite number of parallel occurring reactions so the parameters computed are apparent kinetic parameters but not the real ones. Also, there is no need to provide an elaborate reaction mechanism for the degrading polymer, as this may not be of specific interest for fire simulations purposes.

5.1.2 Poly-methyl methacrylate (PMMA)

The TG and DTG curves of PMMA are shown in Fig. 12

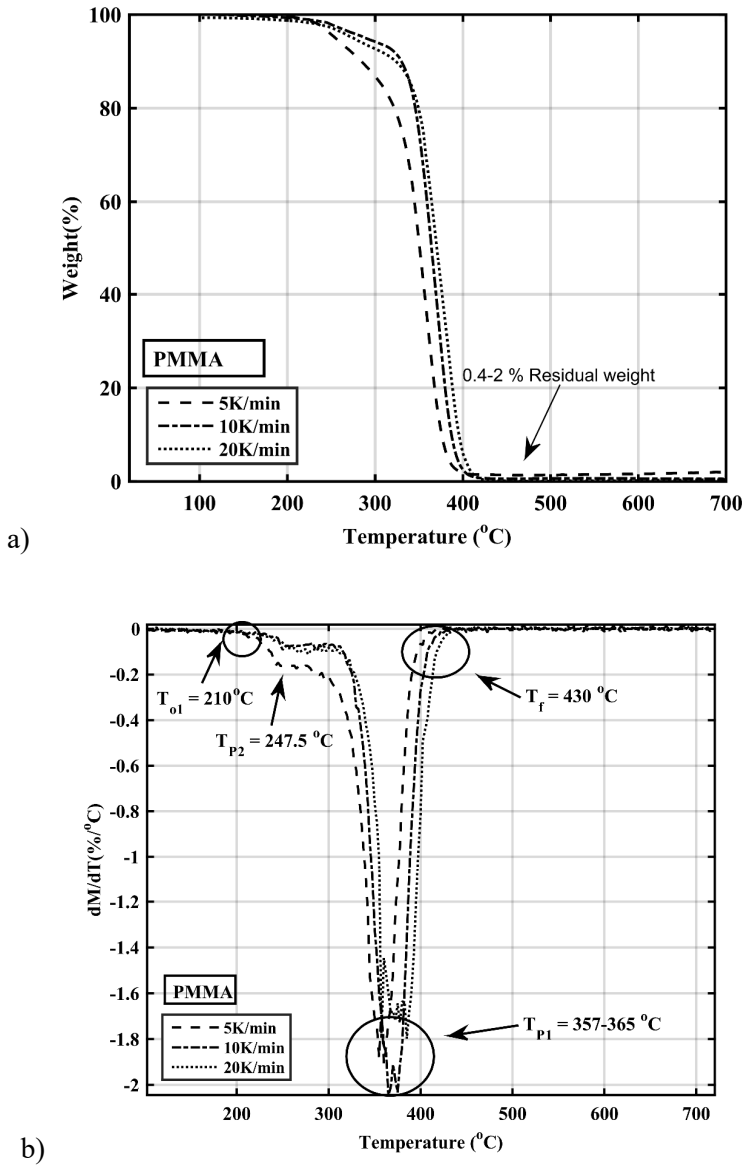

Fig. 12 Experimental TG (above) and DTG (below) curves for PMMA in nitrogen at different heating rates

The experiments were performed in nitrogen atmosphere at three different heating rates. The residual weight of the sample at the end of the reaction is negligible (0.4-2 percent). The weight loss in the PMMA sample seems to occur in one single reaction step. However, weight loss profile from one step decomposition in the above TG does not necessarily imply occurrence of one single reaction. In reality it is plausible several reactions occur in parallel which may not be identifiable via inflections in the TG curve. Manring [75] has written an account on multiplicity of several reactions in PMMA during thermal decomposition process. As shown in Fig. 12 (b) a main broad DTG peak is visible while a minor shoulder peak appears to the left of the main peak, indicating the possibility of more than one reaction occurring during the decomposition process. The onset of the degradation starts at 210°C and ends at 430°C. The main DTG peaks for different heating rates for PMMA lie in the range of 357-365°C. It can be observed from Fig. 12 that the peak temperature increases as the heating rate increases from 5 K/min to 20 K/min. Similar results were reported for PMMA by Janssens et al. [76].

Table 6 Summary of DTG curves for PMMA

Heating Rate	Main Peak Temperature	$DTG_{(main)}$	Minor Peak Temperature	$DTG_{(minor)}$	Residual weight
β(K/min)	T_{P1}/ °C	$(dM/dT)_{P1}$	T_{P2}/°C	$(dM/dT)_{P2}$	Wt.%
5	360	-1.9	247	-0.2	2.0
10	364	-2.0	252	-0.1	0.6
20	365	-1.8	262	-0.1	0.4

A great deal of previous research into PMMA has been focused on the understanding of thermal degradation mechanisms. According to Troitzsch [4], the thermal decomposition of PMMA follows at least two and sometimes three stages by means of reactions occurring at the chain ends and random scission process producing only monomers. It was first shown by Kashiwagi [77] and later by Manring [75] that a radically polymerized sample degrades in three stages. The multi-reaction theory was and later adopted by Ferriol [78] for the modelling work. Ferriol [78] have discussed the detailed account of the reaction mechanisms proposed by Kashiwagi and Manring [77,79] and implemented that approach into the estimation of reaction model by using non-linear fitting algorithm.

5.2 Kinetic Analysis (Model Free –Iso-conversional method)

The test data obtained in TGA experiments was shown in section 5.1 It is used to perform kinetic analysis in accordance with the theory presented in section 4.2.1 on iso-conversional methods. As an end result, in Fig. 13 is shown, E vs α curve. The conversion dependent activation energy is the resultant plot derived from the individual linear fits of corresponding model shown via model equations of Friedman and Kissinger Akhaira Sunose. It can be seen from Fig. 13 the spread of activation energy for both polymers (PVC and PMMA) as calculated by either of the isoconversional methods (Freidman and KAS) follow a similar trend.

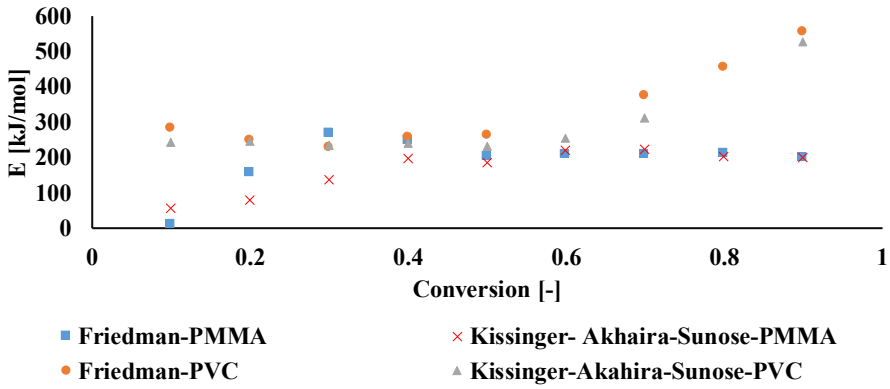

Fig. 13 Spread of activation energy computed using isoconversional methods for PMMA and PVC

For PVC the values of activation energy E were found to vary in the range of 235 - 284 kJ/mol in the conversion range of ($\alpha = 0\ to\ 0.6$) and later it was found to increase from 240 to 550 kJ/mol in the range of ($\alpha = 0.6\ to\ 0.9$) . While, for PMMA activation energy E was found to increase from 50 kJ/mol to 197 kJ/mol in the conversion range of ($\alpha = 0\ to\ 0.4$) , later it was found to follow a constant value at 200 kJ/mol (α = 0.6 - 1). Since the values of the activation energies are spread over the conversion range, it indicates multiplicity in the reaction mechanism of both the materials. The extent of it greater in PVC than in PMMA.

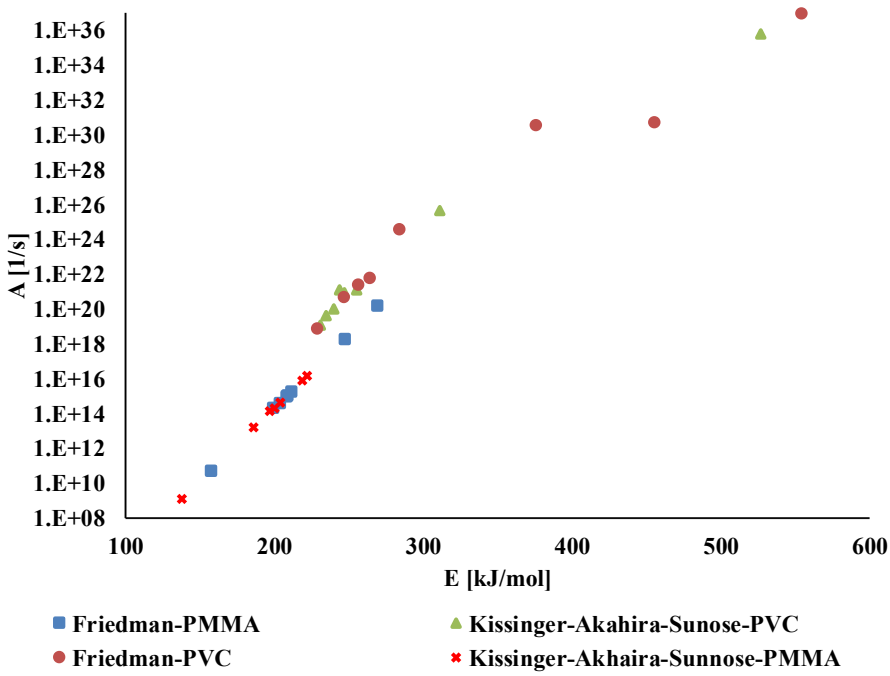

Fig. 14 Spread of pre-exponential factor computed using isoconversional methods for PMMA and PVC

The comparison of the pre-exponential factor A with respect to the activation energy is shown in Fig. 14. The spread of values for A was found to be nearly same by the two methods for each polymer. The wide variation in the values of activation energy and appearance of shoulders in DTG curves indicate that the reaction rate curve is not dominated by a single step reaction and cannot be described by a single step model. The best fit among all the methods discussed was obtained by Kissinger method as shown below in Fig. 15. It can be seen that only the main peak of the curves can be approximated to a large extent however, peak shoulders are not reproducible.

a)

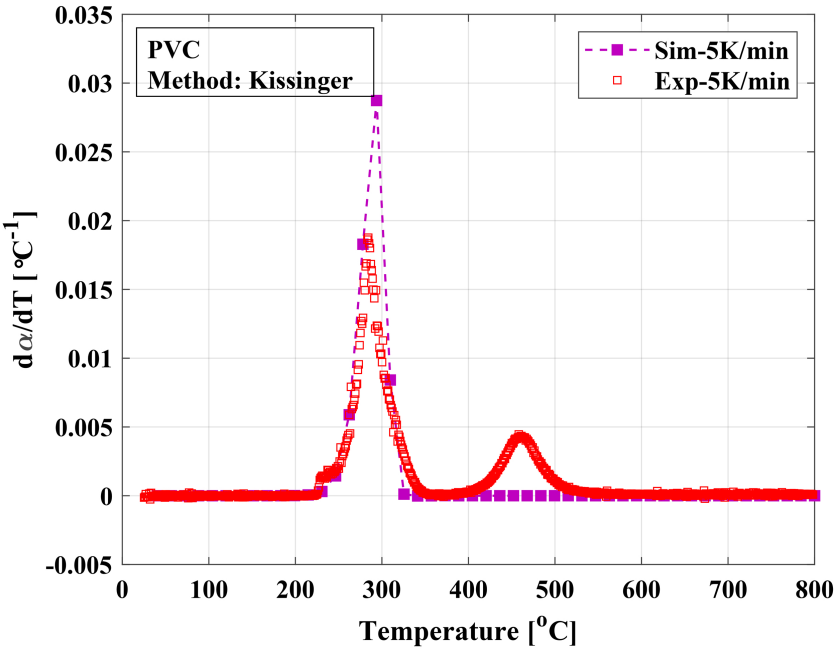
PVC
Method: Kissinger
Sim-5K/min
Exp-5K/min
dα/dT [°C-1]
Temperature [°C]
0.035
0.03
0.025
0.02
0.015
0.01
0.005
0
-0.005
0
100
200
300
400
500
600
700
800

b)

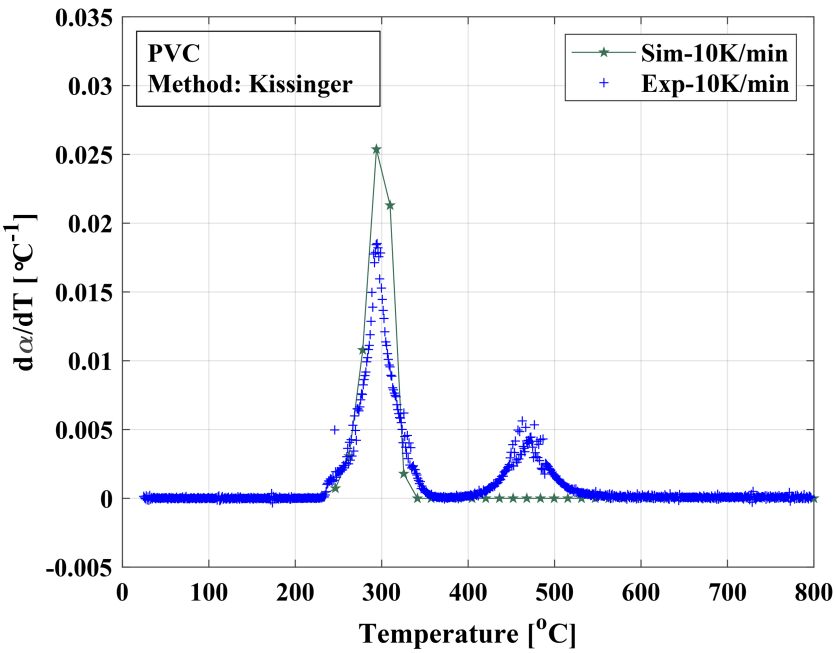
PVC
Method: Kissinger
Sim-10K/min
Exp-10K/min
dα/dT [°C-1]
Temperature [°C]
0.035
0.03
0.025
0.02
0.015
0.01
0.005
0
-0.005
0
100
200
300
400
500
600
700
800

c)

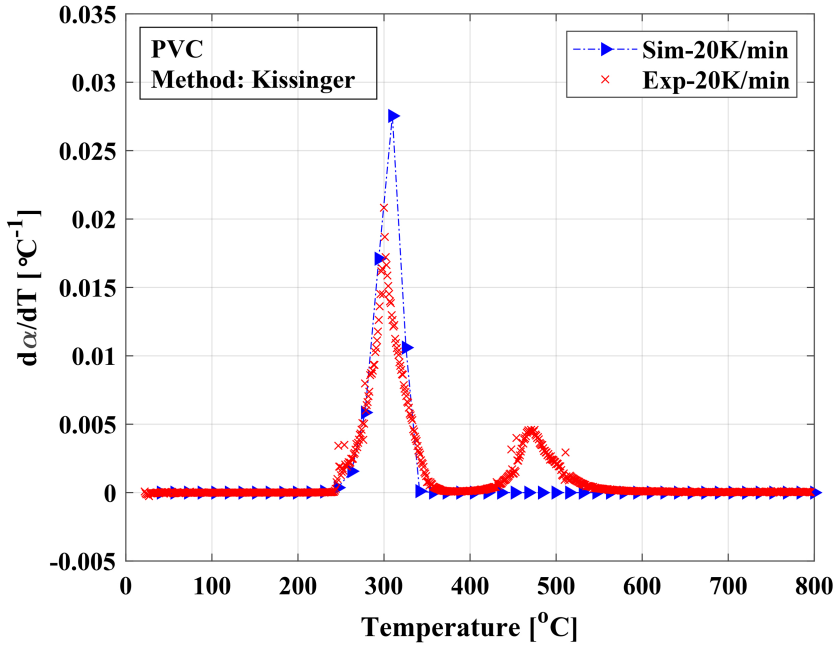
PVC
Method: Kissinger
Sim-20K/min
Exp-20K/min
dα/dT [°C-1]
Temperature [°C]
0.035
0.03
0.025
0.02
0.015
0.01
0.005
0
-0.005
0
100
200
300
400
500
600
700
800

d)

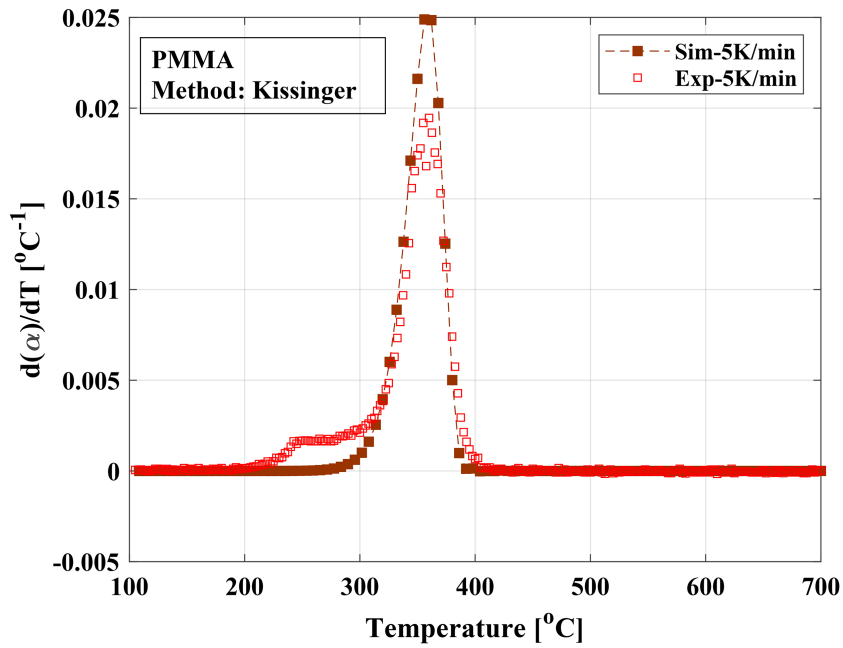
PMMA
Method: Kissinger
Sim-5K/min
Exp-5K/min
d(α)/dT [°C-1]
Temperature [°C]
0.025
0.02
0.015
0.01
0.005
0
-0.005
100
200
300
400
500
600
700

e)

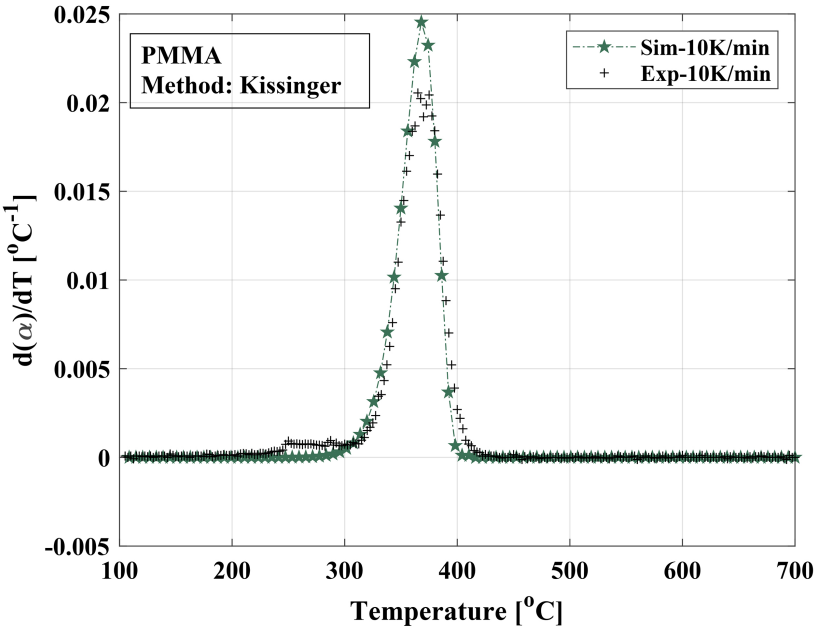

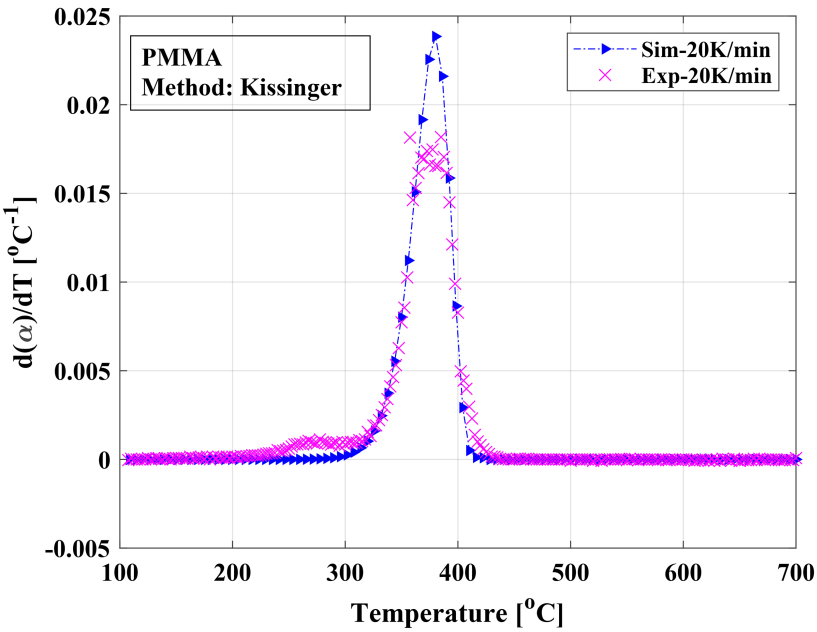

Fig. 15 Comparison of experimental and simulated DTG data with Kissinger method (a-c) PVC and (d-f) PMMA at different heating rates

Although, the reaction rate plots simulated with the parameters obtained with iso-conversional methods match closely with the test data but improvements in fittings is possible via multi-step model fitting methods. The values obtained using these methods can be used to initiate optimization calculations using model fitting methods (as shown in next section).

Table 7 Summary of kinetic parameters obtained by Iso-conversional and Kissinger method

Method	Friedman		Kissinger-Akhaira-Sunose (KAS)		Kissinger	
Kinetic Parameters	PVC	PMMA	PVC	PMMA	PVC	PMMA
Activation Energy, E* [kJ/mol]	333.4	213.4	286.2	166.7	209.7	218.7
Pre-exponential factor, A*[2] [1/s]	$1.0x10^{36}$	$1.8x10^{19}$	7.1×10^{34}	$2.4x10^{15}$	$2.9x10^{17}$	$8.1x10^{15}$

5.3 Kinetic Analysis (Model Fitting-DAEM)

The detailed kinetic analysis shown in previous section was focused on two polymers (PVC and PMMA). The results show the samples experience multi-step chemical reactions during exposure to heat. The observed profiles of the mass loss phenomenon with shoulders in microscale device is a testimony to it. This necessitates the requirement of a multi-step kinetic analysis. Hence, model fitting DAEM is invoked to demonstrate its ability to resolve the several chemical reactions occurring in material samples for a number of polymers. Also, the model fitting analysis is extended to several other polymers including paper (retrieved from common gypsum plaster board), EVA and fabric used in common furniture upholstery. Fig. 16 shows the summary of experimental and modelled DTG curves for various polymers. It can be seen that two main peaks were observed for PVC, EVA and the fabric, while for PMMA and paper only one broad peak is observed. It is apparent that, the broad peak is convoluted in more than one peak. Several inflections in the main peak were also visible near the onset and final temperatures.

[2] *Averaged over conversion

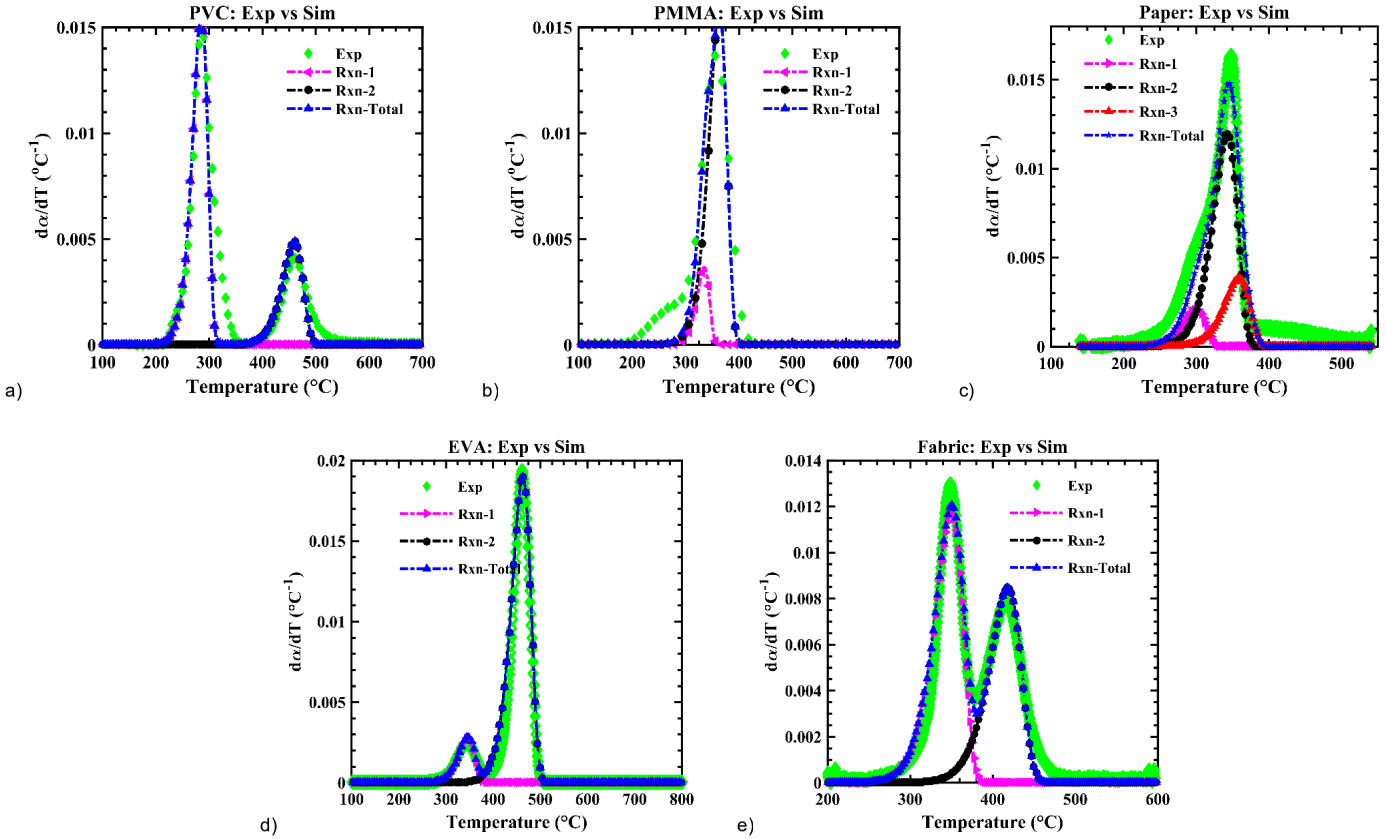

Fig. 16 Experimental and simulated DTG curves for different polymers at 5K/min using multi-Gaussian DAEM

For PVC, PMMA, EVA and the fabric, the DTG curve is modelled as a sum of two peaks, while for paper it is modelled as a sum of three peaks. In the case of PVC and the fabric, the first peak is sharp as compared to the second one, while for PMMA, and EVA the second peak is more prominent. In the case of paper a singular broad peak is clearly visible and slight inflections appear in the beginning and at the end of the pyrolysis reaction. Hence, the de-convolution of this peak was effectively possible using at least three contributing reactions, while for all other cases it was accomplished using two contributing reactions. It can be seen that, in most cases, the modelled curve predicts the experimental data to a high degree of accuracy. However, in some cases, minor inflections in the overall DTG curve could not be reproduced with two reactions e.g. PMMA. It should also be noted that PMMA and EVA left negligible amounts of residues after the test while other materials showed varying amounts of residues. A summary of parameters characterizing the thermal decomposition of the process during the pyrolysis experiment is shown in Table 8.

Table 8 Parameters characterizing the thermal decomposition of different polymers under inert atmosphere for the test at 5K/min

Sample	Peak	T_o (˚C)	T_p (˚C)	T_f (˚C)	Residual Mass (wt. %)
PVC	1	200	284	365	46
	2	365	461	545	27
PMMA	1	210	247	300	87
	2	300	360	420	1
Paper*	1	234	348	380	40
	2	380	450	535	32
EVA	1	277	341	378	85
	2	378	464	500	0
Fabric	1	250	350	375	60
	2	375	417	498	13

*For paper sample 2nd and 3rd DTG peaks were convoluted, but subtle inflections were clearly visible in the beginning and the end of the reactions. T_o: Peak onset temperature, T_p is the peak temperature, T_f is the Final peak temperature.

Table 9 shows the parameters estimated for the DAEM model fittings. Although, the value of the objective function is very low (10^{-3} to 10^{-4}) and the corresponding fit is less than 7 percent, it indicates model predictions show reasonably good agreement with the experimental data.

Table 9. Estimated Parameters for different polymers using multi-Gaussian distributed activation energy model

Material	Peak	E_{0j}	σ_j	c_j	Fit (%)	O.F.
PVC	1	169.4	6.6	0.5	4.7	3.4×10^{-3}
	2	219.1	29.4	0.5		
PMMA	1	182.7	11.8	0.6	2.1	2.1×10^{-4}
	2	190.8	19.6	0.5		
Paper	1	170.0	5.0	0.6	3.4	2.0×10^{-3}
	2	183.0	16.0	0.3		
	3	188.0	20.0	0.1		
EVA	1	184.2	14.9	0.1	2.6	7.5×10^{-4}
	2	219.9	44.0	0.9		
Fabric	1	185.2	14.0	0.6	6.2	5.2×10^{-3}
	2	206.3	29.5	0.4		

5.3.1 Sensitivity Analysis

The results shown in this section are primarily sourced from the sensitivity analysis presented in **Paper II,** in which sensitivity level of each estimated parameter for different materials has been quantified.

The results of a sample sensitivity calculation for PVC is shown in Fig. 17, in which the DTG peak is computed using DAEM with one of the estimated parameters changed to 85% (randomly chosen) of its optimized value (other parameters held constant). The results show the extent of departure of the computed DTG peaks from the experimental and optimized ones. The degree of variation differs from one relative parameter to the other. The effects were observed to be more pronounced for the mean activation energy values (E_{01}, E_{02}) as compared to their standard deviations $(\sigma_{01}, \sigma_{02})$. For PVC, deviation in E_{01} resulted in the first peak to shift to the left of the optimum peak by approximately 70 ºC. Further, the change in σ_{01} resulted in the first peak to diminish to almost half its original value (peak position remains unchanged).

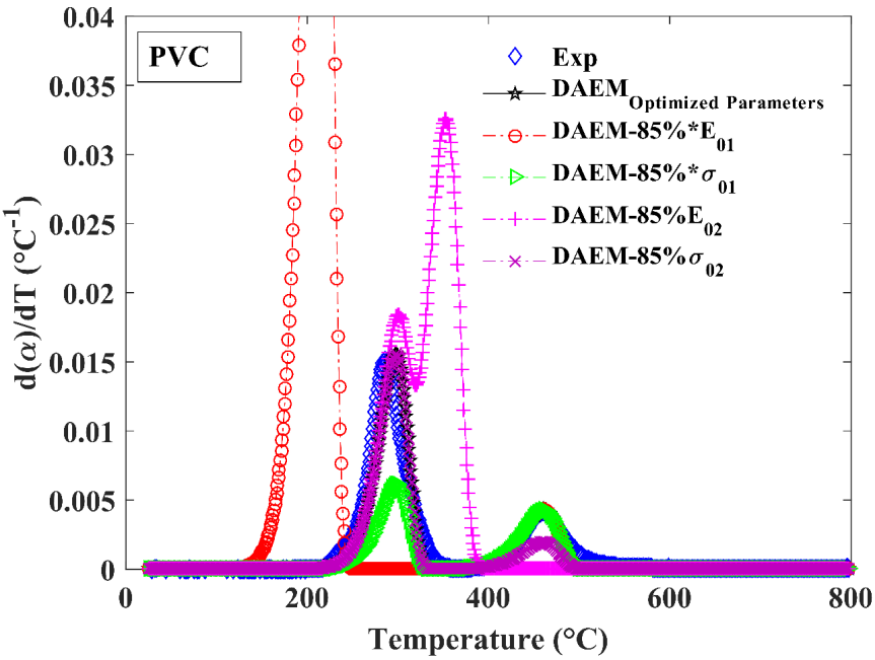

Fig. 17 A sensitivity analysis calculation showing DTG peak deviations in PVC upon variation of one of the estimated parameters to 85% of its optimized value (other parameters being held constant). Maximum peak deviation is seen upon variation of activation energy values.

Further, the change in the E_{02} value resulted in a higher peak. The first peak increased slightly as compared to the optimum one, but the second peak rose sharply in addition. Additionally, a peak shift of 107 degrees Celsius to the left of the optimized peak was observed. Finally, a change in the value of σ_{02} caused the second peak to diminish, but the first peak remained unaffected. The overall inference that may be drawn from the sensitivity analysis is that the model has shown higher sensitivity to activation energy values. A slight deviation of 15 percent (see Fig. 17) in its value causes significant changes in the overall DTG peak properties. This phenomenon is less prominent for standard deviation values, whose variation has less effect on the overall DTG peak. A detailed computation for all the samples is summarized in Fig. 18.

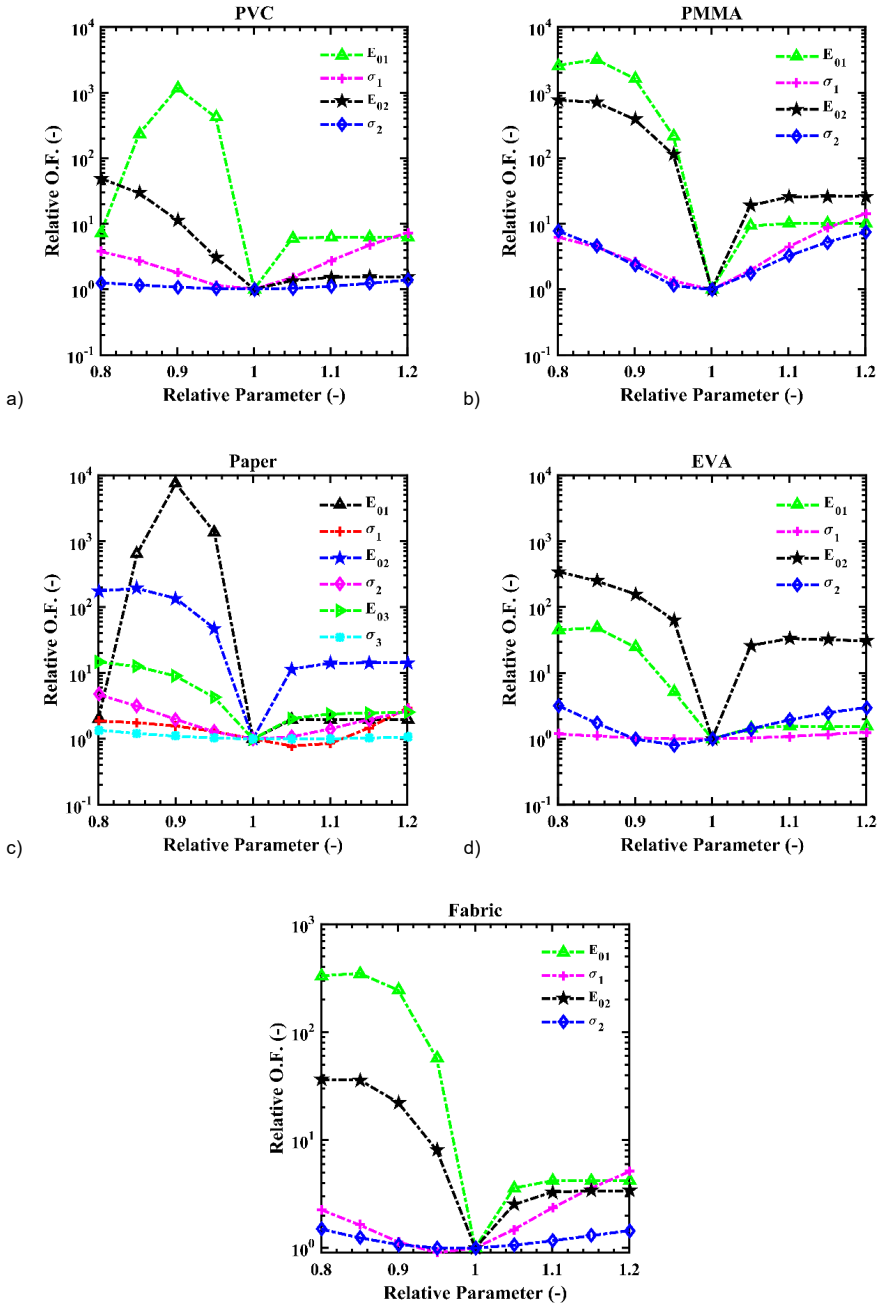

Fig. 18 Local parametric sensitivity analysis of common polymers

For PVC and Paper, the values of relative objective function peaked when E_{01} was deviated to 90 percent of its optimum value, while this was observed at 85 percent for PMMA and Fabric. For EVA, the relative objective function peaked at 80 percent of E_{02} value. A general conclusion that may be drawn from Fig. 18 is that in most cases, the farther the DAEM is computed from the optimized parameters the more the variation is observed in the relative objective function (O.F.). For some values of the relative parameters the deviation is seen to rise exponentially. In this case, the values of activation energies show a higher value of relative O.F. in the order of (10^2-10^4) as compared to standard deviations whose values lie in the range of (1-10). This shows the model's higher sensitivity towards activation energy values as compared to standard deviation. The relative objective functions in most cases show a decreasing trend when the relative parameter increases from 0.8 to 1. It converges to 1 when the relative parameter is 1, followed by an increasing trend as the relative parameter increases from 1 to 1.2.

The sensitivity levels of estimated parameters have been divided into three categories (from low to high). The categorization is based on the range of values computed for the relative objective function for each material (in Fig. 18) at different levels of deviation. The point sensitivities were determined at nine different levels ranging from 80-120 percent of the optimized parameter values. It was found that activation energies were found to have the highest sensitivities for the majority of the points.

For PVC and Fabric, E_{01} was found to be most sensitive while for EVA, E_{02} showed high sensitivity and for PMMA and Paper, E_{01} and E_{02} both showed high sensitivity values. The least sensitive parameters were standard deviation ($\sigma_1, \sigma_2\ \sigma_3$) for all reactions. The result of the sensitivity levels of different parameters is shown in Table 10.

Table 10 Sensitivity levels of estimated parameters of different polymers

		Parameters				
Sensitivity	**Range – Relative O.F.**	**PVC**	**PMMA**	**Paper**	**EVA**	**Fabric**
Low Sensitivity	1 to10	σ_1, σ_2	σ_1, σ_2	$\sigma_1, \sigma_2\ \sigma_3$	σ_1, σ_2	σ_1, σ_2
Medium Sensitivity	10 to 100	E_{02}	-	E_{03}	E_{01}	E_{02}
High Sensitivity	> 100	E_{01}	E_{01}, E_{02}	E_{01}, E_{02}	E_{02}	E_{01}

5.4 Combined heat and mass transfer model

In this section experimental results and model simulations for industrial formulation of PVC and EVA-ATH polymers are shown. These materials are

significantly different from those discussed in earlier section, since they incorporate several additives, fillers, lubricants and thermal stabilizers applicable for real cables. Table 11 and Table 12 show the composition of these test specimens. The polymeric formulations were developed in two separate industrial R&D labs and corresponding experimental support was also provided by them. Braskem A/S (Brazil) was supplier of PVC formulations while Nabaltec AG (Germany) supplied EVA-ATH specimens. Hence the results shown in this section are based on support provided by collaborating work partners. **Paper (III)** has provided adequate background information about the work done in collaboration with the other authors from respective laboratories.

Table 11 Contents of PVC compound formulation [80]

S.No	Material	Trade Name	Amount In phr (Parts per hundred of rubber)
1	PVC resin (K 65)	Norvic SP 1000	100
2	Calcium/Zinc thermal stabilizer	Naftomix XC -1202	3.5
3	Diisodecyl phthalate (plasticizer)	DIDP	45
4	Epoxidized soyabean oil (ESO, plasticizer)	Drapex 6.8	5
5	Calcium carbonate (mineral filler)	Barralev C	40
6	Steraic acid (lubricant)	Naftolub L12	0.2

Table 12 Contents of EVA-ATH compound formulation

S.No	Material	Trade Name	Content
1	Ethylene Vinyl Acetate Copolymer (19% EVA)	Escorene UL00119	34.6 %
2	3-Aminopropyltriethoxysilane	AMEO	0.4 %
3	Aluminum Trihydroxide (ATH)	Apyral 40CD	65 %

The methodology demonstrated in previous sections shows a detailed kinetic analysis on a number of polymers and its corresponding sensitivity studies, renders its application in combined heat and mass transfer model. In this section the theory presented in section 4.2 and the simulations results obtained in section 5.1-5.3 is further applied for two real world cable sheathing PVC and EVA-ATH formulation supplied by two manufacturers.

5.4.1 Kinetic Fittings (DAEM)

Fig. 19 (a-f) shows the result of thermogravimetric analysis of PVC and EVA-ATH formulations. The plots shown are experimental TG curves (a, d) and

their corresponding normalized differential thermogravimetric curves (DTG) (b, e). In the DTG curves, a comparison is drawn between the experimental and simulated plot of dα/dT versus temperature. It can be seen that from the DTG curves that in case of EVA-ATH, two main peaks are visible while for PVC three-four peaks are visible. In EVA-ATH, the onset of first peak occurs at a temperature of 220 °C indicative of dehydration of ATH, releasing water and formation of ceramic residue made up of alumina (Al_2O_3). The second step corresponds to the decomposition of EVA around 350 °C in two steps leading to formation of acetic acid and hydrocarbons at around 450 °C. The decomposition of EVA-ATH is well described by Hewitt et al. [81].

For PVC, the first peak occurs at 323 °C, while the second peak occurs at 456 °C, and the third peak occurs at 737.6 °C. The test is conducted in air atmosphere hence, conditions corresponding to combustion reactions are present in the TGA apparatus. However, the first stage of weight loss is still likely to be attributed to the release of hydrogen chloride (HCl) and this phenomenon is termed as dehydro-chlorination. In the second reaction step many cyclic compounds aromatize via chain scission reactions and undergo combustion reactions in presence of oxygen leading to further weight loss and formation of carbon dioxide, water and other aliphatic and olefinic, aromatic hydrocarbons and char.

DAEM has been used to model the peaks occurring in the DTG curve of both the polymers. The parameter search domain was set for mean activation energy to be (50-350 kJ/mol), standard deviation (1-50 kJ/mol), and pre-exponential factor 10^{10} -10^{16} (1/sec). The estimations were based on an optimization algorithm developed as shown earlier. The code is also programmed to search for random numbers within the above cited range to avoid any negative values. Additionally, a visual manual check of the real time reproduction of the DTG curve is incorporated in the code to monitor the fitting quality. The range of pre-exponential factor was kept in a rather lower range as compared to that cited in the literature in view of the theories of compensation effect discussed by Lakshmanan and White [82] to avoid multiple sets of parameters resulting in fitting of the DTG curve. In both cases, the model is able to capture the peak inflections to a high degree. EVA-ATH has been modelled with only two reactions, while PVC has been modelled with two and four reactions. The two-reaction model reproduces the first two peaks only while the four reaction model which covers the entire range of peaks exhibited by PVC. The corresponding parameters used to model these curves are summarized in Table 13. In the figures below only the best fits with four reactions are shown.

Table 13 DAEM kinetic parameters for EVA-ATH and PVC formulations obtained using pattern search

Reaction	Parameters	EVA-ATH	PVC	PVC
		[2-Rxn Fitting]	[2-Rxn Fitting]	[4-Rxn Fitting]
Rxn -1	E_{01} [kJ/mol]	197.4	180.3	172.3
	σ_1 [kJ/mol]	25.8	42.4	9.0
	A_1 [1/s]	$7.5x10^{15}$	$8.6x10^{13}$	$1.7x10^{13}$
	c_1 [-]	0.1	0.2	0.3
Rxn – 2	E_{02} [kJ/mol]	198.5	190.8	212.0
	σ_2 [kJ/mol]	18.1	12.7	50.0
	A_2 [1/s]	$1.0x10^{12}$	$3.x10^{11}$	$1.7x10^{13}$
	c_2 [-]	0.9	0.8	0.1
Rxn-3	E_{03} [kJ/mol]	-	-	224.0
	σ_3 [kJ/mol]	-	-	40.0
	A_3 [1/s]	-	-	$1.6x10^{13}$
	c_3 [-]	-	-	0.1
Rxn-4	E_{04} [kJ/mol]	-	-	270.4
	σ_4 [kJ/mol]	-	-	50.0
	A_4 [1/s]	-	-	$1.1x10^{12}$
	c_4 [-]	-	-	0.5
Objective Function		$1.2x10^{-5}$	$2.1x10^{-4}$	$1.5x10^{-4}$
Fitness [%]		7.0	4.5	4.2

The normalized probability distribution curve, f(E) versus activation energy *(E)* for each polymer is shown in Fig. 19 c) and f) as a cumulative sum of individual reaction rate curves. It can be seen that for the overall reaction, the mean activation energy was found to lie at 193.8 kJ/mol for EVA-ATH and 173.4 kJ/mol for PVC shown by the peak of the overall reaction rate curve.

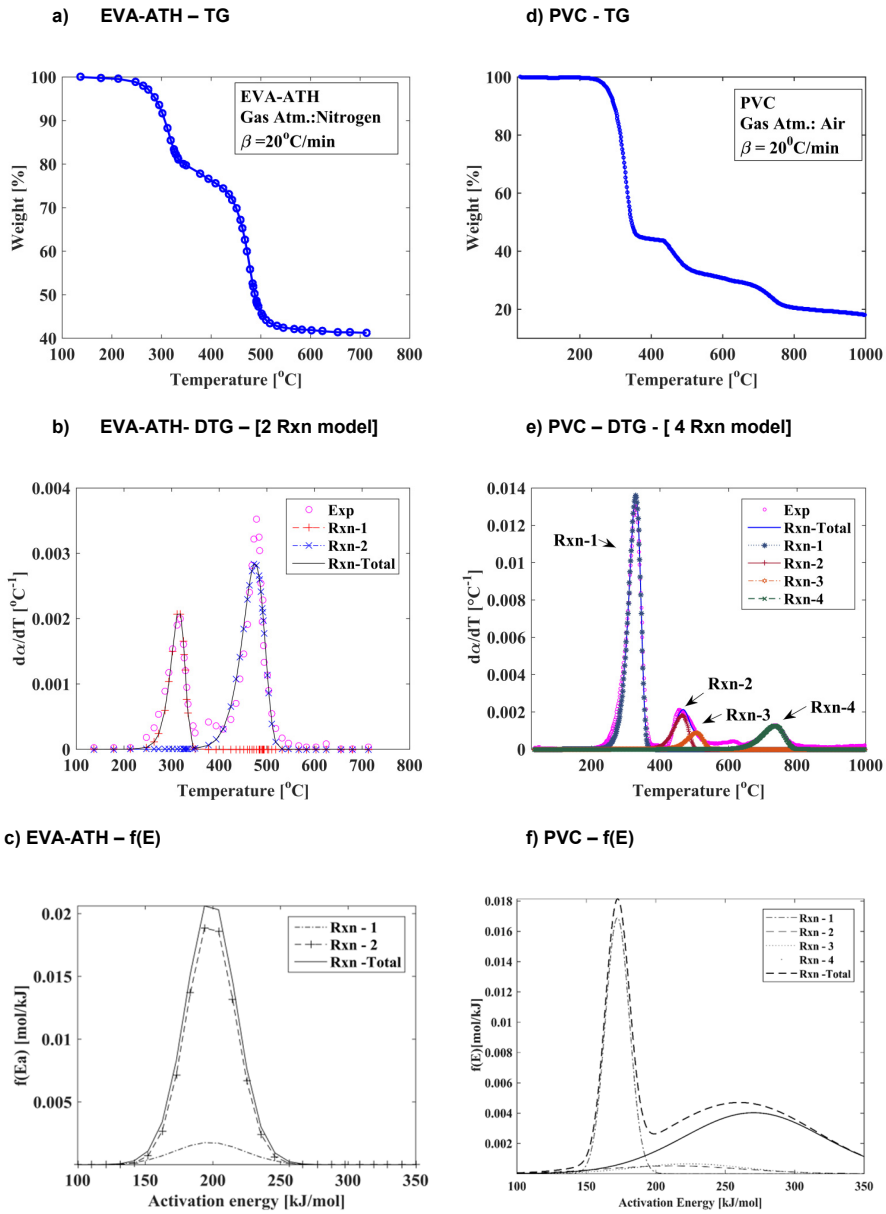

Fig. 19 DAEM model fits for EVA-ATH (a-c) and PVC (d-f) [For PVC fittings shown only for 4 reaction model]

5.4.2 Cone Calorimeter Tests

EVA-ATH

Fig. 20 a) shows the MLR of EVA-ATH polymer. The curve shows linear rise to the peak value at 16 g/m^2/s within first 78 seconds, followed by a linear decay until the end of the experiment. The ignition criterion was defined as the time to reach critical mass flux value of 1 g/m^2/s also used by Stoliarov et al.[26]. For EVA-ATH MLR crosses the threshold of 1 g/m^2/s after 43 seconds, while in the decay phase the MLR falls below this threshold value after 546 seconds. Fig. 20 b) shows the heat release rate curve showing occurrence of a characteristic peak shortly after ignition followed by a steady burning phase with HRR output varying between 120 to 140 kW/m^2. This is followed by steady linear decay until 800 seconds. The peak heat release rate (p-HRR) and the time to peak heat release rate (t_{pHRR}) were found to be 171 kW/m^2 and 84 seconds respectively. Fig. 20 c) shows the total heat released during the experimental run. The total heat released at the end of the run was found to be 63 MJ/m^2. The effective heat of combustion (EHC) was found to show a high degree of variation during the experiment, but overall the values were found to lie below 40 MJ/kg. Largely the values were found to vary between 10-35 MJ/kg.

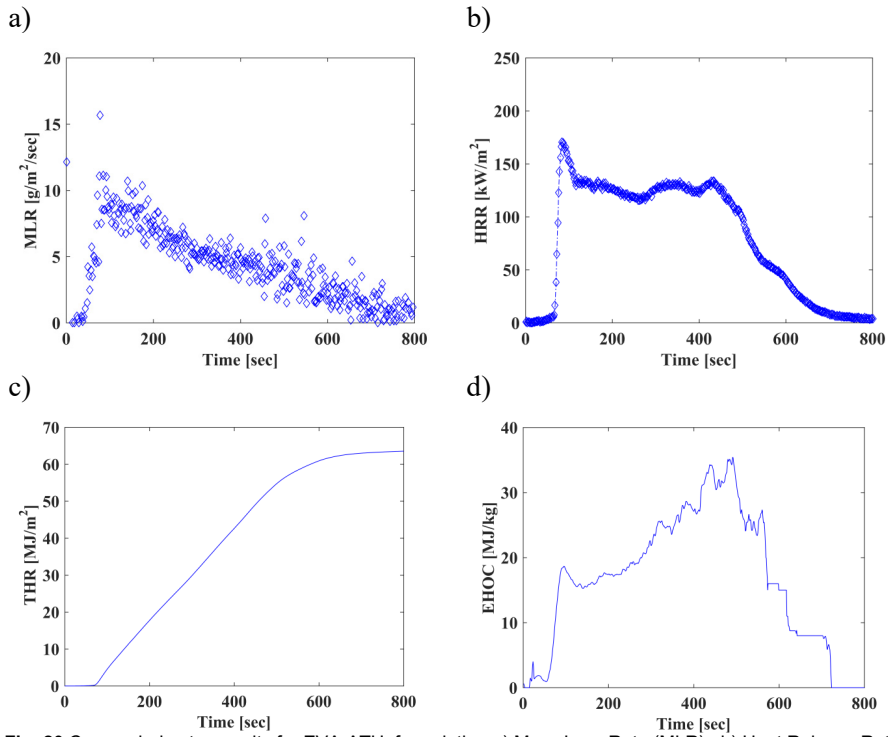

Fig. 20 Cone calorimeter results for EVA-ATH formulation a) Mass Loss Rate (MLR) ; b) Heat Release Rate (HRR); c) Total Heat Released (THR); d) Effective Heat of Combustion (EHC)

PVC

Fig. 21 a) shows the MLR curve of PVC (industrial grade). The curve shows a sharp rise to a peak value of 23 g/m^2/s followed by linear decay phase. During the rise, the MLR crosses the threshold value of 1 g/m^2/s in first 6 seconds of the test. The time to peak MLR was found to be 58 seconds. In the decay phase, the value of MLR falls below the threshold of 1g/m^2/s after 410 seconds. The Fig. 21 b is the HRR curve. The peak HRR and time to peak HRR were found to be 292 kW/m^2/s and 90 seconds respectively. The profile is similar to the MLR curve, in which after a short delay, the curve rises to the peak value followed by a gradual linear decay. Fig. 21 c) is the THR curve, it shows the total heat released at the end of the experiment was 66 MJ/kg. The profile shows zero reading in the beginning of the experiment, indicating towards short delay until the ignition, followed by a linear rise and then a plateau. Fig. 21 d) shows the effective heat of combustion versus time. The peak value of EHC was found to be 35 MJ/kg, overall the curve showed significant fluctuation over the length of the test, with majority of values lying below 35 MJ/kg mark.

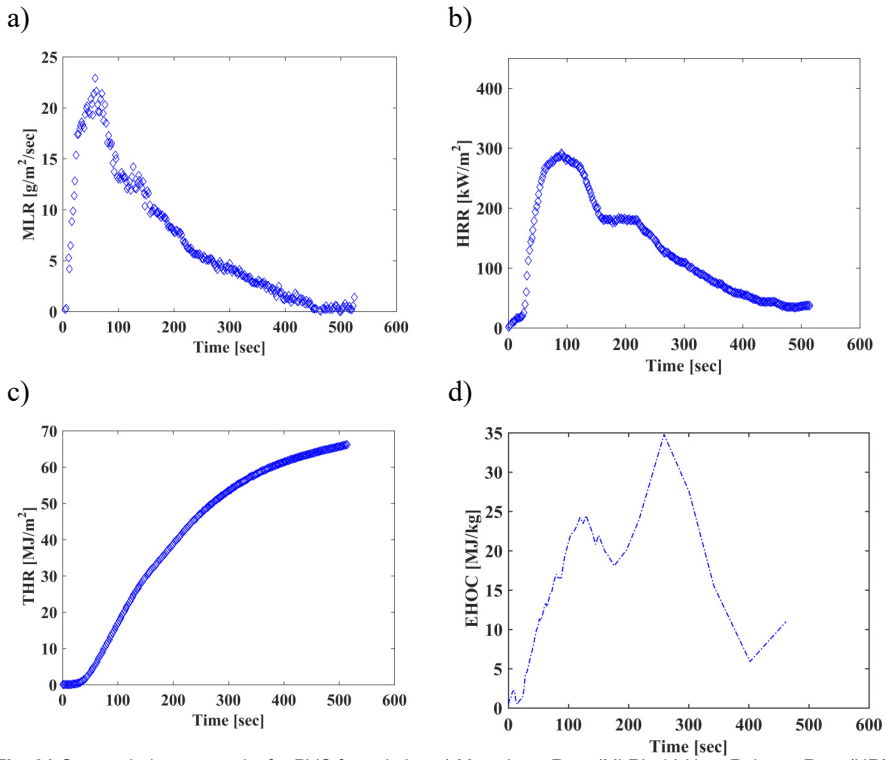

Fig. 21 Cone calorimeter results for PVC formulation a) Mass Loss Rate (MLR) ; b) Heat Release Rate (HRR); c) Total Heat Released (THR); d) Effective Heat of Combustion (EHC)

The cone calorimeter experimental summary is tabulated in Table 14.

Table 14 Short summary of key parameters obtained from cone calorimeter tests*

S. No	Parameters	Symbol	EVA-ATH	PVC
1	Time to Ignition [s]	TTI	40 (44)	6 (10)
2	Time to peak HRR [s]	$t_{p\text{-}HRR}$	84 (88)	90 (180)
3	Peak Heat Release Rate [kW/m^2]	p-HRR	171 (170)	292 (277)
4	Peak Mass Loss Rate [g/m^2/s]	p-MLR	16 (16)	23 (23)
5	Time to peak MLR [s]	$t_{p\text{-}MLR}$	78 (78)	58 (66)
6	Time to flame out [s]	$t_{flame\text{-}out}$	546 (550)	410 (400)

*In brackets are shown the results of repeat tests

From the results above it can be seen PVC shows a higher value of p-HRR and lower time to ignition (TTI) as compared to EVA-ATH specimen. One reason could be the occurrence of dehydration reaction and formation of ceramic residue made up of alumina (Al_2O_3) in the EVA matrix which has significant degree of cooling effect due to production of acetic acid, water and acetone during the thermal decomposition reactions.

5.4.3 Bench Scale Model Predictions

Input Data

For the estimation of mass loss rate, the input data was gathered from two different literature sources as shown in Table 16. The density and specimen thickness values were used as obtained during experimental measurements. The PVC and EVA-ATH specimen was modelled with only two reactions. The four reaction model was not implemented due to lack of other thermo-chemical reaction parameters such as heat of pyrolysis of individual chemical reactions (Rxn-3 and Rxn-4 in case of PVC). For the parameters of chemical reaction model, the values were taken from Table 13 for first two peaks of the DTG curve. The input data of the temperature dependent thermal properties of EVA-ATH are shown in Fig. 22 for virgin and char materials separately, while for PVC, constant values of thermal properties were found and hence used as reported in the literature. Heats of pyrolysis were determined by DSC experiments and literature values were used. Fig. 22a shows the variation of thermal conductivity and specific heat of virgin and charred polymer measured directly by hot disc based on Transient plane source (TPS) method and DSC. The first plot shows linear decline of virgin thermal conductivity until 200 °C followed by slow rise of the thermal conductivity of char. The thermal conductivity of intermediate is shown but not used in the simulations. It can be seen, the majority values of the intermediate and char thermal conductivity are significantly lower than that of virgin polymer. Also, the curve showing variation of specific heat values shows linear rise for virgin and char polymer. But overall, the specific heat of char is significantly lower than that of virgin polymer.

The thermal conductivity curve has been reproduced by using the linear relation proposed by Girardin [83,84] and Witkowski [27]. These relations are shown as a function of temperature in Table 15. Those functions are obtained by linear fitting to the experimental data obtained in test measurements conducted using Hot Disc thermal constant analyser (TPS2500S) from Thermoconcept (Merignac, France) which is based on Transient Plane Source method. The tests were performed separately on virgin, intermediate, and char specimens of EVA-ATH. Each of the test was conducted in inert atmosphere to avoid the oxidation of the Hot disc sensor, which plays a dual role of heater and a thermocouple. The data on virgin specimens was acquired between 50 to 200 ºC at a step size of 50 ºC, while intermediate material and char was first synthesized by heating the virgin polymer upto 350 ºC and 500 ºC respectively and thereafter cooling them to 50 and 100 ºC for intermediate and char respectively. The thermal conductivity measurements were made from 100 to 700 ºC at a step size of 100 ºC on char. Based on the data collected linear correlation trends were found to exist between thermal conductivity and the

temperature at which the measurements were taken, eventually resulting in linear mathematical functions. For modelling tasks in this work, those correlations have been used to generate the thermal conductivity cuve and it been extrapolated only for char beyond 700 ºC (shown in Paper III) so as to avoid problems in numerical convergence during simulation work. In Fig. 22a), thermal conductivity values have been plot using the linear functions from Table 15, while specific heat has been shown in Fig. 22 b) via manual digitization of the reported data.

Table 15 Thermal conductivity functions for EVA-ATH specimens used in simulations reproduced from Girardin et al. [84]

Thermal conductivity [W/m/K]	Specie
$1.10 - 1.7 \times 10^{-3}\ T$	Virgin Formulation (<200 ºC)
$0.20 + 0.28 \times 10^{-4}\ T$	Intermediate (Not considered in simulations) (<350 ºC)
$0.17 + 1.1 \times 10^{-4}\ T$	Residue

a)

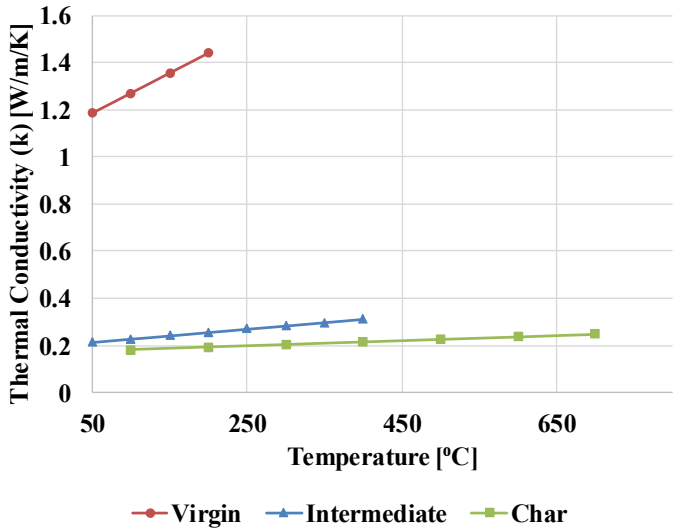

b)

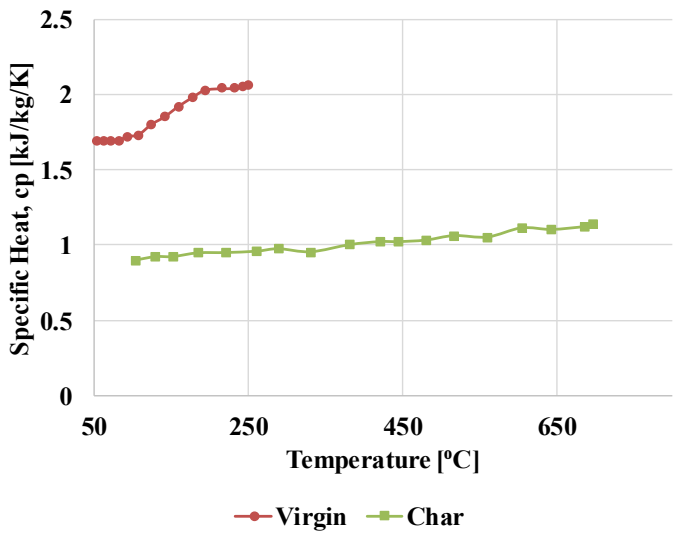

Fig. 22 Temperature dependent thermal properties of virgin and char of EVA-ATH reproduced from Witkowski and Girardin [27,84] using linear relations shown in Table 15 and manual digitization of test data a) Thermal conductivity (linear relations) b) Specific Heat (digitized data).

Table 16 Parameters used for simulation of HT-DAEM model

S.No	Parameters	Units	EVA-ATH- Girardin et al. [83]	PVC- Ghorbani et al. [33]
1	ρ-Density [Virgin]	kg/m^3	950 [Measured]	1425 [Measured]
2	ρ-Density [char]	kg/m^3	397	398
3	$\Delta H_{r,1}$ – Heat of pyrolysis	J/kg	883x10^3 [DSC]	292x10^3 [DSC]
4	L – Thickness	m	6.5x10^{-3} [Measured]	3 x10^{-3} [Measured]
5	h – Convective Heat Transfer Coefficient	W/m^2/K	10	10
6	G – Incident Heat Flux	W/m^2	35x10^3	50x10^3
7	ε –Emissivity [Virgin and Char]	-	0.9	0.9
8	$\Delta H_{r,2}$ – Heat of pyrolysis	kJ/kg	236 [DSC]	292 [DSC- Assumed same as in Rxn 1]
9	$k_{s,virgin}$-Thermal conductivity [Virgin]	W/m/K	See Fig. 22 a)	0.17
10	$k_{s,char}$–Thermal Conductivity [Char]	W/m/K	See Fig. 22 a)	0.10
11	$c_{p,virgin}$- Specific Heat [virgin]	kJ/kg/K	See Fig. 22 b)	1.11
12	$c_{p,char}$- Specific Heat [Char]	kJ/kg/K	See Fig. 22 b)	3.89
13	$\eta_{char,1}$ [Char fraction]	-	0.25 [Measured]	0.56 [Measured]
14	$\eta_{char,2}$ [Char fraction]	-	0.60 [Measured]	0.26 [Measured]
15	$\ddot{q_{fl}}$-Flame heat flux	kW/m^2	6 [Fitting Parameter]	10 [Fitting Parameter]

The flame heat flux ($\ddot{q}_{fl}$)value was chosen as a representative mean of the data provided of several polymers in several references[33,65,85]. It is also treated as model fitting parameter in this study. The values used in simulations for PVC and EVA-ATH were 10kW/m^2 and 6kW/m^2 respectively. Ghorbani et al.[33] have used a similar value for simulation of their PVC specimens, while for EVA-ATH slightly higher values are found in literature (10 or 20 kW/m^2) compared to what is used in this study mainly for fitting purpose. Further, a few other studies were found in which flame heat flux values were obtained by direct measurements for different polymers. Test measurements from Kacem et al. [86] show flame heat flux value obtained for PMMA was found to be 20 kW/m^2, and the results by Quintiere [87] show values for Nylon to be 20 kW/m^2, polyethylene to be 19 kW/m^2 and polypropylene to be 11 kW/m^2 respectively. The values for flame heat flux used in this study are significantly lower than the experimentally obtained values measured for the above polymers due addition of additives for suppression of smoke and heat release in the samples.

The following section shows the comparison of simulated and experimental results of MLR, HRR and THR for the two polymers.

Mass Loss Rate (MLR)

The results for mass loss rates simulation are shown in Fig. 23. It can be seen, that the calculated results match the experimental data to a reasonable extent.

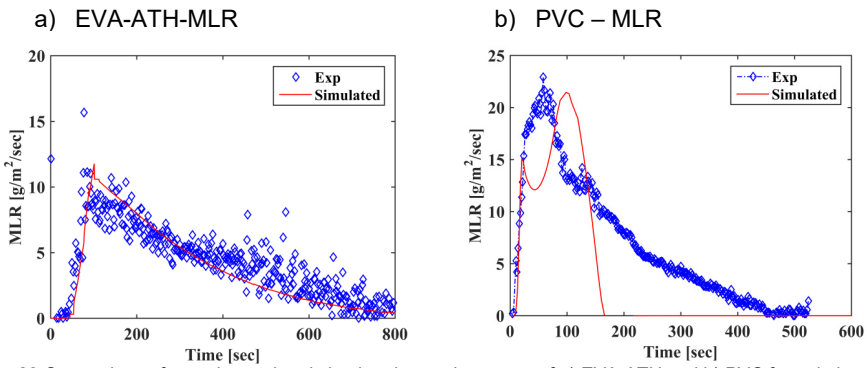

Fig. 23 Comparison of experimental and simulated mass loss rates of a) EVA-ATH and b) PVC formulation

The time to ignition (TTI), p-HRR and $t_{flame\ out}$ follow the experimental results to a high degree especially in case of EVA-ATH, while there is a considerable deviation in the simulated MLR curve of PVC. From the quality of simulations, it can be said the rise and the peak MLR value is captured well in both cases, however there exists significant under prediction in time to flame out and over prediction in time to reach peak heat release rate in case of PVC. This deviation may be attributed to thermo-physical material property data sourced from literature and not acquired by direct measurements. The PVC is a very specific industrial formulation and it is uncertain that generic literature values of material properties would closely represent the actual properties of the complex material. It can also be seen, that in case of PVC, the simulated MLR curve rises to $15 g/m^2/s$ in line with the experimental curve but it drops for a few seconds very sharply followed by a steep rise the top MLR value. This can be attributed to the formation of char layer preventing further oxidation of virgin material by insulating it for a very short period of time. As the exposure time increases the char layer starts oxidizing leading to further increase in MLR value and consumption of virgin fuel until its exhaustion leading to eventual decay of the MLR curve. The interesting observation is that, this effect is not visible in experimental results. The experimental curve decays at a much slower pace and falls to zero value at nearly 500 seconds.

Perhaps one reason could be presence of zinc and calcium thermal stabilizers present in the polymer matrix leading to increase in their burn out time. The impregnated $CaCO_3$ is believed to react with acid (HCl) generated in the

material during thermal decomposition and form $CaCl_2$, CO_2, and H_2O providing overall cooling effect and slowing down the mass loss rate. Shimpi et al.[88] found dispersion of $CaCO_3$ in PVC specimen to have an improvement in thermal stability of the polymer sheet. They found rise in glass transition temperatures for $CaCO_3$ dispersed PVC samples as compared to pure ones. Also, a previous study from Stoliarov et al. [26] has shown that after the flame out in a cone calorimeter experiment, PVC specimens showed smouldering effect leading to heat release at a steady rate for extended period of time.

Also, because of the char formation and intumescence, specimens tend to swell up and trap pyrolysis gases in their air pockets for short period of time. Perhaps non-inclusion of a dedicated radiative porous char-sub model also accounts for under-prediction in this case, since presence of an insulating char layer that would develop upon heat exposure would delay the delivery of external heat flux to virgin material and provide some thermal resistance at higher temperatures when radiative heat transfer plays a dominant role in heat transfer to the material. The absence of two peaks, in the early phase of the development of the MLR may also be attributed to the very thin nature of the sample of PVC in which the decline of MLR due to formation of thin char layer is not very clear and merged into one broad peak. This effect was also observed by Ghorbani et al. [33] for their simulations for very thin samples. The specimens used in this study are closer to real world materials used in cable sheathing industry and differences in modelling output may be attributed to complex thermo-chemical phenomenon occurring in material due to cooling effect provided by water release reactions unlike in pure PVC specimens. In case of EVA-ATH polymer, the values match the experimental data to a high degree. The simulated curve shows initial delay before it climbs to the p-MLR value. Thereafter it shows gradual delay in its decent to zero value at the end of the experiment. The time to ignition is captured well in both cases.

Heat Release Rate (HRR) and Total Heat Released Estimation

The heat release rate curve is estimated based on further computations performed on the simulated MLR curve obtained by solution of model equations. The HRR is computed based on the product of simulated MLR curve and the effective heat of combustion (EHC). EHC is determined using cone calorimeter data in its real time form as discussed in detail by Hshieh et al. [89]. If EHC data is unavailable in real time format literature values may be used as well. In the estimations, it is further hypothesized that flame heat flux contributes to the incident heat flux boundary condition on the top surface of the polymer. In case of EVA-ATH it is assumed to be 6 kW/m^2 of flame heat flux and is rather used as a model fitting parameter. However, in literature Stoliarov [26] have used values up to15 kW/m^2. Comparing the curve features of EVA-ATH, it can be said that the simulated curve matches the experimental one until, the time to peak heat release rate. The value of the p-HRR is slightly over predicted at 209 kW/m^2 as compared to the experimental one which remains at 170 kW/m^2. This is followed by a steady phase of HRR which varies between 100-150 kW/m^2. The simulated curve shows gradual decline until it diminishes at nearly 700 seconds. In the decay phase of the HRR the simulated and the experimental curve do not overlap to a high degree but show a reasonably similar declining trend. Overall, the fitting is satisfactory as compared to the HRR experimental data. The evolution of THR matches the experimental one to a high degree. The total heat released for the experimental curve was found to be 63 MJ/kg, while the simulated ones were found to be 59 MJ/kg.

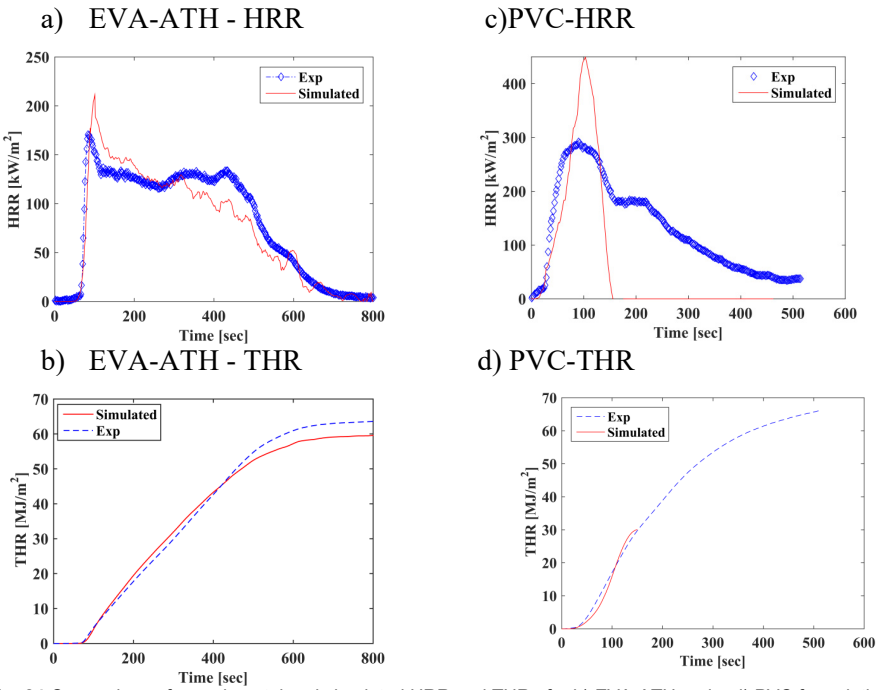

Fig. 24 Comparison of experimental and simulated HRR and THR of a-b) EVA-ATH and c-d) PVC formulations

A similar comparison when drawn for PVC shows that the modelled curve deviates from the HRR curve to a large extent. The simulated HRR curve shows a sharp peak growing as much as 450 kW/m^2 within 103 seconds. It then drops sharply to zero value in 155 seconds. The time to burnout is under predicted by the modelled curve by several hundred seconds. These differences could be attributed to the differences in the material properties and the very thin nature of the sample showing quick burnout with a sharp peak. As a consequence of this, the following THR curve is also under-predicted by a large margin.

6 Discussions

This chapter deals with the analysis on the quality of simulation results obtained with bench scale model and shows ways and means to improve the model performance via inclusion of contributing effects of other sub-models not discussed in mass conservation model.

The analysis is mainly focused towards the reasons for observed deviation in quality of fire simulations and the various factors that may be considered to improve them. From the simulation results itself as shown in the previous chapter, it can be said that there could be several reasons because of which there exists an in-congruence between experimental and simulated results of industrial formulation of PVC. The main factors governing the quality of predictions is the model's ability to predict MLR and temperature distribution. Improvement in the predictive ability of the mass loss rate variation with time may be attributed to various assumptions made during the formulation of the model, which included simplification regarding various phenomenon occurring during the fire which are not considered.

Another issue is the problem in acquiring material property data experimentally at higher temperature levels. For polymeric materials subjected to increasing temperature levels, the material transforms itself into pyrolysis gases and residue. When the measurements are performed to acquire such properties in a dynamic experiment, these processes hinder in obtaining the right signals at the sensor - material interface for some of materials due to physicochemical changes exhibited by the material (such as swelling and shrinking, glass transition). Under these circumstances, the measurements on thermal conductivity and specific heat are challenging and may be performed in special conditions and devices via following specific heating and cooling programs for the sample in question. During the data acquisition process while the sample is subjected to heating, it is difficult to arrest the conversion process and clearly mark the distinction between virgin, intermediate products and residue/char while acquiring temperature dependent material properties. Also, these properties differ for each material corresponding to individual chemical composition and hence literature values may only be representative of the material for which the study is undertaken.

From practical standpoint, access to analytical devices in which these measurements could be made is also limited and their availability is subject to their presence in modern fire laboratories; cost being a major barrier in acquiring them as a part of any portfolio of laboratory devices. Consequently, this restricts the modeller's ability to acquire material property data directly and subjugates its dependency on literature values.

These issues have also been bought forward in selected publications by those researchers who have attempted to acquire thermal conductivity and specific heat for charring polymers experimentally. Those attempts included acquisition of virgin, intermediate and charred materials using individual devices with precise control over the extent of conversion from virgin to char during the heating process of the sample [83,84].

Additionally, some of the causes for deviation in simulated results may be attributed to insufficiency in modelling assumptions. Some of them may be dealt via inclusion of other physical phenomenon is explained in subsequent section where other physical phenomenon such as diffusion of pyrolysis gases, in-depth radiation absorption by specimens is considered. Other factors include gas phase considerations, which are also responsible for the quality of HRR and THR predictions. The main reason being that effective heat of combustion (EHC) and combustion efficiency play an important role in computation of HRR from the MLR curve. Hence the reactions occurring in the gas phase and the amount of heat release through them while the material is decomposing is an important aspect to consider.

Other aspects, which affect the quality of predictions, are connected with the application of boundary conditions. In modelling assumptions, the unexposed side is considered to be insulated and it is assumed there are no heat losses from the edges. However, in reality there are considerable losses of heat via the ceramic insulation penetrating towards the bottom of the test specimen. This also holds true for the heat losses occurring from the sides. However, when the governing equations are solved, the applied boundary conditions negate such considerations allowing all the heat to remain in the material matrix showing faster rate of decomposition as compared to what happens in reality.

From kinetic point of view, especially for material decomposing in multiple steps, sometimes the step in which the heat is released is different that the step in which a major part of weight is lost. Snigrev [90] has shown via complementary experiments performed in MCC and TGA, how each of the peaks observed in MCC corresponds to the heat release step. If the heat released in mass loss step is also accurately quantified, this can also aid in improvement of the solution of governing equations and improve the

confidence in simulated results. The quality of simulations on microscale level is also dependent on quality of experimental data collected. Large amount of noise in the STA signal can be a barrier in performing accurate simulations. Hence, optimum use of data filtering techniques must be employed and this has been used in this work but not mentioned in the previous sections. Another point is the frequency of data collection and which numerical method is used to resolve the equations describing the thermal decomposition process. A higher frequency of data collection ensures sufficient number of points are available for model fitting purpose.

Increasing model complexity: Gas Diffusion and In-Depth Absorption

The model shown in section 4.3 can incorporate further complexities by incorporating other heat transfer effects in the pyrolyzing material by inclusion of gas diffusion and in-depth absorption of radiation. This flexibility in modelling other effects is shown via modified energy conservation equation 30. This considers gas diffusion and in-depth absorption of radiation in the material. The mass flux term $-\sum_{g}^{N*Total\ no.of\ gases)} m_g.\frac{\partial\left(\int_0^T c_{p,g}dT\right)}{\partial x}$ used in this equation implies heating up of the gas from ambient temperature to the temperature of the media in which it diffuses resulting in instantaneous heat transfer between decomposed media and diffusing gases.

Also, the diffusion of the gases in the heat balance equation indicate that when the gases evolve from the decomposing materials it can absorb energy and remove it from the material insides as they diffuse out towards the surface of the material. The mass flux m_g(kg/m^2) and the mass flux rate (kg/m^2/s) of the gases can be defined by equation 31 and 32 respectively where D_g is the diffusion coefficient (m^2/s).

$$\rho c_p \frac{\partial T}{\partial t} = \frac{\partial}{\partial x}\left(k_s \frac{\partial T}{\partial x}\right) - \sum_{i=1}^{n} c_i \omega_{s,i} \Delta H_{r,i} - \sum_{g=1}^{N\ (Total\ no.of\ gases)} m_g.\frac{\partial\left(\int_0^T c_{p,g}dT\right)}{\partial x} + \varepsilon \frac{\partial \ddot{q}_{rad}}{\partial x} \quad [30]$$

$$m_g = -D_g.\frac{\partial m_g}{\partial x} \quad [31]$$

$$\frac{\partial m_g}{\partial t} = \frac{1}{\rho_0}.\frac{\partial \rho}{\partial t}_{Total} - \frac{\partial m_g}{\partial x} \quad [32]$$

Further, the last term in equation 30 accounts for the in-depth radiation absorption of the incident heat flux, which is in accordance with the standard Lambert Beer Law. Here, the absorbed radiation decreases exponentially with the distance to the impacted surface, which is given by equation 33. Here the

absorption coefficient is denoted by κ [m^{-1}] and G is the incident heat flux (kW/m^2) from the cone heater.

$$\ddot{q}_{rad} = G \cdot exp(-\kappa x) \quad [33]$$

The above set of equations [30-33] account for the possibilities to increase the model complexity and incorporate other physical effects during material thermal decomposition. However, in this study to maintain the simplicity of the model, the calculations are limited to equations presented in section 4.3. The reader is apprised about the more complex modelling framework in view of other physical effects that may be included in future for description of combined heat and mass transfer effects in the material.

7 Conclusions

The topic of the thesis was to improve prediction of fire performance of polymeric materials using numerical modelling and simulation tools. The fire behaviour of polymeric materials has been studied using microscale and bench scale experimental techniques. The work shows how numerical modelling and simulation techniques are used on microscale and bench scale level to study material fire behaviour on respective length scales. The appended research papers along with this document aim to address the research objectives presented in the introductory part of the document.

- The first research objective was to investigate some of the main techniques used for evaluation of fire properties of polymeric materials. This area has been mainly addressed in chapter three of this document, where the construction and working principle of some of the main devices (STA, MCC, and Cone calorimeter) have been discussed. Additionally, these devices have been used in the current research work to obtain experimental data shown in the appended publications. The findings show the material properties acquired by these devices play a vital role in fire performance assessment of materials, provide input data to pyrolysis models and aid in comparison of results with the simulation runs.

- The second research objective was to seek which numerical models and simulation techniques were suitable to predict fire behaviour of polymeric materials. This was mainly accomplished in scanning the scientific literature related to one dimensional comprehensive pyrolysis model. The works of Ghorbani et al. [33], Stoliarov et al. [26]. and Girardin et al. [27] were found to be useful in developing the understanding of current level of complexity being incorporated in models developed within last few years. The list of the models reviewed is not limited to only those mentioned above but other research works were also referred as shown in the references enclosed and the appended papers. The chemical kinetic models used as sub-grid models in this study were the main focus of research, as it was considered one of the most significant area of improvement, also highlighted in some of the sensitivity studies found in literature [91]. Literature study shows that a large number of kinetic models exist in the research domain. Among them, iso-conversional

methods of analysing thermal decomposition data was found to be widely accepted way of treating it at first stage for simple materials exhibiting single step reactions. The review paper by Vyazovkin et al. [46] drafted under the guidelines of International Confederation for Thermal Analysis and Calorimetry (ICTAC) was used as a yardstick to develop the analysis further and explore new models for complex materials. The main issues identified in the currently existing kinetic models was to specify the reaction mechanism of investigated material and the difficulties in incorporating multiple reactions as a part of comprehensive pyrolysis models. For materials of unknown composition or those with several additives, the ability of specifying a reaction mechanism is challenging if not straightforward. Hence, the issue has been mainly addressed in attempts to understand complex kinetic models using the concepts of probability and statistics termed under the broad category of distributed reactivity models (DRM).

- Another aim of the third research objective was to identify gaps in existing models and induct new sub-grid models from closely related combustion literature devoted to the study of reactivity of fossil fuels. For, achieving that aim, different forms of distributed reactivity models (DRM) were identified and their evaluation was performed with the focus on DRM with Gaussian distribution function. This has largely been demonstrated under section 4.5 where algorithm for stand-alone distributed reactivity model has been presented followed by a structured method of performing its sensitivity analysis (Section 5.3.1) on several materials. The main simulation techniques that were found useful to conduct such analysis was fourth order runge kutta solvers for non-stiff and stiff ordinary differential equations. In addition, numerical integration using global adaptive quadrature methods (trapezoidal methods) were found to be useful to study the reactivity of materials towards thermal decomposition profiles.

- Overall, the aim for achieving the last research objective was to demonstrate an interlink between microscale and bench scale tests, hence a modified one-dimensional pyrolysis model having the ability to incorporate multiple reactions occurring in the material during the pyrolysis process has been developed. The model takes input values from the tests performed in microscale devices such as MCC, TGA and bomb calorimeter along with thermo-physical parameters (k, ρ, c_p) to predict the results of cone calorimeter. The model has shown satisfactory performance in view of the available experimental resources for the two main polymers. The model has few limitations since it does not address some of the physical phenomenon occurring in the material during pyrolysis process

such as diffusion of pyrolysis gases, intumescence, and radiative heat transfer in porous chars. The developed model is semi-deterministic in nature as some of the parameters required to resolve the model are obtained via parameter estimation method. The main simulation techniques that were found to be useful to conduct such analysis were solvers based on finite volume method and numerical integration using global adaptive quadrature methods. The development of bench scale model lays the foundation for performing reverse engineering study for parameter estimation for un-characterized materials using suitable optimization algorithms such as Genetic Algorithm, Shuffled Complex Algorithm etc. that may be accomplished in future studies. The main simulation techniques that were relevant for resolving the model were solvers based on finite volume methods (Tridiagonal matrix) for solution of coupled partial differential equations. Additionally other techniques such as interpolation functions based on polynomial fitting, data filtering by means of moving average/Gaussian filters and numerical integration were found to be useful.

8 Future Work

The future work entails inducting the developed model in a CFD code for prediction of fire growth rate in buildings. The work could also be used as a contributory sub-grid model for flame spread prediction applications on intermediate scale level such as the SBI test. It is foreseen the method could be used for other building materials of interest apart from the two main polymers discussed in the bench scale modelling work, which are of commercial importance. In addition, it is envisaged that several refinements are necessary from numerical point of view as a first step to minimize the use of analytical approximations and fully resolve the dependent parameters via numerical simulation in the original form. Further, experimental studies at other heat fluxes levels and polymer thicknesses can institute further confidence in prediction ability of the model when it is simulated in those conditions and compared with test results. Also, new studies related to the variation in the choice of parameter estimation algorithms (such as Genetic algorithm, simulated annealing etc.) other than pattern search may be employed to compare the convergence issues, solution uniqueness in the chemical kinetic studies. Another, aspect is to institute further complexities in the model in a step-by-step method via incorporation of other physical processes as discussed in chapter 6. Future research efforts would significantly strengthen the application aspects of it and allow its deployment for large-scale fire simulation studies. Overall, the results summarized in the appended papers will be useful for practicing fire engineers and researchers involved in the field of fire development and CFD based fire risk assessment of buildings.

9 References

[1] B. Evarts, Fire loss in the United States during 2017, NFPA, Quincy, MA. (2018). https://www.nfpa.org.

[2] National Fire Protection Association, SFPE Engineering Guide to Performance based Fire Protection, (2006).

[3] Technical Committee- ISO/TC 92/SC 4, ISO 23932-1:2018 Fire safety engineering-General principles, (2018), 26. https://www.iso.org/standard/63933.html.

[4] J. Troitzsch, Plastics Flammability Handbook, Carl Hanser Verlag GmbH & Co. KG, München, (2004). doi:10.3139/9783446436695.

[5] A. Alvarez, B. Meacham, N. Dembsey, J. Thomas, Twenty years of performance-based fire protection design: challenges faced and a look ahead, J. Fire Prot. Eng. 23 (2013) 249–276. doi:10.1177/1042391513484911.

[6] European Committee for Standardization (CEN), SS-EN 13501-1 Fire classification of construction products and building elements – Part 1: Classification using data from reaction to fire tests, (2019). https://www.sis.se.

[7] International Organization of Standardization (ISO), EN ISO 1716 Reaction to fire tests for products - Determination of gross heat of combustion (calorific value), (2010) 26. https://www.iso.org/standard/45780.html.

[8] International Organization of Standardization (ISO), EN ISO 1182 Reaction to fire tests for products - Non-combustibility test, (2010) 32. https://www.iso.org/standard/45779.html.

[9] European Committee for Standardization (CEN), SS-EN 13823 Reaction to fire tests for building products – Building products excluding floorings exposed to the thermal attack by a single burning item, (2014). https://www.sis.se.

[10] International Organization of Standardization (ISO), SS-ISO 9705-1 Room corner test for wall and ceiling lining products - Part 1: Test method for a small room configuration, (2016) 42. https://www.iso.org/standard/59895.html.

[11] European Committee for Standardization (CEN), EN ISO 11925-2 Reaction to fire tests–Ignitability of products subjected to direct impingement of flame–Part 2: Single-flame source test, (2010). https://www.iso.org/standard/45782.html.

[12] European Committee for Standardization (CEN), EN ISO 9239-1 Reaction to fire tests for floorings - Part 1 : Determination of the burning behaviour using a radiant heat source, (2002) 27. https://www.iso.org/standard/45781.html.

[13] International Organization of Standardization (ISO), ISO 5660-1 Reaction-to-fire tests -- Heat release, smoke production and mass loss rate - Part 1: Heat release rate (cone calorimeter method) and smoke production rate (dynamic measurement), (2015). https://www.iso.org/standard/57957.html.

[14] European Committee for Standardization (CEN), SS-EN 1363-1 Fire resistance tests–Part 1: General Requirements, (2012) 64. https://www-sis-se.ludwig.lub.lu.se/en/sok/?q=en+1363&_t_dtq=true.

[15] European Committee for Standardization (CEN), SS-EN 13501-2 Fire classification of construction products and building elements - Part 2: Classification using data from fire resistance tests, excluding ventilation services, (2016) 56. https://www.sis.se.

[16] K.B. McGrattan, S. Hostikka, R. Mcdermott, J. Floyd, Fire Dynamics Simulator Technical Reference Guide Volume 1: Mathematical Model (FDS6.7.1-0-g14cc738), (2019). https://pages.nist.gov/fds manuals.html.

[17] Ying Zhen Li, C. Huang, J. Anderson, R. Svensson, H. Ingason, B. Husted, M. Runefors, J. Wahlqvist, Verification, validation and evaluation of FireFOAM as a tool for performance design, (2017) 84. http://www.diva-portal.org/smash/record.jsf?pid=diva2:1166638.

[18] U. Wickström, E. Sterner, Tasef: Temperature analysis of structures exposed to fire, (1990). http://www.diva-portal.org/smash/record.jsf?pid=diva2%3A961683&dswid=-3529.

[19] S. Stoliarov, R.Lyon, Thermo-Kinetic Model of Burning for

Pyrolyzing Materials, Fire Saf. Sci. 9 (2008) 1141–1152. doi:10.3801/IAFSS.FSS.9-1141.

[20] A.Y. Snegirev, Generalized approach to model pyrolysis of flammable materials, Thermochim. Acta. 590 (2014) 242–250. doi:10.1016/j.tca.2014.07.009.

[21] K.B. McGrattan, S. Hostikka, R. Mcdermott, J. Floyd, M. Vanella, Fire Dynamics Simulator Technical Reference Guide (FDS6.7.1-0-g14cc738) Volume 3: Validation, 3 (2019). https://pages.nist.gov/fds/manuals.html.

[22] American Society for Testing and Materials, ASTM E1355-12(2018), Standard Guide for Evaluating the Predictive Capabilities of Deterministic Fire Models, (2004). doi:10.1520/E1355-12R18.

[23] K. Livkiss, B. Andres, A. Bhargava, P. van Hees, Characterization of stone wool properties for fire safety engineering calculations, J. Fire Sci. 36 (2018) 202–223. doi:10.1177/0734904118761818.

[24] European Committee for Standardization (CEN), SS-EN 50399 A 1 Common test methods for cables under fire conditions - Heat release and smoke production measurement on cables during flame spread test - Test apparatus, procedures, results, (2011) 57. https://www-sis-se.ludwig.lub.lu.se/en/sok/?q=en+50399.

[25] C. Lautenberger, C. Fernandez-Pello, Generalized pyrolysis model for combustible solids, Fire Saf. J. 44 (2009) 819–839. doi:10.1016/j.firesaf.2009.03.011.

[26] S.I. Stoliarov, S. Crowley, R.N. Walters, R.E. Lyon, Prediction of the burning rates of charring polymers, Combust. Flame. 157 (2010) 2024–2034. doi:10.1016/j.combustflame.2010.03.011.

[27] A. Witkowski, B. Girardin, M. Försth, F. Hewitt, G. Fontaine, S. Duquesne, S. Bourbigot, T.R. Hull, Development of an anaerobic pyrolysis model for fire retardant cable sheathing materials, Polym. Degrad. Stab. 113 (2015) 208–217. doi:10.1016/j.polymdegradstab.2015.01.006.

[28] L.B. Valencia, Experimental and numerical investigation of the thermal decomposition of materials at three scales application to polyether polyurethane foam used in upholstered furniture, ISAE-ENSMA Ecole Nationale Superieure de Mecanique et d'Aerotechique-Poitiers, France, 2010. (PhD Thesis) https://tel.archives-ouvertes.fr/tel-00444898.

[29] S.I. Stoliarov, S. Crowley, R.E. Lyon, G.T. Linteris, Prediction of the burning rates of non-charring polymers, Combust. Flame. 156 (2009) 1068–1083. doi:10.1016/j.combustflame.2008.11.010.

[30] A.Y. Snegirev, V.A. Talalov, V.V. Stepanov, J.N. Harris, A new model to predict pyrolysis, ignition and burning of flammable materials in fire tests, Fire Saf. J. 59 (2013) 132–150. doi:10.1016/j.firesaf.2013.03.012.

[31] D.M. Marquis, M. Pavageau, E. Guillaume, C. Chivas-Joly, Modelling decomposition and fire behaviour of small samples of a glass-fibre-reinforced polyester/balsa-cored sandwich material, Fire Mater. 37 (2013) 413–439. doi:10.1002/fam.2136.

[32] D.M. Marquis, M. Pavageau, E. Guillaume, Multi-scale simulations of fire growth on a sandwich composite structure, J. Fire Sci. 31 (2013) 3–34. doi:10.1177/0734904112453010.

[33] Z. Ghorbani, R. Webster, M. Lázaro, A. Trouvé, Limitations in the predictive capability of pyrolysis models based on a calibrated semi-empirical approach, Fire Saf. J. 61 (2013) 274–288. doi:10.1016/j.firesaf.2013.09.007.

[34] C. Di Blasi, The state of the art of transport models for charring solid degradation, Polym. Int. 49 (2000) 1133–1146. doi:10.1002/1097-0126(200010)49:10<1133::AID-PI519>3.0.CO;2-E.

[35] P. Van Hees, Simulation of Fire Technical Properties of Products and Construction Barriers to Support Fire Safety Engineering - The Fire Tools Project, (2013). http://www.eurofireconference.com/html/programme.htm.

[36] B. Andres, K. Livkiss, J.P. Hidalgo, P. van Hees, L. Bisby, N. Johansson, A. Bhargava, Response of stone wool–insulated building barriers under severe heating exposures, J. Fire Sci. 36 (2018) 315–341. doi:10.1177/0734904118783942.

[37] P. Van Hees, F. Guay, A. Bhargava, K. Wilkens, K. Livkiss, B.A. Valliente, D. Lauridsen, F.V. Lundstrom, Simulation of fire technical properties of products and construction barriers to support efficient product developement in industry, Interflam 2013. (2013). www.intersciencecomms.co.uk.

[38] ASTM E698 - 18 Standard Test Method for Kinetic Parameters for Thermally Unstable Materials Using Differential Scanning Calorimetry and the Flynn/Wall/Ozawa Method, (n.d.). doi:10.1520/E0698-18.

[39] ASTM E1641 - 16 Standard Test Method for Decomposition Kinetics by Thermogravimetry Using the Ozawa/Flynn/Wall Method, (2016). doi:10.1520/E1641-18.

[40] P.J. Haines, M. Reading, F.W. Wilburn, Differential Thermal Analysis and Differential Scanning Calorimetry, Handb. Therm. Anal. Calorim. 1 (1998) 279–361. doi:10.1016/S1573-4374(98)80008-3.

[41] R. Lyon, N. Walters, S. Stoliarov, N. Safronava, Principles and practice of microscale combustion calorimetry, (2014). https://www.fire.tc.faa.gov/pdf/TC-12-53.pdf.

[42] A. Bhargava, P. Van Hees, B. Husted, A.R. Junior, C. Neumeister, Performance analysis of a heat transfer and sub-grid chemical reaction distributed activation energy model for fire simulations, J. Fire Sci. 37 (2019) 18–46. doi:10.1177/0734904118808009.

[43] A. Bhargava, P. van Hees, B. Andersson, Pyrolysis modeling of PVC and PMMA using a distributed reactivity model, Polym. Degrad. Stab. 129 (2016) 199–211. doi:10.1016/j.polymdegradstab.2016.04.016.

[44] A. Bhargava, B. Andersson, P. Van Hees, H. Sina, S. Iyengar, S. Technology, Distributed Reactivity Model to Predict Multistage Pyrolysis of Polymeric Materials and Sensitivity Analysis, Interflam 2016, 14th Int. Conf. Fire Sci. Eng. (2016) 107–118.

[45] A. Bhargava, P. Van Hees, Pyrolysis Modelling of PVC Using Distributed Activation Energy Model- Micro Scale Testing, Appl. Struct. Fire Eng. (2016) 448. doi:10.14311/asfe.2015.071.

[46] S. Vyazovkin, A.K. Burnham, J.M. Criado, L. a. Pérez-Maqueda, C. Popescu, N. Sbirrazzuoli, ICTAC Kinetics Committee recommendations for performing kinetic computations on thermal analysis data, Thermochim. Acta. 520 (2011) 1–19. doi:10.1016/ j.tca.2011.03.034.

[47] B. Janković, Kinetic analysis of the nonisothermal decomposition of potassium metabisulfite using the model-fitting and isoconversional (model-free) methods, Chem. Eng. J. 139 (2008) 128–135. doi:10.1016/j.cej.2007.07.085.

[48] B. Janković, B. Adnadević, J. Jovanović, Application of model-fitting and model-free kinetics to the study of non-isothermal dehydration of equilibrium swollen poly (acrylic acid) hydrogel: Thermogravimetric analysis, Thermochim. Acta. 452 (2007) 106–115.

doi:10.1016/j.tca.2006.07.022.

[49] H.L. Friedman, Kinetics of thermal degradation of char-forming plastics from thermogravimetry. Application to a phenolic plastic, J. Polym. Sci. Part C Polym. Symp. 6 (2007) 183–195. doi:10.1002/ polc.5070060121.

[50] T. Akhaira, Method of determinig activation deterrioration constant of electrical insulating materials, (1971) 22–31.

[51] H.E. Kissinger, Reaction Kinetics in Differential Thermal Analysis, Anal. Chem. 29 (1957) 1702–1706. doi:10.1021/ac60131a045.

[52] J.H. Flynn, The'Temperature Integral'—Its use and abuse, Thermochim. Acta. 300 (1997) 83–92. doi:10.1016/S0040-6031(97)00046-4.

[53] J.J.M. Órfão, Review and evaluation of the approximations to the temperature integral, AIChE J. 53 (2007) 2905–2915. doi:10.1002/aic.11296.

[54] J. Cai, W. Yi, F. He, F. Yao, Obtaining a new approximation for temperature integral by using pattern search method, Chem. Bull. 69 (2006) 272–276.

[55] A.A. Jain, A. Mehra, V. V Ranade, Processing of TGA data : Analysis of isoconversional and model fitting methods, Fuel. 165 (2016) 490–498. doi:10.1016/j.fuel.2015.10.042.

[56] J. Zhang, T. Chen, J. Wu, J. Wu, Multi-Gaussian-DAEM-reaction model for thermal decompositions of cellulose, hemicellulose and lignin: comparison of N2 and CO2 atmosphere., Bioresour. Technol. 166 (2014) 87–95. doi:10.1016/j.biortech.2014.05.030.

[57] J. Cai, W. Wu, R. Liu, G.W. Huber, A distributed activation energy model for the pyrolysis of lignocellulosic biomass, Green Chem. 15 (2013) 1331. doi:10.1039/c3gc36958g.

[58] R.M. Lewis, V. Torczon, Pattern Search Algorithms for Bound Constrained Minimization, SIAM J. Optim. 9 (1999) 1082–1099. doi:10.1137/S1052623496300507.

[59] M. Chaos, M.M. Khan, N. Krishnamoorthy, J.L. de Ris, S.B. Dorofeev, Evaluation of optimization schemes and determination of solid fuel properties for CFD fire models using bench-scale pyrolysis tests, Proc.

Combust. Inst. 33 (2011) 2599–2606. doi:10.1016/j.proci.2010.07.018.

[60] R. Hooke, T.A. Jeeves, "Direct Search''' Solution of Numerical and Statistical Problems," J. ACM. 8 (1961) 212–229. doi:10.1145/321062.321069.

[61] S.K. Rao, R. Imam, K. Ramanathan, S. Pushpavanam, Sensitivity Analysis and Kinetic Parameter Estimation in a Three Way Catalytic Converter, Ind. Eng. Chem. Res. 48 (2009) 3779–3790. doi:10.1021/ie801244w.

[62] W.T. Ramroth, P. Krysl, R.J. Asaro, Sensitivity and uncertainty analyses for FE thermal model of FRP panel exposed to fire, Compos. Part A Appl. Sci. Manuf. 37 (2006) 1082–1091. doi:10.1016/j.compositesa.2005.01.031.

[63] J. Cai, W. Wu, R. Liu, Sensitivity analysis of three-parallel-DAEM-reaction model for describing rice straw pyrolysis, Bioresour. Technol. 132 (2013) 423–426. doi:10.1016/j.biortech.2012.12.073.

[64] J. Cai, W. Wu, R. Liu, An overview of distributed activation energy model and its application in the pyrolysis of lignocellulosic biomass, Renew. Sustain. Energy Rev. 36 (2014) 236–246. doi:10.1016/j.rser.2014.04.052.

[65] P. J DiNenno, D. Drysdale, The SFPE Handbook of Fire Protection Engineering, (2008). https://www.sfpe.org/page/Handbook5thEdition.

[66] R. Lyon, J.G. Quintiere, Criteria for piloted ignition of combustible solids, Combust. Flame. 151 (2007) 551–559. doi:10.1016/j.combustflame.2007.07.020.

[67] R. Miranda, J. Yang, C. Roy, C. Vasile, Vacuum pyrolysis of commingled plastics containing PVC. I. Kinetic study, Polym. Degrad. Stab. 72 (2001) 469–491. doi:10.1016/S0141-3910(01)00048-9.

[68] I.C. McNeill, L. Memetea, W.J. Cole, A study of the products of PVC thermal degradation, Polym. Degrad. Stab. 49 (1995) 181–191. doi:10.1016/0141-3910(95)00064-S.

[69] C.-H. Wu, C.-Y. Chang, J.-L. Hor, S.-M. Shih, L.-W. Chen, F.-W. Chang, Two-Stage pyrolysis model of PVC, Can. J. Chem. Eng. 72 (1994) 644–650. doi:10.1002/cjce.5450720414.

[70] C. Huggett, B.C. Levin, Toxicity of the pyrolysis and combustion

products of poly(vinyl chlorides): A literature assessment, Fire Mater. 11 (1987) 131–142. doi:10.1002/fam.810110303.

[71] A. Matala, S. Hostikka, Pyrolysis modeling of PVC cable materials, Fire Saf. Sci. (2011) 917–930. doi:10.3801/IAFSS.FSS.10-917.

[72] G.M. Anthony, Kinetic and chemical studies of polymer cross-linking using thermal gravimetry and hyphenated methods. Degradation of polyvinylchloride, Polym. Degrad. Stab. 64 (1999) 353–357. doi:10.1016/S0141-3910(98)00129-3.

[73] P.E. Sánchez-Jiménez, A. Perejón, J.M. Criado, M.J. Diánez, L. a. Pérez-Maqueda, Kinetic model for thermal dehydrochlorination of poly(vinyl chloride), Polymer (Guildf). 51 (2010) 3998–4007. doi:10.1016/j.polymer.2010.06.020.

[74] A. Perejón, P.E. Sánchez-Jiménez, J.M. Criado, L. a Pérez-Maqueda, Kinetic analysis of complex solid-state reactions. A new deconvolution procedure., J. Phys. Chem. B. 115 (2011) 1780–1791. doi:10.1021/jp110895z.

[75] L.E. Manring, D.Y. Sogah, G.M. Cohen, Thermal Degradation of Poly(methyl methacrylate). 3. Polymer with Head-to-Head Linkages, Macromolecules. 22 (1989) 4652–4654. doi:10.1021/ma00202a048.

[76] M.L. Janssens, Challenges in Predicting the Pyrolysis Rate of Solid Materials, Fire Mater. 2015 - 14th Int. Conf. Exhib. (2015) 271–284.

[77] T. Kashiwagi, Polymer combustion and flammability—Role of the condensed phase, Symp. Combust. 25 (1994) 1423–1437. doi:10.1016/S0082-0784(06)80786-1.

[78] M. Ferriol, a. Gentilhomme, M. Cochez, N. Oget, J.L. Mieloszynski, Thermal degradation of poly(methyl methacrylate) (PMMA): modelling of DTG and TG curves, Polym. Degrad. Stab. 79 (2003) 271–281. doi:10.1016/S0141-3910(02)00291-4.

[79] L.E. Manring, Thermal degradation of saturated poly(methyl methacrylate), Macromolecules. 21 (1988) 528–530. doi:10.1021/ma00180a046.

[80] A. Rodolfo, L.H. Innocentini-Mei, Poly(vinyl chloride)/metallic oxides/organically modified montmorillonite nanocomposites: Preparation, morphological characterization, and modeling of the mechanical properties, J. Appl. Polym. Sci. 116 (2010) 422–432.

doi:10.1002/app.31442.

[81] F. Hewitt, D.E. Rhebat, A. Witkowski, T.R. Hull, An experimental and numerical model for the release of acetone from decomposing EVA containing aluminium, magnesium or calcium hydroxide fire retardants, Polym. Degrad. Stab. 127 (2016) 65–78. doi:10.1016/j.polymdegradstab.2016.01.007.

[82] C.C. Lakshmanan, N. White, A New Distributed Activation Energy Model Using Weibull Distribution for the Representation of Complex Kinetics, Energy & Fuels. 8 (1994) 1158–1167. doi:10.1021/ef00048a001.

[83] B. Girardin, G. Fontaine, S. Duquesne, M. Försth, S. Bourbigot, Characterization of Thermo-Physical Properties of EVA/ATH: Application to Gasification Experiments and Pyrolysis Modeling, Materials (Basel). 8 (2015) 7837–7863. doi:10.3390/ma8115428.

[84] B. Girardin, G. Fontaine, S. Duquesne, M. Försth, S. Bourbigot, Measurement of kinetics and thermodynamics of the thermal degradation for flame retarded materials: Application to EVA/ATH/NC, J. Anal. Appl. Pyrolysis. 124 (2017) 130–148. doi:10.1016/j.jaap.2016.12.034.

[85] N.A. Dembsey, P.J. Pagni, R.B. Williamson, Compartment fire near-field entrainment measurements, Fire Saf. J. 24 (1995) 383–419. doi:10.1016/0379-7112(95)00030-5.

[86] A. Kacem, M. Mense, Y. Pizzo, G. Boyer, S. Suard, P. Boulet, G. Parent, B. Porterie, A fully coupled fluid/solid model for open air combustion of horizontally-oriented PMMA samples, Combust. Flame. 170 (2016) 135–147. doi:10.1016/j.combustflame.2016.04.009.

[87] D. Hopkins, J.G. Quintiere, Material fire properties and predictions for thermoplastics, Fire Saf. J. 26 (1996) 241–268. doi:10.1016/ S0379-7112(96)00033-1.

[88] N.G. Shimpi, J. Verma, S. Mishra, Dispersion of nano CaCO3on PVC and its influence on mechanical and thermal properties, J. Compos. Mater. 44 (2010) 211–219. doi:10.1177/0021998309344637.

[89] F.-Y. Hshieh, H.D. Beeson, Note: measuring the effective heats of combustion of transformer-insulating fluids using a controlled-atmosphere cone calorimeter, Fire Mater. 26 (2002) 47–49. doi:10.1002/fam.778.

[90] A. Snegirev, V. Talalov, V. Stepanov, J. Harris, A new model to predict multi-stage pyrolysis of flammable materials in standard fire tests, J. Phys. Conf. Ser. 395 (2012) 012012. doi:10.1088/1742-6596/395/1/012012.

[91] M. Chaos, Application of sensitivity analyses to condensed-phase pyrolysis modeling, Fire Saf. J. 61 (2013) 254–264. doi:10.1016/j.firesaf.2013.09.016.

Paper I

Polymer Degradation and Stability 129 (2016) 199–211

Contents lists available at ScienceDirect

Polymer Degradation and Stability

journal homepage: www.elsevier.com/locate/polydegstab

Pyrolysis modeling of PVC and PMMA using a distributed reactivity model

Abhishek Bhargava [a, b, *], Patrick van Hees [b], Berit Andersson [b]

[a] Danish Institute of Fire and Security Technology, Jernholmen 12, DK-2650, Hvidovre, Denmark
[b] Division of Fire Safety Engineering, Lund University, P.O Box 118, SE-22100, Lund, Sweden

ARTICLE INFO

Article history:
Received 17 December 2015
Received in revised form
15 April 2016
Accepted 24 April 2016
Available online 25 April 2016

Keywords:
Pyrolysis modeling
Thermal degradation
Fire behavior
Distributed activation energy model (DAEM)

ABSTRACT

The thermal decomposition kinetics of poly(vinyl chloride) (PVC) and poly(methyl methacrylate) (PMMA) was studied by thermogravimetry using non isothermal experiments. A detailed kinetic analysis was done using the isoconversional methods (model-free) (including Friedman, Kissinger-Akhaira-Sunose (KAS) and Kissinger methods) and distributed reactivity model (model-fitting). The overall aim was to retrieve kinetic parameters of the model describing the differential thermogravimetric (DTG) curve. For distributed reactivity models, both double and multi-Gaussian methods were used to explain the thermal decomposition process in these polymers. Apparent kinetic parameters were retrieved using optimization calculations with a newly developed computer code using MATLAB® involving pattern search algorithm. Modeling results were compared with the experimental data obtained in a simultaneous thermal analyzer (STA). Agreement between experimental tests and simulations showed good results for fire modeling applications for these polymers.

1. Introduction

In the last couple of decades, there has been an increase in the production of polymeric plastic materials on a global scale. The world plastic production is estimated to have reached 299 million tons in the year 2013 as compared to 204 million tons in 2002 [1]. In Europe, building and construction sector is the second largest application area, this constitutes 20.3% of the total plastic demand. Traditional materials such as bricks, concrete, glass, cement and wood now have plastic alternatives due to their excellent physical properties. The main advantages of using plastics are durability, low maintenance costs, corrosion resistance and good insulation properties. PVC and PMMA are two of the many polymers used in this sector. PVC is used in piping work, electrical cabling, roof sealing, floor, wall and ceilings coverings and window profiling. PMMA is used as a lightweight replacement for glass and finds applications in doors, windows, canopies, balustrades and illumination applications. Other polymers used in modern buildings for insulation purpose include poly(urethanes) (PUR), poly(isocyanurate) (PIR), expanded poly(styrene) (EPS), extruded poly(styrene) (XPS). Fire safety of such polymers is an important issue. In case of fire, the heat released and toxic smoke produced poses a potentially fatal hazard to the building occupants. Hence, many studies deal with the thermal degradation of polymers to assess their suitability for real life applications.

Computer simulation on the fire behavior of plastic materials has gained significant attention in the last decade [2]. There has been an increasing number of studies demonstrating that one-dimensional numerical pyrolysis models can be used to predict the outcomes of a standard cone calorimeter test (ISO 5660) [3–5]. One of the main sub-models used in such calculations is the chemical kinetic model. Its function is to mathematically describe the mass loss rate (MLR) and heat generated in the material due to ongoing chemical reactions leading to conversion of solid mass into volatiles, char and smoke. It enables the modeling of the chemical heat source term for the overall solution of the heat transfer equation. The chemical kinetic model and the heat transfer equation are solved simultaneously to compute the heat release rate (HRR) from the material subject to appropriate boundary conditions. The current state of the art methodology for retrieving kinetic input parameters for fire simulation is to perform microscale thermogravimetric analysis (TGA) on the sample followed by computations using isoconversional (model free) or non-linear

* Corresponding author. Danish Institute of Fire and Security Technology, Jernholmen 12, DK-2650, Hvidovre, Denmark.
E-mail addresses: abhishekk.bhargava@gmail.com, abb@dbi-net.dk (A. Bhargava).

http://dx.doi.org/10.1016/j.polymdegradstab.2016.04.016
0141-3910/

least square (model fitting approach) [6,7]. Retrieved kinetic parameters can be used as input values for the overall solution of the pyrolysis model. Several studies have shown that, there are a number of chemical kinetic models available in the literature to describe different types of chemical reactions occurring in solids e.g. power laws, nucleation and diffusion models [6]. As a consequence of this, the results vary considerably from one study to another for the same set of materials depending upon the choice of the reaction model [8–11]. Stoliarov et al. [4] found that the extent of this variation leads to discrepancies in the prediction of HRR and its magnitude was found to be far more in case of charring polymers than the non-charring ones. They further add that the main cause for such discrepancies is the gap in the understanding of the thermo-chemistry of different materials. The FIRETOOLS project investigates the possibilities to predict real scale fire behavior of building products, content and barriers by means of using material data on successively increasing scales [12].

Recently, two different studies were conducted by Vyazovkin et al. [13,14] which aim to provide recommendations for collecting experimental thermal analysis data and perform kinetic computations on them. It provides a pragmatic approach to perform kinetic model fitting calculations. For materials, degrading in single step, isoconversional methods were recommended, while for materials degrading in multiple reaction steps non-linear regression methods and distributed reactivity models were suggested. In this study a preliminary analysis using isoconversional methods was performed followed by a detailed analysis using distributed reactivity concept.

The main aim of this study is to compare the quantitative aspects of the thermal decomposition process in two different polymer specimens (PVC and PMMA) by employing isoconversional approaches and multiple step parallel reaction models. Previous studies have shown that these materials decompose in two or more steps [9–11,15,16]. Therefore, a distributed activation energy model (DAEM) was considered for this study. It is one of the more comprehensive pyrolysis models that has been applied to complex materials such as coal, biomass and sewage sludge, all of which exhibit thermal decomposition in multiple reaction steps [17–21]. As newly manufactured plastics become increasingly complex due to impregnation of several additives and flame-retardants, it is important to investigate the multiple reactions occurring in them during the pyrolysis process. In the first part of the study, TG analysis is undertaken, while in the second part; results of kinetic simulations are presented. The modelling results are compared with the test results from the TG and DTG curves.

2. Theory

2.1. DAEM model

The main assumption in the DAEM reaction model is the thermal degradation of material occurs in multiple parallel overlapping steps. Each reaction step is assumed to consist of an infinite number of simultaneously occurring parallel reactions having different activation energies (E_a) and frequency factors (k_o). In this study, the distribution function of the activation energy has been modeled by a Gaussian function. Recently, Cai et al. [22] and Zhang et al. [20,23,24] have applied this model to explain pyrolysis kinetics of biomass and municipal solid waste but very few studies are reported regarding its application to fire behavior of building materials. In a previous study Bhargava et al. [25,26] used this concept in the form of distribution free approach, however in this study the distribution fitting approach is used.

DAEM uses the thermal decomposition data obtained in a dynamic TG experiment to retrieve the chemical kinetic parameters using an optimization technique. For non-isothermal TGA runs, where temperature is a linear function of time, the temperature function can be modelled as equation (1), where T is the absolute temperature (K), β is the heating rate (K/s) and t is the time (s).

$$T(t) = T_0 + \beta x t \tag{1}$$

The degree of conversion for a sample material is calculated by equation (2). In this equation, α (T) is the degree of conversion at temperature T (K), m_0 (mg) is the initial weight, m_T (mg) is the weight at temperature T (K) and m_f (mg) is the final weight

$$\alpha(T) = \frac{m_0 - m_T}{m_0 - m_f} \tag{2}$$

$$\alpha(T) = \int_0^{\infty} \{1 - \varphi(E_a, T)\} \text{ x } f(E_a) \text{ x } dE_a \tag{3}$$

$$\varphi(E_a, T) = \exp\left(\frac{-k_0}{\beta} \int_0^{T} e^{-E_a/RT}\, dT\right) \tag{4}$$

$$f(E_a) = \frac{1}{\sigma\sqrt{2\pi}} \exp\left[-\frac{E_a - E_{a0}}{2\sigma^2}\right] \tag{5}$$

Equations (3)–(5) show the change in amount of volatiles represented in the terms of DAEM model. In equation (3), $\varphi(E_a,T)$ is the term comprising of temperature integral and $f(E_a)$ is the probability distribution function of the activation energies having the conversion at temperature T (K). In equation (4), k_0 (1/s) is the pre-exponential factor corresponding to the activation energy value, E_a (kJ/mol), β (K/s) is the heating rate, R is the real gas constant having a fixed value of 8.314×10^{-3} kJ mol^{-1} K^{-1}. In equation (5), E_{a0} (kJ/mol) is the mean activation energy and σ (kJ/mol) is the standard deviation. The derivative form of equation (3) can be written as shown in equation (6)

$$\frac{d\alpha(T)}{dT} = \frac{1}{\sigma\sqrt{2\pi}} \int_0^{\infty} \frac{k_0}{\beta} \exp\left[-\frac{E_a}{RT} - \frac{k_0}{\beta} \int_0^{T} \exp\left(-\frac{E_a}{RT}\right) dT - \frac{(E_a - E_{a0})^2}{2\sigma^2}\right] dE_a \tag{6}$$

Previous studies [21,27–30] have shown that other forms of DAEM equation exist in the literature in which the distribution of activation energy is modeled using several forms of probability distribution functions such as weibull, logistic or delta dirac distribution. The primary reason for such an assumption is the fact that activation energies of real materials are rarely symmetric. Hence, other types of distributions are discussed to account for asymmetry. Other authors have also considered single nth order DAEM equation instead of first order assumption [30,31]. However, for simplicity the analysis in this work is based on the assumption of first order having Gaussian distribution of activation energies.

Since there is no analytical solution for the inner temperature integral (dT) in equation (6), a large number of approximations that intend to approximate the values of temperature integral have been discussed in the literature [32,33]. But numerical integration for its evaluation is preferred. Hence, in our computations we have used adaptive quadrature method to evaluate the temperature integral. The algorithm of evaluation of DAEM is shown in the flowcharts below (Figs. 1 and 2).

The two ways of evaluation depend upon the choice of equation used for the formulation of the objective function (O.F.) by the

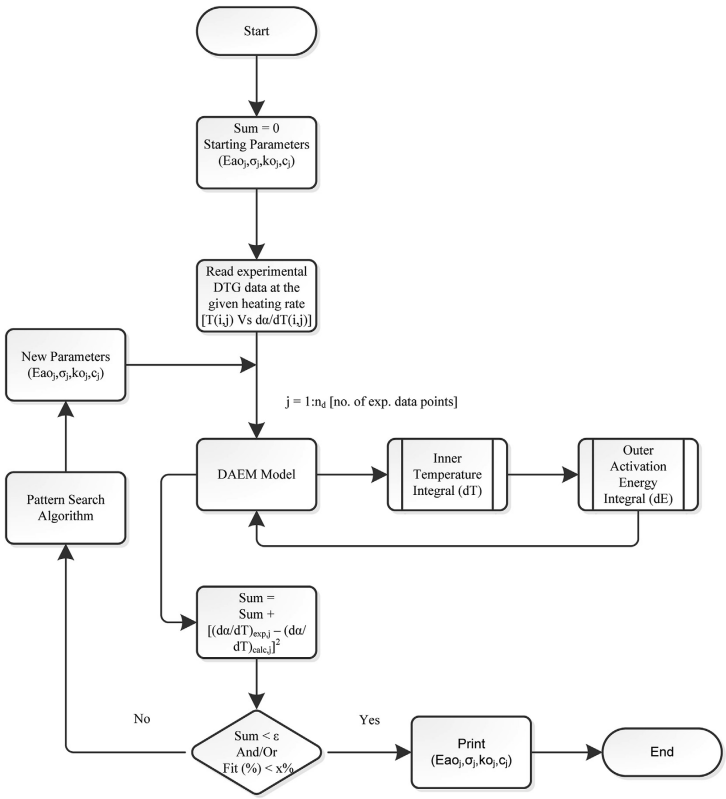

Fig. 1. Algorithm for DAEM evaluation using non-linear least square minimization using a single experiment at one heating rate showing a simplistic minimization procedure.

modeler. In this work we have considered both the formulations (simple and rigorous) for analysis. The simple formulation and corresponding fitness is shown in equations (7) and (8) respectively. In this case the minimization is performed for a single TG experiment conducted at one heating rate.

$$O.F = \sum_{j=1}^{n_d} \left[\left(\frac{d\alpha(T)}{dT}_{exp,j} \right) - \left(\frac{d\alpha(T)}{dT}_{cal,j} \right) \right]^2 \tag{7}$$

$$Fit(\%) = 100 * \frac{\left(\sqrt{\frac{O.F}{n_d}} \right)}{\left(\frac{d\alpha(T)}{dT} \right)_{exp,max}} \tag{8}$$

On the other hand a more rigorous form of the O.F. is shown in equation (9). The corresponding fitness function is given by equation (10). In this case the minimization of the objective function is achieved taking into consideration all the experimental tests performed at different heating rates.

$$O.F. = \sum_{i=1}^{3} \sum_{j=1}^{n_d} \left[\left(\frac{d\alpha}{dT}_{exp,ij} \right) - \left(\frac{d\alpha}{dT}_{cal,ij} \right) \right]^2 \tag{9}$$

$$Fit(\%) = 100 * \frac{\left(\sqrt{\frac{O.F}{n_d}} \right)}{\sum_{j=1}^{3} \frac{d\alpha(T)}{dT}_{exp,max}} \tag{10}$$

The purpose of the O.F. is to minimize the difference between experimental and calculated values of the DTG curve using non-linear least square method for certain chosen values of kinetic parameters. In equations (7) and (9), j is the serial number of the data point used; n_d is the total number of data points logged during the experiment. In equation (9), i = 1 to 3 correspond to experiments at different heating rates (i = 1 represents 5 K/min, i = 2 represents 10 K/min, and i = 3 represents 20 K/min). The term $(d\alpha(T)/dT_{(exp,ij)})$

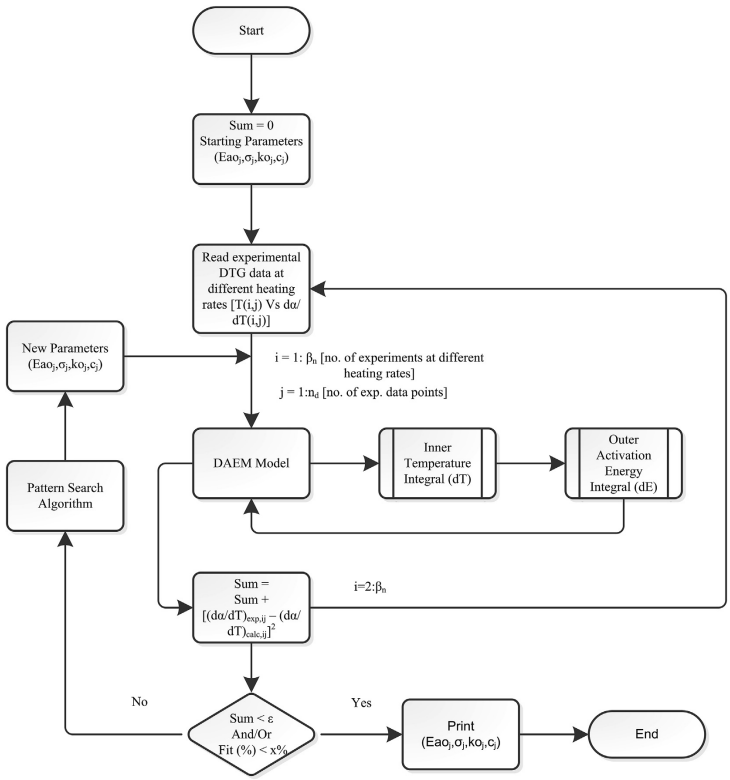

Fig. 2. Algorithm for DAEM evaluation using non-linear least square minimization using a set of three experiments at different heating rates showing a more rigorous minimization procedure.

is the experimental DTG value, while $(d\alpha(T))/dT_{(cal,ij)}$ is the calculated value using equation (6) for a given set of parameters of k_0, E_{a0}, σ. The fitting quality as shown in equations (8) and (10) is based on a previous study by Zhang et al. and Cai et al. [22,24]. A lower value signifies better quality of fitting.

For complex materials decomposing in more than one reaction steps, the single Gaussian model has shown poor fitness quality. There is a significant interest in using multi-Gaussian approach to describe multiple reaction steps and to improve the comprehensiveness of the reaction model. In multi-Gaussian model the overall $d\alpha/dT$ curve is taken as a weighted sum of more than one individual $d\alpha/dT$ curve. Similarly the global $f(E_a)$ curve is a weighted sum of linear combination of individual curves. Hence, equations (5) and (6) are replaced by equations (11) and (12) respectively for the multi-Gaussian fitting. The parameters representing individual weight are denoted by c_j and are also estimated for each reaction in the optimization calculation.

$$f(E_a) = \sum_{1}^{n} c_j f(E_a)_j \tag{11}$$

$$\frac{d\alpha(T)}{dT} = \sum_{1}^{n} c_j \frac{d\alpha_j}{dT} \tag{12}$$

In both equations (11) and (12) c_j physically represents the fraction of volatiles produced by the jth peak and n is the number of peaks. c_j values were estimated between 0 and 1. For overall optimization calculations using this approach four parameters (E_{ao}, σ, k_o, c_j) are optimized corresponding to each reaction step. As the number of assumed reactions increase the number of parameters increase by four folds.

2.2. Solution methodology and parameter estimation

The solution is evaluated using a computer code based on the algorithms presented earlier. The codes work in conjunction with

the optimization toolbox of MATLAB®. It invokes the pattern search algorithm with initial guess parameters (E_{ao}, σ, k_o, c_j) to run the optimization process until a minimum tolerance value in the order 10^{-4} of the objective function is reached. Pattern search is a derivative free direct search subroutine for minimizing the objective function (O.F.). It is considered to be better in terms of robustness and number of function evaluations as compared to other search methods such as Powell method and Simplex method [34]. The arguments of the O.F. are varied until its minimum is obtained. Here this method will be discussed briefly. A detailed account is available in Ref. [35]. In our case, the pattern search routine determines the sequence of values for variables (E_{ao}, σ, k_o, c_j); while the DAEM code computes the functional values of O.F. During the parameter estimation process, successive values of variables are chosen as distinct points in the k dimensional space. For double Gaussian DAEM this value is 8 dimensional while for multi-Gaussian DAEM with four partial reactions, this value is 16 dimensional. The procedure for going from a given point to the next is called a move. This move is termed as a success if the value of objective function decreases; else it is a failure. The first move is exploratory in nature to gain knowledge about variations in the variables leading to a successful move. In each exploratory move only a single variable is changed in a particular direction. The exploratory moves forms a vector base to pursue the search for the arguments in subsequent iterations. The second move is the pattern move, in which the knowledge gained in the exploratory moves is utilized to accomplish the actual minimization of the objective function by moving in the direction of the established pattern. The point from which the pattern move is made is called the base point, and the direct search procedure can be understood as moving from base point to base point. This procedure is repeated until the O.F. value meets the tolerance limit.

2.3. Compensation effect

It is evident from several literature studies [6,27,36,37] that a strong compensation effect exists between pre-exponential factor (k_o) and mean activation energy (E_{a0}). In other words, different pairs of kinetic parameters provide equally good fit to the experimental data. One option was to fix the value of pre-exponential factor (k_0) and estimate the other model parameters (E_{ao}, σ, cj). But, according to Lakshmanan and White [27] for complex reactions such as pyrolysis and combustion it is often difficult to provide a valid justification for fixing pre-exponential factor at an arbitrary value because these are assumed based on different molecular theories. Hence, a fixed value of k_o was not chosen in this study but it was estimated during the optimization process. The range in which these values were estimated was kept in a rather narrow span of 1×10^{14} to 1×10^{22} (1/s) based on experience of [9,10]. For other variables the range of values chosen for the estimation was based on the recommendations of Vyazovkin et al. [14] and Varhgeyi et al. [36]. Candidate values for activation energy (E_a) were chosen between 100 and 350 kJ/mol while for the standard deviation (σ), these values were chosen in the range of 1–50 kJ/mol.

3. Materials and methods

Milligram samples of PVC and PMMA were obtained as reference materials from manufacturers. All experiments were performed in a STA (NETZSCH 449F3) and results have been reported earlier in a study by Matala et al. [38] for PVC and Jannsens et al. [39] for PMMA. The STA enabled simultaneous recording of TG and DTG signals. For each experimental run of PMMA and PVC 10 and 20 mg of sample specimens were used respectively. The samples were placed in the alumina (Al_2O_3) crucible and subjected to different linear heating rates (5, 10, 20 K/min). The experiments were performed by setting the upper limit of the temperature up-to 700 °C. In the STA, nitrogen (N_2) was used as a carrier gas with a flow rate of 40 mL/min. Before measuring each sample, a baseline was recorded using two empty crucibles.

4. Results and discussion

4.1. Thermogravimetric analysis

4.1.1. Poly-vinyl chloride (PVC)

The experimental results obtained from the TG-DTG tests of PVC are shown in Fig. 3. The TG curve (Fig. 3a) shows that weight loss occurs in at least two stages. In the first stage the sample shows a weight loss of 54% (residual weight = 46%), while in the second stage, a further weight loss of 19% is recorded, leading to the final sample residual weight of 27%. The TG curve also shows the appearance of a small plateau between 340 and 420 °C indicating a slight drop in the rate of weight loss during that temperature interval. The DTG curve (Fig. 3b), shows, the first stage of decomposition occurs between 200 and 365 °C while the second stage of decomposition occurs in between 365 °C and 545 °C. The curves show slight sensitivity to the applied heating rate. The DTG curve peaks shift to the right as the heating rate increases. The peaks appear to fall in a very narrow temperature range of 10–15 °C (Fig. 3b). It can be seen from Fig. 3 that main peak temperatures (T_{P1}) increases from 284 °C to 300 °C with increasing heating rate, while the minor peak (T_{P2}) is observed between 461 and 471 °C. These results are consistent with the earlier studies performed by Miranda et al. [10]. For PVC, it is well known that during the first stage of pyrolysis, that mass loss is mainly attributed to the release of hydrogen chloride (HCl) and this phenomenon is termed as dehydro-chlorination. Several authors mentioned that the first stage is a combination of two independent (parallel) reactions associated with head-to-head and head-to-tail linkages [10,11,40]. During this stage small amounts of other aromatic hydrocarbons (e.g. benzene, toluene, xylene and ethyl benzene etc.) and condensed ring aromatics such as naphthalene, anthracene and indene etc. are also evolved. McNiell et al. [40] have explained that most double bonds in such aromatic compounds get accumulated in the polymer to create cross linked network of cyclic compounds in the aliphatic matrix. In the second reaction step these cyclic compounds aromatize via chain scission reactions leading to further weight loss and formation of aliphatic and olefenic, aromatic hydrocarbons and char (see Table 1).

In the past a number of experimental kinetic studies on the thermal decomposition of PVC have been reported [10,11,16,40–42]. Many of the previous research works have shown that PVC degradation occurs in two distinct reaction steps, however it is apparent only from the works of Miranda [10], Wu [11] and Maqueda and Criado [43,44], that DTG curves recorded for PVC have also shown to exhibit three and four distinct peaks. As a consequence, the modeling work for those studies was performed using multiple step reactions through series and parallel kinetic models. The accuracy of these models is very good however, a key issue in these models is to propose a reaction mechanism of the thermal degradation process. For fire engineering work, this is a cumbersome and challenging task. In addition, the profile of the DTG curve is influenced by other factors such as the choice of gas atmosphere in which the TG experiments were performed e.g. N_2, CO_2, O_2, heating rates used and the chemical composition of the polymer. The material shows significantly different reaction profiles under ambient atmosphere due to oxidation reactions as shown by Bhargava et al. [25]. When the reactant gas atmosphere or chemical composition of the material is altered a new reaction mechanism has to be proposed. This task poses a major challenge in

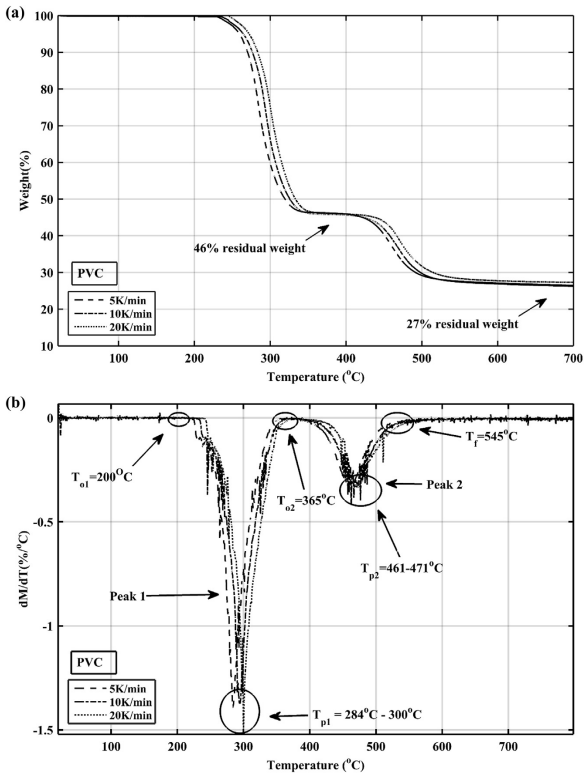

Fig. 3. Experimental TG (above) and DTG (below) curves for PVC in nitrogen at different heating rates.

Table 1
Summary of DTG curves for PVC.

Heating rate	Main peak temperature	$DTG_{(main\ peak)}$	Minor peak temperature	$DTG_{(minor)}$	Residual weight
β (K/min)	T_{P1}/°C	$(dM/dT)_{P1}$	T_{P2}/°C	$(dM/dT)_{P2}$	wt.%
5	284	−1.4	461	−0.3	26
10	295	−1.4	463	−0.4	26
20	300	−1.5	471	−0.3	27

the general implementation of this sub-model to simulate the overall pyrolysis model for HRR predictions for a cone calorimeter test. It is to be noted that for all practical applications the properties of PVC are modified by adding several additives, plasticizers and flame-retardants. The reaction mechanism originally proposed for a specific polymeric composition may not be generalized for a modified material. This problem may be mitigated by using the DAEM approach for the purpose of fire modeling due to its inherent modeling assumptions. In the DAEM model, it is assumed the each reaction step represents infinite number of parallel occurring reactions so the parameters computed are apparent kinetic parameters but not the real ones. Also, there is no need to provide an elaborate reaction mechanism for the degrading polymer, as this may not be of specific interest for fire simulations purposes.

4.1.2. Poly-methyl methacrylate (PMMA)

The TG and DTG curves of PMMA are shown in Fig. 4. The residual weight of the sample at the end of the reaction is negligible (0.4–2%) (Fig. 4a). The weight loss in the PMMA sample seems to occur in one single reaction step. However, in reality it is plausible that this reaction occurs in multiple stages. As shown in Fig. 4b a main broad DTG peak is visible while a minor shoulder peak

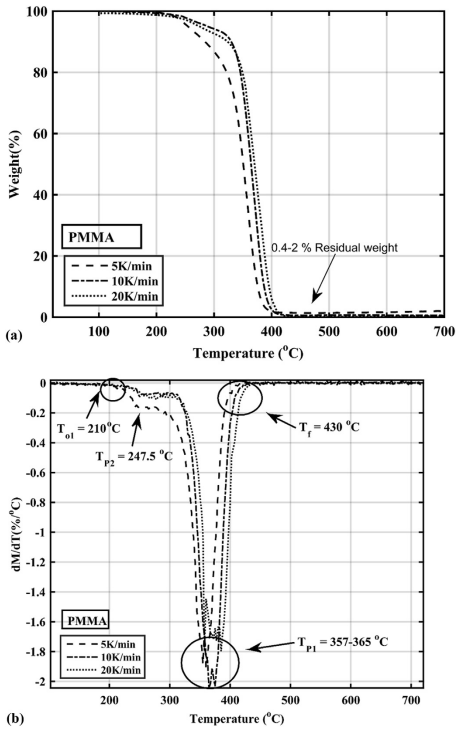

Fig. 4. Experimental TG (above) and DTG (below) curves for PMMA in nitrogen at different heating rates.

appears the left of the main peak, indicating the possibility of more than one reaction occurring during the decomposition process. The onset of the degradation starts at 210 °C and ends at 430 °C. The main DTG peaks for different heating rates for PMMA lie in the range of 357–365 °C. It can be observed from Fig. 4b that the peak temperature increases as the heating rate increases from 5 K/min to 20 K/min. Similar results were reported for PMMA by Ref. [39] (see Table 2).

A great deal of previous research into PMMA has focused on the understanding of thermal degradation mechanism. According to Troitzsch [45], the thermal decomposition of PMMA follows at least two and sometimes three stages by means of reactions occurring at the chain ends and random scission process producing only monomers. It was first shown by Kashiwagi et al. [46] and later by Manring [8] that a radically polymerized sample degrades in three stages. The multi-reaction theory was and later adopted by Ref. [9] for the modeling work. Ferriol et al. [9] have discussed the detailed account of the reaction mechanisms proposed by Refs. [15,46] and implemented that approach into the estimation of reaction model by using non-linear fitting algorithm.

4.2. Kinetic analysis

4.2.1. Isoconversional methods

Vyazovkin and co-workers [47] have suggested that as a apart of any kinetic modeling study it is advisable to perform basic fitting using isoconversional methods. In this analysis, apart from DAEM model, we have used two most commonly practiced isoconversional methods (Friedman and Kissinger-Akhaira-Sunose), along with Kissinger method to calculate the activation energies for the pyrolysis of polymers. The corresponding equations for these methods are shown in Table 3. The detailed discussion of these methods can be found in the cited references.

In all these methods activation energies are calculated by the analysis of multiple curves measured at different heating rates at same level of conversions (α) assuming first order reaction model where $f(\alpha) = (1-\alpha)$ and $g(\alpha) = -\ln(1-\alpha)$. The reason for such an assumption stems from the fact that for most fire simulations, the reaction model is assumed to follow a single first order reaction. It can be seen from Fig. 5 that the spread of activation energy for both polymers as calculated by either of the isoconversional methods (Freidman and KAS) follow a similar trend.

For PVC the values of activation energy (E_a) were found to vary in the range of 235–284 kJ/mol in the conversion range of ($\alpha = 0$–0.6) and later it was found to increase from 240 to 550 kJ/mol in the range of ($\alpha = 0.6$–1). While, for PMMA activation energy (E_a) was found to increase from 50 kJ/mol to 197 kJ/mol in the conversion range of ($\alpha = 0$–0.4), later it was found to follow a constant value at 200 kJ/mol ($\alpha = 0.6$–1). The comparison of the pre-exponential factor (k_0) with respect to the activation energy is shown in Fig. 6. The spread of values for k_0 was found to be same nearly same by the two methods for each polymer. The wide variation in the values of activation energy and appearance of shoulders in DTG curves indicate that the reaction rate curve is not dominated by a single step reaction and cannot be described by a single step model. The best fit among all the methods discussed was obtained by Kissinger method as shown below in Fig. 7. It can be seen that only the main peak of the curves can be approximated to a large extent however, peak shoulders are not reproducible.

Though isoconversional methods do not give us a good match with experimental data, but the kinetic parameters obtained using those values provide us with valuable insights about their range. These values can be used as possible candidates for initiating optimization calculations using model fitting methods (see Table 4).

4.2.2. DAEM model fitting

To improve the accuracy of simulations, we then applied the

Table 2
Summary of DTG curves for PMMA.

Heating rate	Main peak temperature	$DTG_{(main)}$	Minor peak temperature	$DTG_{(minor)}$	Residual weight
β (K/min)	T_{P1}/°C	$(dM/dT)_{P1}$	T_{P2}/°C	$(dM/dT)_{P2}$	wt.%
5	360	−1.9	247	−0.2	2.0
10	364	−2.0	252	−0.1	0.6
20	365	−1.8	262	−0.1	0.4

Table 3
Model equations for isoconversional methods and the Kissinger method.

S. no	Method	Equation	References
1	Friedman	$\ln\left[\beta_i\left(\frac{d\alpha}{dT}\right)_{\alpha,i}\right] = \ln(k_0 f(\alpha)) - \left(\frac{E_\alpha}{RT_{\alpha,i}}\right)$	[48]
2	Kissinger-Akhaira-Sunose (KAS)	$\ln\left(\frac{\beta_i}{T^2_{\alpha,i}}\right) = \ln(\frac{k_0 R}{g(\alpha)E_\alpha}) - \left(\frac{E_\alpha}{RT_\alpha}\right)$	[49]
3	Kissinger	$\ln\left(\frac{\beta_i}{T^2_{max,i}}\right) = \ln\left(-\frac{k_0 R f'(\alpha_{max})}{E_\alpha}\right) - \left(\frac{E}{RT_{max,i}}\right)$	[50]

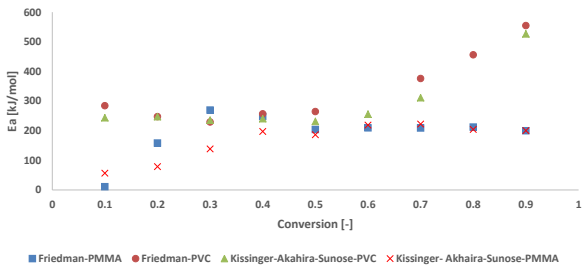

Fig. 5. Spread of activation energy computed using isoconversional methods for PMMA and PVC.

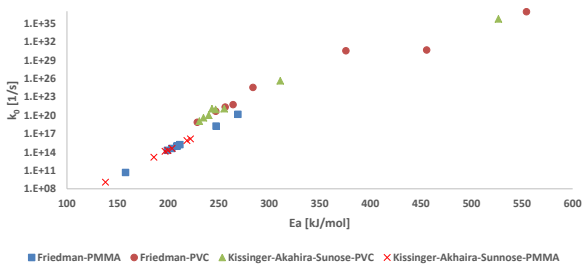

Fig. 6. Spread of pre-exponential factor computed using isoconversional methods for PMMA and PVC.

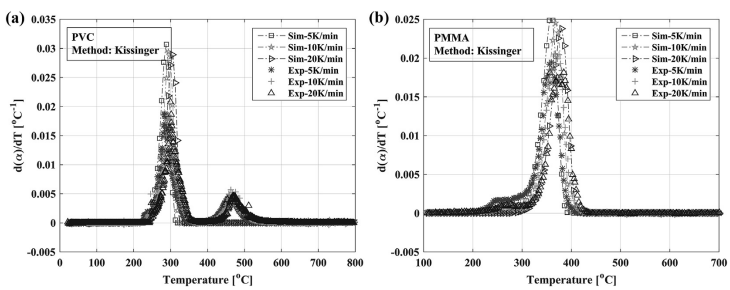

Fig. 7. Comparison of experimental and simulated DTG data with Kissinger method (a) PVC and (b) PMMA.

Table 4
Summary of kinetic parameters obtained by isoconversional and Kissinger method.

Method	Friedman		Kissinger-Akhaira-Sunose (KAS)		Kissinger	
Kinetic Parameters	PVC	PMMA	PVC	PMMA	PVC	PMMA
Activation energy, Ea [kJ/mol]	333.4	213.4	286.2	166.7	209.7	218.7
Pre-exponential factor, k0 [1/s]	1.0E+36	1.8E+19	7.1E+34	2.4E+15	2.9E+17	8.1E+15

distributed reactivity models that were expected to show a better fit with the experimental data. In this section simulation results of DAEM model fitting will be focused for the test run performed at 5 K/min. For results of other test runs and global optimization only, the calculated parameters are shown in Tables 5 and 6.

4.2.2.1. Double Gaussian fit. In the double Gaussian modelling of DTG curves, the overall reaction was modelled as a sum of two individual reaction peaks (Rxn-1 and Rxn-2). Eight parameters (E_{ao1}, σ_1, k_{o1}, c_1, E_{ao2}, σ_2, k_{o2}, c_2) were optimized in the calculations. The results obtained from the model fittings are presented in Table 5. Regarding the test at 5 K/min, the mean value of activation energy (E_{a0}) for PVC for reaction 1 and 2 were found to be 179.7 kJ/mol and 231.5 kJ/mol respectively. These values were comparable with previously reported data in the literature by Zhang et al. [20] who found E_a values in the range of 159–212 kJ/mol and standard deviation (σ) values in the range of 1.5–8.2 kJ/mol. For PMMA, the mean activation energy (E_{a0}) values were found to be 264.4 kJ/mol and 199.0 kJ/mol for step 1 and 2 respectively. However, scarce data is available in the literature related to the distributed reactivity models for comparison purposes. Overall the average fittings were found to be reasonably better for PVC (Fit = 4.1%) than PMMA (Fit = 4.7%).

In Fig. 8 the DTG peaks of PVC and PMMA are shown as a comparison between experimental results and simulations. In case of PVC, both the peaks of the test data can be reproduced with fairly good accuracy; however there exists some deviation from the test data in the fittings. In Fig. 8b the minor shoulder peak of PMMA is not well captured by the model, while for PVC this deviation is visible at the end of first peak.

Fig. 9 shows the normalized probability distribution plots of PVC and PMMA. The f(Ea) curve is shown as a sum of two individual f(Ea) peaks. Both curves have been calculated using the parameters presented in Table 5. The peak value of the f(Ea) curve appears at 178.7 kJ/mol and 201.9 kJ/mol for PVC and PMMA respectively. Overall the activation energy (E_a) values are significantly distributed over the range of 100–350 kJ/mol.

Fig. 10 shows the comparison between experimental and simulated values of normalized conversion using α(T) plots. These plots are obtained by numerically integrating equation (6) and using the optimized parameters obtained in Table 5. Fittings show some deviation from the experimental data, as the model under predicts the instantaneous conversion. Fig. 10 indicates that in the case of PVC, the prediction is accurate only until the alpha = 0.6, later the model shows significant under-prediction from the test result. It is plausible that the two reaction peaks are not sufficient to capture the DTG peaks accurately and additional reaction peaks are required to model the entire reaction. For PMMA, the model predictions are closer to the test results, but these values are slightly deviated from the experimental data in the initial ($\alpha = 0$ to 0.3) and final stages ($\alpha = 0.8$ to 1.0) of the reaction.

4.2.2.2. Multi − Gaussian fit. In the multi Gaussian modelling of DTG curves, four reactions are used to model the DTG curves of PVC and PMMA. Sixteen parameters (E_{ao1}, σ_1, k_{o1}, c_1, E_{ao2}, σ_2, k_{o2}, c_2, E_{ao3}, σ_3, k_{o3}, c_3, E_{ao4}, σ_4, k_{o4}, c_4) were optimized for model fitting (four parameters corresponding to each reaction). In Fig. 11, results of four-step multi-Gaussian DAEM simulation are compared with the experimental test result obtained for the run at 5 K/min.

The DTG peaks of PVC and PMMA were reproduced with better accuracy than with the double Gaussian fittings. The results for optimized kinetic and statistical parameters are shown in Table 6 for the test runs at other heating rates.

For PVC, E_{a0} values lied in the range of 164–230 kJ/mol for the test run at 5 K/min. For comparison purposes, not enough literature data related to the multi-Gaussian DAEM model could be found on PVC. These values are compared with the activation energy values reported for the series and parallel kinetic model by Miranda et al. [10] using non-linear least square method, which lied in the range of 138–245 kJ/mol showing a reasonable agreement. The difference

Table 5
Fitted kinetic and statistical parameters for pyrolysis of PVC and PMMA using double Gaussian DAEM at different heating rates.

PVC											
Heating rate	Rxn-1				Rxn-2						
β (K/min)	E_{a0-1} (kJ/mol)	σ_1 (kJ/mol)	$Log_{10}(k_{0-1})$ (1/s)	C_1	E_{a0-2} (kJ/mol)	σ_2 (kJ/mol)	$Log_{10}(k_{0-2})$ (1/s)	C_2	Fitness (%)	O.F.
5	179.7	11.3	14.4	0.6	231.5	40.3	14.0	0.4	4.9	4E-04
10	177.4	10.1	14.3	0.6	229.8	39.2	14.0	0.4	4.5	3E-04
20	181.0	12.1	14.7	0.6	227.6	37.6	14.0	0.4	4.9	4E-04
Global parameters (i = 1:3; β = 5/10/20) K/min	181.0	12.1	14.7	0.6	229.6	39.6	14.0	0.4	2.0	2E-03
Average	179.8	11.4	14.5	0.6	229.6	39.2	14.0	0.4	4.1	7E-04
PMMA											
Heating rate	Rxn-1				Rxn-2						
β (K/min)	E_{a0-1} (kJ/mol)	σ_1 (kJ/mol)	$Log_{10}(k_{0-1})$ (1/s)	C_1	E_{a0-2} (kJ/mol)	σ_2 (kJ/mol)	$Log_{10}(k_{0-2})$ (1/s)	C_2	Fitness (%)	O.F.
5	264.4	50.0	20.7	0.5	199.0	26.3	14.0	0.5	6.3	2E-04
10	275.6	50.0	21.5	0.5	198.5	28.1	14.0	0.5	5.2	2E-04
20	268.2	50.0	20.9	0.5	197.5	26.5	14.0	0.5	5.2	1E-04
Global parameters (i = 1:3; β = 5/10/20) K/min	268.1	50.0	20.9	0.5	198.5	26.7	14.0	0.5	2.0	5E-04
Average	269.1	50.0	21.0	0.5	198.4	26.9	14.0	0.5	4.7	3E-04

Table 6
Fitted kinetic and statistical parameters for pyrolysis of PVC and PMMA using multi Gaussian DAEM model.

PVC						
Heating rate	β (K/min)	5	10	20	Global parameters (β = 5/10/20) K/min	Average
Rxn-1	E_{a0-1} (kJ/mol)	217.0	224.0	227.0	217.0	221.3
	σ_1 (kJ/mol)	32.6	36.6	36.6	32.6	34.6
	$Log_{10}(k_{0-1})$ (1/s)	13.0	18.0	18.0	13.0	15.5
	C_1	0.3	0.3	0.3	0.3	0.3
Rxn-2	E_{a0-2} (kJ/mol)	230.6	230.6	230.6	233.6	231.3
	σ_2 (kJ/mol)	30.5	46.5	46.5	30.5	38.5
	$Log_{10}(k_{0-2})$ (1/s)	13.0	14.0	14.0	21.0	15.5
	C_2	0.2	0.2	0.2	0.2	0.2
Rxn-3	E_{a0-3} (kJ/mol)	164.3	172.3	172.3	164.3	168.3
	σ_3 (kJ/mol)	49.3	49.3	49.3	49.3	49.3
	$Log_{10}(k_{0-3})$ (1/s)	13.0	14.0	14.0	13.0	13.5
	C_3	0.2	0.2	0.2	0.2	0.2
Rxn-4	E_{a0-4} (kJ/mol)	218.1	266.1	266.1	218.1	242.1
	σ_4 (kJ/mol)	28.8	44.8	48.8	32.8	38.8
	$Log_{10}(k_{0-4})$ (1/s)	17.0	17.0	17.0	17.0	17.0
	C_4	0.3	0.3	0.3	0.3	0.3
Fit (%)		1.8	4.1	1.9	4.1	3.0
O.F.		5.80E-05	2.92E-04	6.15E-05	8.00E-03	2.10E-03
PMMA						
Heating rate	β (K/min)	5	10	20	Global parameters (i = 1:3; β = 5/10/20) K/min	Average
Rxn-1	E_{a0-1} (kJ/mol)	194.8	198.9	198.9	199.9	198.1
	σ_1 (kJ/mol)	15.4	27.6	27.6	27.6	24.6
	$Log_{10}(k_{0-1})$ (1/s)	13.0	14.0	14.0	14.0	13.8
	C_1	0.3	0.3	0.3	0.3	0.3
Rxn-2	E_{a0-2} (kJ/mol)	184.2	206.9	205.9	205.9	200.7
	σ_2 (kJ/mol)	20.4	28.8	24.8	26.8	25.2
	$Log_{10}(k_{0-2})$ (1/s)	13.0	14.0	14.0	14.0	13.8
	C_2	0.2	0.2	0.2	0.2	0.2
Rxn-3	E_{a0-3} (kJ/mol)	166.5	170.5	174.5	170.5	170.5
	σ_3 (kJ/mol)	4.3	4.3	4.3	4.3	4.3
	$Log_{10}(k_{0-3})$ (1/s)	13.6	14.0	14.0	14.0	13.9
	C_3	0.2	0.2	0.2	0.2	0.2
Rxn-4	E_{a0-4} (kJ/mol)	188.9	194.4	190.4	190.4	191.0
	σ_4 (kJ/mol)	16.0	20.2	20.2	20.4	19.2
	$Log_{10}(k_{0-4})$ (1/s)	13.0	14.0	14.0	14.0	13.8
	C_4	0.3	0.3	0.3	0.3	0.3
Fit (%)		4.3	3.1	3.4	1.7	3.1
O.F.		8.50E-05	5.52E-05	5.97E-05	4.00E-04	1.50E-04

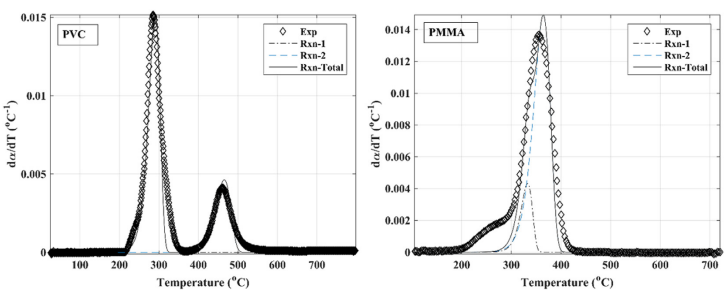

Fig. 8. Experimental and calculated DTG curves for PVC (left) and PMMA (right) at 5 K/min using double Gaussian DAEM (Contributing reactions Rxn1−Rxn2 are hindered due to peak overlaps).

in kinetic parameters can be attributed to experimental conditions, sample characteristics and model choice and the carrier gas used to study the reaction. For PMMA, E_{a0} values are distributed in rather narrow range of 166−195 kJ/mol. These values are comparable with the activation energy values reported by Refs. [9,15,51]. Overall, the simulated DTG curve (Fig. 8) can be approximated to the experimental data to a high degree of accuracy.

In Fig. 12 the normalized probability distribution curves of the activation energy for PVC and PMMA are shown. The f(Ea) curve is taken as a sum of four individual Gaussian peaks (Rxn1−Rxn4). The f(Ea) curve peaks at $E_P = 220.4$ kJ/mol and $E_P = 168.2$ kJ/mol for PVC and PMMA respectively. These results suggest that the activation

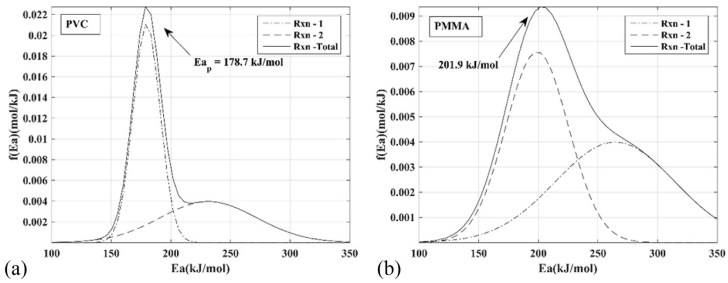

Fig. 9. f(Ea) curve estimated for PVC (left) and PMMA (right) at β = 5 K/min using double-Gaussian DAEM.

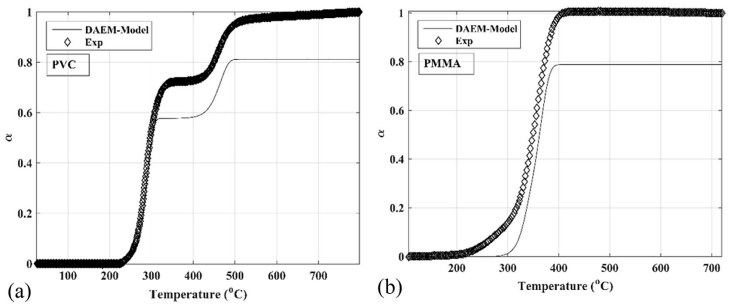

Fig. 10. α(T) curve estimated for PVC (left) and PMMA (right) at β = 5 K/min using double-Gaussian DAEM.

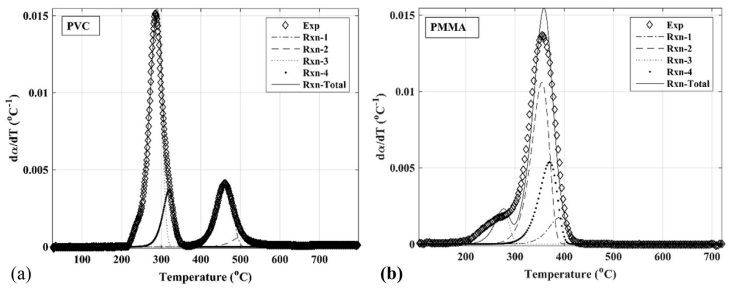

Fig. 11. Experimental and calculated DTG curve for PVC (left) and PMMA (right) at 5 K/min using multi-Gaussian DAEM (Contribution reactions Rxn1–Rxn4 are hindered due to peak overlaps).

energies of numerous individual reactions are during thermal degradation of the material, centered near these peak values, hence they may be possible candidates for use as input parameters in fire simulations.

Fig. 13 shows the comparison between experimental and simulated values of normalized conversion using α(T) curves. Fittings improve significantly and match experimental data to a high degree of accuracy. For PVC the model shows good prediction, while for PMMA it is slightly under-predicted. The overall fitting of multi-Gaussian DAEM model was found to be better than double Gaussian fitting. The average fitness was found to be approximately 3% each for PVC and PMMA, which is slightly lower than double Gaussian fittings. Thus multi-Gaussian modelling with minimum of 4 reaction steps is recommended over the double Gaussian approach.

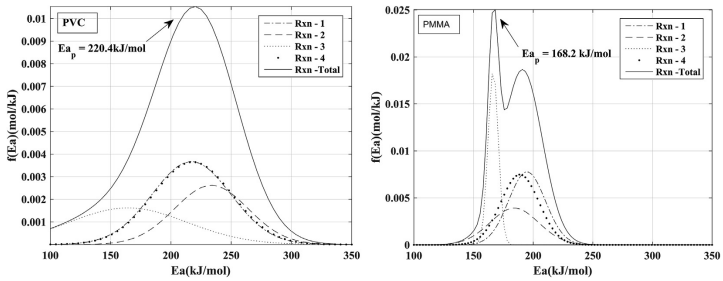

Fig. 12. f(Ea) curve estimated for PVC (left) and PMMA (right) at β = 5 K/min using multi-Gaussian DAEM.

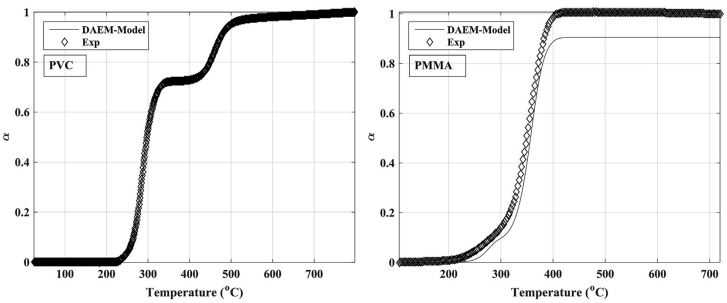

Fig. 13. α(T) curve estimated for PVC (left) and PMMA (right) at β = 5 K/min using multi-Gaussian DAEM.

5. Conclusions

The main conclusions from this study are that, in condensed phase pyrolysis several reactions occur simultaneously and overlap in time and temperature during the thermal degradation process. However, from a fire engineering perspective it is not critical to describe all of them. A robust modelling approach has been adopted using a combination of pattern search optimization and distributed reactivity model to simulate MLR occurring in two different thermoplastics (PVC and PMMA) that are representative of polymers showing charring and non-charring behavior respectively. The overall fitting of MLR has shown to improve considerably with the use of a multi-Gaussian DAEM model as compared with the double-Gaussian DAEM model and isoconversional methods. The DTG curves in the former case were reproduced with higher accuracy, but at computational expense. The main advantage in using this type of methodology is the possibility to extend the scope of its applicability to polymers showing degradation in multiple reaction steps and having complex compositions including several additives and/or flame-retardants. For future work, MLRs computed using DAEM model may be integrated as a sub-model in a commercial CFD package. This can lead to improvement in the results of thermo-kinetic calculations leading to more accurate predictions of HRR. However, it would be useful in such a case to acquire experimental data in a wide range of heating rates (5–80 K/min), so that the estimated parameters can be calibrated for fire simulations. Another advantage of combining DAEM code with the optimization engine is that the parameter estimation can be performed systematically rather than random trial and error basis. Despite this, computational time involved can take from several minutes to a few hours. Nevertheless, these calculations are performed only once for each material. It may also be concluded that the number of reactions that may be used to describe a reaction model should be first based on the visual inspection of the DTG curve and should depend upon the number of peaks clearly visible. If the DTG curve cannot be modeled accurately by the number of clearly visible peaks, additional reactions peaks may be used.

Acknowledgements

This work was supported by the funding received from European Union Seventh Framework Program (FP7/2007–2013) under grant agreement n° 316991 for the project FIRETOOLS. The authors would like to thank Dr. Anna Matala (VTT Technical Research Centre, Finland) and Dr. Marc Janssens (South West Research Institute, Texas, USA) for providing experimental thermogravimetric data. Also, authors are grateful for the whole team of Fire Tools for fruitful discussions.

References

[1] Plastics – the Facts 2014/2015, (n.d.). http://www.plasticseurope.org/documents/document/20150227150049-final_plastics_the_facts_2014_2015_260215.pdf.

[2] A.Y. Snegirev, Generalized approach to model pyrolysis of flammable

materials, Thermochim. Acta 590 (2014) 242–250, http://dx.doi.org/10.1016/j.tca.2014.07.009.
[3] M.B. McKinnon, S.I. Stoliarov, A. Witkowski, Development of a pyrolysis model for corrugated cardboard, Combust. Flame 160 (2013) 2595–2607, http://dx.doi.org/10.1016/j.combustflame.2013.06.001.
[4] S.I. Stoliarov, S. Crowley, R.N. Walters, R.E. Lyon, Prediction of the burning rates of charring polymers, Combust. Flame 157 (2010) 2024–2034, http://dx.doi.org/10.1016/j.combustflame.2010.03.011.
[5] S.I. Stoliarov, S. Crowley, R.E. Lyon, G.T. Linteris, Prediction of the burning rates of non-charring polymers, Combust. Flame 156 (2009) 1068–1083, http://dx.doi.org/10.1016/j.combustflame.2008.11.010.
[6] B. Janković, B. Adnađević, J. Jovanović, Application of model-fitting and model-free kinetics to the study of non-isothermal dehydration of equilibrium swollen poly (acrylic acid) hydrogel: thermogravimetric analysis, Thermochim. Acta 452 (2007) 106–115, http://dx.doi.org/10.1016/j.tca.2006.07.022.
[7] A. Witkowski, B. Girardin, M. Försth, F. Hewitt, G. Fontaine, S. Duquesne, et al., Development of an anaerobic pyrolysis model for fire retardant cable sheathing materials, Polym. Degrad. Stab. 113 (2015) 208–217, http://dx.doi.org/10.1016/j.polymdegradstab.2015.01.006.
[8] L.E. Manring, D.Y. Sogah, G.M. Cohen, Thermal degradation of poly(methyl methacrylate). 3. Polymer with head-to-head linkages, Macromolecules 22 (1989) 4652–4654, http://dx.doi.org/10.1021/ma00202a048.
[9] M. Ferriol, A. Gentilhomme, M. Cochez, N. Oget, J.L. Mieloszynski, Thermal degradation of poly(methyl methacrylate) (PMMA): modelling of DTG and TG curves, Polym. Degrad. Stab. 79 (2003) 271–281, http://dx.doi.org/10.1016/S0141-3910(02)00291-4.
[10] R. Miranda, J. Yang, C. Roy, C. Vasile, Vacuum pyrolysis of commingled plastics containing PVC. I. Kinetic study, Polym. Degrad. Stab. 72 (2001) 469–491, http://dx.doi.org/10.1016/S0141-3910(01)00048-9.
[11] C.-H. Wu, C.-Y. Chang, J.-L. Hor, S.-M. Shih, L.-W. Chen, F.-W. Chang, Two-Stage pyrolysis model of PVC, Can. J. Chem. Eng. 72 (1994) 644–650, http://dx.doi.org/10.1002/cjce.5450720414.
[12] P. van Hees, Simulation of Fire Technical Properties of Products and Construction Barriers to Support Fire Safety Engineering – the Fire Tools Project, Basel, Switzerland, 2013, http://www.eurofireconference.com/html/programme.htm.
[13] S. Vyazovkin, K. Chrissafis, M.L. Di Lorenzo, N. Koga, M. Pijolat, B. Roduit, et al., ICTAC Kinetics Committee recommendations for collecting experimental thermal analysis data for kinetic computations, Thermochim. Acta 590 (2014) 1–23, http://dx.doi.org/10.1016/j.tca.2014.05.036.
[14] S. Vyazovkin, A.K. Burnham, J.M. Criado, L.A. Pérez-Maqueda, C. Popescu, N. Sbirrazzuoli, ICTAC Kinetics Committee recommendations for performing kinetic computations on thermal analysis data, Thermochim. Acta 520 (2011) 1–19, http://dx.doi.org/10.1016/j.tca.2011.03.034.
[15] L.E. Manring, Thermal degradation of saturated poly(methyl methacrylate), Macromolecules 21 (1988) 528–530, http://dx.doi.org/10.1021/ma00180a046.
[16] A. Matala, S. Hostikka, Pyrolysis modelling of PVC cable materials, Fire Saf. Sci. (2011) 917–930, http://dx.doi.org/10.3801/IAFSS.FSS.10-917.
[17] K. Miura, T. Maki, A simple method for estimating f(E) and k0(E) in the distributed activation energy model, Energy Fuels (1998) 864–869.
[18] A. Rostami, M.R.R. Hajaligol, S.E.E. Wrenn, A biomass pyrolysis sub-model for CFD applications, Fuel 83 (2004) 1519–1525, http://dx.doi.org/10.1016/j.fuel.2003.09.024.
[19] J. Cai, W. Wu, R. Liu, An overview of distributed activation energy model and its application in the pyrolysis of lignocellulosic biomass, Renew. Sustain. Energy Rev. 36 (2014) 236–246, http://dx.doi.org/10.1016/j.rser.2014.04.052.
[20] J. Zhang, T. Chen, J. Wu, J. Wu, TG-MS analysis and kinetic study for thermal decomposition of six representative components of municipal solid waste under steam atmosphere, Waste Manag. (2015), http://dx.doi.org/10.1016/j.wasman.2015.05.024.
[21] A.K. Burnham, R.L. Braun, Global kinetic analysis of complex materials, Energy Fuels 13 (1999) 1–22.
[22] J. Cai, W. Wu, R. Liu, G.W. Huber, A distributed activation energy model for the pyrolysis of lignocellulosic biomass, Green Chem. 15 (2013) 1331, http://dx.doi.org/10.1039/c3gc36958g.
[23] J. Zhang, T. Chen, J. Wu, J. Wu, A novel Gaussian-DAEM-reaction model for the pyrolysis of cellulose, hemicellulose and lignin, RSC Adv. 4 (2014) 17513, http://dx.doi.org/10.1039/c4ra01445f.
[24] J. Zhang, T. Chen, J. Wu, J. Wu, Multi-Gaussian-DAEM-reaction model for thermal decompositions of cellulose, hemicellulose and lignin: comparison of N_2 and CO_2 atmosphere, Bioresour. Technol. 166 (2014) 87–95, http://dx.doi.org/10.1016/j.biortech.2014.05.030.
[25] A. Bhargava, P. van Hees, Pyrolysis modeling of PVC using distributed activation energy model – micro scale testing, in: Appl. Struct. Fire Eng., Czech Technical University, Dubrovnik, 2015, p. 448.
[26] A. Bhargava, P. van Hees, Using Distributed Activation Energy Model (DAEM) to predict mass loss rates in PMMA, in: Fire Retard. Polym. Mater., 2015, p. 22. Berlin, http://www.frpm2015.bam.de/en/home/index.htm.
[27] C. Lakshmanan, N. White, A new distributed activation energy model using Weibull distribution for the representation of complex kinetics, Energy Fuels 31 (1994) 1158–1167 (accessed 06.01.15), http://pubs.acs.org/doi/abs/10.1021/ef00048a001.
[28] J. Cai, C. Jin, S. Yang, Y. Chen, Logistic distributed activation energy model—Part 1: derivation and numerical parametric study, Bioresour. Technol. 102 (2011) 1556–1561, http://dx.doi.org/10.1016/j.biortech.2010.08.079.
[29] J. Cai, F. He, F. Yao, Nonisothermal nth-order DAEM equation and its parametric study – use in the kinetic analysis of biomass pyrolysis, J. Math. Chem. 42 (2007) 949–956, http://dx.doi.org/10.1007/s10910-006-9151-4.
[30] A.A. Jain, A. Mehra, V.V. Ranade, Processing of TGA data: analysis of isoconversional and model fitting methods, Fuel 165 (2016) 490–498, http://dx.doi.org/10.1016/j.fuel.2015.10.042.
[31] J. Cai, F. He, F. Yao, Nonisothermal nth-order DAEM equation and its parametric study – use in the kinetic analysis of biomass pyrolysis, J. Math. Chem. 42 (2006) 949–956, http://dx.doi.org/10.1007/s10910-006-9151-4.
[32] J.H. Flynn, The "Temperature Integral"—its use and abuse, Thermochim. Acta 300 (1997) 83–92, http://dx.doi.org/10.1016/S0040-6031(97)00046-4.
[33] J.J.M. Órfão, Review and evaluation of the approximations to the temperature integral, AIChE J. 53 (2007) 2905–2915.
[34] R.M. Lewis, V. Torczon, Pattern search algorithms for bound constrained minimization, SIAM J. Optim. 9 (1999) 1082–1099, http://dx.doi.org/10.1137/S1052623496300507.
[35] R. Hooke, T.A. Jeeves, "Direct Search" solution of numerical and statistical problems, J. ACM 8 (1961) 212–229, http://dx.doi.org/10.1145/321062.321069.
[36] G. Várhegyi, B. Bobály, E. Jakab, H. Chen, Thermogravimetric study of biomass pyrolysis kinetics. A distributed activation energy model with prediction tests, Energy Fuels 25 (2011) 24–32, http://dx.doi.org/10.1021/ef101079r.
[37] E. Kim, N. Dembsey, Parameter estimation for comprehensive pyrolysis modeling: guidance and critical observations, Fire Technol. 51 (2014) 443–477, http://dx.doi.org/10.1007/s10694-014-0399-0.
[38] A. Matala, S. Hostikka, J. Mangs, Estimation of pyrolysis model parameters for solid materials using thermogravimetric data, Fire Saf. Sci. 9 (2008) 1213–1223, http://dx.doi.org/10.3801/IAFSS.FSS.9-1213.
[39] M.L. Janssens, Challenges in predicting the pyrolysis rate of solid materials, in: Fire Mater. 2015–14th Int. Conf. Exhib., Interscience Communications, London, UK, 2015, pp. 271–284.
[40] I.C. McNeill, L. Memetea, W.J. Cole, A study of the products of PVC thermal degradation, Polym. Degrad. Stab. 49 (1995) 181–191, http://dx.doi.org/10.1016/0141-3910(95)00064-S.
[41] C. Huggett, B. Levin, Toxicity of the pyrolysis and combustion products of poly (vinyl chlorides): a literature assessment, Fire Mater. II (1987) 131–142. http://onlinelibrary.wiley.com/doi/10.1002/fam.810110303/abstract.
[42] G.M. Anthony, Kinetic and chemical studies of polymer cross-linking using thermal gravimetry and hyphenated methods. Degradation of polyvinyl-chloride, Polym. Degrad. Stab. 64 (1999) 353–357, http://dx.doi.org/10.1016/S0141-3910(98)00129-3.
[43] P.E. Sánchez-Jiménez, A. Perejón, J.M. Criado, M.J. Diánez, L.A. Pérez-Maqueda, Kinetic model for thermal dehydrochlorination of poly(vinyl chloride), Polymer (Guildf) 51 (2010) 3998–4007, http://dx.doi.org/10.1016/j.polymer.2010.06.020.
[44] A. Perejón, P.E. Sánchez-Jiménez, J.M. Criado, L.A. Pérez-Maqueda, Kinetic analysis of complex solid-state reactions. A new deconvolution procedure, J. Phys. Chem. B 115 (2011) 1780–1791, http://dx.doi.org/10.1021/jp110895z.
[45] J. Troitzsch, Plastics Flammability Handbook – Principles, Regulations, Testing, and Approval, third ed., Hanser Publishers, 2004 (accessed 31.03.15), http://app.knovel.com/web/toc.v/cid:kpPFHPRTA1/viewerType:toc/root_slug:plastics-flammability/url_slug:polyurethane-foam?b-q=polyurethanefoam&b-group-by=true.
[46] T. Kashiwagi, Polymer combustion and flammability—role of the condensed phase, Symp. Combust. (1994) 1423–1437 (accessed 09.12.14), http://www.sciencedirect.com/science/article/pii/S0082078406807861.
[47] S. Vyazovkin, A.K. Burnham, J.M. Criado, L.A. Pérez-Maqueda, C. Popescu, N. Sbirrazzuoli, ICTAC Kinetics Committee recommendations for performing kinetic computations on thermal analysis data, Thermochim. Acta 520 (2011) 1–19, http://dx.doi.org/10.1016/j.tca.2011.03.034.
[48] H.L. Friedman, Kinetics of thermal degradation of char-forming plastics from thermogravimetry. Application to a phenolic plastic, J. Polym. Sci. Part C Polym. Symp. 6 (1964) 183–195, http://dx.doi.org/10.1002/polc.5070060121.
[49] T. Akhaira, Method of Determining Activation Deterioration Constant of Electrical Insulating Materials, 1971.
[50] H.E. Kissinger, Reaction kinetics in differential thermal analysis, Anal. Chem. 29 (1957) 1702–1706. http://www.scopus.com/inward/record.url?eid=2-s2.0-33749213901&partnerID=tZOtx3y1.
[51] B.J. Holland, J.N. Hay, The kinetics and mechanisms of the thermal degradation of poly(methyl methacrylate) studied by thermal analysis-Fourier transform infrared spectroscopy, Polymer (Guildf) 42 (2001) 4825–4835, http://dx.doi.org/10.1016/S0032-3861(00)00923-X.

Paper II

DISTRIBUTED REACTIVITY MODEL TO PREDICT MULTISTAGE PYROLYSIS OF POLYMERIC MATERIALS AND SENSITIVITY ANALYSIS

Abhishek Bhargava[a, b], Berit Andersson[b], Patrick van Hees[b], Hossein Sina[c], Srinivasan Iyengar[c]
[a]Danish Institute of Fire and Security Technology, Denmark
[b]Lund University, Division of Fire Safety Engineering, Sweden
[c]Lund University, Division of Materials Engineering, Sweden

1 ABSTRACT

Based on a statistical approach, a robust chemical kinetic model is presented to explain thermal decomposition in complex, real-world polymer materials during pyrolysis in the condensed phase. The model envisages the material to take part in multiple solid-state chemical reactions during a microscale thermogravimetric (TG) experiment. The model considers the total mass loss rate to include contributions from an infinite number of independent, parallel, first order reactions characterized by unique activation energies. Preliminary calculations have shown good agreement between experimental and simulation data. The sub-model approach could be useful for integration in commercial and open access CFD code for computing HRR (heat release rate) in a cone calorimeter test, particularly in cases where the user has marginal knowledge about the reaction mechanism and exact chemical composition of the sample. The model could also be applicable in cases where the mass loss curve exhibits irregular shapes and multiple peaks are observed in the differential thermogravimetric (DTG) plot. The model parameters were estimated in this work using a pattern search algorithm using a non-linear, least-squares approach. The work has been expanded to include a local sensitivity analysis of the estimated parameters to determine the accuracy and robustness of the model.

2 KEYWORDS

Pyrolysis, TGA, DAEM, Multi-step kinetics, Sensitivity analysis, Fire modelling

3 INTRODUCTION

Polymeric materials find applications in wide-ranging areas such as building construction, electrical works, upholstery, paints and sealants. The versatile applicability of such materials can be attributed to their customizable physio-chemical properties suitable for a large number of products [1]. However, a key issue with such materials is their combustible nature which present a potential fire hazard. One major step to mitigate this problem is the use of flame retardants. As a consequence of this practice, polymeric materials have shown to exhibit increasing complexities in the condensed phase during fire tests. A number of flame retardants (e.g. Dechlorane, ATH, silica gel, phosphates etc.) whose mode of action is based on dehydration, crosslinking, intumescence and char formation are currently being used in many polymeric materials [2].

In the EU and many other countries, fire testing and classification is based on certain parameters such as non-combustibility, fire resistance, ignition temperature, flame spread and smoke development. These are determined by different types of fire tests and are often based on prescriptive rules laid down by EU directives and national regulations. These standard test methods are used to assess the fire behavior of plastics for the estimation of ignition temperatures, smoke density and thermal decomposition. Many of them have been documented by Troitzsch[3]. For the US, most fire test methods have been issued by ASTM and can be found in the document ASTM D 3814-99 [3].

Recently, there has been a growing interest in performance based design approach to fire engineering applications using modelling and simulation techniques. This has resulted in the increasing use of computer calculations in this area. Fire Tools is a research project in this domain, funded by the European Commission under the Marie Curie Actions which aims to predict fire performance of materials used as products, contents and barriers in a building by means of using material properties in a multi-scale approach [4,5]. This paper will focus on modelling of thermal decomposition in polymers using small scale material test (TGA) and evaluating the sensitivities of its input parameters used in the distributed reactivity model. The work shall be linked to product scale calculations (using cone calorimetry) in future publications.

Several studies in the past have shown that the outcomes of cone-calorimeter tests of many polymers can be predicted using one dimensional-numerical pyrolysis model using CFD software packages such as FDS and Thermakin [6–8]. However, some of them have pointed out significant discrepancies between modelling results and experimental data [6,9]. These models apply energy and mass conservation equations to quantify spatial temperature profiles, heat release rates (HRR) and other fire performance parameters. One major reason for such a discrepancy is attributed to the lack of understanding of processes occurring in the condensed phase.

In separate studies, Bhargava and co-workers[10–12] presented an alternate approach to model thermal decomposition in two different polymers using the distributed reactivity concept. In this work, the concept introduced in reference [12] is extended further by performing more validation work on a number of polymers and cellulosic materials. In order to address the issues of multiplicity in the chemical reactions, a model fitting approach is discussed. Further, the influence of estimated parameters on model output has also been studied using local parametric sensitivity analysis.

4 MATERIAL AND METHODS

4.1 Materials

Five polymeric samples of materials commonly used in building constructions or are part of the building components were collected for thermal decomposition tests. These were poly (vinyl chloride) (PVC), poly (methyl methacrylate) (PMMA), paper used in a common plaster board's outer covering, ethylene vinyl acetate (EVA) and a fabric blend of cellulosic cotton and polyester.

4.2 TG-DSC Experiments

Milligram samples (5-8 mg) of each of the above polymers were prepared from the bulk materials. All the experiments were performed in a simultaneous thermal analyser (STA - NETZSCH 449F3 Jupiter) under a controlled environment. It enabled simultaneous recording of TG and DSC signals (DSC curves are not shown in this work). The STA was calibrated for temperature and heat sensitivity at different heating rates using standard reference materials (pure metals). The specimens were placed in aluminium or alumina crucibles and subjected to three different linear heating rates in the range (5 to 30 K/min). At each heating rate, a baseline was recorded using two empty crucibles. For PVC, PMMA and EVA samples, experimental work was shared with other laboratories. Results for these materials have been reported earlier in separate studies by Matala[13] for PVC, by Janssens[14] for PMMA, and by Girardin[15,16] for EVA. For paper samples and the fabric blends, new tests were conducted in co-operation with material testing laboratory at Lund University. The experimental conditions varied from one lab to the other in terms of selection of heating rates and carrier gas availability. Those variations can be attributed to individual choices made by the experimentalists. Table 1 shows the summary of experimental conditions. All tests were done under inert conditions and with 5 and 10 K/min as heating rates in lower range. While the heating rate of 30 K/min was chosen to reflect temperature rise in the material in slightly higher range.

Table 1 Summary of samples and experimental conditions

Sample	Heating Rate (K/min)	Gas Atmosphere
PVC	5,10,20	Nitrogen
PMMA	5,10,20	Nitrogen
EVA	5,10, 20	Nitrogen
Paper – (Plaster board covering)	5,15,30	Argon
Fabric (Blend – 25% Polyester, 75% Cotton)	5,15,30	Argon

4.3 Kinetic Model

The model is based on the distributed reactivity concept. This concept had been used previously for materials such as coal and biomass, which show thermal decomposition in a complex manner and have shown to exhibit irregular mass loss profiles. In this model the overall reaction rate is assumed to be the sum of many parallel and overlapping reactions. Each reaction step is characterized by a pre-exponential factor, a mean value of activation energy and a standard deviation of the activation energy distribution. The derivative form of the DAEM model is:

$$\frac{d\alpha_j}{dT} = \frac{1}{\sigma\sqrt{2\pi}}\int_0^\infty \frac{k_0}{\beta}\exp\left[-\frac{E}{RT} - \frac{k_0}{\beta}\int_0^T \exp\left(-\frac{E}{RT}\right)dT - \frac{(E-E_0)^2}{2\sigma^2}\right]dE \quad [1]$$

$$\frac{d\alpha(T)}{dT} = \sum_{j=1}^{r} w_j \frac{d\alpha_j}{dT} \quad [2]$$

In the Eq. [1] and [2] above, α is the degree of sample conversion, T (K) is the temperature, β (K/s) is the heating rate, E (J/mol) is the activation energy, R (8.314 J/K/mol) is the universal gas constant, k_0(1/s) is the frequency factor, E_0 (J/mol) is the mean activation energy and σ (J/mol) is the standard deviation of the activation energy distribution (Gaussian in this case), w_j is the fraction of volatiles produced by each component. For a detailed explanation of this model see [17–19]. For modelling the multiplicity of reactions and appearance of more than one DTG peak, Eq. [2] is used.

For the parameter estimation of the unknown variables, a non-linear regression method using pattern search algorithm was implemented using a computer program in Matlab. The objective function was minimized using systematically chosen values of kinetic parameters (E_o, σ, w_j). Holstein and co-workers[20] have stated that different pairs of kinetic parameters provide equally good fit to experimental data. Hence, in the present work, a constant value of $k_0 = 1.67 \times 10^{13}$ s^{-1} was chosen to maintain consistency with the transition state theory. This value has been chosen based on previous modelling attempts reported in literature by Zhang[21] and Miranda[22]. Also, this practice reduced the number of parameters to be estimated by one factor reducing the computational effort. In the present case three parameters are estimated per reaction. Our objective was to choose least number of reactions to describe the DTG curve as accurately as possible. For some most cases this was achieved using only two reactions while for one of them it was accomplished with three step mechanism.

The objective function is shown in Eq. 3. In this equation the subscript 'j' refers to the data point used, n_d is the number of data points, $(d\alpha/dT)_{exp,ij}$ represents the experimental values of the i^{th} experiment, while $(d\alpha/dT)_{cal,ij}$ represents those calculated by the DAEM model (Eq. [2]) for a chosen set of parameters. The measure of agreement between experimental and simulation results is given by Eq. [4]. A lower value signifies a better fit[17,23].

$$\mathbf{O.F.} = \sum_{i=1}^{n_e}\sum_{j=1}^{n_d}\left[\left(\frac{d\alpha}{dT_{exp,ij}}\right) - \left(\frac{d\alpha}{dT_{cal,ij}}\right)\right]^2 \quad [3]$$

$$\mathbf{Fit}(\%) = \mathbf{100} * \frac{\left(\sqrt{\frac{\mathbf{O.F}}{\mathbf{n_d}}}\right)}{\sum_{j=1}^{3} \frac{d\alpha(T)}{dT}_{exp,max}} \quad [4]$$

5 RESULTS AND DISCUSSIONS

5.1 Comparison of Experimental and Simulated DTG curves

Fig. 1 shows the summary of experimental and modeled DTG curves for various polymers. It can be seen that two main peaks were observed for PVC, EVA and the fabric, while for PMMA and paper only one broad peak is observed. It is apparent that, the broad peak is convoluted in more than one peak. Also several inflections in the main peak were visible near the onset and final temperatures.

Fig. 1 Experimental and simulated DTG curves for different polymers at 5K/min using multi-Gaussian DAEM-(*Continued on the next page)

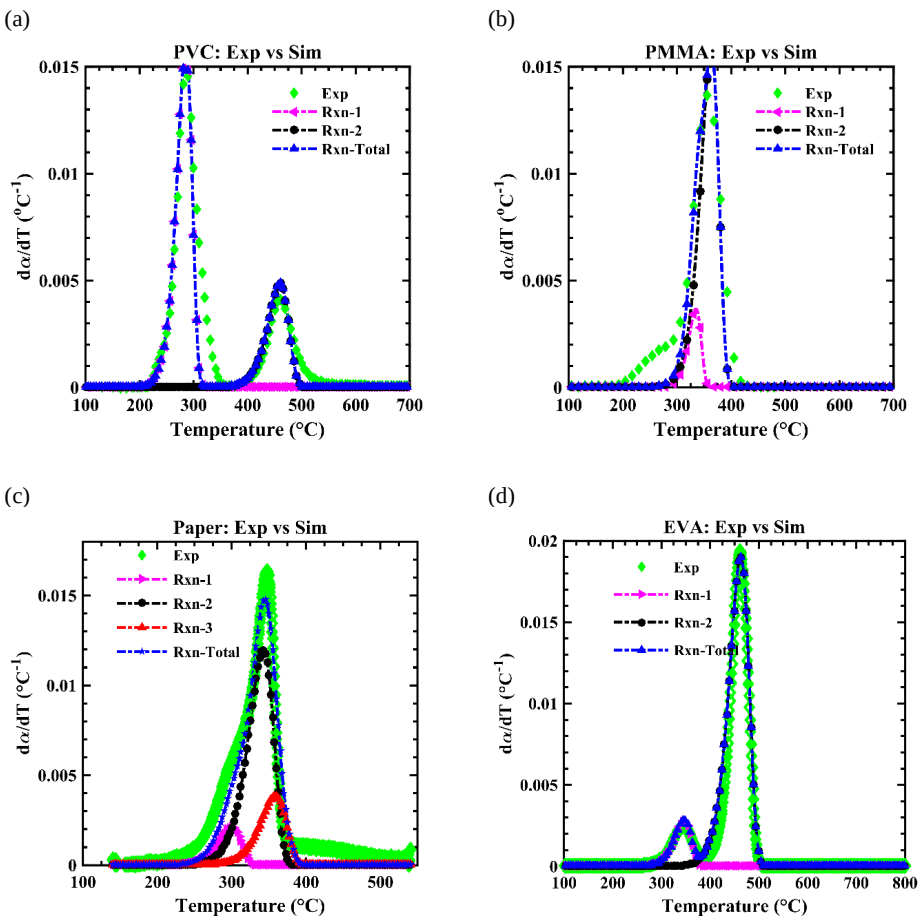

Fig. 1 (*Continued)

(e)

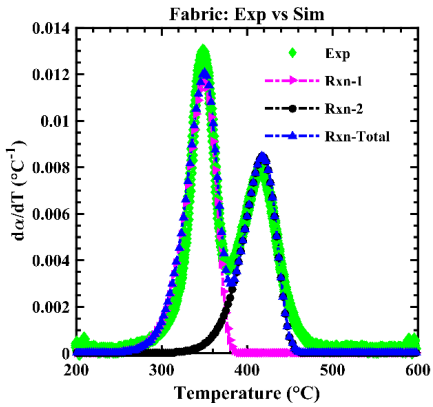

For PVC, PMMA, EVA and the fabric, the DTG curve is modelled as a sum of two peaks, while for paper it is modeled as a sum of three peaks. In the case of PVC and the fabric, the first peak is sharp as compared to the second one, while for PMMA, and EVA the second peak is more prominent. In the case of paper a singular broad peak is clearly visible and slight inflections appear in the beginning and at the end of the pyrolysis reaction. Hence, the de-convolution of this peak was effectively possible using at least three contributing reactions, while for all other cases it was accomplished using two contributing reactions. It can be seen that, in most cases, the modeled curve predicts the experimental data to a high degree of accuracy. However, in some cases, minor inflections in the overall DTG curve could not be reproduced with two reactions e.g. PMMA. It should also be noted that PMMA and EVA left negligible amounts of residues after the test while other materials showed varying amounts of residues. A summary of parameters characterizing the thermal decomposition of the process during the pyrolysis experiment is shown in Table 2.

Table 2 Parameters characterizing the thermal decomposition of different polymers under inert atmosphere for the test at 5K/min

Sample	**Peak**	**T_o (˚C)**	**T_p (˚C)**	**T_f (˚C)**	**Residual Mass (wt. %)**
PVC	1	200	284	365	46
	2	365	461	545	27
PMMA	1	210	247	300	87
	2	300	360	420	1
Paper*	1	234	348	380	40
	2	380	450	535	32
EVA	1	277	341	378	85
	2	378	464	500	0
Fabric	1	250	350	375	60
	2	375	417	498	13

*For paper sample 2nd and 3rd DTG peaks were convoluted, but subtle inflections were clearly visible in the beginning and the end of the reactions. T_o: Peak onset temperature, T_p is the peak temperature, T_f is the Final peak temperature.

Table 3 shows the parameters estimated for the DAEM model fittings. Although, the value of the objective function is very low (10^{-3} to 10^{-4}), and the corresponding fit is less than 7 percent, it indicates model predictions show reasonably good agreement with the experimental data.

Table 3. Estimated Parameters for different polymers using multi-Gaussian distributed activation energy model

Material	Peak	Eo_i	sig_i	w_i	Fit (%)	O.F.
PVC	1	169.4	6.6	0.5	4.7	3.4E-03
	2	219.1	29.4	0.5		
PMMA	1	182.7	11.8	0.6	2.1	2.1E-04
	2	190.8	19.6	0.5		
Paper	1	170.0	5.0	0.6	3.4	2.00E-03
	2	183.0	16.0	0.3		
	3	188.0	20.0	0.1		
EVA	1	184.2	14.9	0.1	2.6	7.5E-04
	2	219.9	44.0	0.9		
Fabric	1	185.2	14.0	0.6	6.2	5.2E-03
	2	206.3	29.5	0.4		

5.2 Sensitivity Analysis of Estimated Model Parameters

A sensitivity analysis allows the study of how changes in input parameters affect the model predictions. It provides a systematic way of analyzing the model's performance and robustness, when one of the input parameters deviates from its optimum value. This technique has been used previously by (Cai and Rao) [24–26] to study parametric changes on their pyrolysis model outputs. In this study, the local sensitivity analysis of estimated DAEM model parameters has been done by varying each kinetic parameter, one at a time, in the range of ±20% of its optimum value at a step size of 5 percent (other parameters being held constant).

Fig. 3 shows a plot of the relative objective function against the relative parameter. In this case the relative objective function (Eq. 5) can be defined as the ratio of the objective function value at the deviated parameter to its value calculated at the optimized parameter.

$$Relative\ O.F. = \frac{O.F._{\cdot Deviated\ Parameter}}{O.F._{\cdot Optimized\ Parameter}} \quad [5]$$

The relative parameter (Eq. 6) represents the ratio of the deviated parameter to its value at the optimized one.

$$Relative\ Parameter = \frac{Deviated\ Parameter}{Optimized\ Parameter} \quad [6]$$

Eq. 7 and Eq. 8 show the relative parameters with respect to mean activation energy and standard deviation of the j^{th} reaction peak respectively.

$$E_{0,j,relative} = \frac{E_{oj,deviated}}{E_{oj,optimized}} \quad [7]$$

$$\sigma_{j,relative} = \frac{\sigma_{j,deviated}}{\sigma_{j,optimized}} \quad [8]$$

A sample calculation for PVC is shown in Fig. 2, in which the DTG peak is computed using DAEM with one of the estimated parameter changed to 85% (randomly chosen) of its optimized value (other parameters held constant).

Fig. 2 A sensitivity analysis calculation showing DTG peak deviations in PVC upon variation of one of the estimated parameters to 85% of its optimized value (other parameters being held constant). Maximum peak deviation is seen upon variation of activation energy values.

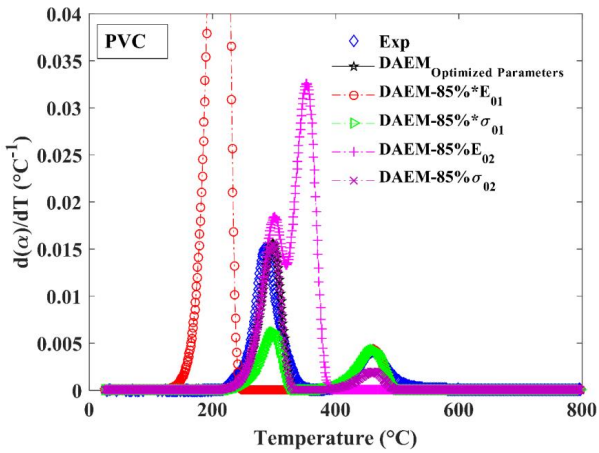

The results show the extent of departure of the computed DTG peaks from the experimental and optimized ones. The degree of variation differs from one relative parameter to the other. The effects were observed to be more pronounced for the mean activation energy values ($E_{01,}$ E_{02}) as compared to their standard deviations ($\sigma_{1,}$ $\sigma_{2,}$). For PVC, deviation in E_{01} resulted in the first peak to shift to the left of the optimum peak by approximately 70 degrees Celsius. Further, the change in σ_{01} resulted in the first peak to diminish to almost half its original value (peak position remain unchanged).

Further, change in E_{02} value resulted in a higher peak. The first peak increased slightly as compared to the optimum one, but the second peak rose sharply in addition. Additionally, a peak shift of 107 degrees Celsius to the left of the optimized peak was observed. Finally, a change in the value of σ_2 caused the second peak to diminish, but the first peak remained unaffected. The overall inference that may be drawn from the sensitivity analysis is that the model has shown higher sensitivity to activation energy values. A slight deviation of 15 percent (see Fig. 2) in its value causes significant changes in the overall DTG peak properties. This phenomenon is less prominent for standard deviation values, whose variation has less effect on the overall DTG peak.

A detailed computation for all the samples is summarized in Fig. 3. For PVC and Paper, the values of relative objective function peaked when E_{01} was deviated to 90 percent of its optimum value, while this was observed at 85 percent for PMMA and Fabric. For EVA, the relative objective function peaked at 80 percent of E_{02} value. A general conclusion that may be drawn from Fig. 3 is that in most cases, the farther the DAEM is computed from the optimized parameters the more the variation is observed in the relative objective function. For some values of the relative parameters the deviation is seen to rise exponentially. In this case, the values of activation energies show a higher value of relative O.F in the order of (10^2-10^4) as compared to standard deviations whose values lie in the range of (1-10). This shows the model's higher sensitivity towards activation energy values as compared to standard deviation. The relative objective functions in most cases show a decreasing trend when the relative parameter increases from 0.8 to 1. It converges to 1 when the relative parameter is 1, followed by an increasing trend as the relative parameter increases from 1 to 1.2.

Fig. 3 Local parametric sensitivity analysis of common polymers

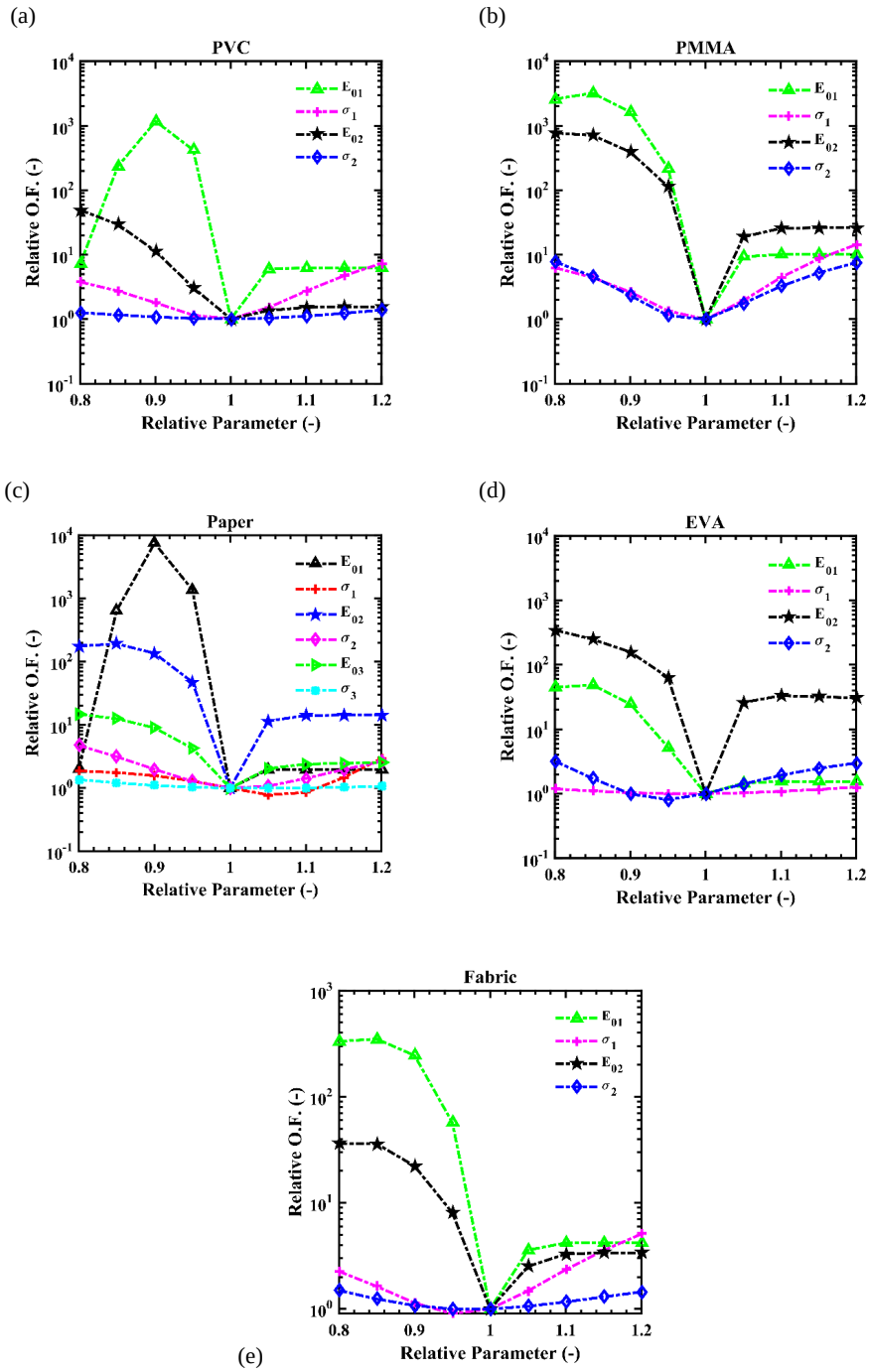

The sensitivity levels of estimated parameters have been divided into three categories (from low to high). The categorization is based on the range of values computed for the relative objective function for each material (in Fig. 3) at different levels of deviation. The point sensitivities were determined at nine different levels ranging from 80-120 percent of the optimized parameter values. It was found that activation energies were found to have the highest sensitivities for the majority of the points.

For PVC and Fabric, E_{01} was found to be most sensitive while for EVA, E_{02} showed high sensitivity and for PMMA and Paper, E_{01} and E_{02} both showed high sensitivity values. The least sensitive parameters were standard deviation (σ_1, σ_2 and σ_3) for all reactions. The result of the sensitivity levels of different parameters is shown in Table 4.

Table 4 Sensitivity levels of estimated parameters of different polymers

		Parameters				
Sensitivity	**Range – Relative O.F.**	**PVC**	**PMMA**	**Paper**	**EVA**	**Fabric**
Low Sensitivity	1 to10	σ_1,σ_2	σ_1,σ_2	$\sigma_1,\sigma_2,\sigma_3$	σ_1,σ_2	σ_1,σ_2
Medium Sensitivity	10 to 100	E_{02}	-	E_{03}	E_{01}	E_{02}
High Sensitivity	> 100	E_{01}	E_{01}, E_{02}	E_{01}, E_{02}	E_{02}	E_{01}

CONCLUSIONS

The multi-Gaussian DAEM model can be used to simulate thermal decomposition phenomena in modern polymers. The complex profile of mass loss and mass loss rate curves observed in the TG experiment can be attributed to many factors. Some of them include multiplicity in the number of reaction steps in the condensed phase, physio-chemical changes occurring in the sample during exposure to heat leading to char formation and intumescence. The appearance of multiple DTG peaks and their minor inflections can now be accounted in the modelled multi-Gaussian DAEM curve by means of optimization technique and non-linear least square approach. The model has the potential to be coupled with the heat transfer equation to estimate HRR and perform flame spread calculations using open source CFD codes. The local sensitivity analysis of the estimated parameters shows model robustness with respect to variation in input parameters. In the present case, higher sensitivities were observed for the model with respect to mean activation energy values as compared to their standard deviations. For future works, when the model is integrated in the overall comprehensive pyrolysis model, this study will augment the current understanding of parametric influences on the overall outputs (such as estimation of HRRs and surface temperatures).

ACKNOWLEDGEMENTS

This work was supported by the funding received from European Union Seventh Framework Program (FP7/2007-2013) under grant agreement n˚ 316991 for the project FIRETOOLS. The authors would like to thank Dr. Anna Matala (VTT Technical Research Centre, Finland), Dr. Marc Janssens (South West Research Institute, Texas, USA) and Dr. Bertrand Girardin (Université Lille1, France) for providing adequate support for experimental work. Also, authors are grateful to the whole team of Fire Tools (Konrad Wilkens, Blanca Andres Valiente, Frida Vermina Lundstrom, Karlis Livkiss, Dan Lauridsen and Fanny Guay) for fruitful discussions.

REFERENCES

1. Van Krevelen, D. W. & Te Nijenhuis, K. *Properties of Polymers*. *Properties of Polymers* (Elsevier, 2009). doi:10.1016/B978-0-08-054819-7.00001-7
2. Wilkie, C. A. & Morgan, A. B. *Fire Retardancy of Fire Retardancy of Polymeric Materials*. (CRC Press, Taylor and Francis Group, LLC, 2010).

3. Troitzsch, J. *Plastics Flammability Handbook - Principles, Regulations, Testing, and Approval (3rd Edition). Hanser Publishers* (Hanser Publishers, 2004). at <http://app.knovel.com/web/toc.v/cid:kpPFHPRTA1/viewerType:toc/root_slug:plastics-flammability/url_slug:polyurethane-foam?b-q=polyurethane foam&b-group-by=true>
4. Van Hees, P. Simulation of Fire Technical Properties of Products and Construction Barriers to Support Fire Safety Engineering - The Fire Tools Project. in (2013). at <http://www.eurofireconference.com/html/programme.htm>
5. Van Hees, P. *et al.* Simulation of fire technical properties of products and construction barriers to support efficient product developement in industry. in *Interflam 2013* (Interscience Communications Ltd, 2013). at <www.intersciencecomms.co.uk>
6. Stoliarov, S. I., Crowley, S., Walters, R. N. & Lyon, R. E. Prediction of the burning rates of charring polymers. *Combust. Flame* **157,** 2024–2034 (2010).
7. Stoliarov, S. I., Crowley, S., Lyon, R. E. & Linteris, G. T. Prediction of the burning rates of non-charring polymers. *Combust. Flame* **156,** 1068–1083 (2009).
8. Shi, L. & Chew, M. Y. L. A review of fire processes modeling of combustible materials under external heat flux. *Fuel* **106,** 30–50 (2013).
9. Snegirev, A. Y. Generalized approach to model pyrolysis of flammable materials. *Thermochim. Acta* **590,** 242–250 (2014).
10. Bhargava, A. & van Hees, P. Using Distributed Activation Energy Model (DAEM) to predict mass loss rates in PMMA. in *Fire Retardancy of Polymeric Materials* P–22 (2015). at <http://www.frpm2015.bam.de/en/home/index.htm>
11. Bhargava, A. & Van Hees, P. Pyrolysis modeling of PVC using distributed activation energy model - micro scale testing. in *Application of Structural Fire Engineering* 448 (Czech Technical University, 2015).
12. Bhargava, A., Van Hees, P. & Andersson, B. Pyrolysis modeling of PVC and PMMA using a distributed reactivity model. *Polym. Degrad. Stab.* (2016). doi:10.1016/j.polymdegradstab.2016.04.016
13. Matala, A. & Hostikka, S. Pyrolysis modeling of PVC cable materials. in *Fire Safety Science* 917–930 (2011). doi:10.3801/IAFSS.FSS.10-917
14. Janssens, M. L. Challenges in Predicting the Pyrolysis Rate of Solid Materials. in *Fire and Materials 2015 - 14th International Conference and Exhibition* 271 – 284 (Interscience Communications, 2015).
15. Witkowski, A. *et al.* Development of an Anaerobic Pyrolysis Model for Fire Retardant Cable Sheathing Materials. *Polym. Degrad. Stab.* **113,** 208–217 (2015).
16. Girardin, B. Small Scale Tests and Numerical Modeling of Fire Performance of Electrical Cable. in *Fire and Materials 2015 - 14th International Conference and Exhibition* 38–52 (2015).
17. Cai, J., Wu, W. & Liu, R. An overview of distributed activation energy model and its application in the pyrolysis of lignocellulosic biomass. *Renew. Sustain. Energy Rev.* **36,** 236–246 (2014).
18. Miura, K. & Maki, T. A Simple Method for Estimating f(E) and k0(E) in the Distributed Activation Energy Model. *Energy & Fuels* 864–869 (1998).
19. Várhegyi, G., Bobály, B., Jakab, E. & Chen, H. Thermogravimetric study of biomass pyrolysis kinetics. A distributed activation energy model with prediction tests. *Energy and Fuels* **25,** 24–32 (2011).
20. Holstein, A., Bassilakis, R., Wójtowicz, M. A. & Serio, M. A. Kinetics of methane and tar evolution during coal pyrolysis. *Proc. Combust. Inst.* **30 II,** 2177–2185 (2005).
21. Zhang, J., Chen, T., Wu, J. & Wu, J. TG-MS analysis and kinetic study for thermal decomposition of six representative components of municipal solid waste under steam atmosphere. *Waste Manag.* (2015). doi:10.1016/j.wasman.2015.05.024
22. Miranda, R., Yang, J., Roy, C. & Vasile, C. Vacuum pyrolysis of commingled plastics containing PVC. I. Kinetic study. *Polym. Degrad. Stab.* **72,** 469–491 (2001).
23. Trninić, M., Wang, L., Várhegyi, G., Grønli, M. & Skreiberg, Ø. Kinetics of corncob pyrolysis. *Energy and Fuels* **26,** 2005–2013 (2012).
24. Rao, S. K., Imam, R., Ramanathan, K. & Pushpavanam, S. Sensitivity Analysis and Kinetic

Parameter Estimation in a Three Way Catalytic Converter. *Ind. Eng. Chem. Res.* **48,** 3779–3790 (2009).
25. Ramroth, W. T., Krysl, P. & Asaro, R. J. Sensitivity and uncertainty analyses for FE thermal model of FRP panel exposed to fire. *Compos. Part A Appl. Sci. Manuf.* **37,** 1082–1091 (2006).
26. Cai, J., Wu, W. & Liu, R. Sensitivity analysis of three-parallel-DAEM-reaction model for describing rice straw pyrolysis. *Bioresour. Technol.* **132,** 423–6 (2013).

Paper III

JOURNAL OF FIRE SCIENCES

Original Article

Journal of Fire Sciences
2019, Vol. 37(1) 18–46

DOI: 10.1177/0734904118808009
journals.sagepub.com/home/jfs
SAGE

Performance analysis of a heat transfer and sub-grid chemical reaction distributed activation energy model for fire simulations

Abhishek Bhargava[1,2], Patrick Van Hees[2], Bjarne Husted[2], Antonio Rodolfo Junior[3] and Corina Neumeister[4]

Date received: 26 June 2018; accepted: 28 September 2018

Abstract

A heat transfer and sub-grid chemical reaction kinetic model for solid phase combustion of a charring polymer is presented based on distributed reactivity modeling approach. The model is used to compute flammability parameters of a polymer sheet of a given thickness to simulate test results of a cone calorimeter experiment. Comparison of model simulations with cone calorimeter test data shows that it gives reasonable prediction of mass loss rate, heat release rate, and total heat released of poly-vinyl chloride (PVC) and ethyl vinyl acetate–aluminum tri-hydroxide (EVA-ATH). The solution of governing equations with the current form of distributed reactivity modeling model poses numerical challenges due to appearance of a double integral in the chemical reaction model. Hence, an analytical approximation has been derived to solve mass and energy conservation equations representing the model. Simulation results indicate that with the approximated form of the distributed reactivity modeling model, along with the input parameters retrieved from literature, the model shows comparatively good predictions for EVA-ATH for mass loss rate, heat release rate, and total heat released, but calculates under-predicted values for PVC.

[1]DBI—Danish Institute of Fire and Security Technology, Hvidovre, Denmark
[2]Division of Fire Safety Engineering, Lund University, Lund, Sweden
[3]Braskem SA, Vinyls Business Unit, Sao Paulo, Brazil
[4]Nabaltec AG, Research and Development (Cables and Polymers) Schwandorf, Germany

Corresponding author:
Abhishek Bhargava, DBI—Danish Institute of Fire and Security Technology, Jernholmen 12, DK-2650 Hvidovre, Denmark.
Email: abb@dbigroup.dk

Keywords
Polymer flammability, distributed activation energy model, Pyrolysis, mass loss rate, PVC, EVA-ATH

Introduction

The past decades have seen increasingly rapid advances in the field of one-dimensional (1D) comprehensive pyrolysis modeling. Several computer programs based on computational fluid dynamics (CFD) framework have been developed such as Fire Dynamics Simulator (FDS),[1,2] ThermaKin,[3] Pyropolis,[4] COMSOL,[5] and MATLAB[6] based applications. These software tools are increasingly being used for initial screening purposes to predict the fire behavior of building materials in standard reaction to fire tests. The availability of such software tools has also provided a possible means to accelerate product development lifecycle and reduce time to market.[7] Some of the notable works in the field of comprehensive pyrolysis modeling include those of McGrattan et al.,[1] Stoliarov and colleagues,[8,9] Snegirev et al.,[10] Marquis et al.,[11,12] Ghorbani et al.,[13] Di Blasi,[14] and Valencia.[6] Their models incorporate different physio-chemical processes to describe material response to thermal abuse in the form of mass and energy conservation equations. More often than not, cone calorimeter is the preferred experimental choice in validating the simulations performed by such 1D pyrolysis models.

Despite elaborate efforts, the results of such simulations deviate considerably from experiments in large number of cases for a variety of materials under different heat exposure conditions and specimen dimensions.[3,13] The main factors accountable for the average quality of predictions made by such deterministic pyrolysis models are poor understanding of heat and mass transfer phenomenon, material property data used in them as input values, sub-model choices, and implementation of boundary conditions.

One way to seek improvements in such models is to make modifications on sub-model level and evaluate the impact on final outcomes on the overall model output. In this study, the performance of distributed reactivity modeling (DRM) sub-model is evaluated to seek improvements in prediction of fire properties of two charring polymers. The main intention of this work is to demonstrate the numerical compatibility of the model equations in a comprehensive pyrolysis model for the solid phase and evaluate the quality of predictions made by it. In addition, it is also the goal of this study to highlight the numerical complexities in modeling the thermal decomposition kinetics of common polymers obtained via data acquired in a small scale device such as a thermogravimetric analyzer (TGA) followed by kinetic computations using conventional approaches. It is discussed how chemical reaction mechanisms suffer from deriving complex reaction pathways followed by hurdles in obtaining their reaction parameters. In contrast, it is shown how DAE approach could act as a possible alternative to model reactions involving several overlapping steps. The scope of modeling work is restricted to heat transfer and chemical reactions to maintain the simplicity of the model during this performance evaluation study and does not cover other physical processes during thermal decomposition such as swelling, shrinkage, intumescence, melting, and diffusion through porous media and in-depth absorption as shown by some of the previously cited detailed research studies.

The implementation of DRM concept is partly based on stochastic approach in which chemical reaction sub-model parameters have been estimated using an optimization scheme

based on pattern search to simulate chemical reactivity tests performed in a small scale device such as a TGA, while the other physio-chemical parameters have been sourced from literature. The DRM modeling approach draws analogy from prior studies performed on pyrolysis of coal and biomass materials in CFD simulations done on entrained flow gasifiers.[15] Some examples of this approach have been discussed in brief along with computational procedures used to implement them in later part of this section. A major reason to seek for an alternative chemical reaction sub-model was that real materials with unknown chemical composition seldom show thermal degradation in a single step. In a large number of cases, they do not show a single well-characterized peak in a small scale differential thermogravimetric (DTG) experiment. In such a case, a typical mass loss TG curve shows several inflections which exhibit multiple peaks in a corresponding DTG curve. This typically creates obstacles in proposing a suitable reaction scheme to estimate kinetic parameters and evaluate the rate of individual reactions and subsequently express the overall rate as a sum of contributing individual ones.

For complex materials, formulation of a very accurate chemical kinetic model requires determination of the reaction mechanisms based on evolved gas analysis using a Mass spectrometer or a Fourier transform infrared (FTIR) spectrometer as a validation tool. Past studies by Valencia and colleagues.[6,16] have shown how FTIR was used as an aid to decipher the five reaction kinetic scheme for poly-urethane. This procedure may be cumbersome to apply for general purpose polymer material showing multiplicity in thermal decomposition process with the release of many species. It will not only pose numerically challenging on sub-model level but is also difficult to implement in existing CFD software. Also, a few studies including that of Snegriev et al.[17] have shown that kinetic computations of several polymers yield activation energy values, which are often reported in conversion averaged format obtained by model free iso-conversional methods such as that of Friedman.[18] However, in many cases, at high conversions apparent activation energy deviates strongly from the conversion average values which can lead to deviations in the predictions of the reaction rate curve. This observation is also indicative of the change in the reaction mechanism. In contrast, distributed activation energy model (DAEM) assumes decomposition of complex polymers occurs through a number of parallel overlapping reactions having different activation energies and frequency factors. Detailed information of exact reaction mechanism of decomposition is not necessary to be known to estimate the reaction rate curve. The activation energy in DRM is not a constant value but a variable that obeys a continuous distribution with probability density function (PDF). Pyrolytic kinetics of different biomass have been extensively investigated by using several PDFs, such as Gaussian, Weibull, Logistic, Gamma, and Log-normal distributions.[19–22] The spread of activation energy may be explained by one or more PDFs as shown in Table 1.

This section will elucidate the brief review of prior research studies which shows successful application of heat transfer and DRM models through simultaneous resolution of chemical kinetics and heat transfer physics.

In a study by Wang et al.,[23] it has been shown how a heat and mass transfer model with DAEM kinetics may be applied to predict mass fraction and temperature profiles inside a coal particle. They were of the opinion that for materials as complex as coal, it was proved that the simple kinetic reaction models were too simple so they have poor adaptability and cannot be applied widely. The research highlighted that DAEM model could be a practical solution and easily couple with CFD simulation as against other kinetic models.

Table 1. A list of probability distribution functions with their respective parameters taken from Xu et al.[22]

PDF	Equation	Parameters	E0
Gamma	$f(E) = \frac{1}{\sigma^{a1}}(E - E_0)^{a1-1}\exp\left(\frac{E-E_0}{\sigma}\right)$	E_0, A, σ, n, $a1$ $(a1 > 1)$	$E_0 + a\sigma$
Logistic	$f(E) = \frac{\pi}{\sigma\sqrt{3}}\exp\left[-\frac{\pi(E-E_0)}{\sqrt{3}\sigma}\right]\left\{1 + \exp\left[-\frac{\pi(E-E_0)}{\sqrt{3}\sigma}\right]\right\}^{-2}$	E_0, A, σ, n	E_0
Log-normal	$f(E) = \frac{1}{(E-E_0)\sigma\sqrt{2\pi}}\exp\left[\frac{-(\ln(E-E_0)-a1)^2}{2\sigma^2}\right]$	E_0, A, σ, n, $a1$	$E_0 + \exp(a + \sigma^2/2)$
Gaussian	$f(E) = \frac{1}{\sigma\sqrt{2\pi}}\exp\left(\frac{-(E-E_0)^2}{2\sigma^2}\right)$	E_0, A, σ, n	E_0
Rayleigh	$f(E) = \frac{E-E_0}{\sigma^2}\exp\left[-\frac{(E-E_0)^2}{2\sigma^2}\right]$	E_0, A, σ, n	$E0 + \sigma\sqrt{\frac{\pi}{2}}$
Weibull	$f(E) = \frac{a1}{\sigma}\left(\frac{E-E_0}{\sigma}\right)^{a1-1}\exp\left[-\left(\frac{E-E_0}{\sigma}\right)^{a1}\right]$	E_0, A, σ, n, $a1$ $(a1 > 1)$	$E_0 + \sigma.\Gamma\left(1 + \frac{1}{a1}\right)^{a}$

PDF, probability density function.
[a]$\Gamma(x)$ denotes the Gamma function in real number range, that is, $\Gamma(x) = \int_0^{\infty} t^{x-1}\exp(-t)dt$.

Another study by Xiong et al.[24] shows results from CFD simulations of an experimental lab scale biomass pyrolysis reactor that included DAEM for kinetic computations. They utilized multi-phase CFD to account for turbulent hydrodynamics and combined it with the DAEM kinetics. Through their results and experience from their simulations, they reported that it was possible to numerically integrate the CFD–DAEM system without significantly increasing the computational overheads. The main reason for inducting DAEM sub-model for biomass pyrolysis was because of the occurrence of highly complex chemical reactions, involving thousands of intermediate products. Regarding numerical implementation, they used the time split approach for joint integration of reaction kinetics and transport processes. The calculated reaction rates were associated with exothermic or endothermic reactions and were used as source terms in the conservation equations for updating field variables at each location.

Another example of this modeling approach involving usage of DAEM kinetics as a sub-model is evident from the work of Rostami et al.[25] In their work, they developed a computer program to solve for the yield and rate of evolution of individual pyrolysis products with given kinetic parameters and heating conditions. They expressed the model integrals in mathematical closed forms so that DAEM can be incorporated more efficiently in a CFD code. They concluded that the complex reactions of biomass pyrolysis and the evolution of different volatile species could be well represented by DAEM.

In another study, Sadhukhan et al.[26] showed the applicability of kinetic scheme with DAEM for coal devolatalization followed by combustion in a batch fluidized bed reactor. They used finite volume method (FVM) to solve fully transient partial differential equations coupled with reaction kinetics. Besides this, some support for usage of DAEM was found in the works of Di Blasi[27,28] who also mentioned the usage of DAEM model for calculating kinetics in view of the complex reactions encountered in biomass pyrolysis.

From the above discussion, it is evident that, so far several studies showing the applicability of this approach have been mainly applicable to the cases involving biomass and coal-based materials. In this work, this approach is extended further to polymeric formulations of poly-vinyl chloride (PVC) and ethyl vinyl acetate (EVA) having a tendency to show multiplicity in the reactions indicating a complex thermal degradation process.

Computational limitations of existing models

There are several computational issues arising in the solution of combined mass and energy conservation equations. The choice of the reaction scheme elucidating the thermal decomposition pathway is one of them. Literature survey shows that there are several reaction schemes available for the mass conservation model characterizing the thermal decomposition pathway of similar polymers. A large number of times reaction schemes are different from one another for a material of same chemical composition and a gas analysis is a perquisite to determine the reaction mechanism. Some examples of proposed reaction schemes for common polymers are shown in Table 2.

From Table 2, it can be said different types of mathematical models exist in literature showing the thermal degradation of similar polymers. Each reaction scheme comprises several ordinary differential equations (ODEs) which indicate a mass loss rate (MLR) curve that should be obtained via integration of the ODEs once they are fed with respective kinetic parameters as input values. More often, these systems of ODEs pose numerical problems to converge when fractional orders of reactions are involved. Also, estimation of parameters is one of the challenging tasks since this involves simultaneous optimization of ODEs accompanied with parameter search algorithms based on least square minimization approach. During minimization process, the appearance of fractional order makes the differential equations stiff to solve and often lead to numerical instabilities and convergence problems. Although, with the advent of inbuilt Runge–Kutta solver in commercial software such as MATLAB, these equations can be readily solvable with commands such as ode15s, ode23tb, ode45, and so on. However, such solvers also fail to converge if the systems of ODEs are extremely stiff despite adjusting tolerance values.

In addition, there are some fundamental problems with the standard methods (ASTM E1641[33] and E698[34]) for kinetic parameter estimation such as for the determination of activation energies. The main limitation of these methods is that degradation kinetics can only be made with first-order kinetic model and assuming constant activation energy. This can lead to erroneous predictions when the process obeys a different reaction model and/or when the process demonstrates significant variation of activation energy with conversion. That is, before using such methods, one should make sure that it does not vary significantly with the conversion and the reaction model is consistent with first-order kinetics.[18]

This highlights the issues and limitations in obtaining the solution of existing kinetic submodels. Also, when it is required to implement the kinetic sub-model in a CFD code numerically, it will prove to be even more challenging, since the convergence problems persist at the sub-model level, and their extended field of application in a CFD code will create further numerical issues. For fire simulations, it is imperative to determine fire growth rate and fuel load in a building for correct assessment of heat release rate (HRR) curve. Hence, in this regard, the requirement of a good sub-grid model that can be easily integrated in a CFD simulation of solid phase would be of high value. Marquis et al.[35] have demonstrated in their research that the prediction accuracy of complex thermal decomposition is no longer hampered by the resolution of the technique used but rather by precision or complexity level of the description regarding chemical pathway. The choice of mechanism is dependent on the degree of knowledge about the studied material. Usually in the fire field, the chemical characteristics of materials are unknown and the mechanisms given in literature rely on parametric approaches.

Table 2. A few examples of different reaction schemes and kinetic models from the literature for PVC and EVA-ATH and poly-urethane.

Material	Kinetic model	Type	Stage	Model	Estimated Parameters	Reference
PVC	$PVC_1 \rightarrow \alpha_1 HCl + \gamma_1 Rs_1$ $PVC_2 \rightarrow \alpha_2(HCl + V_1) + \gamma_2 Rs_2$ $\alpha_3 Rs \rightarrow \alpha_4 V_2 + \gamma_3 Rs_3$ where Rs = Rs1 + Rs2	Parallel	1st 2nd	$\frac{dX}{dt} = \sum_{i=1}^{N} \alpha_i \frac{dX_i}{dt}$ [1] $1 = \sum_{i=1}^{N} \alpha_i$ [2] $\frac{d[PVC]}{dt} = \sum_{i=1}^{2} \alpha_i \frac{d[PVC_i]}{dt} + \alpha_3 \frac{d[R]}{dt}$ [3] $\frac{d[PVC]}{dt} = \sum_{i=1}^{2} \alpha_i \left(-A_i e^{-\frac{E_{ai}}{RT}} [PVC_i]^{n_i}\right) + \alpha_3 \left(-A_3 e^{-\frac{E_{a3}}{RT}} [R_2]^{n3}\right)$ [4]	12 Unknown kinetic parameters; 3 Pre-exponential factors (A_1, A_3, A_3), 3 Activation energies (E_{a1}, E_{a2}, E_{a3}), 3 Reaction orders (n1, n2, n3), 3 Yield Factors (α1, α2, α3)	Wu et al.[29]
PVC	PVC→aHCl + bI bI→cV1 + eR1 eR1→fV2 + gR2	Series	1st 2nd	$\frac{d[PVC]}{dt} = -A_1 e^{-\frac{E_{a1}}{RT}} [PVC]^{n1}$ [1] $\frac{d[I]}{dt} = b\left(A_1 e^{-\frac{E_{a1}}{RT}} [PVC]^{n1} - A_2 e^{-\frac{E_{a2}}{RT}} [I]^{n2}\right)$ [2] $\frac{d[R_1]}{dt} = e\left(A_2 e^{-\frac{E_{a2}}{RT}} [I]^{n2} - A_3 e^{-\frac{E_{a3}}{RT}} [R_1]^{n3}\right)$ [3] $\frac{d[R_2]}{dt} = g\left(A_3 e^{-\frac{E_{a3}}{RT}} [R_1]^{n3}\right)$ [4]	12 Unknown kinetic parameters; 3 Pre-exponential factors (A_1, A_3, A_3), 3 Activation energies (E_{a1}, E_{a2}, E_{a3}), 3 Reaction orders (n1, n2, n3), 3 Yield Coefficients (b, e, g)	Miranda et al.[30]
EVA-ATH	EVA-ATH→Gas1 + R1 R1→Gas2 + R2	Parallel		$\frac{d[EVA-ATH]}{dt} = \sum_{i=1}^{2} \alpha_i \left(-A_i e^{-\frac{E_{ai}}{RT}} [EVA-ATH_i]^{n_i}\right)$ [1]	6 Unknown kinetic parameters 2 Pre-exponential factors (A_1, A_2), 2 Activation energies (E_{a1}, E_{a2}), 2 Reaction orders (n1, n2)	Girardin et al.[31]

(continued)

Table 2. Continued

Material	Kinetic model	Type	Stage	Model		Estimated Parameters	Reference
Poly-urethane	Foam Pyrolysis PU Foam→β-Foam + V1 β-PU Foam→Char1 + V1 Foam Oxidation PU Foam + O_2→Char2 + V2 β-Foam + O_2→Char2 + V2 Char Oxidation Char + O2→R3 + V3	Series	1st 2nd 3rd 4th 5th	$\omega_i = -A_i e^{-\frac{E_{ai}}{RT}}[m_i]^{n_i} y_{O_2}{}^{\delta}$ $\frac{dm_f}{dt} = -\omega_p - \omega_0$ $\frac{dm_\beta}{dt} = \nu_{\beta,p}\omega_p - \omega_{p\beta} - \omega_{0,\beta}$ $\frac{dm_c}{dt} = \nu_{c,p\beta}\omega_{p\beta} + \nu_{c,0}\omega_0 + \nu_{c,0\beta}\omega_{0\beta} - \omega_c$ $\frac{dm}{dt} = \frac{dm_f}{dt} + \frac{dm_\beta}{dt} + \frac{dm_c}{dt} + \frac{dm_r}{dt}$ $\frac{dm_\beta}{dt} = \nu_r\omega_c$ y_{O2} = 0.23 (O_2 mass fraction) δ = Reaction order for oxygen mass fraction (δ = 0 for Nitrogen) Subscripts (p-Pyrolysis reaction, o-Oxidation reaction, c-Char oxidation reaction)	[1] [2] [3] [4] [5] [6]	16 Unknown kinetic parameters 4 Activation energies (E_{a1}, E_{a2}, E_{a3}, E_{a4}) 4 Pre-exponential factors (A_1, A_2, A_3, A_4) 4 Reaction order coefficients (n1, n2, n3, n4) 4 Stotiometric yields ($\nu_{j,i.}$)	Rein et al.[32]

V, Volatiles; I, Intermediate; C, Char; R1, Residue generated in the first stage; R2, Residue generated in the second stage; PVC, poly-vinyl chloride; EVA-ATH, ethyl vinyl acetate–aluminum tri-hydroxide.

In contrast to conventional practice of using purely Arrhenius-based kinetics, the DAEM model comparatively offers a simple parametric approach where ODEs are of parallel and additive in nature. This provides relative ease of its implementation in a CFD code as compared to the multi-reaction mechanism involving interlinked ODEs. It is expected the parallel reaction model will reduce the effort of proposing multi-reaction scheme for material decomposing in several steps when implemented in comprehensive pyrolysis models as evidenced in the literature related to wood, poly-urethane, and several other plastic products discussed earlier. This modeling approach could be used to scale up MLR predictions from a TGA device to bench scale cone calorimeter level computations by defining heat and chemical reaction processes in relevant detail.

Modeling

Governing equations

In this section, the main governing equations of the model are shown. The model is developed based on the work of Ghorbani et al.,[13] Cai et al.,[19] and solid phase model described in Society of Fire Protection Engineers (SFPE) handbook.[36]It is mainly divided between equations of mass and energy conservation followed by description of initial and boundary conditions and finally computation of MLR.

Mass conservation. The mass conservation equations are based on DAEM. It differs from conventional Arrhenius-type kinetics in a way because it assumes that activation energies of chemical reactions are distributed over a finite range. Literature sources reveal the values of mean activation energy lie in the range of $50–350 \times 10^3$ J/mol, while those of pre-exponential factors lie in the range of $10^{10}–10^{30}$ (1/s).[37] The probability of finding mean activation energy is given by normalized PDF, $f(E)$ as shown previously in Table 1. In this work, the discussion is limited to Gaussian PDF whose peaks are characterized by the mean value of activation energy and standard deviation values. These values govern the peak position and width of the DTG curve, respectively. If it is assumed that there are "n" number of reactions occurring in the polymer matrix during thermal decomposition, then the total rate of thermal decomposition reaction is the cumulative sum of the rate of individual sub-reactions multiplied by their assigned weights as shown in equations (1)–(4)

$$\frac{\partial \rho}{\partial t} = -\omega_s \tag{1}$$

$$\omega_s = A(\rho - \eta_{char}\rho_0)\int_0^\infty \exp\left(-\frac{E}{RT}\right) f(E)dE \tag{2}$$

$$f(E) = \frac{1}{\sigma\sqrt{2\pi}}\exp\left[-\frac{(E-E_0)^2}{2\sigma^2}\right] \tag{3}$$

where ρ, ω_s, η_{char}, A, E, E_0, and σ are the density, reaction rate, char fraction, pre-exponential factor, activation energy, mean activation energy, and standard deviation,

respectively. The total reaction rate is expressed as a weighted cumulative sum as shown in equation (4)

$$\frac{\partial \rho}{\partial t}_{Total} = \sum_{i=1}^{n} c_i \frac{\partial \rho}{\partial t}_i = \sum_{i=1}^{n} -c_i \omega_{si} \tag{4}$$

Here, c_i and ω_{si} denote the weight and reaction rate of ith individual reaction, respectively. The parameters A_i, σ_i, E_{0i}, and c_i are determined by optimization routine by minimization of the objective function using least sum of square (LSS) approach as shown in a previous study by Bhargava et al.[38]

Energy conservation. The second part of the model is the heat transfer model, in which the coupling is done via temperature. The main equation of the model formulation is given by equation (5), where ρ, c_p, k_s, and T describe the mass density, heat capacity, thermal conductivity, and temperature of the solid material, x is the spatial coordinate normal to the exposed surface, $\omega_{s,Total}$ is the total mass reaction rate as described above (i.e. amount of virgin material converted to pyrolysis gas per unit time per unit volume), and $\Delta H_{r,i}$ is the heat of pyrolysis of the ith reaction (i.e. heat required to generate unit mass of volatiles at temperature T). Equation (5) describes the heat conduction inside the solid and accounts for endothermic pyrolysis processes

$$\rho c_p \frac{\partial T}{\partial t} = \frac{\partial}{\partial x}\left(k_s \frac{\partial T}{\partial x}\right) - \sum_{i=1}^{n} c_i \omega_{s,i} \Delta H_{r,i} \tag{5}$$

Additional assumptions which are valid for this model are as follows:

- In-depth generated volatiles are instantaneously transported to the surface;
- Surface regression is not captured by the model, the fuel thickness remains intact regardless of the amount of solid fuel consumption;
- Volume expansion is not addressed under the current scope of the model;
- Specimens are assumed to be opaque and hence in-depth absorption of radiation is not considered under the current scope of the model.

Increasing complexity: gas diffusion and in-depth absorption. The model shown above can incorporate further complexities by incorporating other heat transfer effects in the pyrolyzing material by inclusion of gas diffusion and in-depth absorption of radiation. This is shown via modified energy conservation equation (6). It considers gas diffusion and in-depth absorption of radiation in the material. The diffusive mass flux term

$$-\sum_{g}^{N \times Total\ no.\ of\ gases)} m_g \frac{\partial\left(\int_0^T c_{p,g} dT\right)}{\partial x}$$

in this equation implies heating up of the gas from ambient temperature to the temperature of the media in which it diffuses resulting in instantaneous heat transfer between decomposed media and diffusing gases. Also, the diffusion of the gases in the heat balance equation

indicates that when the gases evolve from the decomposing materials, it can absorb energy and remove it from the material as they diffuse out from the surface of the material, the gas mass flux m_g (kg/m^2) and the mass flux rate (kg/m^2/s) of the gases can be defined by equations (7) and (8), respectively, where D_g is the diffusion coefficient (m^2/s)

$$\rho c_p \frac{\partial T}{\partial t} = \frac{\partial}{\partial x}\left(k_s \frac{\partial T}{\partial x}\right) - \sum_{i=1}^{n} c_i \omega_{s,i} \Delta H_{r,i} - \sum_{g=1}^{N(Total\ no.\ of\ gases)} m_g \frac{\partial\left(\int_0^T c_{p,g} dT\right)}{\partial x} + \varepsilon \frac{\partial q_{rad}}{\partial x} \quad (6)$$

$$m_g = -D_g \frac{\partial m_g}{\partial x} \quad (7)$$

$$\frac{\partial m_g}{\partial t} = \frac{1}{\rho_0}\frac{\partial \rho}{\partial t}_{Total} - \frac{\partial m_g}{\partial x} \quad (8)$$

Furthermore, the last term in equation (6) accounts for the in-depth radiation absorption of the incident heat flux which is in accordance with the standard Lambert Beer Law. Here, the absorbed radiation decreases exponentially with the distance to the impacted surface which is given by equation (9). Here, the absorption coefficient is denoted by κ (1/m)

$$q_{rad} = G\exp(-\kappa x) \quad (9)$$

The above set of equations (6)–(9) account for the possibilities to increase the model complexity and incorporate other physical effects during material thermal decomposition. However, in this study, to maintain the simplicity of the model, the calculations are limited to equations presented in the "Energy conservation" section. The reader is apprised about the more complex modeling framework in view of other physical effects that may be included in future for description of combined heat and mass transfer effects in the material.

Initial conditions. The initial conditions for the model is described by equation (10), which states that, before any exposure to thermal radiation, the sample temperature is that of ambient atmosphere and its density is same as that of virgin sample

	Density	Initial temperature
PVC	ρ_0 = 1425 kg/m^3	T_0 = 298°K
EVA-ATH	ρ_0 = 950 kg/m^3	T_0 = 298°K

PVC, poly-vinyl chloride; EVA-ATH, ethyl vinyl acetate–aluminum tri-hydroxide.

$$\text{At } t = 0, \text{ for } 0 \leqslant x \leqslant L,\ T = T_0,\ \rho = \rho_0 \quad (10)$$

Boundary conditions. The boundary conditions define the exposure and insulation on the surface and back side of the sample, respectively. Equation (11) shows the insulated backside condition while equation (12) shows the exposed side conditions on the top surface of the polymer describing the exposure as a sum of incident heat flux from the cone, radiative heat losses, and convective losses from the surface. The addition of flame heat flux is

approximated until the attainment of threshold temperature value for the onset of degradation of polymer sample is reached. More conventionally, the ignition criteria and addition of flame heat flux is determined when the MLR of the pyrolyzing gases attain the lower flammability limit until the critical mass flux value of 1 g/m^2/s is reached also discussed by Lyon and Quintiere.[39] Also, the above cases correspond to thermally thick solids whose Biot number (Bi = hl/k) was found to be higher than 0.1 indicating existence of temperature gradient in studied specimens.

Insulated backside

$$For,\ t>0, \text{at } x=L,\ \frac{\partial T}{\partial x}=0 \tag{11}$$

Exposed side

$$For\ t>0, \text{at } x=0, \ddot{q}_{w(t)}=\varepsilon G-\varepsilon\sigma_c\left(T_s^4-T_{amb}^4\right)-h(T_s-T_{amb})+q_{flame} \tag{12}$$

In the above equations, ε is the material emissivity, G is the incident heat flux from the cone heater, σ_c is the Stefan–Boltzmann constant (5.67×10^{-8} W/m^2/K^4), T_s is the surface temperature of the polymer surface, L is the thickness of the material, h is the convective heat transfer coefficient (W/m^2/K), and q_{flame} is the flame heat flux (W/m^2/K).

MLR. The MLR of the polymer is given by equation (13), which shows the total MLR summed over the thickness of the sample at any instant. It is computed by the line integral of the total reaction rate with respect to the thickness of the sample

$$m_f(t)=\int_0^L \omega_s(x,t)dx \tag{13}$$

Treatment of thermal properties

The model assumes the solid phase thermal conductivity (k_s [W/m/K]) and specific heat (c_p [J/kg/K]) to be temperature-dependent quantities. In addition, thermal conductivity and specific heat are assumed to be a composite function of the amount of virgin material converted into char. As the material is irradiated with the heat from the cone, the combustion reaction is triggered which leads to conversion of solid phase into char. The values of thermal conductivity, specific heat, and reaction progress variable (α) also called as conversion are co-related by equations (14)–16, respectively

$$k_s=k_{virgin}(T)\alpha+(1-\alpha)k_{char}(T) \tag{14}$$

$$c_p=c_{p,\,virgin}(T)\alpha+(1-\alpha)c_{pchar}(T) \tag{15}$$

$$\alpha=\frac{\rho_{virgin}-\rho(t)}{\rho_{virgin}-\rho_{char}} \tag{16}$$

Solution and computational workflow

The solution methodology is divided into two parts. In the first part, an analytical approximation to DAEM model is shown (see Appendix 2), while in the second part, the overall computational workflow is presented. The flowchart below shows the workflow of the

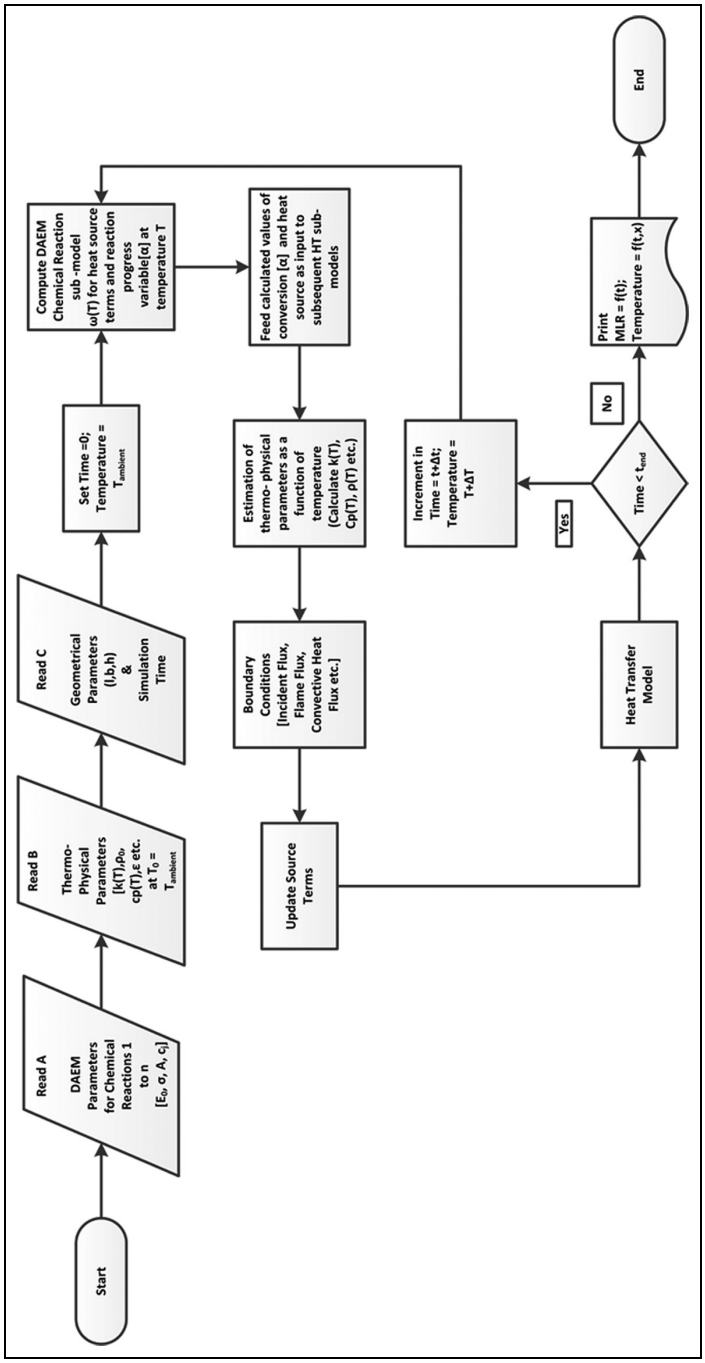

Figure 1. Flowchart depicting combined working of heat transfer and DAEM reaction model for estimation of fire properties of charring polymer.

model computation process. The procedure involves collection of different input parameters (chemical reaction, thermo-physical, and geometrical parameters) of the material in consideration. Previously, such models have been solved with time split approach method as discussed in the introductory part of the article. In this case, COMSOL has been used to solve the differential equations using FVM; however, in this section, only the sequential steps will be described in the form of a flowchart. It can be seen from Figure 1 that in the first step, reaction parameters, thermo-physical parameters, and geometrical parameters are read. Thereafter, the control passes to the DAEM sub-grid model followed by feeding of the calculated conversion values and the source terms to the thermo-physical property estimation module. This is followed by specification of the boundary conditions. With every increasing time step, the boundary conditions provide necessary increment in the temperature (due to irradiation from the cone and the flame heat flux) on the top side or insulation on the bottom surface of the domain. As the temperature increases in the calculation domain, the source terms are updated to provide inputs to heat transfer model and modification of thermo-physical properties. As the conversion increases, the char and virgin material properties change depending upon the converted fraction. The chemical reaction model also provides necessary input in the form of heat generated/consumed from the source to the heat transfer model. Finally at the end of the simulation time, the MLR is computed by integration of MLRs over the space domain, that is, over the thickness of the sample. The time to ignition, peak MLR, and time to extinction may be obtained from the MLR curve, while HRR curve may be obtained as a product of MLR curve and effective heat of combustion (EHC). Similarly, temperature profiles on the front and back side of the polymer sample may be computed once the heat transfer physics is resolved.

Experiments

The experimental part included preparation of the sample specimens for PVC and EVA-ATH (ethyl vinyl acetate–aluminum tri-hydroxide) and carrying out thermogravimetric analysis and cone calorimeter tests on individual specimens.

Polymer extrusion

PVC formulation. The PVC test specimen was manufactured by Braskem polymers S/A using the compounds listed in Table 3 (also reported in another study by Rodolfo and Innocentini-Mei.[40]).

The polymer sheets were prepared by mixing PVC resin, thermal stabilizer, plasticizer, and other additives in a single screw extruder. The constituent materials were added in a mixer (Mecanoplast ML-9) to form a homogeneous mix. The resin, thermal stabilizer, calcium carbonate, and lubricant were added and heated to 80°C and submitted to shear forces in the mixer. This was followed by addition of plasticizer DIDP and ESO. The final composition was discharged at 110°C, and cooled to 35°C–40°C. The formulation was then processed in a heated single screw extruder by subjecting it to gradual increase in temperature from 140°C to 150°C at 80 revolutions per minute (r/min). The test specimen was obtained in the form of pellets in a roll mill. The temperature, processing time, and the rotation to prepare 3 mm-thick plates were 160°C, 3 min, and 20 r.p.m., respectively. Finally, the material pressing was performed in a stainless steel press at 175°C.

Table 3. Contents of PVC compound formulation.[40]

S. no	Material	Trade name	Amount in phr (parts per hundred of rubber)
1.	PVC resin (K 65)	Norvic SP 1000	100
2.	Calcium/Zinc thermal stabilizer	Naftomix XC-1202	3.5
3.	Diisodecyl phthalate (plasticizer)	DIDP	45
4.	Epoxidized soyabean oil (ESO, plasticizer)	Drapex 6.8	5
5.	Calcium carbonate (mineral filler)	Barralev C	40
6.	Steraic acid (lubricant)	Naftolub L12	0.2

PVC, poly-vinyl chloride.

Table 4. Contents of EVA-ATH compound formulation.

S. no	Material	Trade name	Content
1	Ethylene Vinyl Acetate Copolymer (19% EVA)	Escorene UL00119	34.6%
2	3-Aminopropyltriethoxysilane	AMEO	0.4%
3	Aluminum Trihydroxide (ATH)	APYRAL 40CD	65%

EVA-ATH, ethyl vinyl acetate–aluminum tri-hydroxide.

EVA-ATH formulation. The EVA-ATH formulation was prepared in a two-step process using the compounds listed in Table 4. In the first step, the mixture constituents were added to a double shaft kneader (LDUK 1.0 from Werner and Pfleiderer). The mixing chamber was equipped with a thermostat (LTH 303S from Lauda) to control the temperature. The kneading procedure involved the following steps:

(a) 1 h preheating of the kneader at 135°C,
(b) Addition of weighed plastic granules of EVA copolymer resin (Escorene UL00119) to the kneading chamber and kneading for 2 min at 150°C,
(c) Addition of approximately 70% weight of APYRAL 40CD,
(d) Addition of AMEO followed by kneading at 130°C for 5 min, and
(e) Addition of remaining amount of APYRAL 40CD; kneading at 155°C for 6 min, then 8 min at 165°C.

In step 2, the kneaded mixture was pressed in a hydraulic press (Polystat 300S from Servitec) using compression molding at 130°C for 5 min pre-pressing, followed by pressing at 200 bar for 6 min.

Thermogravimetric analysis

For thermogravimetric analysis of PVC, a simultaneous thermal analyzer (STA-409) and mass spectrometer (QMS-403) was used to study the reaction rate of thermal decomposition. The sample size was cut into a thin piece that weighed between 5 and 8 mg and subjected to linear temperature ramp from 20°C to 1000°C at a heating rate of 20°C/min. Sample mass and MLR were recorded as functions of time and temperature. The experiment was

performed in air atmosphere at a gas flow rate of 50 mL/min. For PVC, the material decomposition is approximated to fire-like conditions since the gaseous atmosphere used was not purely inert due to testing limitations. The results are used for model development work only. Alumina crucibles were used as sample holders during the experiment. For EVA-ATH formulation, the TG data of Girardin et al.[31] were used, who tested similar chemical formulation of EVA-ATH in nitrogen atmosphere at a heating rate of 20°C/min. The TG data were converted into digital format and later used for kinetic parameter estimation.

Cone calorimetry

The heat released by burning polymers was measured by cone calorimeter built by Fire Testing Technology (East Grindstead, UK) as per the procedures outlined in ISO 5660-1.[41] The size of the PVC specimen was (length, breadth, thickness) 0.1 m × 0.1 m × 0.003 m and experiments were performed in duplicate at an incident heat flux of 50×10^3 W/m^2. For EVA-ATH, the specimen size used was 0.1 m × 0.1 m × 0.0065 m and the test was performed at an incident heat flux value of 35×10^3 W/m^2. The duct flow rate was kept at 24 L/s. The tests were performed by Braskem and Nabaltec AG as part of two individual research studies in separate laboratories.

Results and discussions

Kinetic fittings

Figure 2(a)–(f) shows the result of thermogravimetric analysis. The plots shown are experimental TG curves (a, d) and their corresponding normalized DTG curves (b, e). In the DTG curves, a comparison is drawn between the experimental and simulated plot of $d\alpha/dT$ versus temperature. It can be seen that from the DTG curves, in case of EVA-ATH, two main peaks are visible while for PVC three to four peaks are visible. In EVA-ATH, the onset of first peak occurs at a temperature of 220°C indicative of dehydration of ATH, releasing water and formation of ceramic residue made up of alumina (Al_2O_3). The second step corresponds to the decomposition of EVA around 350°C in two steps leading to formation of acetic acid and hydrocarbons at around 450°C. The decomposition of EVA-ATH is well described by Hewitt et al.[42]

For PVC, the first peak occurs at 323°C, while the second peak occurs at 456°C, and the third peak occurs at 737.6°C. The test is conducted in air atmosphere; hence, conditions corresponding to combustion reactions are present in the TGA apparatus. However, the first stage of weight loss is still likely to be attributed to the release of hydrogen chloride (HCl) and this phenomenon is termed as dehydro-chlorination. In the second reaction step, many cyclic compounds aromatize via chain scission reactions and undergo combustion reactions in the presence of oxygen leading to further weight loss and formation of carbon dioxide, water and other aliphatic and olefenic, aromatic hydrocarbons and char.

DAEM has been used to model the peaks occurring in the DTG curve of both the polymers. The parameter search domain was set for mean activation energy to be (50–350 kJ/mol), standard deviation (1–50 kJ/mol), and pre-exponential factor 10^{10}–10^{16} (1/s). The estimations were based on an optimization algorithm developed using a MATLAB code which uses the pattern search method to search for optimum kinetic parameters to obtain a good fit for the reaction rate curve. The code is also programmed to search for random numbers

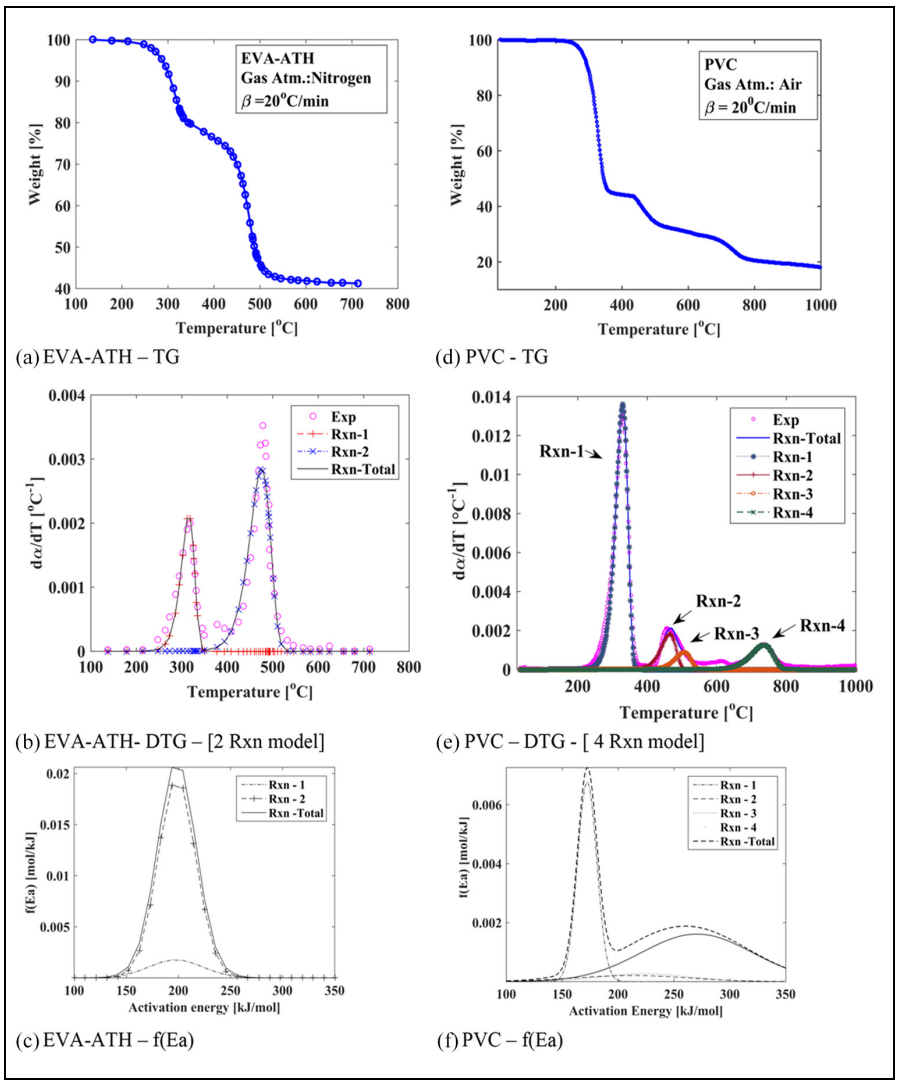

Figure 2. DAEM model fits for EVA-ATH (a-c) and PVC (d-f) (for PVC fittings shown only for four reaction model).

within the above-cited range to avoid any negative values. In addition, a visual manual check of the real time reproduction of the DTG curve is incorporated in the code to monitor the fitting quality. Also, the range of pre-exponential factor was kept in a rather lower range as compared to that cited in the literature in view of the theories of compensation effect

Table 5. DAEM kinetic parameters for EVA-ATH and PVC formulations obtained using pattern search.

Reaction	Parameters	EVA-ATH (2-Rxn fitting)	PVC (2-Rxn fitting)	PVC (4-Rxn fitting)
Rxn-1	E_{01} (kJ/mol)	197.4	180.3	172.3
	σ_1 (kJ/mol)	25.8	42.4	9.0
	A_1 (1/s)	7.5×10^{15}	8.6×10^{13}	1.7×10^{13}
	C_1 (–)	0.1	0.2	0.3
Rxn-2	E_{02} (kJ/mol)	198.5	190.8	212.0
	σ_2 (kJ/mol)	18.1	12.7	50.0
	A_2 (1/s)	1.0×10^{12}	3×10^{11}	1.7×10^{13}
	C_2 (–)	0.9	0.8	0.1
Rxn-3	E_{03} (kJ/mol)	–	–	224.0
	σ_3 (kJ/mol)	–	–	40.0
	A_3 (1/s)	–	–	1.6×10^{13}
	C_3 (–)	–	–	0.1
Rxn-4	E_{04} (kJ/mol)	–	–	270.4
	σ_4 (kJ/mol)	–	–	50.0
	A_4 (1/s)	–	–	1.1×10^{12}
	C_4 (–)	–	–	0.5
Objective function		1.2×10^{-5}	2.1×10^{-4}	1.5×10^{-4}
Fitness (%)		7.0	4.5	4.2

EVA-ATH, ethyl vinyl acetate–aluminum tri-hydroxide; PVC, poly-vinyl chloride; Rxn, reaction.

discussed by Lakshmanan and White[43] to avoid multiple sets of parameters resulting in fitting of the DTG curve. In both cases, the model is able to capture the peak inflections to a high degree. EVA-ATH has been modeled with only two reactions, while PVC has been modeled with two and four reactions. The two reaction model reproduces the first two peaks only while the four reaction model which covers the entire range of peaks exhibited by PVC. The corresponding parameters used to model these curves are summarized in Table 5. In the figures below only the best fits with four reactions are shown.

The above parameters were obtained by minimization of the objective function using an optimization scheme as shown by Bhargava et al.[44] and Cai and Ji[45] in a previous research. The normalized probability distribution curve, $f(Ea)$ versus activation energy for each polymer is shown as a cumulative sum of individual reaction rate curves. It can be seen that for the overall reaction, the mean activation energy was found to lie at 193.8 kJ/mol for EVA-ATH and 173.4 kJ/mol for PVC shown by the peak of the overall reaction rate curve.

Cone calorimeter tests

EVA-ATH. Figure 3 shows the MLR of EVA-ATH polymer. The curve shows linear rise to the peak value at 16 g/m^2/s within first 78 s followed by a linear decay until the end of the experiment. The ignition criterion was defined as the time to reach critical mass flux value of 1 g/m^2/s also used by Stoliarov et al.[3] For EVA-ATH, MLR crosses the threshold of 1 g/m^2/s after 43 s, while in the decay phase, the MLR falls below this threshold value after 546 s. The second curve is the HRR curve showing occurrence of a characteristic peak shortly after ignition followed by a steady burning phase with HRR output varying between 120 and 140 kW/m^2. This is followed by steady linear decay until 800 s. The peak heat release rate

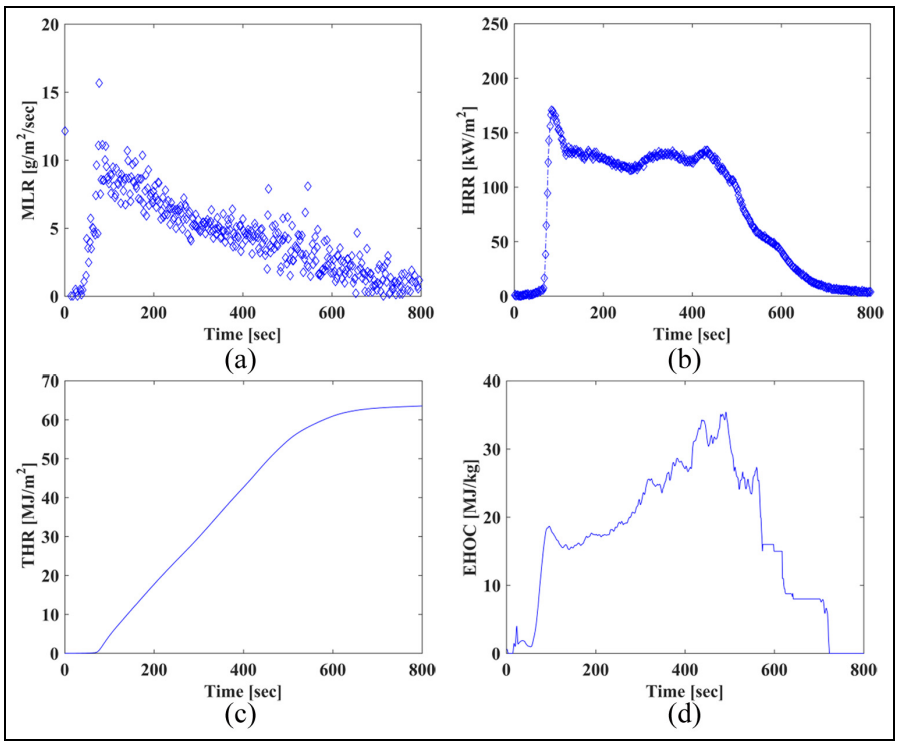

Figure 3. Cone calorimeter results for EVA-ATH formulation: (a) mass loss rate (MLR), (b) heat release rate (HRR), (c) total heat released (THR), and (d) effective heat of combustion (EHC).

(p-HRR) and the time to peak heat release rate (t_{pHRR}) were found to be 171 kW/m^2 and 84 s, respectively. The third curve shows the total heat released (THR) during the experimental run. The THR at the end of the run was found to be 63 MJ/m^2. The EHC was found to show a high degree of variation during the experiment, but overall, the values were found to lie below 40 MJ/kg. Largely the values were found to vary between 10 and 35 MJ/kg.

PVC. Figure 4 shows the MLR curve of PVC. The curve shows a sharp rise to a peak value of 23 g/m^2/s followed by linear decay phase. During the rise, the MLR crosses the threshold value of 1 g/m^2/s in first 6 s of the test. The time to peak MLR was found to be 58 s. In the decay phase, the value of MLR falls below the threshold of 1 g/m^2/s after 410 s. The second curve is the HRR curve. The peak HRR and time to peak HRR were found to be 292 kW/m^2/s and 90 s, respectively. The profile is similar to the MLR curve, in which after a short delay, the curve rises to the peak value followed by a gradual linear decay. The third curve is the THR curve, it shows the THR at the end of the experiment was 66 MJ/kg. The profile shows zero reading in the beginning of the experiment, indicating toward short delay until the ignition, followed by a linear rise and then a plateau. In the end, EHC versus time is

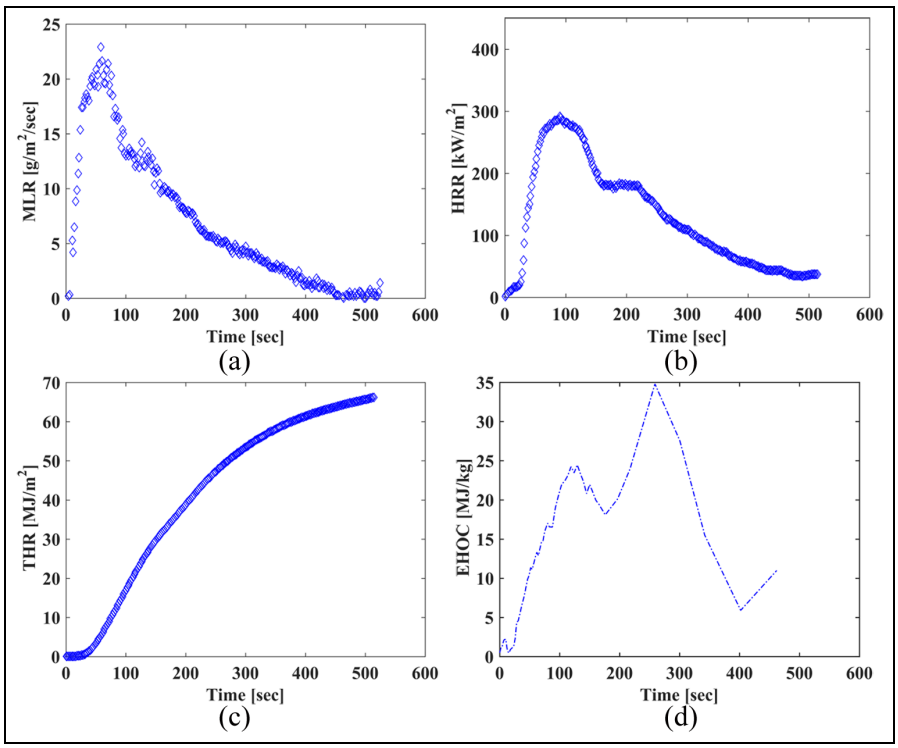

Figure 4. Cone calorimeter results for PVC formulation: (a) mass loss rate (MLR), (b) heat release rate (HRR), (c) total heat released (THR), and (d) effective heat of combustion (EHC).

shown. The peak value of EHC was found to be 35 MJ/kg, overall the curve showed significant fluctuation over the length of the test, with majority of values lying below 35 MJ/kg mark.

The cone calorimeter experimental summary is tabulated in Table 6.

From the results above, it can be seen PVC shows a higher value of p-HRR and lower time to ignition (TTI) as compared to EVA-ATH specimen. One reason could be occurrence of dehydration reaction and formation of ceramic residue made up of alumina (Al_2O_3) in the EVA matrix, which has significant degree of cooling effect due to production of acetic acid, water, and acetone during the thermal decomposition reactions.

Simulation results

Input data. For the estimation of MLR, the input data were gathered from two different literature sources as shown in Table 7. The density and specimen thickness values were used as obtained during experimental measurements. The PVC and EVA-ATH, specimen was modeled with only two reactions. The four reaction model was not implemented due to lack of

Table 6. Short summary of key parameters obtained from cone calorimeter tests.

S. no	Parameters	Symbol	EVA-ATH	PVC
1	Time to ignition (s)	TTI	40 (44)	6 (10)
2	Time to peak HRR (s)	$t_{p\text{-}HRR}$	84 (88)	90 (180)
3	Peak heat release rate (kW/m^2)	p-HRR	171 (170)	292 (277)
4	Peak mass loss rate (g/m^2/s)	p-MLR	16 (16)	23 (23)
5	Time to peak MLR (s)	$t_{p\text{-}MLR}$	78 (78)	58 (66)
6	Time to flame out (s)	$t_{flame\ out}$	546 (550)	410 (400)

The results of repeat tests are shown in parentheses. EVA-ATH, ethyl vinyl acetate–aluminum tri-hydroxide; PVC, poly-vinyl chloride; HRR, heat release rate; MLR, mass loss rate.

other thermo-chemical reaction parameters such as heat of pyrolysis of individual chemical reactions (Rxn-3 and Rxn-4 in case of PVC). For the parameters of chemical reaction model, the values were taken from Table 5 for first two peaks of the DTG curve. The input data of the temperature dependent thermal properties of EVA-ATH are shown in Figure 5 for virgin and char materials separately, while for PVC constant values of thermal properties were found and hence used as reported in the literature. Heats of pyrolysis were determined by differential scanning calorimetry (DSC) experiments and literature values were used. Figure 5 shows the variation of thermal conductivity and specific heat of virgin and charred polymer measured directly by Transient plane source (TPS) method and DSC. The first plot shows linear decline of virgin thermal conductivity until 400°C followed by slow rise of the thermal conductivity of char. The majority values of the char thermal conductivity are significantly lower than that of virgin polymer. Also, the curve showing variation of specific heat values shows linear rise for virgin and char polymer. But overall, the specific heat of char is significantly lower than that of virgin polymer. The flame heat flux value was chosen as a representative mean of the data provided of several polymers in literature.[13,36,46] It is also treated as model fitting parameter in this study. The values used in simulations for PVC and EVA-ATH were 10 kW/m^2 and 6 kW/m^2, respectively. Ghorbani et al.[13] have used a similar value for simulation of their PVC specimens, while for EVA-ATH, slightly higher values are found in literature (10 or 20 kW/m^2) compared to what is used in this study mainly for fitting purpose. Also, a few other studies were found in which flame heat flux values were obtained by direct measurements for different polymers. Test measurements from Kacem et al.[47] show flame heat flux value obtained for PMMA was found to be 20 kW/m^2, and the results by Hopkins and Quintiere et al.[48] show values for Nylon to be 20 kW/m^2, poly-ethylene to be 19 kW/m^2, and poly-propylene to be 11 kW/m^2, respectively. The values for flame heat flux used in this study are significantly lower than the experimentally obtained values measured for the above polymers due to addition of additives for suppression of smoke and heat release in the samples.

The following section shows the comparison of simulated and experimental results of MLR, HRR, and THR for the two polymers.

MLR. The results for MLRs simulation are shown in Figure 6. It can be seen that the calculated results match the experimental data to a reasonable extent.

Table 7. Parameters used for simulation of HT-DAEM model.

S. no	Parameters	Units	EVA-ATH Girardin et al.[31]	PVC Ghorbani et al.[13]
1	ρ–Density (Virgin)	kg/m^3	950 (Measured)	1425 (Measured)
2	ρ–Density (char)	kg/m^3	397	398
3	$\Delta H_{r,1}$–Heat of pyrolysis	J/kg	883 $\times$ 10^3 (DSC)	292 $\times$ 10^3 (DSC)
4	L–Thickness	M	6.5 $\times$ 10^{-3} (Measured)	3 $\times$ 10^{-3} (Measured)
5	h–Convective Heat Transfer Coefficient	W/m^2/K	10	10
6	G–Incident Heat Flux	W/m^2	35 $\times$ 10^3	50 $\times$ 10^3
7	ε–Emissivity (Virgin and Char)	–	0.9	0.9
8	$\Delta H_{r,2}$–Heat of pyrolysis	J/kg	236 $\times$ 10^3 (DSC)	292 $\times$ 10^3 (DSC-Assumed same as in Rxn-1)
9	ks_{virgin}–Thermal conductivity (Virgin)	W/m/K	See Figure 5	0.17
10	k_{char}–Thermal Conductivity (Char)	W/m/K	See Figure 5	0.10
11	$c_{pvirgin}$–Specific Heat (virgin)	J/kg/K	See Figure 5	1111
12	c_{pchar}–Specific Heat (Char)	J/kg/K	See Figure 5	3894
13	$\eta_{char,1}$ (Char fraction)	–	0.25 (Measured)	0.56 (Measured)
14	$\eta_{char,2}$ (Char fraction)	–	0.60 (Measured)	0.26 (Measured)
15	q_{flame}–Flame heat flux	kW/m2	6 (Fitting Parameter)	10 (Fitting Parameter)

HT-DAEM, heat transfer– distributed activation energy model; EVA-ATH, ethyl vinyl acetate–aluminum tri-hydroxide; PVC, poly-vinyl chloride.

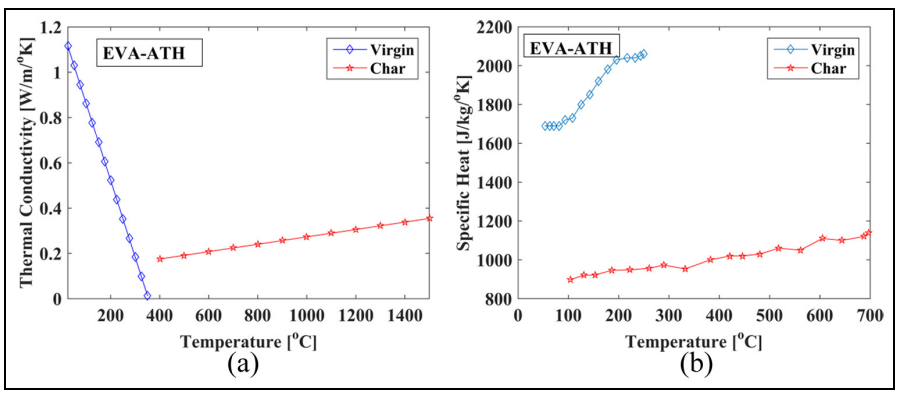

Figure 5. Temperature dependent thermal properties of EVA-ATH obtained by digitizing experimental data from Witkowski et al.[5] for simulating HT-DAEM model: (a) thermal conductivity (measured by transient plane source [Extrapolations beyond T= 700°C]) and (b) specific heat (measured by STA-DSC).

The time to ignition (TTI), p-HRR, and $t_{\text{flame out}}$ follow the experimental results to a high degree especially in case of EVA-ATH, while there is a considerable deviation in the simulated MLR curve of PVC. From the quality of simulations, it can be said the rise and the peak MLR value is captured well in both cases; however, there exists significant under-

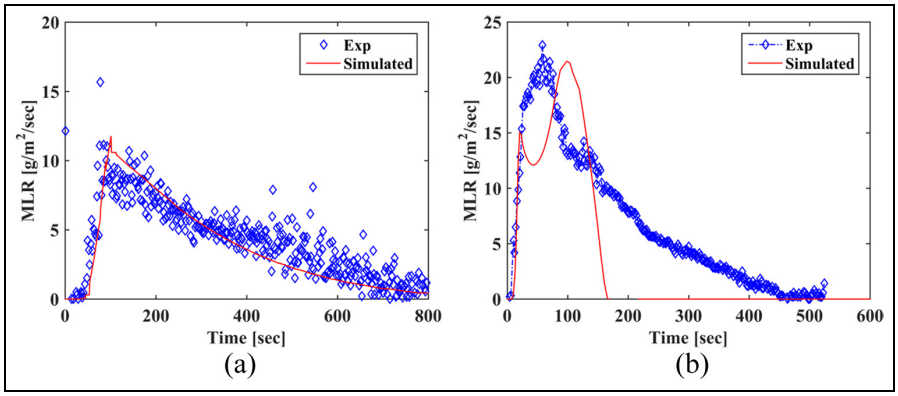

Figure 6. Comparison of experimental and simulated mass loss rates of (a) EVA-ATH–MLR and (b) PVC–MLR formulation.

prediction in time to flame out and over prediction in time to reach peak HRR in case of PVC. This deviation may be attributed to thermo-physical material property data sourced from literature and not acquired by direct measurements. It can also be seen that in case of PVC, the simulated MLR curve rises to 15 $g/m^2/s$ in line with the experimental curve but it drops for a few seconds very sharply followed by a steep rise to p-HRR value. This can be attributed to the formation of char layer preventing further oxidation of virgin material by insulating it for a very short period of time. As the exposure time increases, the char layer starts oxidizing leading to further increase in MLR value and consumption of virgin fuel until its exhaustion leading to eventual decay of the MLR curve. The interesting observation is that this effect is not visible in experimental results. The experimental curve decays at a much slower pace and falls to zero value at nearly 500 s. Perhaps one reason could be presence of zinc and calcium thermal stabilizers present in the polymer matrix leading to increase in their burn out time. The impregnated $CaCO_3$ is considered to react with acid (HCl) generated in the material during thermal decomposition and form $CaCl_2$, CO_2, and H_2O providing overall cooling effect and slowing down the MLR. Shimpi et al.[49] found dispersion of $CaCO_3$ in PVC specimen to have an improvement in thermal stability of the polymer sheet. They found rise in glass transition temperatures for $CaCO_3$ dispersed PVC samples as compared to pure ones. Also, previous study from Stoliarov et al.[3] has shown that after the flame out in a cone calorimeter experiment, PVC specimens showed smoldering effect leading to heat release at a steady rate for extended period of time. Also, because of char formation and intumescence specimens tend to swell up and trap pyrolysis gases in their air pockets for short period of time. Perhaps non-inclusion of a dedicated radiative porous char-sub model also accounts for under-prediction in this case, since presence of an insulating char layer that would develop upon heat exposure would delay the delivery of external heat flux to virgin material and provide some thermal resistance at higher temperatures when radiative heat transfer plays a dominant role in heat transfer to the material. Also absence of two peaks, in the early phase of the development of the MLR may be attributed to the very thin nature of the sample of PVC in which the decline of MLR due to formation of thin char layer is not

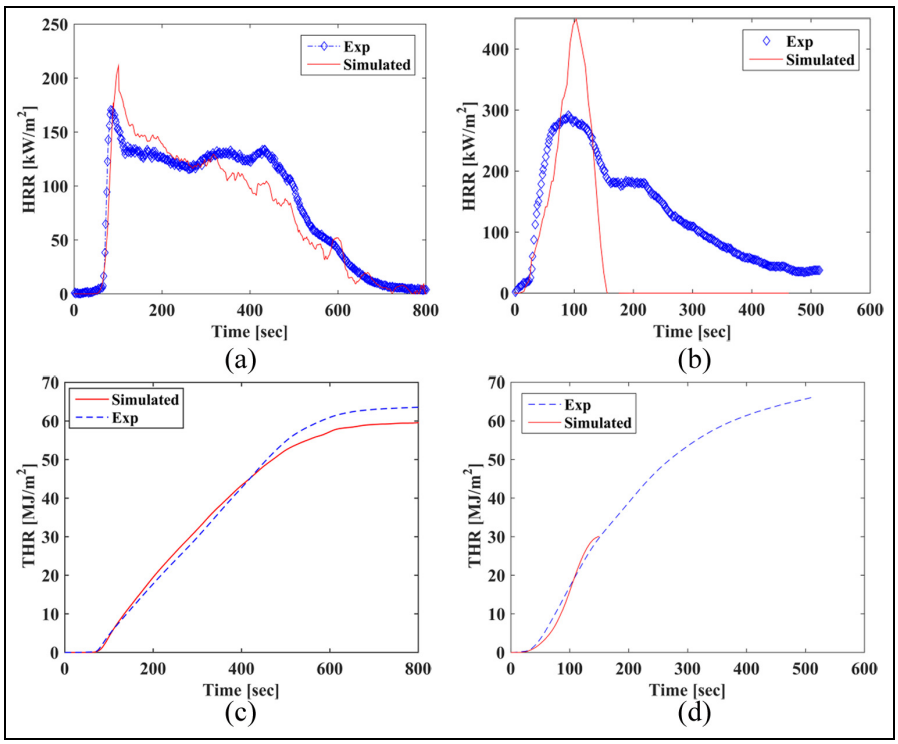

Figure 7. Comparison of experimental and simulated HRR and THR of EVA-ATH and PVC formulations: (a) EVA-ATH–HRR, (b) PVC–HRR, (c) EVA-ATH–THR, and (d) PVC–THR.

very clear and merged into one broad peak. This effect was also observed by Ghorbani et al.[13] for his simulations for very thin samples. The specimens used in this study are closer to real-world materials used in cable sheathing industry and differences in modeling output may be attributed to complex thermo-chemical phenomenon occurring in material due to cooling effect provided by water release reactions unlike in pure PVC specimens. In case of EVA-ATH polymer, the values match the experimental data to a high degree. The simulated curve shows initial delay before it climbs to the p-MLR value. Thereafter it shows gradual delay in its decent to zero value at the end of the experiment. The time to ignition is captured well in both cases.

HRR and THR estimation. The HRR curve is estimated based on further computations performed on the simulated MLR curve obtained by solution of model equations. The HRR is computed based on the product of simulated MLR curve and the EHC. EHC is determined using cone calorimeter data in its real time form as discussed in detail by Hshieh and Beeson.[50] If EHC data are unavailable in real-time format, literature values may be used as well. In the estimations, it is further hypothesized that flame heat flux contributes to the

incident heat flux boundary condition on the top surface of the polymer. In case of EVA-ATH, it is assumed to be 6 kW/m^2 of flame heat flux and is rather used as a model fitting parameter. However, in literature, values up to 15 kW/m^2 can be found as well.[3] Comparing the curve features of EVA-ATH, it can be said that the simulated curve matches the experimental one until, the time to peak HRR. The values of p-HRR is slightly over predicted at 209 kW/m^2 as compared to the experimental one which remains at 170 kW/m^2. This is followed by a steady phase of HRR which varies between 100 and 150 kW/m^2. The simulated curve shows gradual decline until it diminishes at nearly 700 s. In the decay phase of the HRR, the simulated and the experimental curve do not overlap to a high degree but show a reasonably similar declining trend. Overall, the fitting is satisfactory as compared to the HRR experimental data. The evolution of THR matches the experimental one to a high degree. The THR for the experimental curve was found to be 63 MJ/kg, while the simulated ones were found to be 59 MJ/kg (Figure 7).

A similar comparison when drawn for PVC shows that the modeled curve deviates the HRR curve to a large extent. The simulated HRR curve shows a sharp peak growing as much as 450 kW/m^2 within 103 s. It drops sharply to zero value in 155 s. The time to burnout is under-predicted by the modeled curve by several hundred seconds. These differences could be attributed to the differences in the material properties and the very thin nature of the sample showing quick burnout with a sharp peak. As a consequence of this, the following THR curve is also under-predicted by a large margin.

Conclusion

Based on the discussions above, it can be concluded that the concept of distributed reactivity may be applied to predict fire technical properties of materials using heat and mass conservation equations. The combined HT-DAEM model shows promising results for charring polymers but there are several gaps in model physics such as advection, intumescence, and radiative heat transfer in porous chars which have not been addressed fully in the current scope of work. The results show reasonably good predictions for EVA-ATH polymer but relatively under-prediction for PVC. The deviation from the test results may be attributed to sourcing material property data from literature and using analytical approximation of the sub-model instead of original form containing the double integral. In addition to this, presence of error function in the analytical approximation of the sub-model could render numerical convergence issues at higher values of standard deviation values of activation energy. Future work would include refinements in solution of equations by using them in original form instead of reducing them to analytical form. Direct measurement of material property data is still an important aspect of the simulation process by providing right inputs to models. The main uncertainties include choice of the flame heat flux values, heats of reactions of the individual reaction steps, and the values of effective heat of combustion (EHC). Inclusion of four step reaction scheme in 1D pyrolysis model is subject to availability of tests data for heat of reactions and heat of combustion. Also future work could include further details analogous to other pyrolysis model elucidating porous char formation or swelling and shrinkage physics in the material. The model could be further developed to scale up cone calorimeter predictions to single burning item (SBI) test, by implementing the new reaction modeling approach.

Acknowledgements

The authors would like to thank Dr Reiner Sauerwein (Nabeltec AG, Germany) for providing access to experimental resources. The works of Dr Bertand Girardin, Dr Z. Ghorbani, and Dr S. Stoliarov are highly acknowledged as a valuable source of reference to develop this model into a heat transfer–chemical reaction model, that could be used in CFD calculations in future. It is to be noted some of experimental data (Thermogravimetry experiments) and material property characterization has been manually digitized during literature search for solely using as input values for model development work and for that purpose authors would like to thank contributors of such data. Also, authors are grateful for the whole team of Professor Bart Merci (Ghent University) and Advanced Services team at DBI (Karlis Livkiss, Thomas Hulin, Blanca Andres Valiente, Konrad Wilkens, Martin Scott McLaggan and Dan Lauridsen) for fruitful discussions.

Declaration of conflicting interests

The author(s) declared no potential conflicts of interest with respect to the research, authorship, and/or publication of this article.

Funding

The author(s) disclosed receipt of the following financial support for the research, authorship, and/or publication of this article: This work was supported by the funding received from European Union Seventh Framework Program (FP7/2007-2013) under grant agreement no. 316991 for the project FIRETOOLS.

ORCID iD

Abhishek Bhargava https://orcid.org/0000-0002-4095-6133

References

1. McGrattan K, McDermott R, Hostikka S, et al. *Fire dynamics simulator technical reference guide, volume 1: mathematical model*. Gaithersburg, MD: NIST Special Publication, 2013.
2. Lautenberger C and Fernandez-Pello C. Generalized pyrolysis model for combustible solids. *Fire Safety J* 2009; 44: 819–839.
3. Stoliarov SI, Crowley S, Walters RN, et al. Prediction of the burning rates of charring polymers. *Combust Flame* 2010; 157: 2024–2034.
4. Snegirev AY. Generalized approach to model pyrolysis of flammable materials. *Thermochim Acta* 2014; 590: 242–250.
5. Witkowski A, Girardin B, Försth M, et al. Development of an anaerobic pyrolysis model for fire retardant cable sheathing materials. *Polym Degrad Stabil* 2015; 113: 208–217.
6. Valencia LB. *Experimental and numerical investigation of the thermal decomposition of materials at three scales: application to polyether polyurethane foam used in upholstered furniture*. Chasseneuil-du-Poitou: École Nationale Supérieure de Mécanique et d'Aérotechnique (ISAE-ENSMA), 2010.
7. Matala A. Methods and applications of pyrolysis modelling for polymeric materials. Aalto University, 2013, https://www.vtt.fi/inf/pdf/science/2013/S44.pdf
8. Stoliarov SI and Lyon RE. Thermo-kinetic model of burning for pyrolyzing materials. *Fire Safety Sci* 2008; 9: 1141–1152.
9. Stoliarov SI, Crowley S, Lyon RE, et al. Prediction of the burning rates of non-charring polymers. *Combust Flame* 2009; 156: 1068–1083.
10. Snegirev AY, Talalov VA, Stepanov VV, et al. A new model to predict pyrolysis, ignition and burning of flammable materials in fire tests. *Fire Safety J* 2013; 59: 132–150.
11. Marquis DM, Pavageau M, Guillaume E, et al. Modelling decomposition and fire behaviour of small samples of a glass-fibre-reinforced polyester/balsa-cored sandwich material. *Fire Mater* 2013; 37: 413–439.
12. Marquis DM, Pavageau M and Guillaume E. Multi-scale simulations of fire growth on a sandwich composite structure. *J Fire Sci* 2013; 31: 3–34.
13. Ghorbani Z, Webster R, Lázaro M, et al. Limitations in the predictive capability of pyrolysis models based on a calibrated semi-empirical approach. *Fire Safety J* 2013; 61: 274–288.
14. Di Blasi C. The state of the art of transport models for charring solid degradation. *Polym Int* 2000; 49: 1133–1146.
15. Kirtania K and Bhattacharya S. Coupling of a distributed activation energy model with particle simulation for entrained flow pyrolysis of biomass. *Fuel Process Technol* 2015; 137: 131–138.

16. Valencia LB, Rogaume T, Guillaume E, et al. Analysis of principal gas products during combustion of polyether polyurethane foam at different irradiance levels. *Fire Safety J* 2009; 44: 933–940.
17. Snegirev A, Talalov V, Stepanov V, et al. A new model to predict multi-stage pyrolysis of flammable materials in standard fire tests. *J Phys Conf Ser* 2012; 395: 12012.
18. Vyazovkin S, Burnham AK, Criado JM, et al. ICTAC Kinetics Committee recommendations for performing kinetic computations on thermal analysis data. *Thermochim Acta* 2011; 520: 1–19.
19. Cai J, Wu W and Liu R. An overview of distributed activation energy model and its application in the pyrolysis of lignocellulosic biomass. *Renew Sust Energ Rev* 2014; 36: 236–246.
20. Cai J, Jin C, Yang S, et al. Logistic distributed activation energy model—part 1: derivation and numerical parametric study. *Bioresour Technol* 2011; 102: 1556–1561.
21. Cai J, Yang S and Li T. Logistic distributed activation energy model—part 2: application to cellulose pyrolysis. *Bioresour Technol* 2011; 102: 3642–3644.
22. Xu T, Xu F, Hu Z, et al. Non-isothermal kinetics of biomass-pyrolysis-derived-tar (BPDT) thermal decomposition via thermogravimetric analysis. *Energ Convers Manag* 2017; 138: 452–460.
23. Wang J, Lian W, Li P, et al. Simulation of pyrolysis in low rank coal particle by using DAEM kinetics model: reaction behavior and heat transfer. *Fuel* 2017; 207: 126–135.
24. Xiong Q, Zhang J, Xu F, et al. Coupling DAEM and CFD for simulating biomass fast pyrolysis in fluidized beds. *J Anal Appl Pyrolysis* 2016; 117: 176–181.
25. Rostami AA, Hajaligol MR and Wrenn SE. A biomass pyrolysis sub-model for CFD applications. *Fuel* 2004; 83: 1519–1525.
26. Sadhukhan AK, Gupta P and Saha RK. Modeling and experimental studies on single particle coal devolatilization and residual char combustion in fluidized bed. *Fuel* 2011; 90: 2132–2141.
27. Di Blasi C. Modeling and simulation of combustion processes of charring and non-charring solid fuels. *Prog Energ Combust* 1993; 19: 71–104.
28. Di Blasi C. Modeling chemical and physical processes of wood and biomass pyrolysis. *Prog Energ Combust* 2008; 34: 47–90.
29. Wu C-H, Chang C-Y, Hor J-L, et al. Two-stage pyrolysis model of PVC. *Can J Chem Eng* 1994; 72: 644–650.
30. Miranda R, Yang J, Roy C, et al. Vacuum pyrolysis of commingled plastics containing PVC. I. Kinetic study. *Polym Degrad Stabil* 2001; 72: 469–491.
31. Girardin B, Fontaine G, Duquesne S, et al. Characterization of thermo-physical properties of EVA/ATH: application to gasification experiments and pyrolysis modeling. *Materials* 2015; 8: 7837–7863.
32. Rein G, Lautenberger C, Fernandez-Pello A, et al. Application of genetic algorithms and thermogravimetry to determine the kinetics of polyurethane foam in smoldering combustion. *Combust Flame* 2006; 146: 95–108.
33. ASTM E1641-16. Standard test method for decomposition kinetics by thermogravimetry using the Ozawa/Flynn/Wall method, 2016, https://www.astm.org/standards/e1641.htm
34. ASTM E698-18. Standard test method for kinetic parameters for thermally unstable materials using differential scanning calorimetry and the Flynn/Wall/OzawaMethod, http://www.astm.org/cgi-bin/resolver.cgi?E698
35. Marquis DM, Batiot B, Guillaume E, et al. Influence of reaction mechanism accuracy on the chemical reactivity prediction of complex charring material in fire condition. *J Anal Appl Pyrol* 2016; 118: 231–248.
36. DiNenno PJ and Drysdale D. *SFPE handbook of fire protection engineering*. 5th ed. Quincy, MA: National Fire Protection Association.
37. Cai J, Wu W, Liu R, et al. A distributed activation energy model for the pyrolysis of lignocellulosic biomass. *Green Chem* 2013; 15: 1331.
38. Bhargava A, Andersson B, Hees P, et al. Distributed reactivity model to predict multistage pyrolysis of polymeric materials and sensitivity analysis. In: *14th international conference on fire science and engineering (Interflam)*, Windsor, 4–6 July 2016, pp. 107–118. London: Interscience Communications Ltd.
39. Lyon R and Quintiere JG. Criteria for piloted ignition of combustible solids. *Combust Flame* 2007; 151: 551–559.
40. Rodolfo A and Innocentini-Mei LH. Poly(vinyl chloride)/metallic oxides/organically modified montmorillonite nanocomposites: preparation, morphological characterization, and modeling of the mechanical properties. *J Appl Polym Sci* 2010; 116: 422–432.
41. ISO 5660-1:2015. Reaction—to—fire tests—heat release, smoke production and mass loss rate—part 1: heat release rate (cone calorimeter method) and smoke production rate (dynamic. measurement), 2015, https://www.iso.org/standard/57957.html
42. Hewitt F, Rhebat DE, Witkowski A, et al. An experimental and numerical model for the release of acetone from decomposing EVA containing aluminium, magnesium or calcium hydroxide fire retardants. *Polym Degrad Stabil* 2016; 127: 65–78.
43. Lakshmanan C and White N. A new distributed activation energy model using Weibull distribution for the representation of complex kinetics. *Energ Fuel* 1994; 31: 1158–1167.
44. Bhargava A, van Hees P and Andersson B. Pyrolysis modeling of PVC and PMMA using a distributed reactivity model. *Polym Degrad Stabil* 2016; 129: 199–211.
45. Cai J and Ji L. Pattern search method for determination of DAEM kinetic parameters from nonisothermal TGA data of biomass. *J Math Chem* 2007; 42: 547–553.
46. Dembsey NA, Pagni PJ and Williamson RB. Compartment fire near-field entrainment measurements. *Fire Safety J* 1995; 24: 383–419.
47. Kacem A, Mense M, Pizzo Y, et al. A fully coupled fluid/solid model for open air combustion of horizontally-oriented PMMA samples. *Combust Flame* 2016; 170: 135–147.
48. Hopkins D and Quintiere JG. Material fire properties and predictions for thermoplastics. *Fire Safety J* 1996; 26: 241–268.
49. Shimpi NG, Verma J and Mishra S. Dispersion of nano CaCO3 on PVC and its influence on mechanical and thermal properties. *J Compos Mater* 2010; 44: 211–219.
50. Hshieh F-Y and Beeson HD. Note: measuring the effective heats of combustion of transformer-insulating fluids using a controlled-atmosphere cone calorimeter. *Fire Mater* 2002; 26: 47–49.
51. Spiegel MR. *Schaum's outline of mathematical handbook of formulas and tables*. 4th ed. New York: McGraw-Hill Education, 1998.

Author biographies

Abhishek Bhargava works as a Research Consultant at Danish Institute of Fire and Security Technology (DBI). His main research interests lie in the domain of pyrolysis modeling, fire growth, and performance-based design. He graduated with a Master's degree in Materials Engineering from Université Paul Sabatier Toulouse III, France (2009). He is an Industrial PhD candidate in the field of Fire Safety Engineering at Lund University (Sweden).

Patrick van Hees works as a Professor at the Division of Fire Safety Engineering, Lund University, Sweden. Prior to this, he worked as a Research Manager at SP Fire Research in Sweden. He is currently the chairman of ISO TC 92 Fire Safety committee and IAFSS (International Association of Fire Safety Science). He obtained his PhD degree from the University of Ghent in Belgium in 1995. His main research interests lie in the domain of fire development, fire behavior of systems and materials, fire modeling, and performance-based design.

Bjarne Husted works as an Associate Professor at the Division of Fire Safety Engineering, Lund University, Sweden. His main research interests are simulations of fires using zone and CFD models. He has worked extensively with CFX, FDS, FireFOAM, and water mist systems. He obtained his PhD in Fire safety engineering from Lund University in 2007.

Antonio Rodolfo Jr works as Application Engineering and Market Development Manager for vinyls at Braskem S/A (São Paulo, Brazil). He graduated in Materials Engineering with specialization in polymers from the Federal University of São Carlos, Brazil (1994) and holds both a Master's degree in Civil Engineering from the State University of São Paulo, Brazil (2005) and a PhD in Chemical Engineering from the State University of Campinas, Brazi (2010). His main research interests lie in smoke suppression of PVC formulations.

Corina Neumeister heads the department of "Cable & Polymers" in the division R&D/Technical Service at Nabaltec AG (Schwandorf, Germany). She is responsible for the development of new mineral flame retardant solutions and the application thereof in different polymer formulations. She works as Product Manager for fine precipitated ATH globally. Her main research interests lies in mineral flame retardants as well as the optimization of the flame retardant performance. She obtained her PhD degree from the University of Regensburg (Germany) and the ICIQ in Tarragona (Spain).

Appendix 1

Notation

$a1$	parameter used probability distribution function
A	pre-exponential factor (1/s)
c_p	specific Heat (J/kg/K)
C	weight of the individual reaction rate (–)
D_g	diffusion coefficient (m^2/s)
E	activation energy (kJ/mol)
E_0	mean activation energy (kJ/mol)
G	incident heat flux from the cone (W/m^2)
h	convective heat transfer coefficient ($W/m^2/K^1$)
HRR	heat release rate (kW/m^2)
k	thermal conductivity (W/m/K)

L	thickness (m)
m_f	mass loss rate (g/m^2/s)
MLR	mass loss rate (g/m^2/s)
N	total number of gases
q_{flame}	flame heat flux (W/m^2)
q_w	net incident heat flux on the polymer surface (W/m^2)
R	real gas constant (8.314 J/K/mol)
T	temperature (K)
TTI	time to ignition (s)
x	Cartesian coordinate (m)
α	reaction progress variable (–)
ε	emissivity (–)
κ	absorption coefficient (1/m)
ρ	density (kg/m^3)
σ	standard deviation of activation energy (kJ/mol)
σ_c	Stephan–Boltzmann constant (5.67×10^{-8} W/m^2/K^4)
ω	reaction rate (kg/m^3/s)
ΔH_r	heat of pyrolysis (J/kg)

Subscripts

amb	ambient
char	char
g	gas
i	reaction index
p	peak
n	number of reactions
r	reaction
S	solid phase
Total	total
virgin	virgin material
0	initial

Appendix 2

Approximation to distributed activation energy model

The reaction model contains two integrals: the inner one dE and the outer one dt. This creates numerical difficulties in simultaneous solution of energy conservation model and mass conservation model. To resolve such numerical issues, an approximation to the DAEM model is proposed targeted to eliminate the inner dE integral. This is shown via equations (17)–(22), with mathematical manipulations

$$\frac{\partial \rho}{\partial t} = -A\rho \int_0^\infty \exp\left(-\frac{E}{RT}\right) f(E)dE \tag{17}$$

where

$$f(E) = \frac{1}{\sigma\sqrt{2\pi}} \exp\left(-\frac{(E - E_0)^2}{2\sigma^2}\right)$$

Substituting $f(E)$ in equation (13), we get

$$\frac{\partial \rho}{\partial t} = -\frac{A\rho}{\sigma\sqrt{2\pi}} \int_0^\infty \exp\left(-\frac{E}{RT}\right) \exp\left(-\frac{(E - E_0)^2}{2\sigma^2}\right) dE \tag{18}$$

By combining the two exponential terms of equation (14), the above equation may be written as

$$\frac{\partial \rho}{\partial t} = -\frac{A\rho}{\sigma\sqrt{2\pi}} \int_0^\infty \exp\left(-\frac{E}{RT} - \frac{\left(E^2 + {E_0}^2 - 2EE_0\right)}{2\sigma^2}\right) dE \tag{19}$$

Equation (15) can be further rearranged to appear as

$$\frac{\partial \rho}{\partial t} = -\frac{A}{\sigma\sqrt{2\pi}} \rho \int_0^\infty \exp\left[-\left(\frac{1}{2\sigma^2}E^2 + \frac{(2\sigma^2 - 2RTE_0)}{2\sigma^2 RT}E + \frac{{E_0}^2}{2\sigma^2}\right)\right] dE \tag{20}$$

Equation (16) is a Gaussian integral which may be compared to the form shown by Spiegel[51] in equation (17)

$$\int_0^\infty e^{-\left(ax^2 + bx + c\right)} dx = \frac{1}{2}\sqrt{\frac{\pi}{a}} \exp\left(\frac{b^2 - 4ac}{4a}\right) erfc\left(\frac{b}{2\sqrt{a}}\right) \tag{21}$$

where

$$a = \frac{1}{2\sigma^2}$$
$$b = \frac{2\sigma^2 - 2E_0 RT}{2RT\sigma^2}$$
$$c = \frac{E_0^2}{2\sigma^2}$$

This leads to final equation (18)

$$\frac{\partial \rho}{\partial t} = -\left[\frac{A}{\sigma\sqrt{2\pi}} \frac{1}{2} \sqrt{\frac{\pi}{a}} \exp\left(\frac{b^2 - 4ac}{4a}\right) \left(1 - \operatorname{erf}\left(\frac{b}{2\sqrt{a}}\right)\right)\right] \rho \tag{22}$$

The above analytical approximation renders the flexibility for simpler implementation in computational environment due to elimination of the inner dE integral.

Paper IV

PYROLYSIS MODELING OF PVC USING DISTRIBUTED ACTIVATION ENERGY MODEL - MICRO SCALE TESTING

Abhishek Bhargava[a,b], Patrick van Hees[b]

[a] Danish Institute of Fire and Security Technology, Copenhagen, Denmark
[b] Lund University, Lund, Sweden

Abstract
Polyvinyl chloride (PVC) is a common thermoplastic which finds widespread applications in the construction industry for usage in ceiling linings, flooring materials, electrical cables and roofing materials. Several fire requirements are put on these types of applications. For fire safety engineering and product development, thermo-chemical decomposition modeling of PVC is required. The FIRETOOLS project investigates the possibilities to predict real scale fire behavior of building products, content and barriers by means of using material data on successively increasing scale. This paper focuses on the material modeling and studies the thermo-chemical decomposition of PVC using Distributed Activation Energy Model (DAEM).

KEYWORDS: Pyrolysis modeling, Fire behavior, Matlab, DAEM

1 INTRODUCTION

PVC is one of the major plastics manufactured in the world. Some of the end use applications include usage in window frames, drain pipes, wall coverings, flooring materials and insulation materials for wires and cables. Due to its combustible nature, the reaction to fire property of PVC is of great interest, especially at the material level. Pyrolysis modeling enables prediction of mass loss rates at different heating rates using a combination of experimental and simulation technique. The results of these simulations can be used in a CFD code such as fire dynamic simulator (FDS) to perform fire predictions on real scale (Kim & Dembsey 2012; Stoliarov et al. 2010; McGrattan et al. 2013; Marquis et al. 2012).

2 THEORETICAL BACKGROUND

DAEM stands for Distributed Activation Energy Model. It has been used previously to interpret the pyrolysis kinetics of complex multi-component materials such as coal, biomass and sewage sludge (Miura 1995; Miura & Maki 1998; Soria-Verdugo et al. 2013). These materials are heterogeneous in nature, and when they are exposed to heat, no single reaction determines their thermal decomposition into volatile content; rather the conversion of solid phase into different volatile products is characterized by many parallel occurring reactions. So, the accurate reaction mechanism for such materials may be difficult to ascertain. A similar approach is applied for PVC, which exhibits two-step decomposition mechanism due to the release of hydrogen chloride (HCl) followed by pyrolysis of the remaining residue. For real life applications, PVC is not used as pure material, but several additives are added into it. For e.g. addition of plasticizers such as aliphatic and aromatic esters improves the flexibility of PVC, a property desirable for usage in electrical cables (Troitzsch 2004). In the scenario, when information related to the on-going chemical reactions due to material interactions upon exposure to heating profile unavailable for the solid phase, it may be difficult to predict reaction rates, mass loss rates and heat release rate curve. In this work the pyrolysis phenomenon has been modelled using DAEM approach. The main assumptions of the DAEM model are that the reaction mechanism is assumed to consist of infinite set of parallel occurring irreversible single step reactions that have different activation energies and frequency factors. The distribution curve is modelled by a Gaussian distribution function (Miura 1995).
As per the model equation, the change in total volatiles at time t is given by:

$$1 - \frac{V}{V_*} = \int_0^\infty exp(-k_o \int_0^t e^{\frac{-E_a}{RT}} dt) * f(E_a) * dE_a \quad (1)$$

where, V* is the effective volatile content, V is the volatile content at temperature T (K), $f(E_a)$ is the distribution curve of the activation energy- E_a(kJ/mol) representing differences in the energies of all the reactions and $k_0(s^{-1})$ is the frequency factor corresponding to the E_a value, R is the real gas constant (8.314 J/K/mol). The PVC sample temperature at any time t is given by

$$T(t) = T_0 + \beta * t \quad (2)$$

Where, T_o is the starting temperature at which no reaction occurs, β (K/sec) is the heating rate and t is the time (s). Equation (1) can be re-written as:

$$1 - \frac{V}{V_*} = \int_0^\infty \varphi(E_a T) * f(E_a) * dE_a \quad (3)$$

Where, $\varphi(E_a, T) = exp\left(\frac{-k_0}{\beta} \int_0^T e^{-E_a/RT} dT\right)$ (4)

Equation (3) can be reduced to the equation (5) by a procedure detailed by (Miura & Maki 1998; Bhavanam & Sastry 2015).

$$ln\left(\frac{\beta}{T^2}\right) = ln\left(\frac{k_o * R}{E_a}\right) + 0.6075 - \frac{E_a}{R} * \frac{1}{T} \quad (5)$$

A plot of ln (β/T^2) versus 1/T at selected V/V* values at three different heating rates is presented in Fig 2. The procedure can be summarized as follows:

- V/V* values are measured at three different heating rates using a thermal analyzer.
- At selected values of V/V*, using the above data a plot of ln(β/T^2) versus 1/T is made.
- E_a and k_o values are determined from the slope and intercept of these curves for each conversion level using equation 14.
- Finally the $f(E_a)$ curve is obtained by differentiating the V/V* vs E_a curve and using inbuilt fitting functions in MATLAB.

The $f(E_a)$ curve in such models is assumed to follow Gaussian distribution due to its symmetric nature, however in reality, the kinetic parameters follow significantly different distribution having considerable asymmetry. The $f(E_a)$ curve, in such cases may be described by other statistical distribution functions such as Weibull and Logistic functions (Lakshmanan & White 1994; Cai et al. 2014). Table 1 shows the distribution function and different characteristic parameters defining the $f(E_a)$ curve. The main issue however, is the range of applicability of such model equations. Often several materials decompose in a two-step mechanism, exhibiting a shoulder peak and this was evident in the results obtained for PVC, see figure 1.

Table 1 Statistical distribution function to describe chemical kinetic parameters for usage in DAEM model

S.No	f(Ea)	Distribution functions	Parameters
1.	Gaussian	$\frac{1}{\sqrt{2\pi\sigma}}$	Mean Activation Energy - E_{a0} Standard Deviation- σ

3 COMPUTATIONAL CHALLENGES AND SOLUTION TECHNIQUES

The main computational hurdle in the DAEM model is that there is no closed form solution to this model. Equation 1 is a double integral equation and has inner dT integral and an outer dE_a integral.

(Cai et al. 2014) have divided the solution approaches to this model in two main categories namely, distribution free methods and distribution fitting methods. In this paper, the Miura Maki integral method (a form of distribution free method)(Miura & Maki 1998; Soria-Verdugo et al. 2013) has been employed to find the solution to Equation 1.

4 EXPERIMENTAL

The experimental data was provided by VTT and published in (Matala & Hostikka 2011). For the experiments, a simultaneous thermal analyzer NETZSCH STA 449 was used in both air and nitrogen atmosphere for the measurement of mass changes. The samples (≈20mg) were placed in alumina (Al_2O_3) crucibles and subjected to linear heating profiles (2/5/10/20 Kelvin/min) at four different heating rates in the TGA apparatus.

5 RESULTS AND DISCUSSIONS

5.1 Thermal decomposition in inert and air atmosphere – TGA and DTG curves

Figure 1 shows the TGA and DTG curves of the PVC samples as recorded experimentally in ambient and inert conditions. The onset of thermal decomposition of PVC starts at about 500K in air and nitrogen.

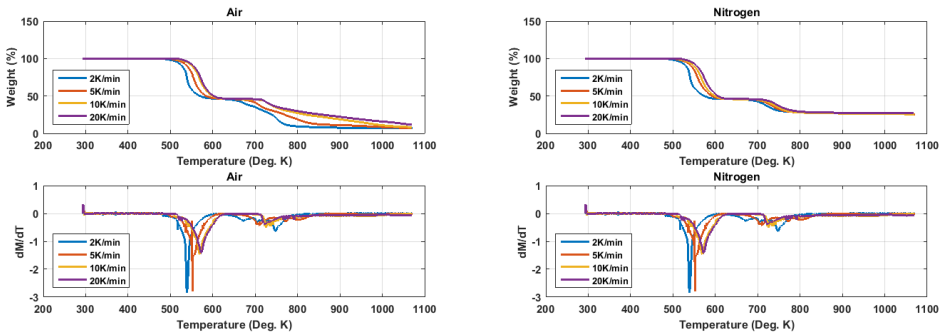

Figure 1 TGA and DTG curves for pure PVC in air and nitrogen at different heating rates

The decomposition occurs in a two-step reaction as evident from the TGA shoulder and two different peaks recorded in the DTG curve. The sample lost about 54% weight in the first reaction in both air and nitrogen. The first reaction pertains to the release of hydrogen chloride (HCl) and is termed as de-hydro-chlorination (Huggett & Levin 1987; Matala & Hostikka 2011). The decomposition mechanism is sensitive to the applied heating rate and shifts towards the right with the increasing heating rate i.e. from 5 K/min to 20 K/min. Also, in ambient atmosphere oxidation reactions occur and further complicate the shape of the mass loss curve. The residual weight in ambient and nitrogen environment is 7-11.5% and 25.5-27% respectively. Due to space constraints, the DAEM model has been applied to the experiments performed under nitrogen atmosphere only, and the two reaction steps have been characterized separately using DAEM parameters.

5.2 Arrhenius fittings for two different reaction steps

Figure 2 shows linear fit of Arrhenius plots for PVC samples. For reaction 1, the plots are straight lines, while for the second reaction due to the onset of gasification; the fittings are not good in the beginning and at the end conversion levels. When the reaction is steady the conversion levels for V/V* are between 0.55-0.71. The fittings follow straight lines.

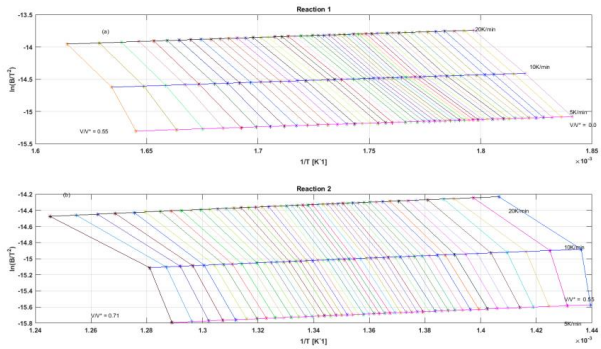

Figure 2 Arrhenius plot of ln(β/T^2) versus 1/T at selected V/V* values for PVC for reaction 1and 2

5.3 Kinetic parameters and their distribution curves

Figure 3 shows the frequency distribution curve of the activation energy (E_a) for both the reactions. The values are distributed over the range 228-351 kJ/mol for the first one, while for the second reaction the values are distributed over the range 218-405 kJ/mol.

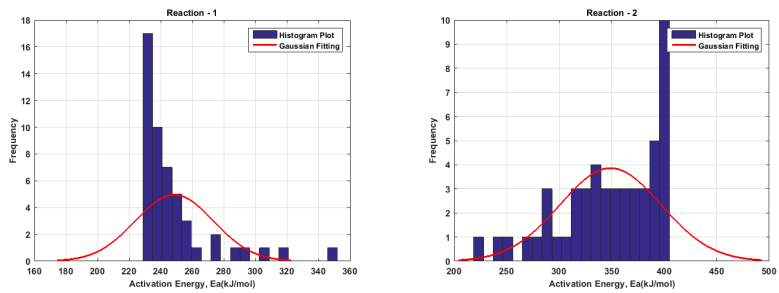

Figure 3 Frequency distribution curve of activation energy for reaction 1 and reaction 2 for PVC in nitrogen

Table 2 shows a summary of the chemical kinetic parameters obtained by the solution of DAEM model.

Table 2 Summary of Arrhenius parameters computed for PVC with DAEM model

Reaction 1	**Mean**	**Standard Deviation**	**Range**
E_a (kJ/mol)	248.7	10.0	228.8-351.8
$k_0(s^{-1})$	$3.6*10^{20}$	$2.5*10^{21}$	$2.2*10^{13}$-$1.8*10^{22}$
Reaction 2			
E_a (kJ/mol)	348.9	48.1	218.5-404.8
$k_o(s^{-1})$	$7.7*10^{19}$	$1.5*10^{20}$	$2.3*10^{6}$- $5.2*10^{20}$

5.4 Experimental Results Vs Numerical Simulations

The model simulations have been performed for all the heating rates (5/10/20 K/min) and for each conversion level by the solution of the non-linear equation using numerical method (bisection method).

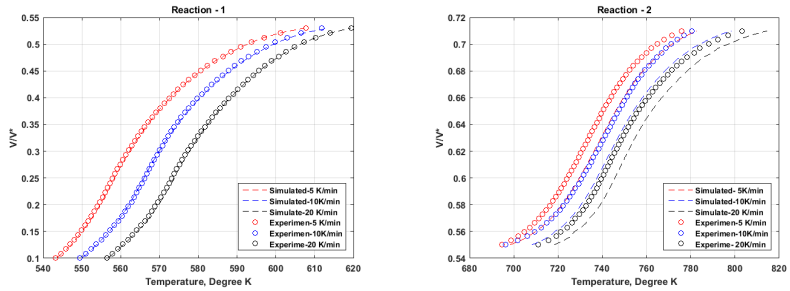

Figure 4 Model validation curve – experimental data and numerical simulations

For reaction 1 the simulations match experimental data very closely. The average percentage error is less than 0.25 percent, however for the reaction 2, the simulations show a slight over-prediction error. However, the percentage error is less than 2.3 percent.

5.5 Prediction of mass loss rates (MLRs) at high linear heating rates

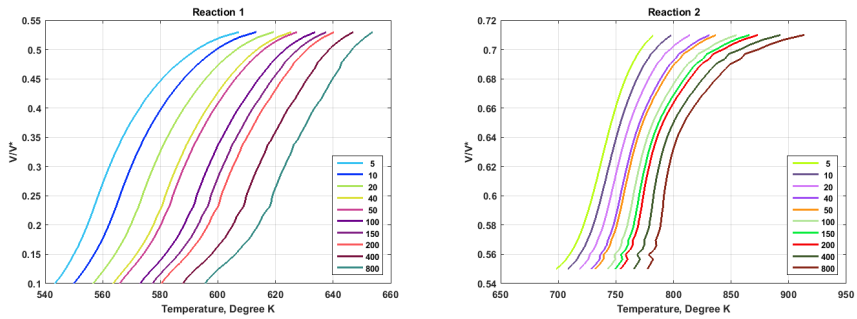

Figure 5 Predicted MLRs for reaction 1 and 2 for PVC in nitrogen at high heating rates (β in K/min)

Figure 5 shows predicted mass loss rate (MLRs) for PVC at increasing heating rates (up to 800K/min) in nitrogen atmosphere. This is obtained by numerical solution of equation 14 for desired heating rate and computed chemical kinetic parameters retrieved using the slopes and intercepts of the Arrhenius plots (Figure 2). Experiments using thermal analyzers at high heating rates are difficult to perform due lack of equipment availability. Although, many simultaneous thermal analyzers (STAs) can obtain a heating rate of 100 degrees K/min but there are several challenges associated with the experimentation at high temperatures. Simulations are a cost effective way of predicting material behavior under experimentally difficult conditions.

6 CONCLUSIONS

For fire simulations, very detailed chemical reactions mechanisms may not be of much significance due to the challenges they pose in the implementation of CFD codes such as fire dynamic simulator (FDS). In this paper, the DAEM method uses the Miura Maki integral approach to retrieve chemical kinetic parameters and predict mass loss rates curves for PVC under inert atmosphere at high linear heating rates. The computed kinetic parameters are distributed over a significant range (modelled by a Gaussian bell curve) for both reactions. The results of these predictions can be used as input parameter in fire simulations of building products but further validation and experience with the method is needed. The model calculations may later be applicable to a variety of building products

such as flooring materials, window frames and drainage pipes in combination with advanced flame spread calculations. With the development of in house computer code, the calculation process is fast and experimental effort reduced.

Acknowledgments

This work was supported by the funding received from European Union Seventh Framework Program (FP7/2007-2013) under grant agreement n° 316991 for the project FIRETOOLS. The authors would like to thank Dr. Anna Matala (VTT Technical Research Centre, Finland) for providing experimental thermo-gravimetric data for the model validation work.

REFERENCES

Bhavanam, A. & Sastry, R.C., 2015. Kinetic study of solid waste pyrolysis using distributed activation energy model. *Bioresource Technology*, 178, pp.126–131.

Cai, J., Wu, W. & Liu, R., 2014. An overview of distributed activation energy model and its application in the pyrolysis of lignocellulosic biomass. *Renewable and Sustainable Energy Reviews*, 36, pp.236–246.

Huggett, C. & Levin, B., 1987. Toxicity of the pyrolysis and combustion products of poly (vinyl chlorides): a literature assessment. *Fire and materials*, II(January), pp.131–142.

Kim, M.E. & Dembsey, N., 2012. *Engineering Guide for Estimating Material Pyrolysis Properties for Fire Modeling*,

Lakshmanan, C. & White, N., 1994. A new distributed activation energy model using Weibull distribution for the representation of complex kinetics. *Energy & fuels*, 31(5), pp.1158–1167.

Marquis, D.M., Pavageau, M. & Guillaume, E., 2012. Multi-scale simulations of fire growth on a sandwich composite structure. *Journal of Fire Sciences*, 31(1), pp.3–34.

Matala, A. & Hostikka, S., 2011. Pyrolysis modelling of PVC cable materials. In *Fire Safety Science*. pp. 917–930.

McGrattan, K. et al., 2013. *Fire Dynamics Dimulator (version 5), Technical reference guide. Volum1: Mathematical Model*,

Miura, K., 1995. A New and Simple Method to Estimate f(E) and ko(E) in the Distributed Activation Energy Model from Three Sets of Experimental Data Kouichi. *Energy & Fuels*, 9(4), pp.302–307.

Miura, K. & Maki, T., 1998. A Simple Method for Estimating f(E) and k0(E) in the Distributed Activation Energy Model. *Energy & Fuels*, (12), pp.864–869.

Soria-Verdugo, A. et al., 2013. Analysis of biomass and sewage sludge devolatilization using the distributed activation energy model. *Energy Conversion and Management*, 65, pp.239–244.

Stoliarov, S.I. et al., 2010. Prediction of the burning rates of charring polymers. *Combustion and Flame*, 157(11), pp.2024–2034.

Troitzsch, J., 2004. *Plastics Flammability Handbook - Principles, Regulations, Testing, and Approval (3rd Edition)*, Hanser Publishers.

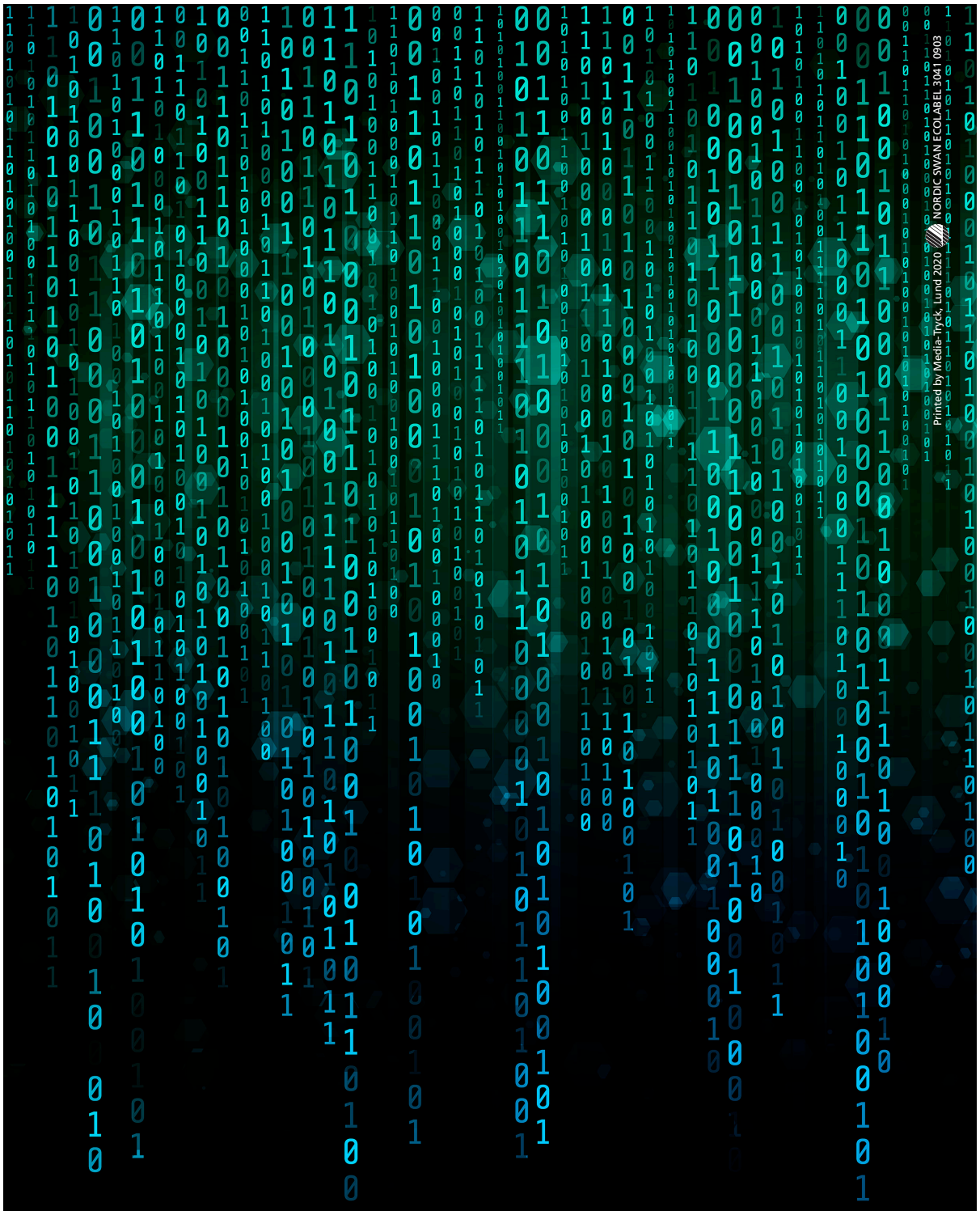

Printed by Media-Tryck, Lund 2020 NORDIC SWAN ECOLABEL 3041 0903

ISBN 978-91-7895-408-7
ISSN 1402-3504
ISRN LUTVDG/TVBB--1063—SE
Report 1063

Fire Safety Engineering
Lund University

LUND UNIVERSITY